Boussinesq type numerical models

Author:
Mera, Mas

Publication Date:
2002

DOI:
https://doi.org/10.26190/unsworks/9257

License:
https://creativecommons.org/licenses/by-nc-nd/3.0/au/
Link to license to see what you are allowed to do with this resource.

Downloaded from http://hdl.handle.net/1959.4/64023 in https://unsworks.unsw.edu.au on 2024-05-05

The University of New South Wales

School of Civil and Environmental Engineering

Sydney, Australia

BOUSSINESQ-TYPE NUMERICAL MODELS

by

Mas MERA

A thesis submitted in fulfilment of the requirements for the degree of

DOCTOR OF PHILOSOPHY

2002

The University of New South Wales
School of Civil and Environmental Engineering
Sydney, Australia

SCIENTIA

MANU ET MENTE

BOUSSINESQ-TYPE NUMERICAL MODELS

by

Mas MERA

Ir. Civil Engineering, 1992. Universitas Andalas, Indonesia

M.T. Civil Engineering, 1995. Institut Teknologi Bandung, Indonesia

Supervisor: Dr. Bruce CATHERS
Co-Supervisor: Assoc. Prof. Ron J. COX

A thesis submitted in fulfilment of the requirements for the degree of

DOCTOR OF PHILOSOPHY

March 2002

U N S W
30 AUG 2005
LIBRARY

Certificate of Originality

I hereby declare that this submission is my own work and to the best of my knowledge it contains no materials previously published or written by another person, nor material which to a substantial extent has been accepted for the award of any other degree or diploma at UNSW or any other educational institution, except where due acknowledgement is made in the thesis. Any contribution made to the research by others, with whom I have worked at UNSW or elsewhere, is explicitly acknowledged in the thesis.

I also declare that the intellectual content of this thesis is the product of my own work, except to the extent that assistance from others in the project's design and conception or in style, presentation and linguistic expression is acknowledged.

(Signed) ....

To: Nasa & Hana

" Verily, along with every hardship is relief,
verily, along with every hardship is relief."

QS.94.5-6

Abstract

Boussinesq-type partial differential equations (BTEs) are a family of 1D or 2D governing equations (i.e. continuity and momentum) to describe the motion of water waves. There are two important parameters associated with BTEs. One parameter (ε) is a measure of non-linearity and is represented by the ratio of typical wave amplitude to characteristic water depth ($\varepsilon = a_{ch}/h_{ch}$). The other parameter ($\mu$) is a measure of frequency dispersion and is represented by the ratio of the characteristic water depth to typical wavelength ($\mu = h_{ch}/L_{ch}$).

This thesis focuses on numerically studying the performance of two existing sets of BTEs. These BTEs are two different extensions of what is termed 'the basic governing equations'. The basic governing equations considered are the existing BTEs which include terms up to $O(\varepsilon,\mu^2)$ and are presented in terms of the horizontal velocity vector at an arbitrary z-elevation. A short description of the limits of the two sets of BTEs studied now follows.

(i) In the first set of BTEs, the basic governing equations were extended to yield a dispersion relation which is valid to deeper water i.e. $h/L \leq 1.0$ whereas the basic governing equations yield a dispersion relation which is

valid for $h/L \leq ½$. (The reference solution is the dispersion relation of Airy wave theory).

(ii) In the second set of BTEs studied, the basic governing equations were extended to include dispersion terms associated with currents. These BTEs are capable of modelling an interacting wave and ambient current field.

Fulfilling the aims of the study requires the development of numerical models based on the two sets of BTEs in (i) and (ii) above, as well as a number of ancillary models. The ancillary models are developed for validating the main numerical models when laboratory data are unavailable. The ancillary models comprise a number of models based on the 1D and 2D non-linear shallow water equations and 1D conservation of wave action equation. All these models are written by the present author.

In this thesis, all the governing equations considered are solved by the present author using an implicit non-staggered finite difference method. In space, the first-order derivatives are discretised using central approximations with fourth-order accuracy. However, the second- and third-order derivatives are approximated using central, second-order accurate finite difference approximations. To advance the solution in time, the third-order Adams-Bashforth predictor and fourth-order Adams-Moulton corrector are used. Emphasis is given to the determination of effective boundary conditions for each set of 1D and 2D governing equations. Due to the Sommerfeld radiation condition being applied at the boundaries, the resulting numerical models are limited to monochromatic waves.

Additionally, a new and systematic approach is developed by the present author for deriving the *existing* BTEs with include terms up to: (i) $O(\varepsilon,\mu^2)$; (ii) $O(\mu^2,\varepsilon^3\mu^2)$; and (iii) $O(\mu^4,\varepsilon^5\mu^4)$.

For making comparisons with the existing BTEs, the author also develops *new* sets of BTEs with terms up to: (a) $O(\varepsilon,\mu^2)$ (4 sets, three of them with dispersion terms associated with currents included); and (b) $O(\mu^2,\varepsilon^3\mu^2)$ (1 set).

Acknowledgements

I would like to express my sincere gratitude to my supervisor *Dr. Bruce Cathers* from the School of Civil and Environmental Engineering, the University of New South Wales (UNSW) for his invaluable guidance, constructive comments, challenging ideas and timely advice.

I would also like to thank my co-supervisor *Assoc. Prof. Ron J. Cox* from the School of Civil and Environmental Engineering, UNSW for reviewing some of the material in my thesis.

I would also like to thank *Cynthia Grant* of NewSouth Global Pty Ltd UNSW for her sustained advice, assistance and helpfulness throughout the duration of my study.

I would like to thank the following organisations for providing the financial assistance and granting me to pursue my study: the Asian Development Bank (ADB), the Government of the Republic of Indonesia, the Central Project Implementation Unit – Engineering Education Development Project (CPIU-EEDP) and NewSouth Global Pty Limited UNSW.

I would like to dedicate this work to a number of people in my family. Firstly to my beloved wife *Yessy Nadewi (Essy)* for her patience and moral support. Secondly to my 'pigeon pair' i.e. my son *Furqano Annasa Essera (Nasa)* and daughter *Hana Fauzia Essera (Hana)*, who missed out on their play time with their father. Finally to my beloved mother *H. Rabaani*, who has always been praying for my success.

Table of Contents

Title Pages i
Abstract v
Acknowledgements vii
Table of Contents ix
Nomenclature xv
List of Figures xx
List of Tables xxix

Chapter One

Introduction

1.1. Background 1
1.2. Objectives 22
1.2.1. Primary objectives 22
1.2.1. Secondary objectives 24
1.3. Outline of contents 27

Chapter Two

Literature Review

2.1. Boussinesq-type equations 33

2.2. Numerical models based on Boussinesq-type equations 38

2.3. Derivation of the equations of Boussinesq (1872) 50

2.4. Derivation of the equations of Peregrine (1967) 54

2.4.1. Non-dimensional variables 54

2.4.2. Continuity equation and Euler equations of motion 54

2.4.3. Boundary conditions 55

2.4.4. Depth-integrated continuity and momentum equations 55

2.4.5. 1D horizontal equations 56

2.4.5.1. First-order 1D horizontal equations 57

2.4.5.2. Second-order 1D horizontal equations 58

2.4.5.3. 1D horizontal equations in terms of $\bar{u}$ 60

2.4.5.4. 1D horizontal equations in terms of $\tilde{u}$ 61

2.4.6. 2D horizontal equations 62

2.4.6.1. 2D horizontal equations in terms of $\tilde{\mathbf{u}}$ 64

2.4.6.2. 2D horizontal equations in terms of $\bar{\mathbf{u}}$ 64

Chapter Three

1D Basic Model

3.1. Introduction 66

3.2. New derivation of the equations of Nwogu (1993) 69

3.3. Review of dispersion relations 75

3.4. Numerical solution algorithm for the 1D basic model (1DBMW-1) 76

3.4.1. Solution method 76

3.4.2. Boundary conditions 79

3.4.2.1. Incoming wave boundary conditions 79

3.4.2.2. Outgoing wave boundary conditions 80

3.5. Model verification 81

3.5.1. Experimental set-up 1: Wave propagation up a slope .. 81

3.5.2. Experimental set-up 2: Wave propagation in a channel with a submerged bar 84

3.6. Conclusions 88

Chapter Four

1D Basic Model with an Improved Dispersion Relation

4.1. Introduction 90

4.2. Derivation of the equations of Schäffer and Madsen (1995) 92

4.3. Dispersion relations 94

4.4. Numerical solution algorithm for 1DDBMW-2 98

4.4.1. Solution method 98

4.4.2. Boundary conditions 99

4.4.2.1. Incoming wave boundary conditions 99

4.4.2.2. Outgoing wave boundary conditions 100

4.5. Model verification 101

4.5.1. Experimental set-up 1: Wave propagation in a constant depth channel 101

4.5.2. Experimental set-up 2: Wave propagation up a slope . 104

4.5.3. Experimental set-up 3: Wave propagation in a channel with a submerged bar 107

4.6. Conclusions 110

Chapter Five

1D Basic Model with Current Effects

5.1. Introduction 112

5.2. Derivation of the equations of Chen *et al.* (1998) 112

5.2.1. Non-dimensionalisation based on wave scaling parameters 112

5.2.2. Non-dimensionalisation based on wave-current scaling parameters 113

5.2.3. *First set* of equations of Chen *et al.* (1998) 115

5.2.4. *Second set* of equations of Chen *et al.* (1998) 119

5.3. Boussinesq-type numerical model (1DBMWC-3) 122
5.3.1. Solution method 122
5.3.2. Boundary conditions for waves only case 124
5.3.2.1. Incoming wave boundary conditions 124
5.3.2.2. Outgoing wave boundary conditions 124
5.3.3. Boundary conditions for current only case 126
5.3.4. Boundary conditions for wave-current interaction case 127
5.4. 1D steady, non-linear shallow water numerical model (1DSSWM) 129
5.5. 1D conservation of wave action numerical model (1DWACM) 131
5.6. Experimental set-up 1: a slope 132
5.7. Experimental set-up 2: a submerged bar 135
5.7.1. Test 1 with submerged bar (set-up 2): Steady current only case 135
5.7.2. Test 2 with submerged bar (set-up 2): Waves and steady strong opposing current 137
5.7.3. Test 3 with submerged bar (set-up 2): Waves and steady weak opposing current 138
5.7.4. Test 4 with submerged bar (set-up 2): Steady current only case 139
5.4.5. Test 5 with submerged bar (set-up 2): Waves and steady current in same direction 140
5.8. Conclusions 141

Chapter Six

2D Basic Model

6.1. Introduction 143
6.2. Governing equations 146
6.3. Numerical solution algorithm for 2DBMW-4 147
6.3.1. Solution method 147
6.3.2. Boundary conditions 150
6.3.2.1. Incoming wave boundary conditions in 2D 150
6.3.2.2. Outgoing wave boundary conditions in 2D 151
6.3.2.3. Reflecting wave boundary conditions in 2D 153

6.3.3. Filter 155

6.4. Model verification 157

6.4.1. Scenario 1: Wave propagation over a circular shoal on a flat bottom basin 157

6.4.2. Scenario 2: Wave propagation over an elliptic shoal on a sloping bottom basin 162

6.5. Conclusions 167

Chapter Seven

2D Basic Model with Current Effects

7.1. Introduction 168

7.2. 2D Boussinesq-type numerical model (2DBMWC-5) 169

7.2.1. Governing equations 169

7.2.2. Numerical solution algorithms for 2DBMWC-5 172

7.2.2.1. Solution method 172

7.2.2.2. Boundary conditions for waves only case in 2D 173

7.2.2.3. Boundary conditions for current only case in 2D 177

7.2.2.4. Boundary conditions for wave-current interaction case 178

7.3. 2D Unsteady non-linear shallow water model (2DUSWM-6) . 180

7.3.1. Governing equations 180

7.3.2. Numerical solution algorithms for 2DUSWM-6 180

7.3.2.1. Solution method 180

7.3.2.2. Boundary conditions for current only case in 2D 182

7.4. Experimental set-up 184

7.4.1. Test 1: Waves only case 184

7.4.2. Test 2: Current only case 187

7.4.3. Test 3: Waves and opposing current 193

7.4.4. Test 4: Current only case 197

7.4.5. Test 5: Waves and current in same direction 197

7.5. Conclusions 201

Chapter Eight

Summary, Conclusions and Recommendations

8.1. Summary 202
8.2. Conclusions 204
8.3. Recommendations 206

References

207

Appendix A

Coordinate Systems and Orientations

212

Appendix B

Central, Finite Difference Operators

215

Appendix C

Alternative 2D Boussinesq-Type Equations

217

Nomenclature

Symbol	Description
a	Wave amplitude
a_{ch}	Typical or characteristic wave amplitude
$\mathbf{C}$	Wave celerity vector
C	Wave celerity (in the x-direction)
$C_{[2,2]}$	Wave celerity (in the x-direction) corresponding to a Padé [2,2] approximation of the dispersion relation in terms of kh
$C_{[4,4]}$	Wave celerity (in the x-direction) corresponding to a Padé [4,4] approximation of the dispersion relation in terms of kh
C_{Airy}	Wave celerity (in the x-direction) from Airy wave theory
Cr	Courant number i.e. $Cr = \sqrt{gh}\frac{\Delta t}{\Delta x}$ for 1D and $Cr = \sqrt{gh}\frac{\Delta t}{\sqrt{\Delta x^2 + \Delta y^2}}$ for 2D
C_c	Chezy coefficient
E	Variable grouping for spatial derivatives in the continuity equations
F	Variable grouping for spatial derivatives in the momentum equations in the x-direction

F_1	Variable grouping for combining temporal with cross-derivatives in the momentum equations in the x-direction
G	Variable grouping for spatial derivatives in the momentum equations in the y-direction
G_1	Variable grouping for combining temporal with cross-derivatives in the momentum equations in the y-direction
g	Gravitational acceleration
h	Local still water depth
h_{ch}	Characteristic water depth
h_i	Still water depth at the incoming wave boundary
H	Wave height
H_i	Wave height at the incoming wave boundary
H_{rms}	Root-mean-square wave height
$\mathbf{k}$	Wave number vector
k	Wave number (in the x-direction)
k_i	Wave number (in the x-direction) at the incoming wave boundary
L	Wavelength (in the x-direction)
L_o	Wavelength (in the x-direction) in deep water
L_{ch}	Typical or characteristic wavelength
p	Pressure field
$\mathbf{Q}$	Volume flux vector
R_c	Bottom friction in Chapter five
t	Time
T	Wave period
$\mathbf{u}$	Horizontal velocity vector, $\mathbf{u}\,(x,y,z,t) = (u,v)$
u	Horizontal velocity (in the x-direction), $u\,(x,y,z,t)$
$\mathbf{u}_b$	Horizontal velocity vector at the seabed, $\mathbf{u}_b = \mathbf{u}\,(x,y,-h,t) = (u_b,v_b)$
u_b	Horizontal velocity (in the x-direction) at the seabed ($z = -h$), $u_b = u\,(x,y,-h,t)$

$\overline{\mathbf{u}}$	Depth-averaged horizontal velocity vector, $\overline{\mathbf{u}} = (\overline{u}, \overline{v})$
$\overline{u}$	Depth-averaged horizontal velocity (in the x-direction), $\overline{u}\,(x,y,t)$
$\tilde{\mathbf{u}}$	Horizontal velocity vector at still water level (z = 0), $\tilde{\mathbf{u}} = \mathbf{u}\,(x,y,0,t) = (\tilde{u}, \tilde{v})$
$\tilde{u}$	Horizontal velocity (in the x-direction) at still water level, $\tilde{u} = u\,(x,y,0,t)$
$\hat{u}_c$	Current horizontal velocity, which is assumed to be uniform over the depth
$\mathbf{u}_\alpha$	Horizontal velocity vector at an arbitrary elevation ($z = z_\alpha$), $\mathbf{u}_\alpha = (u_\alpha, v_\alpha)$
u_α	Horizontal velocity at $z = z_\alpha$ in the x-direction
$u_{\alpha a}$, $\mathbf{u}_{\alpha a}$	Amplitudes of u_α and $\mathbf{u}_\alpha$ respectively
u_{α_x}, $(\,)_x$	$\dfrac{\partial u_\alpha}{\partial x}$, $\dfrac{\partial}{\partial x}(\,)$
U_α	Part of the momentum equations containing temporal derivatives in the x-direction
$\mathbf{v}$	Velocity vector, $\mathbf{v} = (\mathbf{u}, w) = (u, v, w)$
v	Horizontal velocity (in the y-direction), $v\,(x,y,z,t)$
V_α	Part of the momentum equations containing temporal derivatives in the y-direction
v_α	Horizontal velocity at $z = z_\alpha$ in the y-direction
w	Vertical velocity, $w\,(x,y,z,t)$
z_α	z-location at which $\mathbf{u}_\alpha$ is taken, $z_\alpha = z_{c\alpha}\,h$, $-1 \le z_{c\alpha} \le 0$
α	$= \frac{1}{2}(z_{c\alpha})^2 + z_{c\alpha}$, $-0.5 \le \alpha \le 0$
β, β_1, β_2	Free coefficients in the continuity equation in Chapter Four
Δt	Time increment
Δx	Grid size in the x-direction
Δy	Grid size in the y-direction
ε	Scaling parameter, which is a measure of the non-linearity ($= a_{ch}/h_{ch}$)

Φ	Velocity potential
$\gamma, \gamma_1, \gamma_2$	Free coefficients in the momentum equation in Chapter Four
η	Free surface elevation
η_a	Amplitude of η
η_t, η_x	$\frac{\partial\eta}{\partial t}, \frac{\partial\eta}{\partial x}$
Λ	Dispersion terms in the Boussinesq-type momentum equations
μ	Scaling parameter, which is a measure of the frequency dispersion (= h_{ch}/L_{ch})
ν	$\varepsilon \leq \nu \leq 1$; $\nu = O(\varepsilon)$ indicates weak current and $\nu = O(1)$ indicates strong current. This parameter is used when currents are present and terms up to $O(\varepsilon,\mu^2)$ are retained in the governing equations.
Π	Dispersion terms in the Boussinesq-type continuity equations
θ	Local wave angle with respect to the x-axis
θ_i	Wave angle at the incident wave boundary with respect to the x-axis
ρ	Fluid density
σ	Scaling parameter, which is a measure of spatial variation, $\sigma = \varepsilon / \nu$. This parameter is used when currents are present and terms up to $O(\varepsilon,\mu^2)$ are retained in the governing equations.
σ_i	Intrinsic angular frequency or frequency without any currents present.
τ_η	Surface tension effects
Ω	Fluid domain
ω	Angular frequency. In the case of pure wave motion, $\omega = \omega = \sigma_i$.
ω_a	Absolute angular frequency
$\partial\Omega$	Boundary
Ξ	Part of the continuity equation containing temporal derivatives in Chapter Four
Ψ	Stream function
∇	Horizontal gradient operator, $\nabla = (\partial/\partial x, \partial/\partial y) = \partial/\partial x\,\mathbf{i} + \partial/\partial y\,\mathbf{j}$

$\nabla \bullet \mathbf{u}$	$= u_x + v_y$
$(\mathbf{u} \bullet \nabla)\mathbf{u}$	$= (uu_x + vu_y)\,\mathbf{i} + (uv_x + vv_y)\,\mathbf{j}$
$\mathbf{u} \bullet \nabla\eta$	$= u\eta_x + v\eta_y$
$\nabla \bullet (h\mathbf{u})$	$= (hu)_x + (hv)_y$
$\nabla\phi$	$= (\phi_x, \phi_y) = \phi_x\,\mathbf{i} + \phi_y\,\mathbf{j}$
$\overline{\nabla}$	3D gradient operator, $\overline{\nabla} = (\partial/\partial x, \partial/\partial y, \partial/\partial z) = \partial/\partial x\,\mathbf{i} + \partial/\partial y\,\mathbf{j} + \partial/\partial z\,\mathbf{k}$

List of Figures

1.1 Domain of validity of three wave theories based on a criterion of goodness of fit to dynamic free surface boundary condition. Source: Dean and Dalrymple (1984).

1.2 Ratio of wave celerity, C/C_{Airy}, C_{Airy} is the Airy wave celerity and C is the wave celerity of various Boussinesq-type equations including terms up to $O(\mu^2)$ in terms of the horizontal velocity at: (1) an arbitrary z-level, $\mathbf{u}_\alpha$; (2) the seabed, $\mathbf{u}_b$; (3) still water level, $\tilde{\mathbf{u}}$; and (4) depth-averaged horizontal velocity, $\overline{\mathbf{u}}$.

1.3 Ratio of wave celerity, C/C_{Airy}, where C_{Airy} is determined by wave celerity of the Airy wave theory and C by the wave celerity of the equations of: (1) Schäffer and Madsen (1995); and (2) Nwogu (1993).

1.4 Family tree of various Boussinesq-type momentum equations.

3.1 New derivation of Nwogu's (1993) momentum equation.

3.2 Effect of α ($-0.5 \leq \alpha \leq 0$) on the ratio of the wave celerity corresponding to the 1D linearised form of the equations of Nwogu (1993) over the wave celerity corresponding to Airy wave theory: $\alpha = -0.5$, $\alpha = 0$, $\alpha = -1/3$ (or equivalently the equations by Peregrine), and $\alpha = -0.390$ (obtained by Nwogu).

3.3. Boundary conditions for 1DBMW-1

3.4. Experimental set-up 1 (Nwogu, 1993): the basin terminates with a 1:25 constant slope, concrete beach.

3.5. Incident deep water waves ($h_i/L_o = 0.5$): time series of the free surface elevation at 0.28 m depth predicted by the present model (bold line) and the laboratory measurements of Nwogu (thin line). Data: $T = 0.85$ s, $H_i = 0.04$ m, $H_i/h = 0.143$, $k_ih_i = \pi$ and $Cr_i = 1.00$.

3.6. Incident deep water waves ($h_i/L_o = 0.5$): time series of the free surface elevation at the outgoing wave boundary ($h = 0.07$ m) predicted by the present model (bold line) and the laboratory measurements of Nwogu (thin line). Data: $T = 0.85$ s, $H_i = 0.04$ m, $H_i/h = 0.571$, $k_ih_i = \pi$ and $Cr_i = 1.00$.

3.7. Intermediate depth water waves ($h_i/L_o = 0.36$): time series of the free surface elevation at 0.24 m depth predicted by the present model (bold line) and the laboratory measurements of Nwogu (thin line). Data: $T = 1$ s, $H_i = 0.066$ m, $H_i/h = 0.275$, $k_ih_i = 2.30$ and $Cr_i = 1.00$.

3.8. Intermediate depth water waves ($h_i/L_o = 0.36$): time series of the free surface elevation at the outgoing wave boundary ($h = 0.10$ m) predicted by the present model (bold line) and the laboratory measurements of Nwogu (thin line). Data: $T = 1$ s, $H_i = 0.066$ m, $H_i/h = 0.66$, $k_ih_i = 2.30$ and $Cr_i = 1.00$.

3.9. Experimental set-up 2 (Luth *et al.*, 1994): submerged bar topography with 25 m long channel, 0.4 m deep on both sides of the bar and 0.1 m deep on top of the bar.

3.10. Top of the bar (i.e. 11.5 m before the outgoing wave boundary): time series of the water surface elevation predicted by the present model (bold line) and the laboratory measurements of Luth *et al.* (thin line). Data: $T = 2.02$ s, $H_i = 0.02$ m, $H_i/h = 0.2$, $k_ih_i = 0.67$, $h_i/L_o = 0.06$ and $Cr_i = 0.99$.

3.11. Behind the bar (i.e. 7.7 m before the outgoing wave boundary): time series of the water surface elevation predicted by the present model (bold line) and the laboratory measurements of Luth *et al.* (thin line). Data: $T = 2.02$ s, $H_i = 0.02$ m, $H_i/h = 0.05$, $k_ih_i = 0.67$, $h_i/L_o = 0.06$ and $Cr_i = 0.99$.

3.12. Top of the bar (i.e. 11.5 m before the outgoing wave boundary): time series of the water surface elevation predicted by the present model (bold line) and the laboratory measurements of Luth *et al.* (thin line). Data: $T = 1.01$ s, $H_i = 0.041$ m, $H_i/h = 0.2$, $k_ih_i = 1.69$, $h_i/L_o = 0.25$ and $Cr_i = 0.74$.

3.13. Behind the bar (i.e. 7.7 m before the outgoing wave boundary): time series of the water surface elevation predicted by the present model (bold line) and the laboratory measurements of Luth *et al.* (thin line). Data: $T = 1.01$ s, $H_i = 0.041$ m, $H_i/h = 0.05$, $k_ih_i = 1.69$, $h_i/L_o = 0.25$ and $Cr_i = 0.74$.

4.1. A comparison of normalised celerity errors of the linearised Boussinesq-type wave equations of Schäffer and Madsen (1995) for different values of the free coefficients (α,β,γ): (1) the three solutions (4.14b – d) which result in identical dispersion relations; and (2) the particular solution $(\alpha,\beta,\gamma) = (-0.395, 0.0398, 0.01051)$ adopted in this study (1DDBMW-2).

4.2. A comparison of normalised celerity errors of various linearised Boussinesq-type equations of: (1) Schäffer and Madsen (1995) with $(\alpha,\beta,\gamma) = (-0.395, 0.0398, 0.01051)$ (1DDBMW-2); (2) Madsen *et al.* (1991), Madsen and Sørensen (1992) and Nwogu (1993) or equivalently the equations of Schäffer and Madsen with $(\alpha,\beta,\gamma) = (-0.39,0,0)$; and (3) Peregrine (1967) or equivalently the equations by Schäffer and Madsen with $(\alpha,\beta,\gamma) = (-1/3,0,0)$.

4.3. Experimental set-up 1: the channel with a flat bottom.

4.4. Deeper water ($h/L_o = 1.0$): the free surface elevation along the channel at $t = 15$, 20 and 25 s predicted by 1DDBMW-2 (bold lines) and Airy wave theory (thin lines). Data: $T = 0.85$ s, $H_i = 0.04$ m, $h = 1.13$ m, $\Delta x = 0.02$ m and $\Delta t = 0.01$ s.

4.5. Incident deep water waves ($h_i/L_o = 0.5$): time series of the free surface elevation at 0.28 m depth predicted by 1DDBMW-2 (bold line), the laboratory measurements of Nwogu (thin line) and 1DBMW-1 (dashed line). Data: $T = 0.85$ s, $H_i = 0.04$ m, $h_i = 0.56$ m, $\Delta x = 0.02$ m and $\Delta t = 0.01$ s.

4.6. Incident deep water waves ($h_i/L_o = 0.5$): time series of the free surface elevation at the outgoing wave boundary ($h = 0.07$ m) predicted by 1DBMW-2 (bold line), the laboratory measurements of Nwogu (thin line) and 1DBMW-1 (dashed line). Data: $T = 0.85$ s, $H_i = 0.04$ m, $h_i = 0.56$, $\Delta x = 0.02$ m and $\Delta t = 0.01$ s.

4.7. Intermediate depth water waves ($h_i/L_o = 0.36$): time series of the free surface elevation at 0.24 m depth predicted by 1DDBMW-2 (bold line), the laboratory measurements of Nwogu (thin line) and 1DBMW-1 (dashed line). Data: $T = 1$ s, $H_i = 0.066$ m, $h_i = 0.56$ m, $\Delta x = 0.02$ m and $\Delta t = 0.01$ s.

4.8. Intermediate depth water waves ($h_i/L_o = 0.36$): time series of the free surface elevation at the outgoing wave boundary ($h = 0.10$ m) predicted by 1DDBMW-2 (bold line), the laboratory measurements of Nwogu (thin line) and 1DBMW-1 (dashed line). Data: $T = 1$ s, $H_i = 0.066$ m, $h_i = 0.56$ m, $\Delta x = 0.02$ m and $\Delta t = 0.01$ s.

4.9. Top of the bar (i.e. 11.5 m before the outgoing wave boundary): time series of the water surface elevation predicted by 1DDBMW-2 (bold line), the laboratory measurements of Luth *et al.* (thin line) and 1DBMW-1 (dashed line). Data: $T = 2.02$ s, $H_i = 0.02$ m, $h_i = 0.4$ m, $h_i/L_o = 0.06$, $\Delta x = 0.08$ m and $\Delta t = 0.02$ s.

4.10. Behind the bar (i.e. 7.7 m before the outgoing wave boundary): time series of the water surface elevation predicted by 1DDBMW-2 (bold line), the laboratory measurements of Luth *et al.* (thin line) and 1DBMW-1 (dashed line). Data: $T = 2.02$ s, $H_i = 0.02$ m, $h_i = 0.4$ m, $h_i/L_o = 0.06$, $\Delta x = 0.08$ m and $\Delta t = 0.02$ s.

4.11. Top of the bar (i.e. 11.5 m before the outgoing wave boundary): time series of the water surface elevation predicted by 1DDBMW-2 (bold line), the laboratory measurements of Luth *et al.* (thin line) and 1DBMW-1 (dashed line). Data: $T = 1.01$ s, $H_i = 0.041$ m, $h_i = 0.4$ m, $h_i/L_o = 0.25$, $\Delta x = 0.08$ m and $\Delta t = 0.02$ s.

4.12. Behind the bar (i.e. 7.7 m before the outgoing wave boundary): time series of the water surface elevation predicted by 1DDBMW-2 (bold line), the laboratory measurements of Luth *et al.* (thin line) and 1DBMW-1 (dashed line). Data: $T = 1.01$ s, $H_i = 0.041$ m, $h_i = 0.4$ m, $h_i/L_o = 0.25$, $\Delta x = 0.08$ m and $\Delta t = 0.02$ s.

5.1. Waves only case: the free surface elevation η at the incoming wave boundary is varied sinusoidally with time.

5.2. Current only case: (a) the imposed current flows from the right to the left hand boundaries; and (b) the imposed current flows from the left to the right hand boundaries. Note: $c = \sqrt{gh}$.

5.3. Wave-current interaction case: (a) waves and steady opposing current; and (b) waves and steady current in same direction.

5.4. Definitions for d, h and η.

5.5. Incident deep water waves propagating over a slope: time series of the free surface elevation at 0.28 and 0.07 m depth predicted by 1DBMWC-3 (bold lines), the laboratory measurements (thin lines) and 1DBMW-1 (dashed lines). Test condition: $h_i = 0.56$ m, $H_i = 0.04$ m, $T = 0.85$ s, $\Delta x = 0.04$ m and $\Delta t = 0.017$ s.

5.6. Incident intermediate depth water waves propagating over a slope: time series of the free surface elevation at 0.24 and 0.10 m depth predicted by 1DBMWC-3 (bold lines), the laboratory measurements (thin lines) and 1DBMW-1 (dashed lines). Test condition: $h_i = 0.56$ m, $H_i = 0.066$ m, $T = 1$ s, $\Delta x = 0.05$ m and $\Delta t = 0.02$ s.

5.7. Channel with a submerged bar: the channel is 60 m long, 0.8 m deep on both sides of the bar and 0.2 m deep on top of the bar.

5.8. Steady flow in open channel with a submerged bar (Test 1): comparison of the free surface elevation predicted by 1DBMWC-3 (bold line) at $t = 120$ s and 1DSSWM (thin line). Test condition: $h_i = 0.8$ m, $\bar{u}_{c(x=0)} = 0.17$ m/s, $\Delta x = 0.2$ m and $\Delta t = 0.05$ s.

5.9. Steady flow in open channel with a submerged bar (Test 1): comparison of the horizontal velocity predicted by 1DBMWC-3 (bold line) at $t = 120$ s and 1DSSWM (thin line). Test condition: $h_i = 0.8$ m, $\bar{u}_{c(x=0)} = 0.17$ m/s, $\Delta x = 0.2$ m and $\Delta t = 0.05$ s.

5.10. Waves propagating over a submerged bar against a steady, strong opposing current (Test 2). The bold line denotes the computed instantaneous solution by 1DBMWC-3 at $t = 120 + 75 = 195$ s. The thin lines defining the wave envelope denote the results of 1DWACM. Test condition: $h_i = 0.8$ m, $H_i = 0.02$ m, $T = 1.2$ s, $\bar{u}_{c(x=0)} = 0.17$ m/s, $\Delta x = 0.1$ m and $\Delta t = 0.025$ s.

5.11. Waves propagating over a submerged bar against a steady, strong opposing current (Test 2): the relationship between the absolute local current velocity (bold line) and the local wave celerity (circles) and the local group velocity (crosses) predicted by 1DBMWC-3 at $t = 120 + 75 = 195$ s. Test condition: $h_i = 0.8$ m, $H_i = 0.02$ m, $T = 1.2$ s, $\bar{u}_{c(x=0)} = 0.17$ m/s, $\Delta x = 0.1$ m and $\Delta t = 0.025$ s.

5.12. Waves propagating over a submerged bar against a steady, weak opposing current (Test 3). The oscillatory motion of the free surface elevation predicted 1DBMWC-3 at $t = 120 + 47.5 = 167.5$ s is enclosed by the wave envelope (thin lines) of the results of 1DWACM. Test condition: $h_i = 0.8$ m, $H_i = 0.02$ m, $T = 2.4$ s, $\bar{u}_{c(x=0)} = 0.17$ m/s, $\Delta x = 0.2$ m and $\Delta t = 0.025$ s.

5.13. Waves propagating over a submerged bar against a steady, weak opposing current (Test 3): the relationship between the absolute local current velocity (line) and local wave celerity (circles) and local group velocity (crosses) predicted by 1DBMWC-3 at $t = 120 + 47.5 = 167.5$ s. Test condition: $h_i = 0.8$ m, $H_i = 0.02$ m, $T = 2.4$ s, $\bar{u}_{c(x=0)} = 0.17$ m/s, $\Delta x = 0.2$ m and $\Delta t = 0.025$ s.

5.14. Steady flow in open channel with a submerged bar (Test 4): comparison of the free surface elevation predicted by 1DBMWC-3 (bold line) at $t = 120$ s and 1DSSWM (thin line). Test condition: $h_i = 0.8$ m, $\bar{u}_{c(x=60)} = 0.17$ m/s, $\Delta x = 0.2$ m and $\Delta t = 0.05$ s.

5.15. Waves and steady current in same direction moving over a submerged bar (Test 5): The bold line denotes the instantaneous water surface (with waves) from 1DBMWC-3 and the thin lines denote 1DWACM. Test condition: $h_i = 0.8$ m, $H_i = 0.02$ m, $T = 1.2$ s, $\bar{u}_{c(x=60)} = 0.17$ m/s, $\Delta x = 0.1$ m and $\Delta t = 0.025$ s.

6.1. Filter.

6.2. Plan (top) and perspective (bottom) views of numerical bathymetry following Chawla and Kirby's (1996) laboratory set-up. Basin size is 18 m long and 18.2 m wide. Side walls are at $y = 0$ and 18.2 m. Centre of the circular shoal is located at $(x,y) = (13,9.22)$ m. Transects of wave gauge locations: Sections A–A at $y = 9.22$ m, B–B at $x = 6.88$ m, C–C at $x = 8.35$ m, D–D at $x = 10.005$ m, E–E at $x = 11.5$ m, F–F at $x = 13$ m and G–G at $x = 14.5$ m.

6.3. Wave heights (H_{rms}) normalised with respect to the incoming wave height: comparisons between 2DBMW-4 (——) and laboratory data (∘ ∘ ∘) along various transects for the experiment of Chawla and Kirby (1996). Data: $T = 1.0$ s, $H_i = 0.0118$ m, $\theta_i = 0^o$, $h_{even} = 0.45$ m, $\Delta x = 0.05$ m, $\Delta y = 0.10$ m and $\Delta t = 0.01$ s.

6.4. Results of 2DBMW-4: perspective views of monochromatic wave fields at $t = 20$ s (top) and $t = 40$ s (bottom). Data: $T = 1.0$ s, $H_i = 0.0118$ m, $\theta_i = 0^o$, $h_{even} = 0.45$ m, $\Delta x = 0.05$ m, $\Delta y = 0.10$ m and $\Delta t = 0.01$ s.

6.5. Plan (top) and perspective (bottom) views of numerical bathymetry following Berkhoff *et al.*'s (1982) laboratory set-up. Basin size is 22 m long and 20 m wide. Side walls are at $y = 0$ and 20 m. Centre of the elliptic shoal is located at $(x,y) = (12,10)$ m. Transects of wave gauge locations: Sections 1–1 at $x = 11$ m, 2–2 at $x = 9$ m, 3–3 at $x = 7$ m, 4–4 at $x = 5$ m, 5–5 at $x = 3$ m, 6–6 at $y = 12$ m, 7–7 at $y = 10$ m and 8–8 at $y = 8$ m, $h_{even} = 0.45$ m.

6.6. Wave height (H_{rms}) normalised with respect to the incoming wave height: comparisons between 2DBMW-4 (——) and laboratory data (∘ ∘ ∘) along various Sections for the experiment of Berkhoff *et al.* (1982). Data: $T = 1.0$ s, $\eta_i = 0.0232$ m, $\theta_i = 0^o$, $h_{even} = 0.45$ m, $\Delta x = \Delta y = 0.10$ m and $\Delta t = 0.02$ s.

6.7. Results of 2DBMW-4: perspective views of monochromatic wave fields at $t = 16$ s (top) and $t = 32$ s (bottom). Data: $T = 1.0$ s, $\eta_i = 0.0232$ m, $\theta_i = 0^o$, $h_{even} = 0.45$ m, $\Delta x = \Delta y = 0.10$ m and $\Delta t = 0.02$ s.

7.1. Boundary conditions for wave only case. The imposed monochromatic wave propagates from $i = L$ to $i = 1$. Side walls are located at $j = 1$ and $j = M$. Note: $i = 1,2,3,\ldots L.$ and $j = 1,2,3,\ldots,M$.

7.2. Boundary conditions for current only case. The imposed current flows from $i=1$ to $i=L$. Side walls are located at $j=1$ and $j=M$. Note: $i=1,2,3,...L$; $j=1,2,3,...,M$ and $c=\sqrt{gh}$. Explanations for equations to determine η and $\bar{u}$ at inflow and outflow boundaries can be found in Section 5.3.3.

7.3. Boundary conditions for wave-current interaction case: (a) waves and steady opposing current; and (b) waves and steady current in same direction. Note: no-flow boundary conditions are same as those for waves or current only (see Figure 7.2). Explanations for equations to determine η and $\bar{u}$ at inflow and outflow boundaries can be found in Section 5.3.3.

7.4. Boundary conditions for current only case. The imposed current flows from $i=1$ to $i=L$. Side walls are located at $j=1$ and $j=M$. Note: $i=1,2,3,...L$; $j=1,2,3,...,M$ and $c=\sqrt{gh}$.

7.5. Wave heights (H_{rms}) normalised with respect to the incoming wave height in the case of pure wave motion: comparisons between the results of 2DBMWC-5 (bold lines), 2DBMW-4 (thin lines) and laboratory data (circles) along various sections for the experiment of Chawla and Kirby (1996). Data: $T=1.0$ s, $H_i=0.0118$ m, $\theta_i=0^\circ$, $h_{even}=0.45$ m, $\Delta x=\Delta y=0.10$ m and $\Delta t=0.02$ s.

7.6. Wave only case: plan (top) and perspective (bottom) views of the free surface elevation at $t=40$ s predicted by 2DBMWC-5. Data: $T=1.0$ s, $H_i=0.0118$ m, $\theta_i=0^\circ$, $h_{even}=0.45$ m, $\Delta x=\Delta y=0.10$ m and $\Delta t=0.02$ s.

7.7. Current only case (flow from $x=0$ to $x=18$ m): comparisons of the free surface elevation at $t=65$ s between results of 2DBMWC-5 (bold lines) and 2DUSWM-6 (thin lines) for $x=11$, 13 and 15 m and for $y=0$, 2, 5, 7 and 9 m. Data: $\theta_i=0^\circ$, $h_{even}=0.45$ m, $\bar{u}_{c(x=0)}=0.10$ m/s, $\bar{v}_{c(x=0)}=0$ m/s, $\Delta x=\Delta y=0.10$ m and $\Delta t=0.02$ s.

7.8. Current only case (flow from $x=0$ to $x=18$ m): comparisons of the magnitude of the x-component of velocity at $t=65$ s between results of 2DBMWC-5 (bold lines) and 2DUSWM-6 (thin lines) for $x=11$, 13 and 15 m and for $y=0$, 2, 5, 7 and 9 m. Data: $\theta_i=0^\circ$, $h_{even}=0.45$ m, $\bar{u}_{c(x=0)}=0.10$ m/s, $\bar{v}_{c(x=0)}=0$ m/s, $\Delta x=\Delta y=0.10$ m and $\Delta t=0.02$ s.

7.9. Current only case (flow from $x=0$ to $x=18$ m): comparisons of the magnitude of the y-component of velocity at $t=65$ s between results of 2DBMWC-5 (bold lines) and 2DUSWM-6 (thin lines) for $x=11$, 13 and 15 m and for $y=0$, 2, 5, 7 and 9 m. Data: $\theta_i=0^\circ$, $h_{even}=0.45$ m, $\bar{u}_{c(x=0)}=0.10$ m/s, $\bar{v}_{c(x=0)}=0$ m/s, $\Delta x=\Delta y=0.10$ m and $\Delta t=0.02$ s.

7.10. Current only case (flow from $x = 0$ to $x = 18$ m): perspective views of the free surface elevation (upside down) at $t = 65$ s predicted by 2DBMWC-5 (top) and by 2DUSWM-6 (bottom). Data: $\theta_i = 0^o$, $h_{even} = 0.45$ m, $\bar{u}_{c_{(x=0)}} = 0.10$ m/s, $\bar{v}_{c_{(x=0)}} = 0$ m/s, $\Delta x = \Delta y = 0.10$ m and $\Delta t = 0.02$ s.

7.11. Current only case (flow from $x = 0$ to $x = 18$ m): the velocity vectors at $t = 65$ s predicted by 2DBMWC-5 (top) and by 2DUSWM-6 (bottom). Data: $\theta_i = 0^o$, $h_{even} = 0.45$ m, $\bar{u}_{c_{(x=0)}} = 0.10$ m/s, $\bar{v}_{c_{(x=0)}} = 0$ m/s, $\Delta x = \Delta y = 0.10$ m and $\Delta t = 0.02$ s.

7.12. Waves with period $T = 1$ s propagating against a steady, opposing current with steady inflow velocity of 0.1 m/s along the $x = 0$ boundary. Both free surface elevation predicted by 2DBMWC-5 at $t = 40$ s. The waves with (bold lines) and without (thin lines) the presence of the ambient current for $y = 2$, 5, 7 and 9 m. Data: $T = 1$ s, $H_i = 0.0118$ m, $\theta_i = 0^o$, $h_{even} = 0.45$ m, $\Delta x = \Delta y = 0.10$ m and $\Delta t = 0.02$ s.

7.13. Waves with period $T = 1$ s propagating against a steady, opposing current with steady inflow velocity of 0.1 m/s along the $x = 0$ boundary. Perspective views of the free surface elevation predicted by 2DBMWC-5 at $t = 20$ s (top) and at $t = 40$ s (bottom). Data: $T = 1$ s, $H_i = 0.0118$ m, $\theta_i = 0^o$, $h_{even} = 0.45$ m, $\Delta x = \Delta y = 0.10$ m and $\Delta t = 0.02$ s.

7.14. Waves with period $T = 1$ s propagating against a steady, opposing current with steady inflow velocity of 0.1 m/s along the $x = 0$ boundary. The velocity vectors predicted by 2DBMWC-5 at $t = 20$ s (top) and at $t = 40$ s (bottom). The velocities shown in figures above are the total velocity (i.e. combined orbital waves and ambient current velocities at the particular times. Data: $T = 1$ s, $H_i = 0.0118$ m, $\theta_i = 0^o$, $h_{even} = 0.45$ m, $\Delta x = \Delta y = 0.10$ m and $\Delta t = 0.02$ s.

7.15. Waves with period $T = 1$ s propagating with a co-flowing steady current with steady inflow velocity of 0.1 m/s along the $x = 18$ m boundary. The free surface elevation predicted by 2DBMWC-5 at $t = 40$ s. The waves with (bold lines) and without (thin lines) the presence of the ambient current for $y = 2$, 5, 7 and 9 m. Data: $T = 1$ s, $H_i = 0.0118$ m, $\theta_i = 0^o$, $h_{even} = 0.45$ m, $\Delta x = \Delta y = 0.10$ m and $\Delta t = 0.02$ s.

7.16. Waves with period $T = 1$ s propagating with a co-flowing steady current with steady inflow velocity of 0.1 m/s along the $x = 18$ m boundary. Perspective views of the free surface elevation predicted by 2DBMWC-5 at $t = 20$ s (top) and at $t = 40$ s (bottom). Data: $T = 1$ s, $H_i = 0.0118$ m, $\theta_i = 0^o$, $h_{even} = 0.45$ m, $\Delta x = \Delta y = 0.10$ m and $\Delta t = 0.02$ s.

7.17. Waves with period $T = 1$ s propagating with a co-flowing steady current with steady inflow velocity of 0.1 m/s along the $x = 18$ m boundary. The velocity vectors predicted by 2DBMWC-5 at $t = 20$ s (top) and at $t = 40$ s (bottom). The velocities shown in figures above are the total velocity (i.e. combined orbital waves and ambient current velocities at the particular times. Data: $T = 1$ s, $H_i = 0.0118$ m, $\theta_i = 0^o$, $h_{even} = 0.45$ m, $\Delta x = \Delta y = 0.10$ m and $\Delta t = 0.02$ s.

A.1. Definition for η, u_α, v_α, z, z_α, x, y and their positive directions.

A.2. 1D Cartesian coordinate system and the positive direction for u_α.

A.3. 2D Cartesian coordinate system and the positive directions for the velocity components u_α, v_α and the incident wave direction θ_i.

A.4. Vector components and the positive directions for **C**, **k**, **u** and $\mathbf{u}_\alpha$.

B.1. Convention adopted for positive slopes.

C.1. New derivations of four new and three existing (ε,μ^2) momentum equations.

C.2. New derivations of Wei *et al.*'s (1993) and new $(\mu^2,\varepsilon^3\mu^2)$ momentum equations.

C.3. New derivations for Madsen and Schäffer's (1998) and new $(\mu^4,\varepsilon^5\mu^4)$ momentum equations.

C.4. Wave celerity ratio, C/C_{Stokes}, where C is determined by: (1) equation (C.65) (with $\alpha = -0.39$); (2) equation (C.56); (3) equation (C.59); and (4) equation (C.62). [Boussinesq-type equations include terms up to $O(\mu^2)$], and C_{Stokes} from (C.69).

C.5. Wave celerity ratio, C/C_{stokes}, where C is determined by equation (C.68), and C_{Stokes} from equation (C.69). Boussinesq-type equations include terms up to $O(\mu^4)$. (1) $\alpha = -0.429648$, (2) $\alpha = -4/9$, (3) $\alpha = -2/5$ and (4) $\alpha = -1/2$, (2) $\alpha = 0$.

C.6. Ratio of second harmonic, $\eta_2/\eta_{2Stokes}$, where η_2 is determined by equation (C.87) and $\eta_{2Stokes}$ by equation (C.88). (1) FBE2O-E and Wei *et al.*'s (1995) equations include terms up to $O(\mu^2,\varepsilon\mu^2)$; (2) BEWCAV-A, Nwogu's (1993) and second Chen et *al.*'s (1998) equations include terms up to $O(\mu^2,\varepsilon)$; (3) BEWCBV-B and BEWBV-D include terms up to $O(\mu^2,\varepsilon)$; (4) BEWCSV-C include terms up to $O(\mu^2,\varepsilon)$; (5) The first Chen et *al.*'s equations include terms up to $O(\mu^2,\varepsilon)$; and (6) Schäffer and Madsen's (1995) equations include terms up to $O(\mu^2,\varepsilon)$.

C.7. Ratio of second harmonic, $\eta_2/\eta_{2Stokes}$, where η_2 is determined by equation (C.87) and $\eta_{2Stokes}$ by equation (C.88). Boussinesq-type equations include terms up to $O(\mu^4,\varepsilon\mu^4)$. (1) $\alpha = -0.429648$; (2) $\alpha = -4/9$; (3) $\alpha = -2/5$; (4) $\alpha = -1/2$; and (5) $\alpha = 0$.

List of Tables

1.1. Comparison of the order of frequency dispersion terms retained, the dispersion relations and dispersion terms associated with currents in the equations of Nwogu (1993), Schäffer and Madsen (1995) and Chen *et al.* (1998).

2.1. Various Boussinesq-type equations based on different definitions of the velocity vector. The superscript * denotes that the investigators presented more than one set of Boussinesq-type equations.

3.1. Differences between the current and previous research studies.

4.1. Wave celerity of various linearised Boussinesq-type equations relative to the wave celerity of Airy wave theory.

6.1. Differences the current and previous researches.

Chapter One

Introduction

1.1. Background

Water waves and currents are natural phenomena, which occur in channels, lakes, estuaries and oceans. Waves are most commonly generated by winds, while currents may be generated by wind waves, tides, river flows and density differences. In coastal regions, waves and currents might cause erosion and sedimentation. To develop a safe recreational resort by a beach or in the coastal zone for example, an understanding of waves and currents is needed. The layout of the resort is usually designed by considering existing waves and currents as well as the predicted waves and currents due to the presence of the proposed resort.

An optimised design for a development can be obtained by modelling and simulating the significant factors mentioned above. Modelling and simulation can be undertaken in laboratories or on computers. Physical modelling in laboratories is well established, but can be relatively expensive compared to numerical modelling. Nevertheless, numerical modelling of wave processes on computers is less well established. This is because of the difficulty in deriving the governing equations and boundary conditions, which constitute the mathematical model[1] and which accurately describe the physical processes (e.g. wave shoaling, refraction, diffraction, reflection and breaking) associated with waves. The next barrier is the difficulty in discretising the governing equations and boundary conditions using numerical methods to form a stable numerical model with solutions, which converge to the true solution as the computational mesh is refined.

There are various forms of the wave equations that can be used to describe wave processes; these are limited by the exclusion of those regions in which waves would be expected to break. (i.e. $H/h < 0.78$, where $H =$ wave height and $h =$ water depth). This breaker criterion was proposed by McCowan (1894). Five formulations of the wave equations will now be introduced.

A. Non-linear shallow water wave theory.

The governing equations from this theory are generally known as the long wave equations. These are more fully enunciated in Chapter Seven. In what follows, the second set of equation numbers refers to the equation numbers in Chapter Seven.

$$\eta_t + \nabla \bullet [(\eta + h)\overline{\mathbf{u}}] = 0 \qquad (1.1),(7.23)$$

$$\overline{\mathbf{u}}_t + (\overline{\mathbf{u}} \bullet \nabla)\overline{\mathbf{u}} + g\nabla\eta = 0 \qquad (1.2),(7.24)$$

where η is the free surface elevation, $\overline{\mathbf{u}}$ is the depth-averaged horizontal velocity, $\nabla = (\partial/\partial x, \partial/\partial y)$, g is the gravitational acceleration and the subscript t denotes partial differentiation with respect to time. The shallow water region is defined by $kh < \pi/10$ i.e. $h/L < 1/20$, where k is the wave number and L is the wavelength (Dean and Dalrymple, 1984). These equations retain the non-linear terms in both the continuity and momentum equations and the vertical

[1] Terminology: mathematical model is the generic term which includes (i) the governing equations, initial and boundary conditions and (ii) numerical model. For brevity in this thesis, the term 'model' used on its own will be taken to denote a numerical model.

component of the motion is completely neglected. The resulting wave shapes are of non-permanent form and are similar to the sinusoidal solutions of the linear shallow water wave equations. That the solutions are non-permanent is due to the fact that in the absence of friction, any forward facing slope of a wave will continue to steepen. However, the free surface elevation in the shallow water region is increasingly affected by the seabed. As a result, the long wave equations are increasingly incapable of reproducing the correct wave shapes in shallow water.

B. Stokes wave theory.

Other alternative wave equations are based on the Stokes expansions with the inclusion of three-dimensional kinematic and dynamic free surface boundary conditions. Imposition of these 3D boundary conditions in a model is computationally intensive and time demanding. As reported by Dean and Dalrymple (1984), the asymptotic values in shallow water for Stokes second-order wave theory are defined by $ka < 8(kh)^3/3$ (where a is the wave amplitude). Thus, for $kh = \pi/10$, the maximum ratio a/h which can be obtained when using Stokes second-order wave theory is $8\pi^2/300$ (i.e. $a/h \approx 0.263$). However, based on the breaker criterion proposed by McCowan (1894) the ratio of a/h is closer to 0.4 (if $a = H/2$). Consequently, Stokes second-order wave theory does not perform well in shallow water near wave break. Dean and Dalrymple also reported that the details of the second-order Stokes wave theory are quite arduous to follow. Clearly, higher order Stokian wave theories (such as the fifth-order wave theory of Skjelbreia and Hendrickson, 1960) become complicated. The velocity potential of Stokes second-order wave theory is

$$\Phi = \underbrace{\underbrace{\frac{H_1}{2}\frac{g}{\omega}\frac{\cosh[k(h+z)]}{\cosh(kh)}\sin(kx-\omega t)}_{\text{First-order wave theory}} + \underbrace{\frac{3H_1^2\omega}{32}\frac{\cosh[2k(h+z)]}{\sinh^4(kh)}\sin[2(kx-\omega t)]}_{\text{Second-order correction term}}}_{\text{Second-order wave theory}}$$

(1.3a)

where subscript 1 denotes Stokes first-order wave theory. The associated free surface elevation and dispersion relation (i.e. the relationship between angular frequency ω and wave number k) are respectively

$$\underbrace{\underbrace{\eta = \frac{H_1}{2}\cos(kx - \omega t)}_{\text{First-order}} + \frac{H_1^2 k}{16}\frac{\cosh(kh)}{\sinh^3(kh)}[2 + \cosh(2kh)]\cos[2(kx - \omega t)]}_{\text{Second-order}} \tag{1.3b}$$

$$\omega^2 = gk\tanh(kh) \tag{1.3c}$$

in which the orbital velocities in the x- and z-directions are $u = \Phi_x$ and $w = \Phi_z$ respectively. The subscripts x and z denote partial differentiation with respect to the x- and z-directions respectively.

C. The stream function wave theory.

Dean (1965) developed the second-order stream function wave theory with the assumption that the N^{th}-order stream function is

$$\Psi(x,z) = Cz + \sum_{n=1}^{N} X(n)\sinh[nk(h+z)]\cos(nkx) \tag{1.4a}$$

where $u = -\Psi_z$ and $w = \Psi_x$, C is the wave celerity and X(n) is a set of N coefficients. The dynamic and kinematic boundary conditions at the free surface can be respectively stated in stream function form as

$$\tfrac{1}{2}[(\Psi_z)^2 + (\Psi_x)^2] + g\eta = Q_B \qquad \text{at } z = \eta(x) \tag{1.4b}$$

$$\Psi_x = -\Psi_z \eta_x \qquad \text{at } z = \eta(x) \tag{1.4c}$$

where Q_B is a constant. It is noted that the free surface, dynamic boundary condition (1.4b) is not satisfied by equation (1.4a). The coefficients X(n) in the description (1.4a) are therefore chosen to satisfy this dynamic boundary condition at a number of discrete points along the wave profile, each point is denoted by i. The free surface, dynamic boundary condition is then evaluated at each i point along the profile, giving Q_{Bi}. In this dynamic boundary condition, all the Q_{Bi} must be equal to Q_B, where Q_B is a constant. This results in

$$Q_{Bi} = \tfrac{1}{2}[(\Psi_z)_i^2 + (\Psi_x)_i^2] + g\eta_i = Q_B \qquad (1.4d)$$

The free surface elevation is obtained from the free surface, kinematic boundary condition (1.4c). To calculate equations (1.4a) and (1.4d), the X(n) must be known. This can be accomplished by an iterative procedure until the free surface, dynamic boundary condition is satisfied (i.e. $Q_{Bi} = Q_B$). To provide the best fit of the dynamic boundary condition, very high order stream function wave theory (e.g. 20th-order) is necessary (Dean and Dalrymple, 1984).

D. Finite-amplitude wave theory for shallow water.

In this theory, the shallow water wave is assumed to be propagating without change in form; thus, by moving with the wave celerity C, the waveform and wave motion become steady. The steady-state form of the equation of the Korteweg-De Vries (1895) (see Dean and Dalrymple, 1984), was derived from this theory and is

$$\frac{1}{3}\frac{d^3\eta}{dx^3} + \frac{3\alpha\eta}{\beta}\frac{d\eta}{dx} + \frac{d\eta}{dx}\left(\frac{ga}{\beta C^2\alpha} - \frac{1}{\beta}\right) = 0 \qquad (1.5a)$$

where $C = \sqrt{gh}$ is the wave celerity, $\alpha = a/h$ and $\beta = (h/L)^2$. There are two solutions of the Korteweg-De Vries equations.

<u>First solution:</u> One of the solutions of equation (1.5a) is the solitary wave of Boussinesq (1872), that is

$$\eta = a\,\mathrm{sech}^2\left(x\sqrt{\frac{3}{4}\frac{a}{h^3}}\right) \qquad (1.5b)$$

In a solitary wave, the free surface elevation is positive everywhere.

Second solution: The other solution is a periodic wave is known as a cnoidal wave for which the theory spans the range between linear and solitary wave theories. The cnoidal wave shape is expressed in terms of the Jacobian elliptic function. The word *cnoidal* (to be 'consonant' with the sinusoidal or Airy theory) was coined by Korteweg-De Vries and the cnoidal function is represented by the letters ***cn*** (see e.g. Dean and Dalrymple, 1984 and Mei, 1992). The free surface solution of equation (1.5a) for cnoidal waves can be expressed as

$$\eta = a\,\boldsymbol{cn}^2\left(x\sqrt{\frac{3\alpha}{4h^3 k^2}}\right) \tag{1.5c}$$

where the parameter k is obtained from a graph of k versus the Ursell parameter $[U_r = (a/h)(h/L)^2]$. Both solutions [(1.5b) and (1.5c)] of the Korteweg-De Vries equation are only valid in shallow water.

In addition, Dean and Dalrymple (1984) examined the analytical validity of the three wave theories cnoidal, Airy and Stokes fifth-order (see Figure 1.1). The basis for assessing the accuracy of the wave theory was how well the free surface, dynamic boundary condition was satisfied. Cnoidal wave theory is applicable to shallow water, the Stokes V can be applied to deep water, and Airy wave theory does well for intermediate water depths.

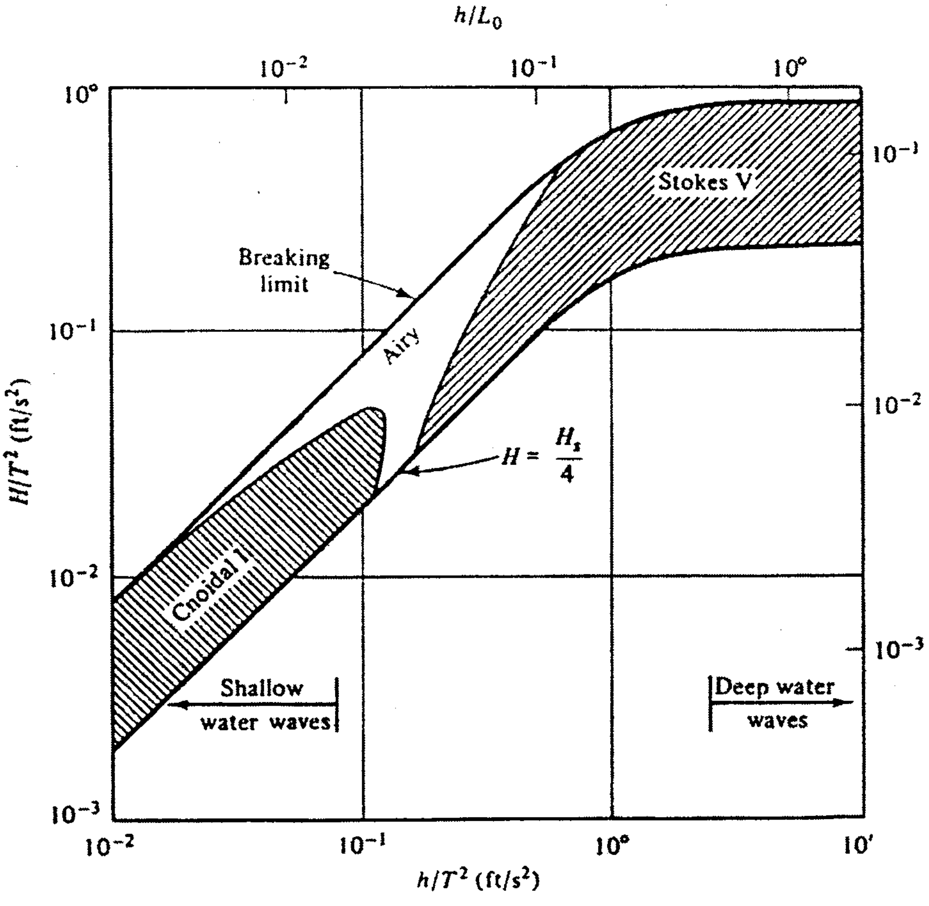

Figure 1.1. Domain of validity of three wave theories based on a criterion of goodness of fit to dynamic free surface boundary condition. Source: Dean and Dalrymple (1984).

E. Boussinesq theory.

Two important parameters used in connection with Boussinesq-type equations are the non-linearity parameter (ε), which represents the ratio of the typical wave amplitude to the characteristic water depth, and the frequency dispersion parameter (μ), which represents the ratio of the characteristic water depth to a typical wavelength. The terms (i) 'weakly non-linear' or 'weak non-linearity', (ii) 'fully non-linear' or 'full non-linearity' and (iii) 'linearised' equations are associated with Boussinesq-type equations. By making recourse to the *non-dimensional* continuity equation (1.13a) in terms of $\mathbf{u}_\alpha$, the meaning of these terms can be clarified.

$$\eta_t + \nabla \bullet [(\varepsilon\eta + h)\mathbf{u}_\alpha] + \mu^2(\Pi^8_{20} + \varepsilon\Pi^8_{21} + \varepsilon^2\Pi^8_{22} + \varepsilon^3\Pi^8_{23}) = O(\mu^4) \qquad (1.13a)$$

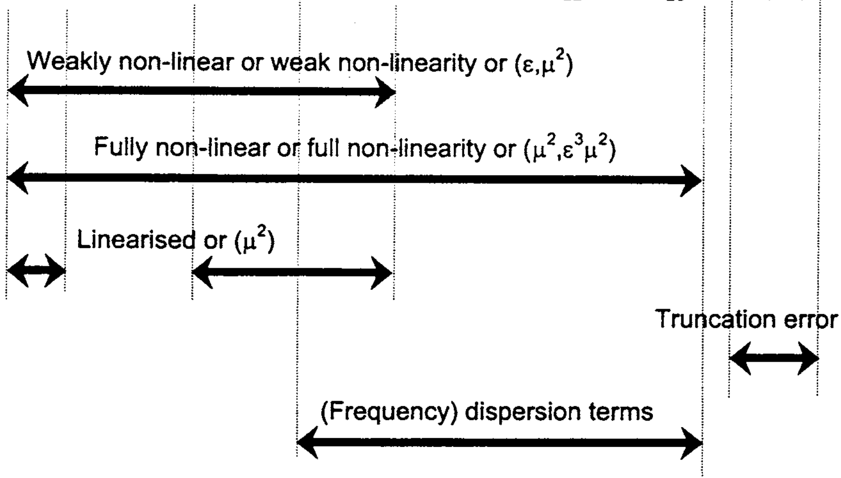

where the Π parameters stand for dispersion terms[2] and involve third-order derivatives[3].

[2] A dispersion term is a dispersive term. In non-dimensional Boussinesq (-type) equations, the dispersive term always contains the (frequency) dispersion parameter such as μ^2 or μ^4 and μ^2. As a result, this term is called (frequency) dispersion term. For brevity, the dispersion term is often written as μ^2 term or μ^4 term and depend on what order of the dispersion parameter retained is.

[3] If μ^4 terms are retained, Π parameters involve fifth-order derivatives.

(i) Boussinesq equations as derived by Boussinesq in terms of bed velocity, $\mathbf{u}_b$.

Boussinesq's most extensive publication on wave theory is dated 1872 and is written in terms of bed velocity (p477 in Dingemans, 1977). In *non-dimensional* form, they are

$$\eta_t + \varepsilon \mathbf{u}_b \bullet \nabla\eta + (\varepsilon\eta + h)(\nabla \bullet \mathbf{u}_b) - \mu^2 \tfrac{1}{6} h^3 \nabla^2 (\nabla \bullet \mathbf{u}_b) = O(\varepsilon\mu^2, \mu^4) \quad (1.6),(2.29)$$

$$\mathbf{u}_{b_t} + \varepsilon(\mathbf{u}_b \bullet \nabla)\mathbf{u}_b + \nabla\eta - \mu^2 \tfrac{1}{2} h^2 \nabla(\nabla \bullet \mathbf{u}_{b_t}) = O(\varepsilon\mu^2, \mu^4) \quad (1.7),(2.30)$$

where $\mathbf{u}_b$ is the horizontal velocity vector at the seabed. Boussinesq reduced the description of the fluid motion to two horizontal dimensions. This was done by introducing a polynomial approximation of the vertical distribution of the flow field into the integral conservation laws of mass and momentum.

Following on from Boussinesq (1872), a number of investigators (e.g. Peregrine, 1967; Nwogu, 1993; and Chen *et al.*, 1998) have developed similar equations, which are termed as 'Boussinesq-type equations'.

(ii) Boussinesq-type equations as derived by Peregrine in terms of depth-averaged velocity, $\overline{u}$.

Peregrine (1967) derived two sets of Boussinesq-type equations. One set (i.e. the first set) of equations was presented in terms of the depth-averaged horizontal velocity vector $\overline{u}$ and is known as the 'standard' form of Boussinesq-type equations. In *non-dimensional* form, the standard Boussinesq-type equations of Peregrine are

$$\eta_t + \nabla \bullet [(h + \varepsilon\eta)\overline{u}] = 0 \quad (1.8),(2.111)$$

$$\overline{u}_t + \varepsilon(\overline{u} \bullet \nabla)\overline{u} + \nabla\eta = \mu^2\left\{\tfrac{1}{2} h\nabla[\nabla \bullet (h\overline{u}_t)] - \tfrac{1}{6} h^2 \nabla(\nabla \bullet \overline{u}_t)\right\} + O(\varepsilon\mu^2, \mu^4) \quad (1.9),(2.112)$$

The Boussinesq equations [(2.29) and (2.30)] and the standard Boussinesq-type equations [(2.111) and (2.112)] are only capable of reproducing weakly non-linear shallow water waves. This is due to the weak non-linearity and dispersion properties retained in the both sets of equations [since they only include terms up to $O(\varepsilon,\mu^2)$]. In the last two decades however, Boussinesq-type equations have been extended and shown to be capable of modelling free surface elevation and wave propagation from deep to shallow water over varying bathymetric and current conditions.

(iii) Boussinesq-type equations as derived by Nwogu in terms of velocity at an arbitrary elevation, $\mathbf{u}_\alpha$.

In 1993, Nwogu derived an alternative set of Boussinesq-type (ε,μ^2) equations[4], which is presented in terms of the horizontal velocity at an arbitrary elevation $\mathbf{u}_\alpha$, that is (in *non-dimensional* form)

$$\eta_t + \nabla \bullet [(h+\varepsilon\eta)\mathbf{u}_\alpha] + \mu^2 \Pi_{20}^{8} = O(\varepsilon\mu^2,\mu^4) \qquad (1.10a)$$

$$\mathbf{u}_{\alpha_t} + \nabla\eta + \varepsilon(\mathbf{u}_\alpha \bullet \nabla)\mathbf{u}_\alpha + \mu^2 \Lambda_{20}^{8} = O(\varepsilon\mu^2,\mu^4) \qquad (1.10b)$$

where Π_{20}^{8} and Λ_{20}^{8} are dispersion terms. This formulation gives an excellent dispersion relation in that there is close agreement with $\omega^2 = gk\tanh(kh)$ for depth to wavelength ratios (h/L) up to ½, even though the μ^4 terms are excluded.

Figure 1.2 shows the dispersion relations (in terms of wave celerity C) for various linearised Boussinesq-type equations (i.e. ε terms dropped) include terms up to $O(\mu^2)$ in terms of: $\mathbf{u}_\alpha$, $\mathbf{u}_b$, $\tilde{\mathbf{u}}$ (the horizontal velocity vector at still water level) and $\bar{\mathbf{u}}$. The reference solution is the dispersion relation of Stokes linear wave theory or Airy wave theory. The good performance of the dispersion relation of Nwogu's equations in terms of $\mathbf{u}_\alpha$ (compared to that of Boussinesq-type equations in terms of others horizontal velocities) is one of

[4] For brevity in this thesis, 'equations including terms up to $O(\varepsilon,\mu^2)$' is often written as '(ε,μ^2) equations' (see also Madsen and Schäffer, 1998).

the reasons why the Boussinesq-type equations of Nwogu (1993) are chosen as the basic governing equations for a number of numerical models.

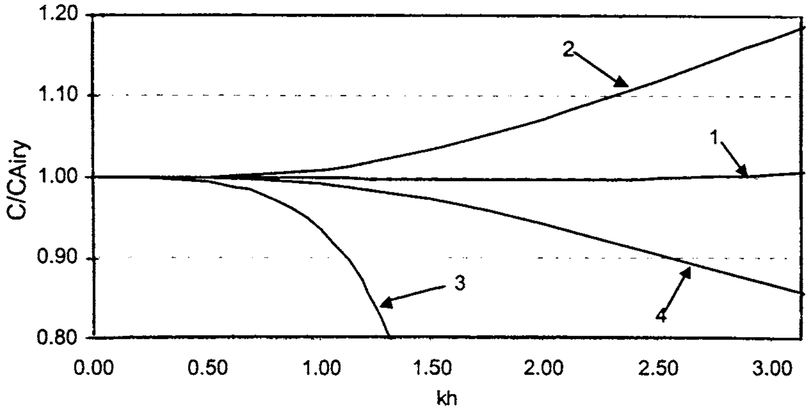

Figure 1.2. Ratio of wave celerity, C/C_{Airy}, C_{Airy} is the Airy wave celerity and C is the wave celerity of various Boussinesq-type equations including terms up to $O(\mu^2)$ in terms of the horizontal velocity at: (1) an arbitrary z-level, $\mathbf{u}_\alpha$; (2) the seabed, $\mathbf{u}_b$; (3) still water level, $\tilde{\mathbf{u}}$; and (4) depth-averaged horizontal velocity, $\bar{\mathbf{u}}$.

In 1995, Schäffer and Madsen extended the Boussinesq-type equations of Nwogu (1993) by incorporating some extra terms in the governing equations thereby improving the dispersion relation. This resulted in a new set of (*dimensionless*) Boussinesq-type equations

$$\underbrace{\eta_t + \nabla \bullet [(h+\varepsilon\eta)\mathbf{u}_\alpha] + \mu^2\Pi_{20}^{8}}_{\text{Nwogu's continuity equation}} + \mu^2\nabla \bullet \{-\beta_1 h^2 \nabla[\nabla \bullet (h\mathbf{u}_\alpha)]$$
$$+ \beta_2 \nabla[h^2\nabla \bullet (h\mathbf{u}_\alpha)] - \beta_1 h^2 \nabla\eta_t + \beta_2\nabla(h^2\eta_t)\} = O(\varepsilon\mu^2, \mu^4) \qquad (1.11a)$$

$$\underbrace{\mathbf{u}_{\alpha_t} + \nabla\eta + \varepsilon(\mathbf{u}_\alpha \bullet \nabla)\mathbf{u}_\alpha + \mu^2\{\Lambda_{20}^{8}}_{\text{Nwogu's momentum equation}} - \gamma_1 h^2 \nabla(\nabla \bullet \mathbf{u}_{\alpha_t}) + \gamma_2 h \nabla[\nabla \bullet (h\mathbf{u}_{\alpha_t})]$$
$$- \gamma_1 h^2 \nabla(\nabla \bullet \nabla\eta) + \gamma_2 h \nabla[\nabla \bullet (h\nabla\eta)]\} = O(\varepsilon\mu^2, \mu^4) \qquad (1.11b)$$

where α, β_1, β_2, γ_1 and γ_2 are the 'free coefficients'. In Chapter Four, these equations are used to investigate the Boussinesq-type equations of Nwogu (1993) extended by Schäffer and Madsen (1995). This resulted in an improved dispersion relation albeit with the same order of the frequency dispersion. In other words, while the order of the frequency dispersion retained in Nwogu's equations (1.10) and Schäffer and Madsen's equations

(1.11) is identical [i.e. $O(\mu^2)$], their dispersion relations (in terms of wave celerity) are significantly different (Figure 1.3). The dispersion relation of Nwogu's equations corresponds to a Padé [2,2] approximation in terms of (kh), and the dispersion relation of Schäffer and Madsen's equations corresponds to a Padé [4,4] approximation in terms of (kh).

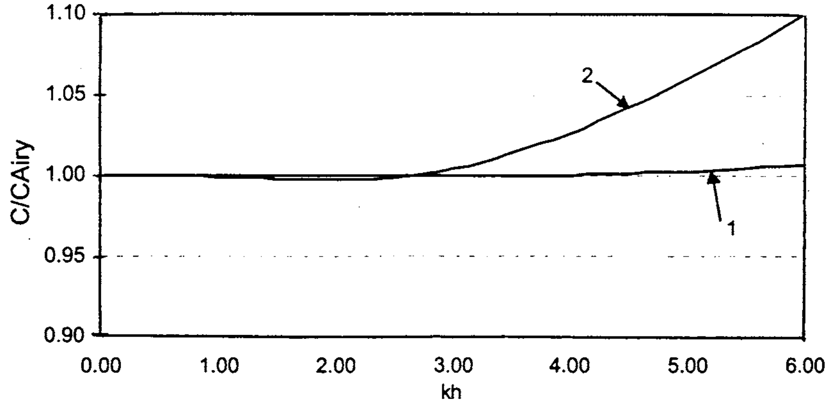

Figure 1.3. Ratio of wave celerity, C/C_{Airy}, where C_{Airy} is determined by wave celerity of the Airy wave theory and C by the wave celerity of the equations of: (1) Schäffer and Madsen (1995); and (2) Nwogu (1993).

The equations of Chen *et al.* (1998) in Chapters Five and Seven are used to assess dispersion terms associated with currents, which are not included in Nwogu's equations. In *non-dimensional* form, the equations of Chen *et al.* (1998) are:

$$\underbrace{\eta_t + \nabla \bullet (h\mathbf{u}_\alpha) + \delta\eta\nabla \bullet \mathbf{u}_\alpha + \nu\mathbf{u}_\alpha \bullet \nabla\eta + \mu^2(\Pi_{20}^{8}}_{\text{Nwogu's continuity equation}}$$

$$\underbrace{+\,\delta\Pi_1^2 + \delta^2\Pi_2^2}_{\text{Dispersion terms associated with currents}} + \delta^3\Pi_3^2) = O(\varepsilon\mu^2, \mu^4) \tag{1.12a}$$

$$\underbrace{\mathbf{u}_{\alpha_t} + \nu(\mathbf{u}_\alpha \bullet \nabla)\mathbf{u}_\alpha + \nabla\eta + \mu^2[\Lambda_{20}^{8}}_{\text{Nwogu's momentum equation}}$$

$$\underbrace{+\,\nu\Lambda_1^2 + \delta(\Lambda_2^2 + \nu\Lambda_3^2) + \delta^2(\Lambda_4^2 + \nu\Lambda_5^2)]}_{\text{Dispersion terms associated with currents}} = O(\varepsilon\mu^2, \mu^4) \tag{1.12b}$$

where ν and δ are additional scales associated with the presence of a current. Again Π and Λ are the dispersion terms, which involve third-order derivatives.

The superscripts and subscripts in the dispersion terms are used to distinguish between them.

It can be concluded that:

- Schäffer and Madsen's equations are equivalent to Nwogu's equations with some additional dispersion terms. These terms in the governing equations result in an improved dispersion relation.
- Chen *et al.*'s equations are equivalent to Nwogu's equations extended to include a current.

Additionally, a comparison of the order of frequency dispersion terms retained, the dispersion relations and dispersion terms associated with currents in the governing equations is contained in Table 1.1.

Investigators	**Nwogu (1993)**	**Schäffer and Madsen (1995)**	**Chen *et al.* (1998)**
Governing equations	Equations (1.10a,b)	Equations (1.11a,b)	Equations (1.12a,b)
Order of frequency dispersion terms retained	μ^2	μ^2	μ^2
Dispersion relation	$\omega^2 = gk^2h\frac{1-(\alpha+1/3)(kh)^2}{1-\alpha(kh)^2}$	$\omega^2 = gk^2h\frac{[1+\gamma(kh)^2][1-(\alpha-\beta+1/3)(kh)^2]}{[1+\beta(kh)^2][1-(\alpha-\gamma)(kh)^2]}$	$\omega^2 = gk^2h\frac{1-(\alpha+1/3)(kh)^2}{1-\alpha(kh)^2}$
Dispersion terms associated with currents	Not included	Not included	Depth-uniform current [i.e. terms $\mu^2(\delta\Pi_1^2 + \delta^2\Pi_2^2 + \delta^3\Pi_3^2)$ and $\mu^2[\nu\Lambda_1^2 + \delta(\Lambda_2^2 + \nu\Lambda_3^2) + \delta^2(\Lambda_4^2 + \nu\Lambda_5^2)]$ in equations (1.12a,b)]

Table 1.1. Comparison of the order of frequency dispersion terms retained, the dispersion relations and dispersion terms associated with currents in the equations of Nwogu (1993), Schäffer and Madsen (1995) and Chen *et al.* (1998).

Boussinesq-type equations have been solved by numerical models using various schemes. Peregrine (1967) proposed the first published finite difference method for the standard Boussinesq-type equations. Abbott *et al.* (1978) were probably the first investigators to develop a Boussinesq-type numerical model that can be used for practical engineering problems. There are a variety of widely published finite difference methods to solve Boussinesq-type equations. They are:

(i) the non-staggered explicit leapfrog scheme (utilised by Witting, 1984);

(ii) the implicit Crank-Nicholson finite difference scheme (used by Liu *et al.*, 1985; Yoon and Liu, 1989; Nwogu, 1993 and Kaihatu and Kirby, 1998) and

(iii) the time-centred, implicit scheme with the method based on the alternating direction implicit algorithm (employed by Abbott *et al.*, 1984; Murray, 1989; Madsen *et al.*, 1991 and Madsen and Sørensen, 1992).

Recently, Wei and Kirby (1995) presented an alternative implicit finite difference scheme for discretising the equations of Nwogu (1993). This alternative scheme was then adopted to solve Boussinesq-type equations in the lowest order frequency dispersion terms with either an improved dispersion relation (e.g. by Chen *et al.*, 1998) or the highest order non-linearity (e.g. by Wei *et al.*, 1995). Therefore, it is finally decided to apply the numerical scheme of Wei and Kirby (1995) to all the governing equations considered in this thesis including the unsteady, non-linear shallow water equations in Chapter Seven.

An important aspect in developing a numerical model is to determine appropriate boundary conditions for the governing equations. A set of boundary conditions, which is suitable for one particular set of governing equations, is not necessarily appropriate for another set of governing equations. Many numerical models based on Boussinesq-type equations have been widely published, but detailed discussion of the 2D boundary conditions were not usually included. The present study is concerned with determining suitable boundary conditions for the 1D and 2D governing equations of Nwogu (1993), the 1D governing equations of Schäffer and Madsen (1995), the 1D and 2D governing equations of Chen *et al.* (1998), and the 2D unsteady, non-linear shallow water equations.

At the outgoing wave boundary, the Sommerfeld radiation condition is used to allow the passage and egress of the wave energy arriving from within the domain. Conversely, as revealed by Nwogu (1993), there will be some wave reflection from the boundary due to: (i) truncation errors, (ii) the initial transient, steep waves and (iii) the approximation of a single wave celerity for irregular waves.

Therefore, in the present study, three-point filters are introduced to reduce these problems as well as to enhance computational stability. On the other hand, the filters must be 'soft' so as not to have much effect on the order of the truncation error retained by the dispersion terms of the particular governing equations under consideration (Chapters Five, Six, and Seven).

The main concept behind the Boussinesq (-type) equations is the reduced mathematical description of the fluid motion to one or two horizontal dimensions. This can be explained through a derivation of the equations of Boussinesq (1872) and the various Boussinesq-type equations derived by Peregrine (1967), Schäffer and Madsen (1995) and Chen *et al.* (1998) in Sections 2.3, 2.4, 4.2 and 5.2 respectively.

In this study, a different and new approach has also been developed for deriving:

(i) the Boussinesq-type (ε,μ^2) equations of Nwogu (1993) in Chapter Three and Appendix C;

(ii) the Boussinesq (ε,μ^2) equations of Boussinesq (1872) in Appendix C;

(iii) the Boussinesq-type (ε,μ^2) equations of Peregrine (1967) in terms of the still water level horizontal velocity in Appendix C;

(iv) the fully non-linear Boussinesq-type equations with the lowest order frequency dispersion [i.e. including terms up to $O(\mu^2,\varepsilon^3\mu^2)$] of Wei *et al.* (1995) in Appendix C; and

(v) the fully non-linear Boussinesq-type equations with fourth-order frequency dispersion [including terms up to $O(\mu^4,\varepsilon^5\mu^4)$] of Madsen and Schäffer (1998) in Appendix C.

All Boussinesq-type momentum equations in the new approach are based on the Euler equation of motion together with the irrotationality condition. However, the Boussinesq-type continuity equations are still based on the depth-integrated continuity equation as in the work of Nwogu (1993), Wei *et al.* (1995) and Madsen and Schäffer (1998).

Previous approaches to develop Boussinesq-type momentum equations include:

a) Nwogu's (1993) work:

The momentum equation (1.10b) in the work of Nwogu was based on the depth-integrated momentum equation.

b) Wei *et al.*'s (1995) work:

In the work of Wei *et al.*, the momentum equation (1.13b) was obtained by substituting an approximate expression for the velocity potential directly into the Bernoulli equation at the free surface (the free surface, dynamic boundary condition). The equations of Wei *et al.* can be written as

$$\underbrace{\eta_t + \nabla \bullet [(\varepsilon\eta + h)\mathbf{u}_\alpha]}_{\text{Nwogu's continuity equation}} + \mu^2\underbrace{(\Pi^8_{20} + \varepsilon\Pi^8_{21} + \varepsilon^2\Pi^8_{22} + \varepsilon^3\Pi^8_{23})}_{\text{Dispersion terms with non-linearity}} = O(\mu^4) \qquad (1.13a)$$

$$\underbrace{\mathbf{u}_{\alpha_t} + \varepsilon(\mathbf{u}_\alpha \bullet \nabla)\mathbf{u}_\alpha + \nabla\eta}_{\text{Nwogu's momentum equation}} + \mu^2\underbrace{(\Lambda^8_{20} + \varepsilon\Lambda^8_{21} + \varepsilon^2\Lambda^8_{22} + \varepsilon^3\Lambda^8_{23})}_{\text{Dispersion terms with non-linearity}} = O(\mu^4) \qquad (1.13b)$$

where the general parameters Π and Λ involve third order derivatives in η and/or u_α. The equations of Wei *et al.* above are Serre-type equations[5] since

[5] Serre-type equations are Boussinesq-type equations with all μ^2 terms retained [i.e. including terms up to $O(\mu^2,\varepsilon^3\mu^2)$]. Serre-type equations can be called as fully non-linear Boussinesq-

they include all dispersion terms with non-linearity. It can be seen that the equations of Wei *et al.* [(1.13a) and (1.13b)] contain the Boussinesq-type (ε,μ^2) equations of Nwogu (1993).

c) Madsen and Schäffer's (1998) work:

Madsen and Schäffer introduced an expansion of the velocity potential as a power series in the vertical coordinate to form the horizontal and vertical velocities. They then incorporated the free surface, dynamic boundary condition (i.e. the Bernoulli equation at the free surface) to develop a momentum equation (C.35). The fully non-linear Boussinesq-type equations of Madsen and Schäffer are

$$\underbrace{\eta_t + \nabla \bullet [(\varepsilon\eta + h)\mathbf{u}_\alpha] + \mu^2(\Pi_{20}^{8} + \varepsilon\Pi_{21}^{8} + \varepsilon^2\Pi_{22}^{8} + \varepsilon^3\Pi_{23}^{8})}_{\text{Wei } et\ al.\text{'s continuity equation}}$$
$$\mu^4(\Pi_{40}^{8} + \varepsilon\Pi_{41}^{8} + \varepsilon^2\Pi_{42}^{8} + \varepsilon^3\Pi_{43}^{8} + \varepsilon^4\Pi_{44}^{8} + \varepsilon^5\Pi_{45}^{8}) = O(\mu^6) \quad (1.14),(C.34)$$

$$\underbrace{\mathbf{u}_{\alpha_t} + \varepsilon(\mathbf{u}_\alpha \bullet \nabla)\mathbf{u}_\alpha + \nabla\eta + \mu^2(\Lambda_{20}^{8} + \varepsilon\Lambda_{21}^{8} + \varepsilon^2\Lambda_{22}^{8} + \varepsilon^3\Lambda_{23}^{8})}_{\text{Wei } et\ al.\text{'s momentum equation}}$$
$$\mu^4(\Lambda_{40}^{8} + \varepsilon\Lambda_{41}^{8} + \varepsilon^2\Lambda_{42}^{8} + \varepsilon^3\Lambda_{43}^{8} + \varepsilon^4\Lambda_{44}^{8} + \varepsilon^5\Lambda_{45}^{8}) = O(\mu^6) \quad (1.15),(C.35)$$

where the general parameters Π and Λ involve third-order derivatives when multiplied by μ^2 and fifth-order derivatives when multiplied by μ^4. (More details can be found in Appendix C). If the μ^4 terms are excluded, the Madsen and Schäffer's $(\mu^4,\varepsilon^5\mu^4)$ equations reduce to the Serre-type equations of Wei *et al.* (1995)

(i) New $(\mu^2,\varepsilon^3\mu^2)$ equations developed by the present author.

It is noted that the pressure distributions of both the fully non-linear Boussinesq-type momentum equations [(1.13b) and (C.35)] do not involve the free surface, kinematic boundary condition. Consequently, there is scope to

---

type equations in $O(\mu^2)$ [i.e. accurate to $O(\mu^2)$]. Second-order is the lowest order in the frequency dispersion parameter (μ).

develop new sets of fully non-linear Boussinesq-type equations which do include the free surface, kinematic boundary condition in the momentum equation. In the present study, a new set of fully non-linear Boussinesq-type equations with the lowest order frequency dispersion terms is developed, that is

$$\underbrace{\eta_t + \nabla \bullet [(\varepsilon\eta + h)\mathbf{u}_\alpha] + \mu^2(\Pi^8_{20}}_{\text{Nwogu's continuity equation}} + \varepsilon\Pi^8_{21} + \varepsilon^2\Pi^8_{22} + \varepsilon^3\Pi^8_{23}) = O(\mu^4) \qquad (1.13a)$$

$$\underbrace{\mathbf{u}_{\alpha_t} + \varepsilon(\mathbf{u}_\alpha \bullet \nabla)\mathbf{u}_\alpha + \nabla\eta + \mu^2(\Lambda^8_{20}}_{\text{Nwogu's momentum equation}} + \varepsilon\Lambda^7_{21} + \varepsilon^2\Lambda^7_{22} + \varepsilon^3\Lambda^7_{23}) = O(\mu^4) \qquad (1.13c)$$

The equations above are a new alternative set of equations to that of Wei *et al.* (1995) [(1.13a) and (1.13b)]. The new equations incorporate all boundary conditions and are derived in full in Appendix C.

(ii) New (ε,μ^2) equations with currents developed by the present author.

By the same method used to derive the equations (1.13a) and (1.13c), three new sets of Boussinesq-type equations with an ambient current treated explicitly[6] on the basis of weakly non-linear waves are developed by the present author. The new equations are presented in terms of:

(i) the horizontal velocity at an arbitrary elevation $\mathbf{u}_\alpha$,

$$\begin{aligned}&\underbrace{\eta_t + \nabla \bullet (h\mathbf{u}_\alpha) + \delta\eta\nabla \bullet \mathbf{u}_\alpha + \nu\mathbf{u}_\alpha \bullet \nabla\eta + \mu^2(\Pi^8_{20}}_{\text{Nwogu's continuity equation}} \\ &\qquad + \underbrace{\delta\Pi^3_1}_{\text{Dispersion terms associated with currents}} + \delta^2\Pi^3_2 + \delta^3\Pi^3_3) = O(\varepsilon\mu^2, \mu^4)\end{aligned} \qquad (1.16a)$$

$$\begin{aligned}&\underbrace{\mathbf{u}_{\alpha_t} + \nu(\mathbf{u}_\alpha \bullet \nabla)\mathbf{u}_\alpha + \nabla\eta + \mu^2[\Lambda^8_{20}}_{\text{Nwogu's momentum equation}} \\ &\qquad + \underbrace{\nu\Lambda^3_1 + \delta(\Lambda^3_2 + \nu\Lambda^3_3) + \delta^2(\Lambda^3_4 + \nu\Lambda^3_5)}_{\text{Dispersion terms associated with currents}}] = O(\varepsilon\mu^2, \mu^4)\end{aligned} \qquad (1.16b)$$

(ii) the horizontal velocity at the seabed $\mathbf{u}_b$,

---

[6] The word 'explicit' is used here in the sense that there are extra terms in the governing equations, which are dispersion terms associated with the ambient current, even though the velocity **u** includes both orbital velocity and ambient current.

$$\eta_t + \nabla \bullet (h\mathbf{u}_b) + \delta\eta\nabla \bullet \mathbf{u}_b + \nu\mathbf{u}_b \bullet \nabla\eta + \mu^2(\Pi_0^4$$

$$+ \underbrace{\delta\Pi_1^4 + \delta^2\Pi_2^4 + \delta^3\Pi_3^4}_{\text{Dispersion terms associated with current}}) = O(\varepsilon\mu^2, \mu^4) \qquad (1.17),(C.17)$$

$$\mathbf{u}_{\alpha_t} + \nu(\mathbf{u}_b \bullet \nabla)\mathbf{u}_b + \nabla\eta + \mu^2[\Lambda_0^4$$

$$+ \underbrace{\nu\Lambda_1^4 + \delta(\Lambda_2^4 + \nu\Lambda_3^4) + \delta^2(\Lambda_4^4 + \nu\Lambda_5^4)}_{\text{Dispersion terms associated with current}})] = O(\varepsilon\mu^2, \mu^4) \qquad (1.18),(C.18)$$

(iii) the horizontal velocity at still water level $\tilde{\mathbf{u}}$,

$$\underbrace{\eta_t + \nabla \bullet (h\tilde{\mathbf{u}}) + \delta\eta\nabla \bullet \tilde{\mathbf{u}} + \nu\tilde{\mathbf{u}} \bullet \nabla\eta + \mu^2(\Pi_0^5}_{\text{Peregrine's (1967) second continuity equation}} + \underbrace{\delta^2\Pi_2^5 + \delta^3\Pi_3^5}_{\text{Dispersion terms associated with current}}) = O(\varepsilon\mu^2, \mu^4)$$

(1.19),(C.24)

$$\underbrace{\tilde{\mathbf{u}}_t + \nu(\tilde{\mathbf{u}} \bullet \nabla)\tilde{\mathbf{u}} + \nabla\eta + \mu^2[\nu\Lambda_1^5}_{\text{Peregrine's (1967) second momentum equation}} + \underbrace{\delta(\Lambda_2^5 + \nu\Lambda_3^5) + \delta^2(\Lambda_4^5 + \nu\Lambda_5^5)]}_{\text{Dispersion terms associated with current}} = O(\varepsilon\mu^2, \mu^4)$$

(1.20),(C.25)

These three new sets of equations are alternative sets to those derived by Chen *et al.* (1998). The main differences between the present study and that of Chen *et al.*'s work are:

(i) the method of derivation for the momentum equations and

(ii) vertical variations in the horizontal and vertical velocities are permitted in the new formulations. This is in contrast to the equations of Chen *et al.* in which these velocities are uniform through the water column.

A family tree of the various Boussinesq-type momentum equations, including those which were developed by earlier investigators as well as those developed by the present author are displayed in Figure 1.4.

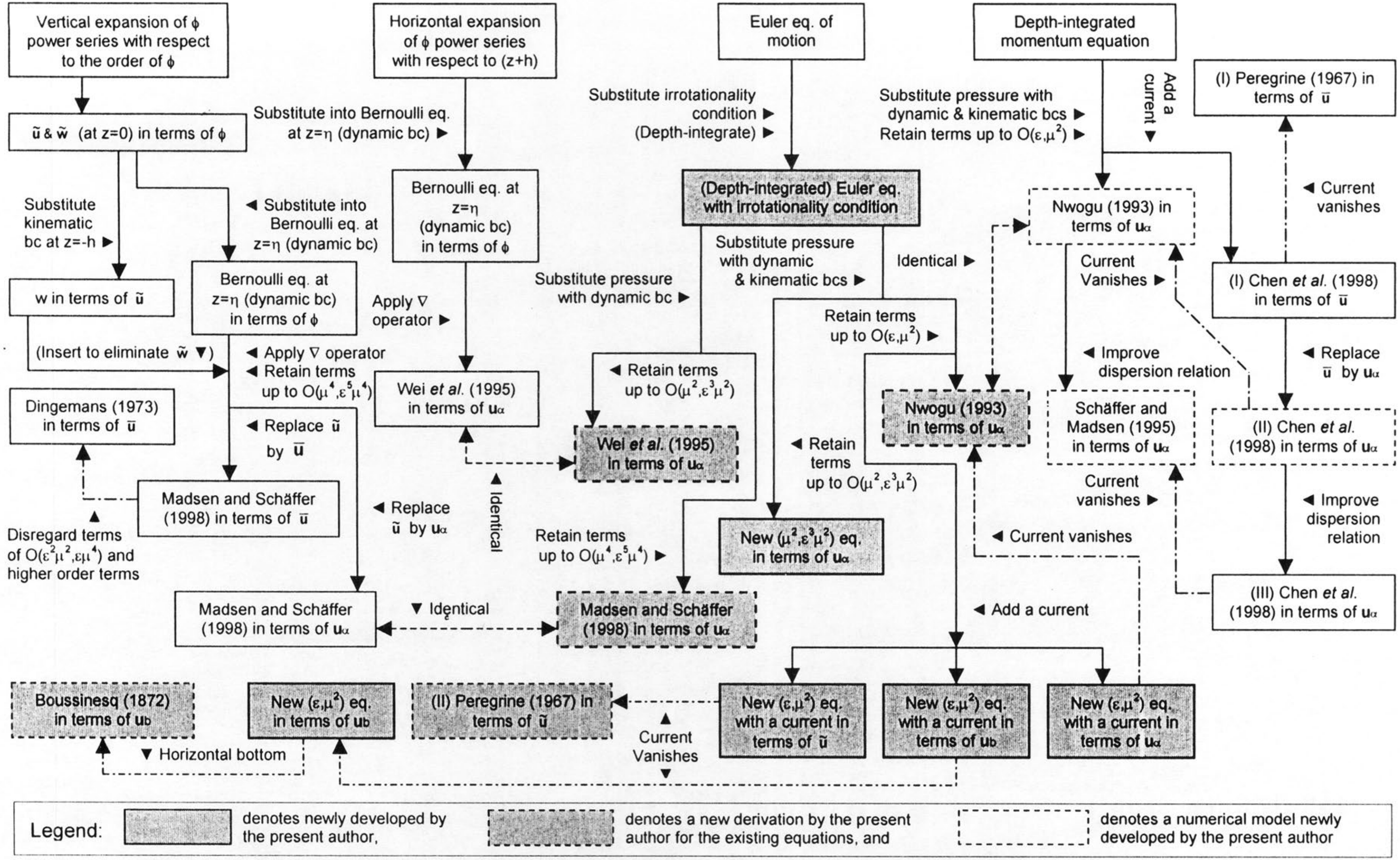

Figure 1.4. Family tree of various Boussinesq-type momentum equations.

The main aims of this study are to develop and asses the performance of numerical models based on two extensions of Nwogu's (1993) Boussinesq-type equations [i.e. the governing equations developed by Schäffer and Madsen (1995) and Chen *et al.* (1998)]. To the present author's knowledge, no numerical models have been based on those governing equations, which are unproven in their performance. Some details of the untested governing equations follow:

(i) Schäffer and Madsen (1995) extended Nwogu's equations to yield a dispersion relation which was valid in deeper water for h/L ratios up to or equal to 1.0, whereas Nwogu's equations yield a dispersion relation which was valid for $h/L \leq 0.5$. The reference solution is the dispersion relation of Airy wave theory.

(ii) Chen *et al.*'s (1998) *second set* of equations (see the right hand column of Figure 1.4), which are equivalent to Nwogu's equations extended to include an ambient current.

To fulfill the aims of the study, a number of numerical models is required:

1. 1D and 2D numerical models based on Nwogu's (1993) equations. These are the basic models whose results are compared against the results of various other models.

2. 1D numerical model based on Schäffer and Madsen's (1995) equations. The improved dispersion relation of this model permits the simulation of waves in deeper water.

3. 1D and 2D numerical models based on Chen *et al.*'s (1998) equations. These models permit the effects of waves and co-flowing and counter-flowing ambient currents to be simulated. Ambient currents are not included in the basic models based on Nwogu's (1993) work.

4. 2D numerical model based on the (unsteady) non-linear shallow water equations. This model is used for validation purposes where laboratory data are unavailable in the study of 2D current effects.

5. Following Chen *et al.* (1998) for comparing the numerical solutions based on their *third set* of equations (see the right hand column of Figure 1.4) in the study of 1D current effects, two 1D simple numerical models are developed by the present author. These two models are based on (i) the (steady) non-linear shallow water equations and (ii) the conservation of wave action equation.

1.2. Objectives

Six numerical models have been developed and coded up in this study. These models have been labelled using the following strategy.

$$\begin{pmatrix} 1\,\mathrm{D} \\ 2\,\mathrm{D} \end{pmatrix} \text{letters - no. (1 to 6)}$$

While the primary objectives of this study are to assess the performance of the two new numerical models based on the untested governing equations of Schäffer and Madsen (1995) and of Chen *et al.* (1998), the specific objectives are detailed below.

1.2.1. Primary objectives

1.a. **1DDBMW-2** (**1D** '**D**eeper water' **B**oussinesq-type numerical **M**odel for **W**aves only - Model No. **2**). The present author develops a 1D numerical model for wave transformation based on the Boussinesq-type equations derived by Schäffer and Madsen (1995). Appropriate boundary conditions are determined and incorporated into the numerical model.

1.b. Compare the solutions from 1DDBMW-2 against:

(i) sinusoidal waves in deep water for h/L = 1 and

(ii) 1DBMW-1 and laboratory data for h/L ≤ ½

to assess the effects of the extended governing equations of 1DDBMW-2 (i.e. Schäffer and Madsen, 1995).

2.a. **1DBMWC-3** (**1D B**oussinesq-type numerical **M**odel for **W**ave-**C**urrent interaction - Model No. **3**). The present author develops a 1D numerical model with boundary conditions for full wave-current interaction based on the *second set* of Boussinesq-type equations derived by Chen *et al.* (1998). The boundary conditions are applicable to the 3 cases: waves only, currents only and fully combined wave-current interaction.

2.b. Compare the numerical solutions from 1DBMWC-3 against the those from 1DBMW-1, **1DSSWM** (**1D S**teady, non-linear **S**hallow **W**ater numerical **M**odel) and **1DWACM** (**1D** principle of **W**ave **A**ction **C**onservation numerical **M**odel) to analyse the effects of an ambient current included in one-dimensional formulation.

---

3. **2DBMWC-5** (**2D B**oussinesq-type numerical **M**odel for **W**ave-**C**urrent interaction - Model No. **5**). The present author develops a 2D numerical model for full wave-current motion based on the *second set* of Boussinesq-type equations derived by Chen *et al.* (1998). Determine suitable boundary conditions for the 3 cases of waves only, currents only and combined waves and currents.

To carry out the above primary objectives related to model development and testing, it has also been necessary to develop several numerical models based on well established governing equations to test particular scenarios of models 1DDBMW-2, 1DBMWC-3 and 1DBMWC-5. The development of the specialised models is briefly described under the heading of Secondary Objectives.

1.2.2. Secondary objectives

4.a. **1DBMW-1** (**1D** **B**oussinesq-type numerical **M**odel for **W**aves only - Model No. **1**). The present author develops a 1D numerical model for wave propagation based on the Boussinesq-type equations derived by Nwogu (1993). Appropriate boundary conditions are determined.

4.b. Verify 1DBMW-1 against existing laboratory data.

5.a. **2DBMW-4** (**2D** **B**oussinesq-type numerical **M**odel for **W**aves only - Model No. **4**). The present author develops a 2D numerical model, including the boundary conditions, for wave propagation based on the Boussinesq-type equations derived by Nwogu (1993).

5.b. Verify 2DBMW-4 against existing laboratory data.

6.a. **2DUSWM-6** (**2D** **U**nstedy, non-linear **S**hallow **W**ater numerical **M**odel - Model No. **6**). The present author develops a 2D numerical model with appropriate boundary conditions, based on the unsteady, non-linear shallow water equations.

6.b. Compare the results of 2DBMWC-5 against those of 2DBMW-4 and laboratory data for the waves only case and against the results of 2DUSWM-6 for the current only case to assess the effects of an ambient current included in two-dimensions.

All discrete forms of the considered governing equations, including the matrix systems and boundary conditions are developed and then coded up in Fortran by the present author. There is no part of the codes (including for instance, the matrix solvers), which has been supplied by or adapted from someone else's work.

This study is limited to the consideration of periodic waves with a single frequency due to the application of the Sommerfeld radiation condition at the outgoing wave boundaries. Application of the Sommerfeld radiation condition to irregular, multi-directional waves is considerably more difficult and is not a focus of the present study.

The existing approaches for deriving the original Boussinesq equations of Boussinesq (1872) and the Boussinesq-type equations of Peregrine (1967) are presented in Chapter Two. A new and systematic approach is introduced by the present author to formulate:

- existing Boussinesq-type equations of Nwogu (1993) in Chapter Three and Appendix C. Both these derivations are novel and different to each other as well as Nwogu's original derivation,
- existing original Boussinesq equations of Boussinesq (1872), existing Boussinesq-type equations of Peregrine (1967) (in terms of the still water level horizontal velocity), Wei *et al.* (1995) and Madsen and Schäffer (1998) in Appendix C.

This derivation is for the purpose of the comparison with the existing approaches.

Five new Boussinesq-type equations have been developed by the present author during the course of this study. Their development can be found in Appendix C. These equations have been labelled using the following strategy:

Letters - no. (A to E)

While these equations are developed here, the assessment of how well they simulate wave behaviour is a recommendation for future work.

- **BEWCAV-A** (2D **B**oussinesq-type **E**quations for **W**ave-**C**urrent interaction presented in terms of the **A**rbitrary horizontal **V**elocity – Equations **A**). The present author derives a new set of 2D Boussinesq-type (ε,μ^2) equations for the interaction of waves and vertically varied currents in terms of the horizontal velocity at an arbitrary elevation $(z = z_\alpha)$.
- **BEWCBV-B** (2D **B**oussinesq-type **E**quations for **W**ave-**C**urrent interaction presented in terms of the **B**ottom horizontal **V**elocity – Equations **B**). The present author derives a new set of 2D Boussinesq-type (ε,μ^2) equations for the interaction of waves and vertically varied currents in terms of the horizontal velocity at elevation $z = -h$.
- **BEWCSV-C** (2D **B**oussinesq-type **E**quations for **W**ave-**C**urrent interaction presented in terms of the **S**till water level horizontal **V**elocity – Equations **C**). The present author derives a new set of 2D Boussinesq-type (ε,μ^2) equations for the interaction of waves and vertically varied currents in terms of the horizontal velocity at elevation $z = 0$
- **BEWSV-D** (2D **B**oussinesq-type **E**quations for **W**aves only presented in terms of the **B**ottom horizontal **V**elocity – Equations **D**). The present author derives a new set of 2D Boussinesq-type (ε,μ^2) wave equations in terms of the horizontal velocity at elevation $z = -h$ by removing all dispersion terms associated with currents from BEWCBV-B.

- **FBE2O-E** (2D **F**ully non-linear **B**oussinesq-type **E**quations accurate to **2**nd **O**rder frequency dispersion terms – Equations **E**). The present author derives a new set of second-order fully non-linear 2D Boussinesq-type equations [i.e. including terms up to $O(\mu^2,\varepsilon^3\mu^2)$] in terms of the horizontal velocity at an arbitrary z-elevation.

1.3. Outline of contents

This thesis consists of eight chapters and is organised as follows:

Chapter One: Introduction

In Section 1.1, a brief explanation of the background to this research is given. This consists of:

(i) motivation for the selection of the basic governing equations of Nwogu;

(ii) a discussion of the basis for extending the basic equations to improve the range of applicability of the dispersion relation into deeper water through a study of Schäffer and Madsen's (1995) equations;

(iii) a discussion of the basis for extending the basic equations to include ambient currents through a study of Chen *et al.*'s (1995) equations;

(iv) the reasoning for the selection of the particular numerical scheme in the numerical models developed in this thesis;

(v) the background to the determination of suitable boundary conditions for the governing equations under consideration;

(vi) the motivation for the development of new sets of Boussinesq-type equations and of the new alternative derivations for the existing Boussinesq-type equations.

Section 1.2 is concerned with the study objectives and how they contribute to new knowledge. A short description of the structure of this thesis is given in Section 1.3.

Chapter Two: Literature Review

In Section 2.1, the evolution of the Boussinesq-type equations is reviewed beginning with those originally derived by Boussinesq (1872). The selection of the equations being reviewed is based on their relevance to the present study. Similarly in Section 2.2, the numerical models based on those Boussinesq-type equations, which are relevant to this study are reviewed.

Boussinesq's (1872) equations are presented in terms of the bottom horizontal velocity and are re-derived by the existing approach in Section 2.3. Additionally, in Section 2.4, two sets of Boussinesq-type equations originally derived by Peregrine (1967), which are presented in terms of the depth-averaged and still water level horizontal velocities, are re-derived by the existing method.

Chapter Three: 1D Basic Model

The differences between the present and previous numerical models are tabulated in Section 3.1. Section 3.2 focuses on the new derivation of the existing Boussinesq-type wave equations of Nwogu (1993). The concept behind the free coefficient α for specifying a particular elevation for the velocities, which is contained in Nwogu's (ε,μ^2) equations, is explained in Section 3.3 under the heading "Review of dispersion relations". Numerical solution algorithms, which consist of the solution method and the formulation and incorporation of appropriate boundary conditions, are considered in Section 3.4.

Finally, in Section 3.5, verification of 1DBMW-1 (the numerical model developed in this chapter) using existing laboratory data for two different cases of a monochromatic wave train propagating in a channel is included. The first set-up includes a channel with a single slope. The second set-up incorporates a submerged bar.

Chapter Four: 1D Basic Model with an Improved Dispersion Relation

The governing equations considered in this chapter will be referred to as 'deeper water' Boussinesq-type equations, because they are applicable for the range in relative depth $h/L \leq 1$. The other Boussinesq-type equations which include terms up to $O(\varepsilon,\mu^2)$ (e.g. the governing equation in Chapter Three) are only applicable up to $h/L = 0.5$ (see also Figure 1.3).

Comparisons of various Boussinesq-type (ε,μ^2) equations based on Padé expansions of the dispersion relation in terms of (kh) are explained in Section 4.1. Schäffer and Madsen's (1995) derivation of the Boussinesq-type wave equations is in Section 4.2. The free coefficients (α,β,γ) contained in Schäffer and Madsen's (ε,μ^2) equations are tuned by the present author using the exact dispersion relation of the linear wave theory instead of the approximate one (Section 4.3). In Section 4.4, the solution method and boundary conditions from Section 4.2 are applied.

Section 4.5 deals with verification of 1DDBMW-2 (the numerical model developed in this chapter) to assess the corresponding governing equations with the additional terms. These terms result in an improved dispersion relation but with the same order of the frequency dispersion i.e. $O(\mu^2)$. This verification consists of three experimental set-ups:

(i) wave propagation in very deep water ($h/L = 1$) in a constant depth channel;

(ii) wave propagation up a slope; and

(iii) wave propagation in a channel with a submerged bar.

The numerical solutions of 1DDBMW-2 for the last two experimental set-ups are compared to those of 1DBMW-1 (from Chapter Three). This comparison enables the evaluation of the effects of non-linear wave shape due to the additional terms in the corresponding governing equations, which result in an improved dispersion relation.

Chapter Five: 1D Basic Model with Current Effects

Section 5.2 deals with the derivation of the *first* and *second sets* of Boussinesq-type (ε,μ^2) equations of Chen *et al.* (1998). In this section, *non-dimensional* variables based on wave only and wave-current scaling parameters are considered where an ambient current is explicitly mentioned in separate terms in the governing equations. The *second set* of (ε,μ^2) equations of Chen *et al.* with a current is discretised, and suitable boundary conditions for three cases (waves only, current only and wave-current motion) are developed by the present author for 1DBMWC-3 in Section 5.3.

In Section 5.4, a simple numerical model (1DSSWM) based on the steady, non-linear shallow water equations is developed. A second simple numerical model (1DWACM) based on the conservation of wave action is developed in Section 5.5. Both these simple numerical models are used for making comparisons with 1DBMWC-3 where laboratory data are unavailable.

Two experimental set-ups are used to verify 1DBMWC-3 (Section 5.6). The first one is a channel with a single slope, which is the same as in Chapter Three. This is used to assess the effects of the dispersion terms associated with currents in the case of wave motion only. In other words, 1DBMWC-3 (with the dispersion terms associated with currents included) is operated without currents being present. Under this condition, the *second set* of equations of Chen *et al.* mathematically reduces to Nwogu's (1993) equations. The second set-up is a channel with a submerged bar (Section 5.7). This is used to evaluate 1DBMWC-3 in the cases of current motion only and also wave-current interaction.

Chapter Six: 2D Basic Model

In Section 6.1, the differences between the present basic numerical model (i.e. 2DBMW-4) and previous models based on Nwogu's (1993) equations are tabled. The 2D governing equations being considered are written in *dimensional* form in Section 6.2. The particular numerical algorithms and appropriate boundary conditions for the corresponding equations are considered in Section 6.3. The filter, which is introduced by the present author and is used to enhance computational stability, is also given in this section. Finally, 2DBMW-4 is verified using existing laboratory data in scenarios of wave propagation over a circular shoal on a flat bottom basin and of wave propagation over an elliptic shoal on a sloping bottom basin.

Chapter Seven: 2D Basic Model with Current Effects

Section 7.2 focuses on the development of the new model 2DBMWC-5, which is based on the *second set* of equations of Chen *et al.*, where the dispersion terms associated with currents are included. The solution method and determination of suitable boundary conditions for the three cases of waves only, current only, and for wave-current interaction are also considered in this section.

Section 7.3 deals with the development of 2DUSWM-6, which is based on the 2D unsteady, non-linear shallow water equations, and is used to assess the new model 2DBMWC-5. Numerical solution of the governing equations together with the determination of appropriate boundary conditions for the current only case is undertaken in this section.

In Section 7.4, a circular shoal on a flat bottom basin is used for the experimental set-up. In the first test, 2DBMW-4 and 2DBMWC-5 are run to simulate wave propagation only. The solutions from both models are compared to evaluate the effects of the inclusion of the dispersion terms associated with currents in 2DBMWC-5. In the second test, 2DBMWC-5 and 2DUSWM-6 are run to simulate current motion only. The results of both models are then compared. The last set of tests is concerned with modelling co-flowing and counter-flowing current and waves.

Chapter Eight: Conclusions and Recommendations

Chapter Eight contains the general conclusions from the present research. Some recommendations for further research into numerical models based on Boussinesq-type equations are also presented.

Chapter Two

Literature Review

2.1. Boussinesq-type equations

Boussinesq (1872) developed the original formulation of the governing equations for a free surface flow, which included the effects of surface waves but in which the vertical dimension was eliminated. The formulation was in terms of the bottom velocity and was restricted to simulating waves moving over bathymetry with a flat bottom. Mei and LeMéhauté (1966) extended the formulation to varying depth in one-dimension. Peregrine (1967) developed two new formulations in two horizontal dimensions for the case of varying depth in terms of (i) the depth-averaged velocity vector and (ii) the velocity vector at still water level. The first formulation became known as the standard form of Boussinesq-type equations.

There are two important parameters in association with the non-dimensional forms of Boussinesq-type equations. One parameter is a measure of the non-linearity and is represented by the ratio of the typical wave amplitude to the characteristic water depth ($\varepsilon = a_{ch}/h_{ch}$). The other parameter is a measure of the frequency dispersion and is represented by the ratio of the characteristic water depth to the typical wavelength ($\mu = h_{ch}/L_{ch}$).

The Boussinesq-type equations have been extended based on these two parameters.

For many applications, Boussinesq-type equations with lowest order (frequency) dispersion terms (i.e. μ^2 terms) usually give a weak dispersion relation. A weak dispersion relation imposes a restrictive water depth limitation i.e. an upper limit on the relative depth h/L. To address this problem requires Boussinesq-type equations (i.e. the governing equations) with an improved dispersion relation, which holds in deeper water. Several alternative Boussinesq-type equations with an improved dispersion relation have been reported, for example by Witting (1984), Murray (1989), Madsen *et al.* (1991), Madsen and Sørensen (1992), Nwogu (1993) and Schäffer and Madsen (1995). Although the dispersion relation of these Boussinesq-type equations had been improved, the order of dispersion terms in the partial differential equations was unchanged i.e. $O(\mu^2)$.

Witting (1984) first presented the Padé approximation technique in connection with the dispersion relations of linear or Airy wave celerity. This was intended to develop Boussinesq-type equations (i.e. partial differential equations) with an improved dispersion relation. As a result, a number of free coefficients appeared in the resulting Boussinesq-type equations. These coefficients were determined by matching a Padé approximation[1] to the dispersion relation of the linear wave celerity. The dispersion relation for Witting's equations corresponded to a Padé [2,2] approximation in terms of wave number k multiplied by the water depth h i.e. $kh = 2\pi h/L$. The same dispersion relation was also obtained, for example from the equations of Madsen *et al.* (1991), Madsen and Sørensen (1992) and Nwogu (1993). Schäffer and Madsen (1995) extended Nwogu's Boussinesq-type equations by incorporating some extra terms in the governing equations thereby improving the dispersion relation in deeper water. The resulting Boussinesq-

[1] Padé [m,n] approximations are rational functions in which the numerator is a polynomial of order m and the denominator is a polynomial of order n. While polynomial approximations suffer from the disadvantage of their tendency for oscillations and hence errors. Padé approximations tend to spread the approximation error. [Faires and Burden (2003) p459]

type equations had a dispersion relation corresponding to a Padé [4,4] approximation in terms of (kh).

In contrast to the above investigators, Serre approached the problem of non-linearity. Serre (1953) developed an alternative Boussinesq theory by combining lowest-order frequency dispersion with full non-linearity (i.e. ε is arbitrary). In other words, Serre's equations included terms up to $O(\mu^2, \varepsilon^3\mu^2)$. In 1993, Madsen and Sørensen studied the non-linearity properties of Boussinesq-type equations. They developed the evolutionary equations for triads of wave-wave interaction and second-order transfer functions for sub- and super-harmonics. More recently, Wei *et al.* (1995) derived a new set of Boussinesq-type equations, which they called 'fully non-linear Boussinesq-type equations'. These equations were derived in terms of the velocity at an arbitrary z-level as first formulated by Nwogu (1993) instead of the depth-averaged velocity as used in the equations of Serre.

Boussinesq-type equations with high order frequency dispersion terms with or without non-linearity [including terms up to $O(\mu^4)$ and $O(\varepsilon\mu^2)$ or higher] were presented in unpublished work by Dingemans (1973). As reported by Dingemans (1997), the equations of Dingemans (1973) were presented in two versions; one version was given in terms of the depth-averaged velocity as the velocity variable and the other in terms of the velocity variable at still water level. Both versions of the partial differential equations retained terms up to $O(\mu^4)$ and $O(\varepsilon\mu^2)$ with the assumption that $O(\varepsilon) = O(\mu^2)$. In 1998, Madsen and Schäffer introduced higher order Boussinesq-type equations by retaining all the terms up to $O(\mu^4)$, which allowed ε to be arbitrary [i.e. retaining terms up to $O(\mu^4, \varepsilon^5\mu^4)$].

The study of Boussinesq-type equations for wave-current interaction has achieved much less attention. As reported by Madsen and Schäffer (1998), one consequence of the non-linearity of Boussinesq-type equations is the automatic inclusion of wave-averaged effects such as radiation stress, setup, undertow and wave-induced currents. This however, is not a guarantee for a correct representation of for example, the Doppler shift in connection with current refraction and, in fact, it turns out that most Boussinesq-type equations fail to model this phenomenon accurately. The Doppler shift describes the kinematics of wave-current interaction for waves on a homogeneous current field. The Doppler shift is defined by $(\omega_a - \hat{u}_c k)^2 = \sigma_i^2$, where ω_a is the absolute angular frequency, $\hat{u}_c$ is the horizontal ambient current velocity, which is assumed to be uniform over the depth, and σ_i is the intrinsic angular frequency. When the current disappears, $\omega = \omega_a = \sigma_i$ where ω is the angular frequency.

Work in wave-current interaction, where the current is explicitly[2] treated, for Boussinesq-type equations was pioneered by Yoon and Liu (1989) and then followed by Prüser and Zielke (1990). The equations of Yoon and Liu and of Prüser and Zielke achieved a correct Doppler shift with a dispersion relation corresponding to a Padé [0,2] approximation in terms of (kh). Consequently, because of the relatively low order of Padé approximations, both sets of equations were only applicable to the case of relatively small wave number (i.e. long wavelength). In the case of waves and ambient current motion being in opposite directions, the Doppler shift became invalid as the wave numbers increased rapidly (i.e. wavelength become shorter) due to the interaction, especially with a strong opposing current.

Chen *et al.* (1998) presented *three sets* of Boussinesq-type equations for full wave-current motion with a correct representation of the Doppler shift.

(a) Firstly, they generalised the set of partial differential equations of Yoon and Liu (1989) to allow for stronger currents. The corresponding dispersion relation and the velocity variable of the *first set* of equations derived by Chen *et al.* (1998) remained identical to that of Yoon and Liu.

(b) Secondly, they extended the derivation of their *first set* of equations by replacing the depth-averaged velocity ($\overline{\mathbf{u}}$) with the velocity at an

[2] The word 'explicit' is used here in the sense that there are extra terms in the governing equations, which are dispersion terms associated with the ambient current.

arbitrary elevation ($\mathbf{u}_\alpha$) as the velocity variable. This resulted in *a second new set* of Boussinesq-type equations with a dispersion relation corresponding to a Padé [2,2] approximation in terms of (kh) instead of a Padé [0,2] approximation.

(c) Thirdly, following the approach of Schäffer and Madsen (1995), Chen *et al.* extended their *second set* of partial differential equations by incorporating some extra terms in the governing equations thereby improving the dispersion relation. The resulting Boussinesq-type equations had a dispersion relation corresponding to a Padé [4,4] approximation in terms of (kh).

In addition, the problem of wave-current interaction in the works of Yoon and Liu (1989), Prüser and Zielke (1990) and Chen *et al.* (1998) have been explicitly treated within the framework of weakly non-linear waves of Boussinesq-type equations. In other words, these sets of equations only retained the lowest-order frequency dispersion and non-linearity terms [i.e. $O(\varepsilon,\mu^2)$] in those terms in the governing equations associated with wave motion.

It is seen that Boussinesq-type equations can be derived in terms of various types of velocity vector. Typical velocity variables are the still water level velocity ($\tilde{\mathbf{u}}$), bottom velocity ($\mathbf{u}_b$), depth-averaged velocity ($\overline{\mathbf{u}}$), depth-integrated velocity component (i.e. volume flux, **Q**) and the velocity at an arbitrary z-level ($\mathbf{u}_\alpha$) (see Table 2.1).

Velocity Vector	Investigators
Still water level velocity, $\tilde{\mathbf{u}}$	Peregrine (1967)*, Dingemans (1973)*, Madsen and Schäffer (1998)* and Mera (Present study)*
Bottom velocity, $\mathbf{u}_b$	Boussinesq (1872), Witting (1984) and Mera (Present study)*
Depth-averaged velocity, $\overline{\mathbf{u}}$	Serre (1953), Peregrine (1967)*, Dingemans (1973)*, Freilich and Guza (1984), Yoon and Liu (1989), Chen *et. al.* (1998)* and Madsen and Schäffer (1998)*
Depth-integrated velocity (i.e. volume flux), $\mathbf{Q}$	Abbott *et. al.* (1978), Hauguel (1980), Murray (1989), Madsen *et. al.* (1991), Madsen and Sørensen (1992), Schäffer and Madsen (1995)* and Borsboom *et al.* (2000)
Velocity at an arbitrary z-level, $\mathbf{u}_\alpha$	Nwogu (1993), Schäffer and Madsen (1995)*, Wei *et al.* (1995), Chen *et al.* (1998)*, Madsen and Schäffer (1998)* and Mera (Present study)*

Table 2.1. Various Boussinesq-type equations based on different definitions of the velocity vector. The superscript * denotes that the investigators presented more than one set of Boussinesq-type equations.

2.2. Numerical models based on Boussinesq-type equations

Peregrine (1967) developed a 1D numerical wave model based on his own Boussinesq-type equations with the depth-averaged velocity as the velocity variable. This model was used to simulate a solitary wave approaching a beach of uniform slope. Using a frequency domain wave transformation derived from the equations of Peregrine, Freilich and Guza (1984) developed two numerical models for the evolution of the wave field in a region of shoaling based on the equations of Peregrine. They showed that Fourier coefficients of the wave field through the shoaling region were accurately predicted. By considering wave spectra derived from Peregrine's equations, Elgar and Guza (1985) showed that the evolution of wave energy spectra, wave celerity, free surface elevation skewness and group velocity were well represented. Elgar *et al.* (1990) subsequently demonstrated that the evolution of second and third moments of the horizontal velocity and acceleration fields was also well predicted.

Abbott *et al.* (1978) converted the Boussinesq-type equations[3] of Peregrine (1967) from being in terms of the depth-averaged horizontal velocity to being in terms of the depth-integrated velocity (i.e. volume flux). The corresponding equations were then augmented with other terms such as those that account for a reduced flow area as occurs especially at permeable breakwaters. Porosity, which was included in Abbott *et al.*'s equations, was set to unity in the open water and set to its physical value in the breakwater. The resulting equations were discretised using Preissmann's implicit finite difference scheme. In 1D, the resulting numerical model was tested for simulation of:

- shoaling waves,
- wave reflection, and
- transmission of waves through permeable breakwaters.

Agreement between computed and mean measured results was within 5% of elevation. In 2D, the resulting numerical model was tested to simulate a real harbour (i.e. the Danish harbour of Hanstholm). In the case of periodic wave inputs, it was seen that the agreement between the numerical solutions and the results obtained in the physical model of the real harbour were highly satisfactory. In the case of irregular waves, comparisons were made between root mean square elevation in physical and numerical models. These comparisons agreed reasonably well. Further demonstrations of Abbott *et al.*'s numerical model for shoaling, refraction, diffraction and partial reflection cases were given by Madsen and Warren (1984). They compared Abbott *et*

[3] All Boussinesq-type equations considered here are in 2D unless stated otherwise.

al.'s numerical solutions against analytical and experimental results in which these comparisons were entirely satisfactory.

The 1D version of the equations of Abbott *et al.* (1978) was approximated by Schaper and Zielke (1984) using their own finite difference scheme. Schaper and Zielke also discussed the boundary conditions corresponding to total, partial and non-reflecting wave boundary conditions. The resulting numerical model was applied to simulate solitary, cnoidal and irregular waves. It appears that agreement between the numerical and analytical solutions were acceptable.

In 1980, Hauguel converted the equations of Serre (1953) from being in terms of the depth-averaged velocity to being in terms of the depth-integrated velocity (i.e. volume flux). This conversion gave rise to new terms α and β in the resulting equations. (It is noted that these terms α and β are completely different to the free coefficients in the equations of Schäffer and Madsen, 1995, and also the coefficients in the equation of Korteweg De-Vries, 1895). The resulting equations were then discretised using a fractional step, finite difference method[4] to form Hauguel's 1D and 2D numerical models. The 1D numerical model was tested at various Courant numbers and numbers of points per wavelengths ($L/\Delta x$) against analytical solutions. The results showed that the best agreement was obtained with a Courant number equal to 1 and a spatial resolution of $L/\Delta x = 20$. The influence of the bathymetry against solitary wave propagation was also studied. A solitary wave propagating over a slope showed an incident solitary wave disintegrating into several trains of solitary waves of decreasing wavelength.

Meanwhile, the 2D numerical model was applied in coastal engineering practice to the case of the solitary waves. The first computations were done in the port of Fecamp (a French port on the English Channel). All the computational tests were carried out without any bottom friction, so there was

[4] The fractional step, finite difference method was used to compute the effect of the advective terms in the first step and the friction terms in the second step.

no damping to cause attenuation of the computed waves. Furthermore, Hauguel made no 2D comparisons between his numerical solutions and analytical solutions or laboratory/field measurements.

Liu *et al.* (1985) converted the Boussinesq-type equations of Peregrine (1967) from elliptic equations into a set of parabolic equations. A Crank-Nicholson implicit finite difference method was used to discretise the new set of Boussinesq-type equations. The resulting numerical model was applied to the propagation of monochromatic waves together with their non-linearly generated harmonics in a wave tank with a bottom topography that acted as a focusing lens. Good agreement was obtained between the numerical results and the laboratory data.

Murray (1989) presented a new set of Boussinesq-type equations with an improved dispersion relation for a water depth up to the incident deep water (i.e. $h/L = \frac{1}{2}$). The equations of Murray were in terms of the surface elevation and the depth-integrated volume flux as dependent variables. A 1D version of these equations was solved by Murray using a finite difference method with a space-staggered grid and the alternating direction implicit algorithm. Murray did not compare the results from his model with laboratory or field data. Instead he compared his model results with those of Abbott *et al.* (1978) and noted that there were significant differences.

In 1991, Madsen *et al.* also derived a set of Boussinesq-type equations, which was presented in terms of the free surface elevation and the depth-integrated velocity components (i.e. volume fluxes) as the dependent variables. As confirmed by Madsen and Sørensen (1992), the derivation of the equations of Madsen *et al.* (1991) neglected all spatial derivatives of the seabed in the dispersion terms. For this reason, Madsen and Sørensen (1993) revealed that the equations of Madsen *et al.* (1991) should not be applied to a variable bathymetry. Schäffer and Madsen (1995) also stated that the equations of Madsen *et al.* (1991) were valid for constant depth only. However, they were applicable up to deep water. Although the equations of

Madsen *et al.* were effectively linear in deep water, the non-linear behaviour of Madsen *et al.*'s equations was similar to that of Peregrine's (1967) equations in shallow water.

The equations of Madsen *et al.* (1991) were discretised using a time-centred implicit finite difference scheme with variables defined on a space-staggered rectangular grid and the solution obtained using the alternative direction implicit (ADI) algorithm. The resulting numerical model was then used to simulate the propagation of monochromatic and bichromatic wave trains in a channel with a horizontal bottom. To reduce the reflected waves at the outgoing wave boundary, a sponge layer technique was applied. Comparisons of the results from the model of Madsen *et al.* and a previous model (Abbott *et al.*, 1978) showed that the equations of Madsen *et al.* were seen to improve the solution dramatically. For the 2D case, the waves were generated internally at the centre of the fluid domain. Absorbing sponge layers were applied along all surrounding boundaries. The computed results showed that circular wave patterns occurred perfectly. Finally, the model was applied to study wave diffraction in deep water and gave excellent agreement with the diffraction curves for wave height in the Shore Protection Manual (1984).

Madsen and Sørensen (1992) re-derived the standard form of the Boussinesq-type equations of Peregrine (1967) in terms of the depth-integrated velocity component (i.e. volume flux) instead of the depth-averaged velocity. The resulting equations were capable of describing irregular wave propagation over slowly varying bathymetry from deep to shallow water. A 2D Boussinesq-type numerical model based on their equations was developed using a time-centred, implicit finite difference scheme with variables defined on a space-staggered rectangular grid and the solution obtained using the ADI algorithm. The numerical model was used to simulate non-linear refraction-diffraction waves over a semicircular shoal. Considerable scatter in the data was evident in front of the shoal but behind the shoal the agreement between the data and the numerical results was acceptable. Generally, the amplitude of the first harmonic was slightly overestimated while that of the second harmonic was slightly underestimated.

In addition, Sørensen *et al.* (1998) extended the Boussinesq-type numerical wave models of Madsen *et al.* (1991) and Madsen and Sørensen (1992) to the surf zone and swash zone by including wave breaking and a moving boundary at the shoreline.

Beji and Battjes (1994) extended the 1D version of the equations of Peregrine (1967) by adding two terms into the 1D momentum equation thereby improving the dispersion relation. A numerical model based on the resulting equations was developed. The model was then applied to a channel with a submerged bar. Comparisons of the model results with measured surface elevations showed that the model was capable of reproducing the essential features of the wave field and non-linear wave transformations.

Witting (1984) developed a new set of Boussinesq-type equations in which the bottom velocity was the velocity variable. The governing equations were solved using a non-staggered leapfrog finite difference method. The resulting numerical model was used to simulate solitary wave propagation. No detailed comparison was made with either the results from other numerical models or laboratory measurements for specific problems. By referring to analytical solutions for solitary wave speeds and amplitudes, it was demonstrated that the equations of Witting predicted the wave celerity more accurately than the earlier theory of Korteweg and de Vries (KdeV) and the regularised long wave (RLW) equations (which were an alternative form of the KdeV equations).

Nwogu (1993) introduced a novel form of Boussinesq-type equations using the velocity at an arbitrary distance from still water level as the velocity variable. This resulted in a significantly improved dispersion relation and made the Boussinesq-type equations of Nwogu applicable to a wider range of water depth ($h/L \leq 0.5$). A 1D version of the corresponding equations was solved using the implicit, Crank-Nicholson finite difference scheme. The numerical model was then applied to the simulation of regular and irregular waves propagating over a concrete beach with a constant slope. Comparisons of the model results with laboratory measurements indicated that the model was capable of reasonably simulating several non-linear effects that occurred in the shoaling of surface waves from deep water. These effects included the amplification of the forced lower and higher frequency wave harmonics and the associated increase in the horizontal and vertical asymmetry of the waves.

Wei and Kirby (1995) presented a Boussinesq-type numerical model based on the equations of Nwogu (1993). A high order predictor-corrector method was used to advance the solution in time and the spatial derivatives were discretised to a sufficient order of accuracy to avoid unwanted numerical diffusion errors. The numerical model was then applied to several cases of wave propagation in variable depth. Comparisons of the computed solutions with laboratory data showed that the model was capable of simulating wave transformation from relatively deep water to shallow water. Other comparisons of the model results with laboratory measurements indicated that the model gave accurate predictions of the height and shape of both regular and irregular shoaled waves. The numerical scheme used in the work of Wei and Kirby is later adopted to solve all the governing equations in the present studies.

Chen and Liu (1995) re-derived the equations of Nwogu (1993) but in terms of the velocity potential (instead of the horizontal velocity) at an arbitrary elevation and the free surface displacement. The dispersion relation of the corresponding equations was found to depend strongly on the choice of a free coefficient value, as was the case for Nwogu's original formulation. The modified Boussinesq-type equations of Chen and Liu contained fourth-order spatial derivatives. This made the equations more complicated to solve in the time domain. For this reason, Chen and Liu then applied the parabolic approximation to the modified equations in the frequency domain. Chen and Liu next developed 2 Boussinesq-type numerical models: (i) a small-angle, parabolic model for waves propagating primarily in a dominant direction; and

(ii) an angular-spectrum, parabolic model for studying the effect of approach directions on the oblique interaction of two identical cnoidal wave trains in shallow water.

Kaihatu and Kirby (1998) presented an alternative parabolic, frequency domain, wave transformation equation starting with the equations of Nwogu (1993). The equation was then discretised using a Crank-Nicholson finite difference scheme. The discretisation was similar to that used by Liu *et al.* (1985). To investigate the linear characteristics of the new equation, the linearised version of the numerical model was compared to:

- the measurements of Berkhoff *et al.* (1982) and
- the linear parabolic mild-slope model.

The comparison showed that the linear characteristics of the model were very similar to those of Airy wave theory well beyond the shallow water limit i.e. $h/L > 1/20$. Finally, Kaihatu and Kirby compared the numerical solutions of their numerical model with non-linear terms included to:

- laboratory measurements in an unpublished work by Whalin (1971),
- the solutions of Liu *et al.*'s (1985) 2D model and
- the solutions of Chen and Liu's (1995) 2D model.

The comparisons showed that the models of Kaihatu and Kirby and of Chen and Liu were in better agreement with laboratory data in intermediate water depth than the model of Liu *et al.*.

Wei *et al.* (1995) derived a set of fully non-linear Boussinesq-type equations using the velocity at an arbitrary z-level as the velocity variable. A high order finite difference model, based on the new equations was developed and applied to the study of two canonical problems

- solitary wave shoaling on a slope and
- an undular bore propagating over a horizontal bed.

Results of the model with strong non-linearity (i.e. fully non-linear) and without strong non-linearity (i.e. weakly non-linear) were compared in detail to the solutions from a boundary element model of the fully non-linear, potential flow problem developed by Grilli *et al.* (1989). The comparisons showed that the fully non-linear variant of the Boussinesq-type numerical wave model of Wei *et al.* was found to predict wave heights, wave celerities and particle kinematics more accurately than the weakly non-linear wave model.

Furthermore, Nwogu (1996) extended the set of fully non-linear Boussinesq-type equations of Wei *et al.* (1995) to include depth limited wave breaking, run-up and breaking-induced currents. Nwogu achieved this by coupling the mass and momentum equations with a one-equation model for the temporal and spatial evolution of the turbulent kinetic energy produced by wave breaking. A 2D numerical model based on the new equations was developed and applied to simulate the shoaling and run-up of regular and irregular waves on a constant slope beach and wave-induced currents behind a detached breakwater. An iterative Crank-Nicholson finite difference scheme was employed to solve the governing equations, with a predictor-corrector scheme to predict the initial values. The computational domain was discretised using a rectangular staggered grid. Comparisons of the model results with measured laboratory data showed that it was capable of reproducing:

(i) a highly asymmetric wave profile in the surf zone,

(ii) the breaking of individual waves in an irregular wave train,

(iii) the cross-spectral transfer of energy due to non-linear wave-wave interactions and

(iv) the decrease in wave energy through the surf zone in an irregular wave train.

Borsboom *et al.* (2000) developed a new set of Boussinesq-type equations that was based on the depth-integrated transport of continuity and momentum. Both mass and momentum were strictly conserved. This set of equations was presented in terms of the depth-integrated velocity (i.e. volume flux). To assess the performance of these equations, a 1D numerical model based on the equations was developed and then applied to the simulation of a monochromatic wave train propagating over a submerged bar. The agreement with measurements was not as good for the shorter waves behind the bar, and for higher amplitude waves.

Yoon and Liu (1989) derived a new set of Boussinesq-type equations, which included the effects of both depth variations and varying currents[5] on weakly non-linear waves. These equations were derived by assuming the magnitude of the current velocity to be greater than the wave orbital velocity but weaker than the group velocity. The effects of vorticity in the current field were considered. The depth-averaged horizontal velocity components and the free surface elevation were decomposed into the wave and current components. They developed a 2D numerical model based on their equations using a Crank-Nicholson finite difference scheme. The resulting numerical model was applied to simulate the propagation of shallow water waves over rip currents on a uniform slope to study the effects of the non-linearity. Comparisons of the results of the full model with those of the linearised model showed that the non-linearity grew and the Boussinesq-type equations were fully utilised as the waves propagated into shallow water and encountered the current. Another scenario modelled was the propagation of cnoidal waves over an isolated vortex ring in constant depth to analyse the effects of refraction and diffraction. Comparisons of the wave height in the focal zones indicated that the predictions of the model with non-linear terms included were lower than those of the linearised model. The non-linearity improved the diffraction in which there is a transfer of wave energy in the lateral direction.

Prüser and Zielke (1990) extended the Boussinesq-type equations of Peregrine (1967) to include ambient current effects. The resulting equations

---

[5] The currents horizontal velocity varied appreciably within a characteristic wavelength. However, the horizontal velocity components were nearly uniform throughout the entire depth.

were used to investigate irregular, weakly non-linear waves propagating and refracting on an ambient current. The validity of the equations of Prüser and Zielke was analysed by comparing their governing equations with Airy wave theory. In the case of sinusoidal waves, these equations were valid if the ratio of the water depth to wave length (h/L) < 0.1 and Froude number (Fr) was in the range of $-0.2 < Fr < 0.2$. $Fr < 0$ indicates waves and a current in opposite directions. A 2D numerical model based on these Boussinesq-type equations was developed and used to simulate irregular waves with a current in a flume. The model results were in good agreement with the solution of Longuet-Higgins and Stewart (1961).

As explained above, Chen *et al.* (1998) presented *three sets* of Boussinesq-type equations for fully combined wave-current motion. Following the approach of Yoon and Liu (1989), Chen *et al.* (1998) derived a set of Boussinesq-type equations based on the depth-integrated continuity equation and Euler equations of motion. The equations of Chen *et al.* and those of Yoon and Liu were presented in terms of the depth-averaged velocity as the velocity variable. Both formulations achieved a correct representation of the Doppler shift with the dispersion relation corresponding to a Padé [0,2] approximation in terms of (kh). When the current vanished, both sets of equations reduced to those of Peregrine (1967) in terms of the depth-averaged horizontal velocity.

The next advance by Chen *et al.* (1998) was to re-formulate their equations by replacing the depth-averaged velocity with the velocity at an arbitrary elevation as the velocity variable. The elevation was expressed as a proportion of the depth. Consequently if the depth was varying in space, so too was the elevation at which the horizontal velocity was defined. This resulted in a new set of Boussinesq-type equations with a correct Doppler shift in which the dispersion relation corresponded to a Padé [2,2] expansion in terms of (kh). These equations reduced to those of Nwogu (1993) for the wave only case.

The third and last development by Chen *et al.* (1998) was to extend these equations by introducing four new free coefficients $(\beta_1,\beta_2,\gamma_1,\gamma_2) \leq O(1)$ into the governing equations thereby improving the dispersion relation. The resulting equations had a dispersion relation corresponding to a Padé [4,4] approximation in terms of (kh). This development technique followed the approach of Schäffer and Madsen (1995). In the case of pure wave propagation, these formulations reduce to those of Schäffer and Madsen.

Chen *et al.* solved a 1D version of their *third set* of equations using an implicit finite difference method with a space-staggered grid. The governing equations were discretised using a fourth-order centred finite difference approximation for the first-order spatial derivative terms and second-order centred finite difference approximations for the second- and third-order spatial derivative terms. This numerical approach was adopted from the work of Wei *et al.* (1995). At the outgoing wave and outflow boundaries, the Sommerfeld radiation condition (i.e. $\eta_t + C\eta_x = 0$) and the sponge layer technique introduced by Larsen and Dancy (1983) were combined to radiate long waves and dissipate unwanted currents. In the case of pure current motion, comparisons of the results of the Boussinesq-type numerical model of Chen *et al.* with those of the numerical model for the steady, non-linear shallow water equations gave excellent agreement. For fully coupled, wave-current motion, wave envelopes determined from the results of the numerical model for wave action conservation equation were compared with those of the Boussinesq-type numerical model.

2.3. Derivation of the equations of Boussinesq (1872)

Unlike the Boussinesq-type equations, the original Boussinesq equations developed by Boussinesq (1872) can be obtained directly without passing through *non-dimensional* forms. These Boussinesq equations consist of the continuity equation and two horizontal momentum equations, and are only applicable to a horizontal bottom. The basic idea can be explained as follows.

Consideration of incompressible inviscid fluid flow, the governing equation is given by the 3D continuity equation as

$$\nabla \bullet \mathbf{u} + w_z = 0 \tag{2.1}$$

where ∇ is the 2D operator as defined as $\nabla = (\partial/\partial x, \partial/\partial y)$, $\mathbf{u} = (u,v)$ is the horizontal velocity, w is the vertical velocity and the subscript z again denotes partial differentiation with respect to the z-direction. The dynamic free surface boundary condition and kinematic boundary conditions at the free surface elevation and seabed are respectively

$$p = p_a \qquad \text{at } z = \eta(x,y,t) \tag{2.2}$$

$$\eta_t + \mathbf{u} \bullet \nabla \eta = w \qquad \text{at } z = \eta(x,y,t) \tag{2.3}$$

$$w + \mathbf{u} \bullet \nabla h = 0 \qquad \text{at } z = -h(x,y) \tag{2.4}$$

where surface tension has been neglected, p_a is atmospheric pressure and the subscript t denotes partial differentiation with respect to time.

The unsteady Bernoulli equation can be expressed as

$$\Phi_t + \tfrac{1}{2}(\mathbf{u}^2 + w^2) + \frac{p}{\rho} + gz = 0 \tag{2.5}$$

where Φ is the velocity potential.

For an irrotational flow, the curl of the velocity vector **v** [where $\mathbf{v} = (u,w)$] must be zero

$$\overline{\nabla} \times \mathbf{v} = 0 = (w_y - v_z)\mathbf{i} + (u_z - w_x)\mathbf{j} + (v_x - u_y)\mathbf{k} \tag{2.6}$$

where $\overline{\nabla}$ is the 3D operator defined by $\overline{\nabla} = (\partial/\partial x, \partial/\partial y, \partial/\partial z)$. The curl of the velocity vector is a measure of the vorticity. The velocity vector can therefore be conveniently represented as

$$\mathbf{u} = \nabla\Phi, \qquad w = \Phi_z \tag{2.7}$$

The continuity equation (2.1) and the irrotationality condition (2.6) can be combined to form the Laplace equation

$$\nabla \bullet \nabla\Phi(x,y,z,t) + \Phi_{zz}(x,y,z,t) = 0 \tag{2.8}$$

Similarly, the kinematic boundary conditions become

$$\eta_t + \nabla\Phi \bullet \nabla\eta = \Phi_z \qquad \text{at } z = \eta(x,y,t) \tag{2.9}$$

$$\Phi_z + \nabla\Phi \bullet \nabla h = 0 \qquad \text{at } z = -h(x,y) \tag{2.10}$$

and the unsteady Bernoulli equation becomes

$$\Phi_t + \tfrac{1}{2}[(\nabla\Phi)^2 + (\Phi_z)^2] + \frac{p}{\rho} + gz = 0 \tag{2.11}$$

The Bernoulli equation (2.11) can be applied at the water surface and is

$$\Phi_t + \tfrac{1}{2}[(\nabla\Phi)^2 + (\Phi_z)^2] + \frac{p}{\rho} + g\eta = 0 \qquad \text{at } z = \eta(x,y,t) \tag{2.12}$$

Equation (2.12) is the new free surface, dynamic boundary condition in terms of the velocity potential Φ. The fluid is assumed to be at atmospheric pressure i.e. $p_a = 0$. As a result, the free surface, dynamic boundary conditions [(2.2) and (2.12)] then become

$$p = 0 \qquad \text{at } z = \eta(x,y,t) \tag{2.13}$$

$$\Phi_t + \tfrac{1}{2}[(\nabla\Phi)^2 + (\Phi_z)^2] + g\eta = 0 \qquad \text{at } z = \eta(x,y,t) \tag{2.14}$$

Applying the ∇ operator to equation (2.14) then allows this equation to be recast in terms of $\mathbf{u}$

$$\mathbf{u}_t + (\mathbf{u} \bullet \nabla)\mathbf{u} + w\nabla w + g\nabla\eta = 0 \qquad \text{at } z = \eta(x,y,t) \tag{2.15}$$

By the use of the kinematic, bottom boundary condition for a *horizontal* bottom $\Phi_z = 0$ at $z = -h$, the Laplace equation (2.8) is integrated twice with respect to z leading to

$$\Phi(x,y,z,t) = \Phi(x,y,-h,t) - \int_{-h}^{z}\int_{-h}^{z}[\nabla \bullet \nabla\Phi(x,y,z,t)]dzdz \tag{2.16}$$

As reported by Dingemans (1997), the principal approximation now consists of the observation that for shallow water, the horizontal velocity $\nabla\Phi$ is not much different from the velocity at the bottom $\nabla\Phi_b$, where $\Phi_b(x,y,t)$ = $\Phi(x,y,-h,t)$ is the value of the velocity potential at the bottom. The horizontal acceleration is also assumed to be nearly equal to its value at the bottom i.e. $\nabla\bullet\nabla\Phi \cong \nabla\bullet\nabla\Phi_b$. Equation (2.16) can be solved as

$$\Phi(x,y,z,t) \cong \Phi_b(x,y,t) - \frac{(z+h)^2}{2!}\nabla \bullet \nabla\Phi_b \tag{2.17}$$

Substitution of the approximation (2.17) into equation (2.16) leads to

$$\Phi(x,y,z,t) \cong \Phi_b(x,y,t) - \frac{(z+h)^2}{2!}\nabla \bullet \nabla\Phi_b + \frac{(z+h)^4}{4!}\nabla^2(\nabla \bullet \nabla\Phi_b) \tag{2.18}$$

The approximation (2.18) can be re-written in terms of the velocities $\mathbf{u} = \nabla\Phi$ and $w = \Phi_z$, (again assuming the seabed to be *flat*), that is

$$\mathbf{u}(x,y,t) = \nabla\Phi(x,y,z,t) \cong \mathbf{u}_b(x,y,t) - \frac{(z+h)^2}{2!}\nabla(\nabla \bullet \mathbf{u}_b) + \frac{(z+h)^4}{4!}\nabla[\nabla^2(\nabla \bullet \mathbf{u}_b)] \tag{2.19}$$

$$w(z,t) = \Phi_z(x,y,z,t) \cong -(z+h)\nabla \bullet \mathbf{u}_b + \frac{(z+h)^3}{3!}\nabla^2(\nabla \bullet \mathbf{u}_b) \tag{2.20}$$

where again $\mathbf{u}_b$ is the horizontal velocity vector at the seabed. Substituting the approximations (2.19) and (2.20) into the kinematic and dynamic boundary conditions at the free surface elevation [(2.9) and (2.15)] and retaining the derivatives up to the third-order gives the set of original Boussinesq equations as

$$\eta_t + \mathbf{u}_b \bullet \nabla\eta + (\eta + h)(\nabla \bullet \mathbf{u}_b) = \tfrac{1}{6}h^3\nabla^2(\nabla \bullet \mathbf{u}_b) \tag{2.21}$$

$$\mathbf{u}_{b_t} + (\mathbf{u}_b \bullet \nabla)\mathbf{u}_b + g\nabla\eta = \tfrac{1}{2}h^2\nabla(\nabla \bullet \mathbf{u}_{b_t}) \tag{2.22}$$

The original Boussinesq equations can be presented in *non-dimensional* forms by making use of the *non-dimensional* variables defined in Section 2.4.1 below. Substitution of equations (2.31) and (2.32) into equations (2.9), (2.15), (2.19) and (2.20) leads to the following *non-dimensional* equations

$$\eta'_{t'} + \varepsilon\mathbf{u}' \bullet \nabla'\eta' - \frac{1}{\mu^2}w' = 0 \qquad \text{at } z' = \varepsilon\eta' \tag{2.23}$$

$$\mathbf{u}'_{t'} + \varepsilon(\mathbf{u}' \bullet \nabla')\mathbf{u}' + \frac{\varepsilon}{\mu^2}w'\nabla'w' + \nabla'\eta' = 0 \qquad \text{at } z' = \varepsilon\eta' \tag{2.24}$$

$$\mathbf{u}' \cong \mathbf{u}'_b - \mu^2\frac{(z'+h')^2}{2!}\nabla'(\nabla' \bullet \mathbf{u}'_b) + \mu^4\frac{(z'+h')^4}{4!}\nabla'[\nabla'^2(\nabla' \bullet \mathbf{u}'_b)] + O(\mu^6) \tag{2.25}$$

$$w' \cong -\mu^2(z'+h')\nabla' \bullet \mathbf{u}'_b + \mu^4\frac{(z'+h')^3}{3!}\nabla'^2(\nabla' \bullet \mathbf{u}'_b) + O(\mu^6) \tag{2.26}$$

where $\nabla' = (\partial/\partial x', \partial/\partial y')$. Substituting the *non-dimensional* velocities [(2.25) and (2.26)] into the *non-dimensional* kinematic and dynamic boundary equations at the free surface elevation [(2.23) and (2.24)] and assuming $O(\varepsilon) = O(\mu^2) << 1$ to give the *non-dimensional* forms of the original Boussinesq equations

$$\eta'_{t'} + \varepsilon\mathbf{u}'_b \bullet \nabla'\eta' + (\varepsilon\eta' + h')(\nabla' \bullet \mathbf{u}'_b) - \mu^2\tfrac{1}{6}h'^3\nabla'^2(\nabla' \bullet \mathbf{u}'_b) = O(\varepsilon\mu^2, \mu^4) \tag{2.27}$$

$$\mathbf{u}'_{b_{t'}} + \varepsilon(\mathbf{u}'_b \bullet \nabla')\mathbf{u}'_b + \nabla'\eta' - \mu^2\tfrac{1}{2}h'^2\nabla'(\nabla' \bullet \mathbf{u}'_{b_{t'}}) = O(\varepsilon\mu^2, \mu^4) \tag{2.28}$$

It is clear that only terms up to $O(\varepsilon, \mu^2)$ are retained in equations (2.27) and (2.28). If the primes are dropped, these equations become

$$\eta_t + \varepsilon\mathbf{u}_b \bullet \nabla\eta + (\varepsilon\eta + h)(\nabla \bullet \mathbf{u}_b) - \mu^2\tfrac{1}{6}h^3\nabla^2(\nabla \bullet \mathbf{u}_b) = O(\varepsilon\mu^2, \mu^4) \tag{2.29}$$

$$\mathbf{u}_{b_t} + \varepsilon(\mathbf{u}_b \bullet \nabla)\mathbf{u}_b + \nabla\eta - \mu^2\tfrac{1}{2}h^2\nabla(\nabla \bullet \mathbf{u}_{b_t}) = O(\varepsilon\mu^2, \mu^4) \tag{2.30}$$

2.4. Derivation of the equations of Peregrine (1967)

2.4.1. Non-dimensional variables

Two important length scales are the characteristic water depth h_{ch} for the vertical direction and the typical wavelength L_{ch} for the horizontal direction. For effects due to the motion of the free surface, the typical wave amplitude a_{ch} is an important length scale. The parameters $\varepsilon = a_{ch}/h_{ch}$ and $\mu = h_{ch}/L_{ch}$ are measures of the non-linearity and frequency dispersion respectively, and are assumed to be small i.e. $O(\varepsilon) << 1$ and $O(\mu) << 1$. The independent, *non-dimensional* variables are defined as follows

$$x' = \frac{x}{L_{ch}}\ ,\ y' = \frac{y}{L_{ch}}\ ,\ z' = \frac{z}{h_{ch}}\ ,\ t' = \frac{\sqrt{gh_{ch}}}{L_{ch}}t \tag{2.31}$$

where again g is the gravitational acceleration and primes are used to denote *non-dimensional* variables. However, the definitions of the dependent, *non-dimensional* variables adopted here follow those used by Nwogu (1993) rather than those used by Peregrine (1967). The dependent, *non-dimensional* variables are defined as follows

$$u' = \frac{u}{\varepsilon\sqrt{gh_{ch}}},\ v' = \frac{v}{\varepsilon\sqrt{gh_{ch}}},\ w' = \frac{\mu}{\varepsilon\sqrt{gh_{ch}}}w \tag{2.32a}$$

$$\eta' = \frac{\eta}{a_{ch}},\ h' = \frac{h}{h_{ch}},\ p' = \frac{p}{\rho g a_{ch}} \tag{2.32b}$$

2.4.2. Continuity equation and Euler equations of motion

The governing equations for an inviscid, incompressible fluid in motion are the continuity equation and Euler equations of motion

$$\nabla \bullet \mathbf{u} + w_z = 0 \tag{2.1}$$

$$\mathbf{u}_t + (\mathbf{u} \bullet \nabla)\mathbf{u} + w\mathbf{u}_z + \frac{1}{\rho}\nabla p = 0 \tag{2.33}$$

$$w_t + (\mathbf{u} \bullet \nabla)w + ww_z + \frac{1}{\rho}p_z + g = 0 \qquad (2.34)$$

where $\mathbf{u} = \mathbf{u}(x,y,z,t)$, $\mathbf{u} = (u,v)$, $w = w(x,y,z,t)$ and $p = p(x,y,z,t)$.

2.4.3. Boundary conditions

The fluid motion must satisfy the dynamic boundary condition at the free surface and the kinematic boundary conditions at the free surface and seabed

$$p = 0 \qquad \text{at } z = \eta \qquad (2.13)$$

$$w = \eta_t + \mathbf{u} \bullet \nabla\eta \qquad \text{at } z = \eta \qquad (2.3)$$

$$w = -\mathbf{u} \bullet \nabla h \qquad \text{at } z = -h \qquad (2.4)$$

where $\eta = \eta(x, y, t)$ and $h = h(x, y)$. The irrotationality condition (2.6) can be written as

$$\mathbf{u}_z - \nabla w = 0 \qquad (2.35a)$$

$$u_y - v_x = 0 \qquad (2.35b)$$

where subscripts x and y denote partial differentiation with respect to the x- and y-directions respectively.

2.4.4. Depth-integrated continuity and momentum equations

The depth-integrated continuity equation can be obtained by integrating the continuity equation (2.1) from the seabed to the free surface elevation and applying the kinematic boundary conditions [(2.3) and (2.4)], that is

$$\eta_t + \nabla \bullet \mathbf{Q} = 0 \qquad (2.36)$$

where $\mathbf{Q} = \int_{-h}^{\eta} \mathbf{u}\, dz$ and $\mathbf{Q} = \mathbf{Q}(x, y, z, t)$. Similarly, the depth-integrated momentum equation is obtained by integrating the horizontal momentum equation (2.33) from –h to η and applying the dynamic and kinematic boundary conditions [(2.13), (2.3) and (2.4)]. This results in

$$\frac{\partial}{\partial t}\int_{-h}^{\eta} \mathbf{u}\,dz + (\mathbf{u}\bullet\nabla)\int_{-h}^{\eta} \mathbf{u}\,dz + \frac{1}{\rho}[\nabla\int_{-h}^{\eta} p\,dz - p|_{z=-h}\nabla h] = 0 \tag{2.37}$$

Alternatively, by following Phillips (1977), both Nwogu (1993) and Chen *et al.* (1998) expressed the depth-integrated momentum equations as defined by equations (2.38) instead of (2.37).

$$\frac{\partial}{\partial t}\int_{-h}^{\eta} u\,dz + \frac{\partial}{\partial x}\int_{-h}^{\eta} u^2\,dz + \frac{\partial}{\partial y}\int_{-h}^{\eta} uv\,dz + \frac{1}{\rho}[\frac{\partial}{\partial x}\int_{-h}^{\eta} p\,dz - p|_{z=-h}h_x] = 0 \tag{2.38a}$$

$$\frac{\partial}{\partial t}\int_{-h}^{\eta} v\,dz + \frac{\partial}{\partial x}\int_{-h}^{\eta} uv\,dz + \frac{\partial}{\partial y}\int_{-h}^{\eta} v^2\,dz + \frac{1}{\rho}[\frac{\partial}{\partial y}\int_{-h}^{\eta} p\,dz - p|_{z=-h}h_y] = 0 \tag{2.38b}$$

2.4.5. 1D horizontal equations

Using the *non-dimensional* variables defined by equations (2.31) and (2.32), equations (2.1), (2.33), (2.34), (2.13), (2.3), (2.4), (2.35a) and (2.36) can be converted into *non-dimensional* forms. After non-dimensionalising and dropping the primes, for one-dimensional horizontal equations, these equations become (2.39) through to (2.46)

Governing equations:

$$\mu^2 u_x + w_z = 0 \qquad \text{(continuity)} \tag{2.39}$$

$$\mu^2 u_t + \varepsilon\mu^2 u u_x + \varepsilon w u_z + \mu^2 p_x = 0 \qquad \text{(x-momentum)} \tag{2.40}$$

$$\varepsilon w_t + \varepsilon^2 u w_x + \frac{\varepsilon^2}{\mu^2} w w_z + \varepsilon p_z + 1 = 0 \qquad \text{(z-momentum)} \tag{2.41}$$

Boundary conditions:

$$p = 0 \qquad \text{at } z = \varepsilon\eta \tag{2.42}$$

$$w = \mu^2\eta_t + \varepsilon\mu^2 u\eta_x \qquad \text{at } z = \varepsilon\eta \tag{2.43}$$

$$w = -\mu^2 u h_x \qquad \text{at } z = -h \tag{2.44}$$

$$u_z - w_x = 0 \qquad \text{(irrotational flow)} \tag{2.45}$$

and

$$\eta_t + Q_x = 0 \qquad \text{(depth-integrated continuity)} \tag{2.46}$$

where $Q = \int_{-h}^{\varepsilon\eta} u\,dz$, $u = u(x,z,t)$, $w = w(x,z,t)$, $p = p(x,z,t)$, $\eta = \eta(x,t)$ and $h = h(x)$

2.4.5.1. *First-order 1D horizontal equations*

Following the perturbation approach by Dingemans (1997), the dependent variables η, u, w, p and Q are expanded as a series

$$f(x,z,t) = f_0(x,z,t) + \varepsilon f_1(x,z,t) + \varepsilon^2 f_3(x,z,t) + \ldots \tag{2.47}$$

with all $f_i = O(1)$.

Equation (2.41) can be stated as

$$p_{0_z} + 1 = O(\varepsilon\mu^2) \tag{2.48}$$

Integrating equation (2.48) over z to give

$$p_0 = -z + O(\varepsilon\mu^2) \tag{2.49}$$

The first-order form of the vertical Euler equation of motion (2.41) is $p_{1_z} = 0$, so that

$$p_1 = c_1(x,t) \tag{2.50}$$

where c_1 is an integration constant and found from the first-order form of the dynamic, free surface boundary condition (2.42), that is

$$p_0 + \varepsilon p_1 = 0 \qquad \text{at} \quad z = \varepsilon\eta_1 \tag{2.51}$$

Substitution of equation (2.49) into (2.51) leads to

$$p_1 = \eta_1 \tag{2.52}$$

The first-order form of the irrotational condition (2.45) is $u_{1_z} = 0$ and so

$$u_1 = U_1(x,t) \tag{2.53}$$

where U_1 is an integration constant and obtained by integrating the first-order form of equation (2.39) for the continuity equation from –h to z and applying the first-order form of equation (2.44) for the kinematic, seabed boundary condition to give

$$w_1 = -\mu^2[(h+z)U_1]_x \tag{2.54}$$

The depth-integrated continuity equation (2.46) and the horizontal momentum equation (2.40) in the first-order forms respectively become

$$\eta_{1_t} + Q_{1_x} = 0 \tag{2.55}$$

$$U_{1_t} + \eta_{1_x} = 0 \tag{2.56}$$

where $Q_1 = hU_1$.

2.4.5.2. Second-order 1D horizontal equations

The second-order vertical Euler equations of motion is

$$\varepsilon p_{2_z} = -w_{1_t} \tag{2.57}$$

Substituting equation (2.54) for w_1 into equation (2.57) and integrating over z to give

$$p_2 = c_2 + \frac{\mu^2}{\varepsilon} z(hU_1)_{xt} + \frac{\mu^2}{\varepsilon}\tfrac{1}{2} z^2 U_{1_{xt}} \tag{2.58}$$

where c_2 is an integration constant and obtained from the second-order form of the dynamic, free surface boundary condition (2.42), that is

$$p_0 + \varepsilon p_1 + \varepsilon^2 p_2 = 0 \qquad \text{at } z = \varepsilon^2 \eta_2 \tag{2.59}$$

Substitution of equations (2.49) for p_0, (2.52) for p_1 and (2.58) for p_2 into (2.59) gives

$$c_2 = \eta_2 \tag{2.60}$$

As a result, equation (2.58) can be re-written as

$$p_2 = \eta_2 + \frac{\mu^2}{\varepsilon} z(hU_{1_t})_x + \frac{\mu^2}{\varepsilon} \tfrac{1}{2} z^2 U_{1_{xt}} \tag{2.61}$$

The second-order form of the irrotational condition (2.45) is

$$u_{2_z} = \frac{1}{\varepsilon} w_{1_x} \tag{2.62}$$

Substituting equation (2.54) for w_1 into (2.62) and integrating over z to obtain

$$u_2 = U_2 - \frac{\mu^2}{\varepsilon} z(hU_1)_{xx} - \frac{\mu^2}{\varepsilon} \tfrac{1}{2} z^2 U_{1_{xx}} \tag{2.63}$$

where U_2 is an integration constant and function of (x,t). The second-order form of the depth-integrated continuity equation (2.46) and of the horizontal momentum equation (2.40) are

$$\eta_{2_t} + Q_{2_x} = 0 \tag{2.64}$$

$$u_{2_t} + \varepsilon u_1 u_{1_x} + p_{2_x} = 0 \tag{2.65}$$

Expressions for Q_1 and Q_2 can be found from the definition of Q

$$Q_1 + \varepsilon Q_2 = \int_{-h}^{\varepsilon\eta} (u_1 + \varepsilon u_2)\, dz \tag{2.66}$$

Substituting equations (2.53) for u_1 and (2.63) for u_2 into (2.66) to give

$$Q_1 = hU_1 \tag{2.67}$$

$$Q_2 = hU_2 + \eta_1 U_1 + \frac{\mu^2}{\varepsilon}\left[\tfrac{1}{2}h^2(hU_1)_{xx} - \tfrac{1}{6}h^3 U_{1_{xx}}\right] \tag{2.68}$$

The first-order depth-integrated continuity equation (2.55) and the first-order horizontal momentum equation (2.56) become

$$\eta_{1_t} + (hU_1)_x = 0 \tag{2.69}$$

$$U_{1_t} + \eta_{1_x} = 0 \tag{2.70}$$

and the second-order equations (2.64) and (2.65) become

$$\eta_{2_t} + (hU_2)_x = -(\eta_1 U_1)_x - \frac{\mu^2}{\varepsilon}\left[\tfrac{1}{2}h^2(hU_1)_{xx} - \tfrac{1}{6}h^3 U_{1_{xx}}\right]_x \tag{2.71}$$

$$U_{2_t} + \varepsilon U_1 U_{1_x} + \eta_{2_x} = 0 \tag{2.72}$$

The first- and second-order equations are therefore combined by adding ε times the second-order equations to the corresponding first-order equations. This results in

$$(\eta_1 + \varepsilon\eta_2)_t + (hU_1 + \varepsilon hU_2)_x + \varepsilon(\eta_1 U_1)_x = -\mu^2\left[\tfrac{1}{2}h^2(hU_1)_{xx} - \tfrac{1}{6}h^3 U_{1_{xx}}\right]_x \tag{2.73}$$

$$(U_1 + \varepsilon U_2)_t + \varepsilon U_1 U_{1_x} + (\eta_1 + \varepsilon\eta_2)_x = 0 \tag{2.74}$$

2.4.5.3. 1D horizontal equations in terms of $\bar{u}$

Equation (2.69) can be written in terms of Q_1 and Q_2 as

$$(\eta_1 + \varepsilon\eta_2)_t + (Q_1 + \varepsilon Q_2)_x = 0 \tag{2.75}$$

where

$$Q_1 + \varepsilon Q_2 = hU_1 + \varepsilon hU_2 + \varepsilon\eta_1 U_1 + \mu^2\left[\tfrac{1}{2}h^2(hU_1)_{xx} - \tfrac{1}{6}h^3 U_{1_{xx}}\right] \tag{2.76}$$

The depth-averaged horizontal velocity $\bar{u}$ is defined as

$$\varepsilon\bar{u}(x,t) = \frac{1}{h + \varepsilon\eta}\int_{-h}^{\varepsilon\eta} u(x,z,t)\,dz \tag{2.77}$$

therefore

$$Q_1+\varepsilon Q_2=(h+\varepsilon\eta)\overline{u} \tag{2.78}$$

$$h\overline{u}=Q_1-\varepsilon\eta_1 U_1+\varepsilon Q_2+O(\varepsilon^2) \tag{2.79}$$

Substitution of equation (2.76) into (2.79) leads to

$$\overline{u}=U_1+\varepsilon U_2+\mu^2\left[\tfrac{1}{2}h(hU_1)_{xx}-\tfrac{1}{6}h^2 U_{1_{xx}}\right] \tag{2.80}$$

or

$$U_1+\varepsilon U_2=\overline{u}-\mu^2\left[\tfrac{1}{2}h(h\overline{u})_{xx}-\tfrac{1}{6}h^2\overline{u}_{xx}\right] \tag{2.81}$$

From equation (2.81), it is clear that $U_1 U_{1_x}=\overline{u}\,\overline{u}_x+O(\varepsilon^2)$. Substituting equation (2.81) into equations (2.73) and (2.74) gives the 1D Boussinesq-type equations of Peregrine (1967) in terms of the depth-averaged horizontal velocity $\overline{u}$ as

$$\eta_t+\left[(h+\varepsilon\eta)\overline{u}\right]_x=0 \tag{2.82}$$

$$\overline{u}_t+\varepsilon\overline{u}\,\overline{u}_x+\eta_x=\mu^2\left[\tfrac{1}{2}h(h\overline{u}_t)_{xx}-\tfrac{1}{6}h^2\overline{u}_{xxt}\right]+O(\varepsilon\mu^2,\mu^4) \tag{2.83}$$

2.4.5.4. 1D horizontal equations in terms of $\tilde{u}$

The horizontal velocity at $z=0$ is defined as

$$\varepsilon\tilde{u}(x,t)=u(x,0,t) \tag{2.84}$$

Considering equations (2.53) for u_1 and (2.63) for u_2, $u(x,z,t)$ can be expressed as

$$\begin{aligned} u(x,z,t)&=\varepsilon u_1(x,z,t)+\varepsilon^2 u_2(x,z,t)\\ &=\varepsilon U_1(x,t)+\varepsilon^2 U_2(x,t)-\varepsilon\mu^2\left[z(hU_1)_{xx}-\tfrac{1}{2}z^2 U_{1_{xx}}\right] \end{aligned} \tag{2.85}$$

Substitution of $z=0$ into equation (2.85) gives the expression for $\tilde{u}$

$$\tilde{u}=U_1+\varepsilon U_2 \tag{2.86}$$

Substituting equation (2.86) into (2.73) and (2.74) gives the 1D Boussinesq-type equations of Peregrine (1967) in terms of the still water level horizontal velocity $\tilde{u}$ as

$$\eta_t + [(h+\varepsilon\eta)\tilde{u}]_x = -\mu^2[\tfrac{1}{2}h^2(h\tilde{u})_{xx} - \tfrac{1}{6}h^3\tilde{u}_{xx}]_x + O(\varepsilon\mu^2,\mu^4) \qquad (2.87)$$

$$\tilde{u}_t + \varepsilon\tilde{u}\tilde{u}_x + \eta_x = O(\varepsilon\mu^2,\mu^4) \qquad (2.88)$$

2.4.6. 2D horizontal equations

In the two-dimensional horizontal plane, the derivation of the Boussinesq-type equations of Peregrine (1967) follows the same lines as the 1D case in Section 2.4.5. Instead of equations (2.39) through to (2.46) in one-dimension, the two-dimensional analogues are written below with vector quantities such as $\mathbf{u} = (u,v)$ written in bold letters.

Governing equations:

$$\mu^2\nabla\bullet\mathbf{u} + w_z = 0 \qquad (2.89)$$

$$\mu^2\mathbf{u}_t + \varepsilon\mu^2(\mathbf{u}\bullet\nabla)\mathbf{u} + \varepsilon w\mathbf{u}_z + \mu^2\nabla p = 0 \qquad (2.90)$$

$$\varepsilon w_t + \varepsilon^2(\mathbf{u}\bullet\nabla)w + \frac{\varepsilon^2}{\mu^2}ww_z + \varepsilon p_z + 1 = 0 \qquad (2.91)$$

Boundary conditions:

$$p = 0 \quad \text{at } z = \varepsilon\eta \qquad (2.92)$$

$$w = \mu^2\eta_t + \varepsilon\mu^2(\mathbf{u}\bullet\nabla\eta) \quad \text{at } z = \varepsilon\eta \qquad (2.93)$$

$$w = -\mu^2(\mathbf{u}\bullet\nabla h) \quad \text{at } z = -h \qquad (2.94)$$

Irrotational conditions:

$$\mathbf{u}_z - \nabla w = 0 \qquad (2.95a)$$

$$u_y - v_x = 0 \qquad (2.95b)$$

<u>Depth-integrated continuity equation:</u>

$$\eta_t + \nabla \bullet \mathbf{Q} = 0 \tag{2.96}$$

where $\mathbf{Q} = \int_{-h}^{\varepsilon\eta} \mathbf{u}\, dz$, $\mathbf{u} = \mathbf{u}(x,y,z,t)$, $w = w(x,y,z,t)$, $p = p(x,y,z,t)$, $\eta = \eta(x,y,t)$ and $h = h(x,y)$. The dependent variables η, $\mathbf{u}$, w, p and $\mathbf{Q}$ are then expanded as

$$f(x,y,z,t) = f_0(x,y,z,t) + \varepsilon f_1(x,y,z,t) + \varepsilon^2 f_3(x,y,z,t) + \ldots \tag{2.97}$$

where all $f_i = O(1)$.

Equations (2.53) for u_1 and (2.63) for u_2 are converted to two-dimensional forms

$$\mathbf{u}_1(x,y,z,t) = \mathbf{U}_1(x,y,t) \tag{2.98}$$

$$\mathbf{u}_2 = \mathbf{U}_2 - \frac{\mu^2}{\varepsilon} z\nabla[\nabla \bullet (h\mathbf{U}_1)] - \frac{\mu^2}{\varepsilon}\tfrac{1}{2}z^2\nabla(\nabla \bullet \mathbf{U}_1) \tag{2.99}$$

The 2D equivalent of equation (2.85) for u becomes

$$\mathbf{u}(x,y,z,t) = \varepsilon \mathbf{u}_1(x,y,z,t) + \varepsilon^2 \mathbf{u}_2(x,y,z,t)$$

$$= \varepsilon \mathbf{U}_1(x,y,t) + \varepsilon^2 \mathbf{U}_2(x,y,t) - \varepsilon\mu^2\{z\nabla[\nabla \bullet (h\mathbf{U}_1)] - \tfrac{1}{2}z^2\nabla(\nabla \bullet \mathbf{U}_1)\}$$

(2.100)

The 2D version of the combined first- and second-order 1D depth-integrated continuity equation (2.75) becomes

$$(\eta_1 + \varepsilon\eta_2)_t + \nabla \bullet (\mathbf{Q}_1 + \varepsilon\mathbf{Q}_2) = 0 \tag{2.101}$$

In the same way, the 2D version of the 1D horizontal momentum equation (2.74) becomes

$$(\mathbf{U}_1 + \varepsilon\mathbf{U}_2)_t + \varepsilon(\mathbf{U}_1 \bullet \nabla)\mathbf{U}_1 + \nabla(\eta_1 + \varepsilon\eta_2) = 0 \tag{2.102}$$

2.4.6.1. 2D horizontal equations in terms of $\tilde{\mathbf{u}}$

Introducing $\varepsilon\tilde{\mathbf{u}}(x,y,t) = \mathbf{u}(x,y,0,t)$ and substituting into equation (2.100) gives

$$\tilde{\mathbf{u}}(x,y,t) = \mathbf{U}_1(x,y,t) + \varepsilon\mathbf{U}_2(x,y,t) \tag{2.103}$$

thus

$$\mathbf{Q}_1 + \varepsilon\mathbf{Q}_2 = h\tilde{\mathbf{u}} + \varepsilon\eta\tilde{\mathbf{u}} + \mu^2\left\{\tfrac{1}{2}h^2\nabla[\nabla\bullet(h\tilde{\mathbf{u}})] - \tfrac{1}{6}h^3\nabla(\nabla\bullet\tilde{\mathbf{u}})\right\} \tag{2.104}$$

Equations (2.103) and (2.104) are substituted into equations (2.101) and (2.102) to give the 2D Boussinesq-type equations of Peregrine (1967) in terms of the still water level velocity $\tilde{\mathbf{u}}$ (i.e. $\mathbf{u}$ at $z = 0$)

$$\eta_t + \nabla\bullet[(h+\varepsilon\eta)\tilde{\mathbf{u}}] = -\mu^2\nabla\left\{\tfrac{1}{2}h^2\nabla[\nabla\bullet(h\tilde{\mathbf{u}})] - \tfrac{1}{6}h^3\nabla(\nabla\bullet\tilde{\mathbf{u}})\right\} + O(\varepsilon\mu^2,\mu^4) \tag{2.105}$$

$$\tilde{\mathbf{u}}_t + \varepsilon(\tilde{\mathbf{u}}\bullet\nabla)\tilde{\mathbf{u}} + \nabla\eta = O(\varepsilon\mu^2,\mu^4) \tag{2.106}$$

In dimensional variables, equations (2.105) and (2.106) are

$$\eta_t + \nabla\bullet[(h+\eta)\tilde{\mathbf{u}}] = -\nabla\left\{\tfrac{1}{2}h^2\nabla[\nabla\bullet(h\tilde{\mathbf{u}})] - \tfrac{1}{6}h^3\nabla(\nabla\bullet\tilde{\mathbf{u}})\right\} \tag{2.107}$$

$$\tilde{\mathbf{u}}_t + (\tilde{\mathbf{u}}\bullet\nabla)\tilde{\mathbf{u}} + g\nabla\eta = 0 \tag{2.108}$$

2.4.6.2. 2D horizontal equations in terms of $\overline{\mathbf{u}}$

The 1D equations (2.78) and (2.81) can be converted into the 2D forms

$$\mathbf{Q}_1 + \varepsilon\mathbf{Q}_2 = (h+\varepsilon\eta)\overline{\mathbf{u}} \tag{2.109}$$

$$\mathbf{U}_1 + \varepsilon\mathbf{U}_2 = \overline{\mathbf{u}} - \mu^2\tfrac{1}{2}h\nabla[\nabla\bullet(h\overline{\mathbf{u}})] + \mu^2\tfrac{1}{6}h^2\nabla(\nabla\bullet\overline{\mathbf{u}}) \tag{2.110}$$

Substituting equations (2.109) and (2.110) into equations (2.101) and (2.102) leads to the 2D Boussinesq-type equations of Peregrine (1967) in terms of the depth-averaged horizontal velocity $\overline{\mathbf{u}}$

$$\eta_t + \nabla \bullet [(h + \varepsilon\eta)\bar{\mathbf{u}}] = 0 \tag{2.111}$$

$$\bar{\mathbf{u}}_t + \varepsilon(\bar{\mathbf{u}} \bullet \nabla)\bar{\mathbf{u}} + \nabla\eta = \mu^2\left\{\tfrac{1}{2}h\nabla[\nabla \bullet (h\bar{\mathbf{u}}_t)] - \tfrac{1}{6}h^2\nabla(\nabla \bullet \bar{\mathbf{u}}_t)\right\} + O(\varepsilon\mu^2, \mu^4) \tag{2.112}$$

In dimensional quantities, equations (2.111) and (2.112) are

$$\eta_t + \nabla \bullet [(h + \eta)\bar{\mathbf{u}}] = 0 \tag{2.113}$$

$$\bar{\mathbf{u}}_t + (\bar{\mathbf{u}} \bullet \nabla)\bar{\mathbf{u}} + g\nabla\eta = \tfrac{1}{2}h\nabla[\nabla \bullet (h\bar{\mathbf{u}}_t)] - \tfrac{1}{6}h^2\nabla(\nabla \bullet \bar{\mathbf{u}}_t) \tag{2.114}$$

Chapter Three

1D Basic Model

3.1. Introduction

In recent investigations, Boussinesq-type equations have been developed to enable the prediction of the shape of waves as they propagate from deep water to shallow water. Peregrine (1967) derived two sets of Boussinesq-type equations for water of varying depth, which were able to describe the non-linear transformation of irregular, multidirectional waves in shallow water. These formulations were based on the Euler equation of motion and the depth-integrated equation for the conservation of mass of an incompressible, inviscid fluid.

Nwogu (1993) developed a new approach in the derivation of a novel set of Boussinesq-type equations that were expressed in terms of the velocity at an arbitrary elevation or z-level as the velocity variable. This was in contrast to the commonly used depth-averaged velocity, which was used in the standard form of the Boussinesq-type equations derived by Peregrine (1967), or depth-integrated velocity components (i.e. volume flux) as developed, for example by Abbott *et al.* (1978), Madsen *et al.* (1991) and Madsen and Sørensen (1992). Numerical experimentation to determine the wave celerity error in the linearised formulations of Nwogu showed that Nwogu's equations were applicable to incident deep water waves (i.e. h/L = ½) with a particular value of α, where $\alpha = 0.5\,(z_\alpha/h)^2 + z_\alpha/h$ (Figures 3.2, 4.1 and 4.2). z_α defines the elevation of the horizontal velocity. A Crank-Nicholson implicit finite difference scheme was employed by Nwogu together with a predictor-corrector method to estimate the initial values of the dependent variables when advancing each time step.

Nwogu demonstrated that the water surface elevation of a regular wave train and the surface elevation spectra of irregular wave trains were well predicted. Although the effect of bottom friction was not included in Nwogu's model, comparisons of Nwogu's numerical model results and laboratory data seemed to indicate that bottom friction was not an important factor for the extent of the concrete beach, wave conditions and beach slope used in Nwogu's experiments.

Subsequently, Wei and Kirby (1995) developed a high order numerical scheme for Nwogu's formulations. A fourth-order predictor-corrector method was used to advance the solution in time and the spatial derivatives were discretised to a sufficient order of accuracy to avoid contamination of the second- and third-order spatial derivatives in the governing equations by the truncation errors. For the 1D version of the numerical model, Wei and Kirby also showed good predictions for the simulation of solitary waves propagating over a very long, flat bottom and for the simulation of random waves evolving on a slope. In another investigation of the 1D version of the numerical model reported in the same reference, they studied random waves propagating over a channel with a slope. Comparisons of the numerical model results with laboratory measurements showed that the numerical model reproduced the waveform quite well.

In spite of the equations of Nwogu (1993) having been solved by Nwogu and by Wei and Kirby (1995), these equations are still of interest to study. In the present study, the 1D version of the Boussinesq-type equations derived by Nwogu (1993) is discretised by the present author using the numerical approach used by Wei and Kirby (1995). However, the boundary conditions, which are determined here, are different to the boundary conditions in the work of Wei and Kirby (1995). A comparison of the differences in the approaches taken by various investigators can be found in Table 3.1.

Investigators	**Nwogu (1993)**	**Wei and Kirby (1995)**	**Mera (present study)**
Governing equations	Nwogu (1993)	Nwogu (1993)	Nwogu (1993)
Numerical scheme	Crank-Nicholson and Predictor-Corrector	Wei and Kirby (1995) (Fourth- and second-order accurate finite difference schemes for spatial derivatives. Third-order predictor & fourth-order corrector schemes for time integration)	Wei and Kirby (1995) (Fourth- and second-order accurate finite difference schemes for spatial derivatives. Third-order predictor & fourth-order corrector schemes for time integration)
Incoming wave boundary condition	1) Regular waves: sinusoidal monochromatic waves 2) Random waves: JONSWAP spectrum	1) Regular waves: sinusoidal monochromatic waves 2) Random waves: Pierson-Moskowitz spectrum	Regular waves: sinusoidal monochromatic waves
Outgoing wave boundary condition	Sommerfeld radiation condition	Engquist and Majda (1977)	Sommerfeld radiation condition
Other explanation relating to the outgoing wave boundary condition	Not discussed	Damping terms added to the momentum equation	Sommerfeld radiation condition is discretised explicitly and implicitly.
Test cases	1) Monochromatic wave propagation over a sloping bed. 2) Irregular waves.	1) Solitary wave propagation over a flat bottom. 2) Random wave evolution on a slope.	1) Monochromatic wave propagation over a sloping bed. 2) Monochromatic wave propagation over a submerged bar.

Table 3.1. Differences between the current and previous research studies.

At the incoming wave boundary, the free surface elevation is varied sinusoidally with time and the horizontal orbital velocity is obtained by considering a small amplitude, periodic wave. The Sommerfeld radiation condition is then discretised explicitly and implicitly by the present author to estimate predicted and corrected values of the free surface elevation at the outgoing wave boundary. Meanwhile, by substituting the Sommerfeld radiation condition and a small amplitude, periodic wave into the continuity equation with a locally constant depth, the horizontal velocity at the outgoing wave boundary is obtained. In this way, implementing non-reflecting wave boundary conditions, which use a sponge or damping layer, are not needed.

Finally in this chapter, an alternative numerical model is developed herein and is referred to as 1DBMW-1. This model is run for two experimental set-ups in which wave shoaling is significant. The first set-up considered is the propagation of regular waves over a constant slope. The second set-up modelled is of a regular wave train propagating in a channel with a submerged bar.

3.2. New derivation of the equations of Nwogu (1993)

Nwogu (1993) proposed a set of Boussinesq-type equations applicable to the horizontal propagation of regular or irregular, multi-directional waves in water of varying depth. Using the non-dimensional governing equations and boundary conditions for an inviscid, incompressible fluid motion (Section 2.4), the present author derives the equations of Nwogu (1993) as follows (see Figures 1.4 or 3.1).

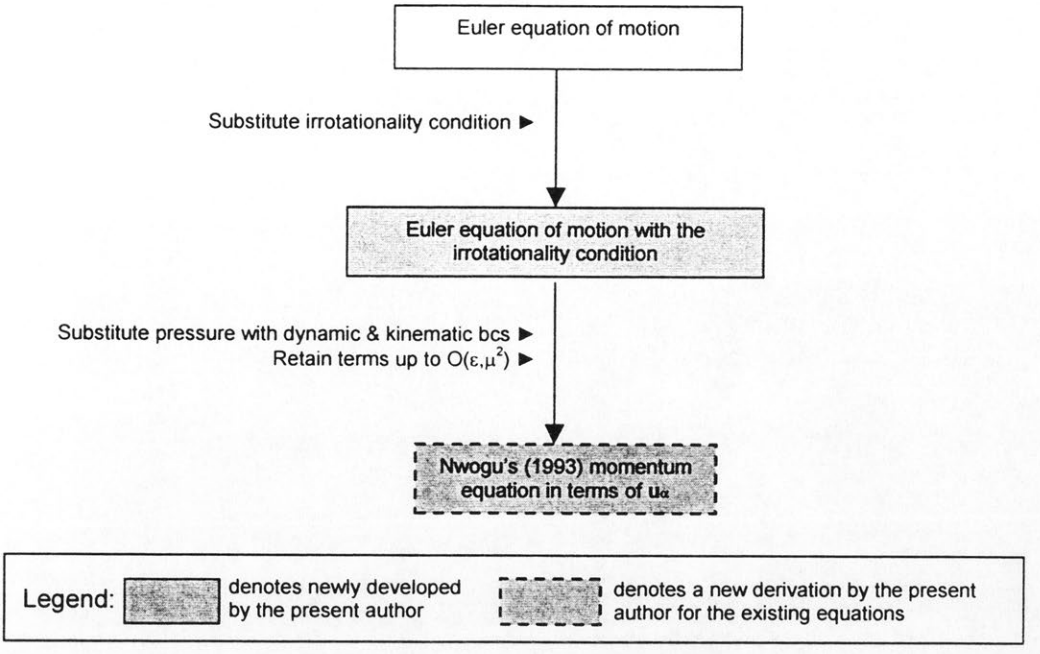

Figure 3.1. New derivation of Nwogu's (1993) momentum equation.

In the work of Nwogu (1993) and Chen et *al.* (1998), the Boussinesq-type momentum equations were obtained from the depth-integrated momentum equation (2.37) [or (2.38)]. This depth-integrated momentum equation was obtained by integrating the horizontal Euler equation of motion (2.90) and applying the boundary conditions for the free surface and seabed [(2.92) through to (2.94)]. Based on the *non-dimensional* variables defined by equations (2.31) and (2.32), equation (2.37) can be written in *non-dimensional* form as

$$\frac{\partial}{\partial t}\int_{-h}^{\varepsilon\eta}\mathbf{u}\,dz+\varepsilon(\mathbf{u}\bullet\nabla)\int_{-h}^{\varepsilon\eta}\mathbf{u}\,dz+\nabla\int_{-h}^{\varepsilon\eta}p\,dz-p\big|_{z=-h}\nabla h=0 \tag{3.1}$$

where the primes have been dropped. The resulting equation (3.1) becomes difficult and complicated when applied to derivations of Boussinesq-type equations with higher order terms than those with terms of $O(\varepsilon,\mu^2)$ included. Consequently, a different approach is developed in this study in which the irrotationality condition (2.95a) is applied to the horizontal Euler equation of motion (2.90) to give

$$\mathbf{u}_t + \varepsilon(\mathbf{u} \bullet \nabla)\mathbf{u} + \frac{\varepsilon}{\mu^2} w\nabla w + \nabla p = 0 \tag{3.2}$$

The Boussinesq-type momentum equation is then obtained directly from equation (3.2) instead of from the depth-integrated momentum equation such as equation (3.1). The boundary conditions at (i) the free surface and (ii) the bed will now be incorporated into the pressure and vertical velocity terms in equation (3.2).

(i) Free surface boundary conditions:

Integration of the vertical Euler equation of motion (2.91) from z to $\varepsilon\eta$ leads to an expression for pressure. The dynamic and kinematic boundary conditions at the free surface [(2.92) and (2.93)] are subsequently incorporated into the equation of pressure and this results in

$$p = \eta - \frac{z}{\varepsilon} + \frac{\partial}{\partial t}\int_z^{\varepsilon\eta} w\,dz + \varepsilon(\mathbf{u} \bullet \nabla)\int_z^{\varepsilon\eta} w\,dz - \frac{\varepsilon}{\mu^2} w^2 \tag{3.3}$$

(ii) Bed boundary condition:

An expression for the vertical velocity w is obtained by integration of the continuity equation (2.89) from the seabed to z. Subsequent substitution of the seabed kinematic boundary condition (2.94) leads to

$$w = -\mu^2 \nabla \bullet \int_{-h}^{z} \mathbf{u}\,dz \tag{3.4}$$

Equation (3.4) is also utilised in the work of Nwogů (1993) and Chen et *al.* (1998).

The horizontal velocity of the fluid is expanded as a Taylor series with respect to the arbitrary level velocities $\mathbf{u}_\alpha = \mathbf{u}(x, y, z_\alpha, t)$ instead of the seabed velocities $\mathbf{u}_b = \mathbf{u}(x, y, -h, t)$ as utilised by Nwogu.

$$\begin{aligned} \mathbf{u}(x,y,z,t) &= \mathbf{u}(x,y,z_\alpha,t) + (z - z_\alpha)\mathbf{u}_z(x,y,z_\alpha,t) + \tfrac{1}{2}(z - z_\alpha)^2\mathbf{u}_{zz}(x,y,z_\alpha,t) + \ldots \\ &= \mathbf{u}_\alpha + (z - z_\alpha)\mathbf{u}_{\alpha_z} + \tfrac{1}{2}(z - z_\alpha)^2\mathbf{u}_{\alpha_{zz}} + \ldots \end{aligned} \tag{3.5}$$

The vertical velocity equation (3.4) can be written as

$$w = -\mu^2 \nabla \bullet [\mathbf{u}(z+h)]$$

$$= -\mu^2 [z \nabla \bullet \mathbf{u} + \nabla \bullet (h\mathbf{u})] \tag{3.6}$$

Making use of equation (2.95a) (i.e. $\mathbf{u}_z = \nabla w$) for the irrotationality condition, $\mathbf{u}_z$ and $\mathbf{u}_{zz}$ can be obtained as

$$\mathbf{u}_z = -\mu^2 \{ z \nabla (\nabla \bullet \mathbf{u}) + \nabla [\nabla \bullet (h\mathbf{u})] \} \tag{3.7}$$

and

$$\mathbf{u}_{zz} = -\mu^2 \nabla (\nabla \bullet \mathbf{u}) \tag{3.8}$$

Evaluating the horizontal velocity in equations (3.7) and (3.8) at $z = z_\alpha$ gives

$$\mathbf{u}_{\alpha_z} \cong -\mu^2 \{ z_\alpha \nabla (\nabla \bullet \mathbf{u}_\alpha) + \nabla [\nabla \bullet (h\mathbf{u}_\alpha)] \} \tag{3.9}$$

and

$$\mathbf{u}_{\alpha_{zz}} \cong -\mu^2 \nabla (\nabla \bullet \mathbf{u}_\alpha) \tag{3.10}$$

Substituting equations (3.9) and (3.10) into (3.5) leads to the horizontal velocity as

$$\mathbf{u} = \mathbf{u}_\alpha - \mu^2 (z - z_\alpha) \{ z_\alpha \nabla (\nabla \bullet \mathbf{u}_\alpha) + \nabla [\nabla \bullet (h\mathbf{u}_\alpha)] \} - \mu^2 \tfrac{1}{2} (z - z_\alpha)^2 \nabla (\nabla \bullet \mathbf{u}_\alpha) + ..$$

$$= \mathbf{u}_\alpha + \mu^2 \{ \Gamma_\alpha - \tfrac{1}{2} z^2 \nabla (\nabla \bullet \mathbf{u}_\alpha) - z \nabla [\nabla \bullet (h\mathbf{u}_\alpha)] \} + \text{truncation error} \tag{3.11}$$

where

$$\Gamma_\alpha = \tfrac{1}{2} z_\alpha^{\ 2} \nabla (\nabla \bullet \mathbf{u}_\alpha) + z_\alpha \nabla [\nabla \bullet (h\mathbf{u}_\alpha)] \tag{3.11a}$$

Substituting equation (3.11) into (3.4) for w and retaining terms of $O(\mu^2)$ gives the vertical velocity, that is

$$w = -\mu^2 [z \nabla \bullet \mathbf{u}_\alpha + \nabla \bullet (h\mathbf{u}_\alpha)] + O(\mu^4) \tag{3.12}$$

The truncation error for equation (3.11) can be determined by integrating the irrotationality condition (2.95a) from z_α to z. This reads

$$\mathbf{u} - \mathbf{u}_\alpha = \int_{z_\alpha}^{z} \nabla w \, dz \tag{3.13}$$

Substitution of equation (3.12) into (3.13) leads to

$$\mathbf{u} = \mathbf{u}_\alpha + \mu^2 \left\{ \Gamma_\alpha - \tfrac{1}{2} z^2 \nabla(\nabla \bullet \mathbf{u}_\alpha) - z \nabla[\nabla \bullet (h\mathbf{u}_\alpha)] \right\} + O(\mu^4) \tag{3.14}$$

The 'spirit' of the *classical* Boussinesq-type equations is a balance between $O(\varepsilon)$ (non-linearity) and $O(\mu^2)$ (frequency dispersion), which these terms are small, i.e. $O(\varepsilon) = O(\mu^2) << 1$. With this in mind, the pressure field is then obtained by inserting equation (3.12) for w and (3.14) for **u** into equation (3.3) for p and retaining terms up to $O(\varepsilon)$ and $O(\mu^2)$. This leads to

$$p = \eta - \frac{z}{\varepsilon} + \mu^2 \left[\tfrac{1}{2} z^2 \nabla \bullet \mathbf{u}_{\alpha_t} + z \nabla \bullet (h \mathbf{u}_{\alpha_t}) \right] + O(\varepsilon \mu^2, \mu^4) \tag{3.15}$$

With terms up to $O(\varepsilon)$ and $O(\mu^2)$, equations (3.14) and (3.15) show that the horizontal velocity vector and pressured field vary quadratically through the water column.

Substituting equation (3.14) for **u** into the depth-integrated continuity equation (2.96) and retaining terms up to $O(\varepsilon)$ and $O(\mu^2)$ leads to equation (3.16). Substituting equations (3.12) for w, (3.14) for **u** and (3.15) for p into equation (3.2) and retaining terms up to $O(\varepsilon)$ and $O(\mu^2)$ gives equation (3.17).

$$\eta_t + \nabla \bullet [(h + \varepsilon\eta)\mathbf{u}_\alpha] + \mu^2 \nabla \bullet (h\overline{\Gamma}) = O(\varepsilon\mu^2, \mu^4) \tag{3.16}$$

$$\mathbf{u}_{\alpha_t} + \nabla\eta + \varepsilon(\mathbf{u}_\alpha \bullet \nabla)\mathbf{u}_\alpha + \mu^2 \Gamma_{\alpha_t} = O(\varepsilon\mu^2, \mu^4) \tag{3.17}$$

where Γ_α is defined by equation (3.11a) and

$$\overline{\Gamma} = \Gamma_\alpha - \tfrac{1}{6} h^2 \nabla(\nabla \bullet \mathbf{u}_\alpha) + \tfrac{1}{2} z \nabla[\nabla \bullet (h\mathbf{u}_\alpha)] \tag{3.18}$$

Equations (3.16) and (3.17) are exactly the same as the set of Boussinesq-type equations derived by Nwogu (1993)

It can be seen that the present derivation for the equations of Nwogu is different to the derivation of the equations of Peregrine (1967) in Chapter Two, which uses a perturbation method. However, both approaches retain the same orders in the terms of the measures of non-linearity and frequency dispersion, i.e. up to $O(\varepsilon,\mu^2)$. This indicates that both formulations are applicable for simulating weakly non-linear waves.

The continuity and momentum equations respectively [(3.16) and (3.17)] can be expressed in 1D *dimensional* form as

$$\eta_t + [(h+\eta)u_\alpha]_x + \left(\tfrac{1}{2}z_{c\alpha}^2 - \tfrac{1}{6}\right)(h^3 u_{\alpha_{xx}})_x + \left(z_{c\alpha} + \tfrac{1}{2}\right)[h^2(hu_\alpha)_{xx}]_x = 0 \qquad (3.19)$$

$$u_{\alpha_t} + g\eta_x + u_\alpha u_{\alpha_x} + z_\alpha\left[\tfrac{1}{2} z_\alpha u_{\alpha_{txx}} + (hu_{\alpha_t})_{xx}\right] = 0 \qquad (3.20)$$

where again the subscripts x and t denote partial differentiation with respect to the x-direction and time respectively, η = free surface elevation, h = local water depth, u_α = horizontal velocity at an arbitrary level ($z = z_\alpha$) below still water level, g = gravitational acceleration,

$$z_\alpha = z_{c\alpha}\, h \qquad -1 \le z_{c\alpha} \le 0 \qquad (3.21)$$

and

$$\alpha = \tfrac{1}{2}(z_{c\alpha})^2 + z_{c\alpha} \qquad -0.5 \le \alpha \le 0 \qquad (3.22)$$

$\alpha = 0$ corresponds to $z_{c\alpha} = 0$ and $z_\alpha = 0$ (at still water)

$\alpha = -½$ corresponds to $z_{c\alpha} = -1$ and $z_\alpha = -h$ (at the bed)

(See Appendix A for definition for η, u_α, v_α, z, z_α, x, y).

3.3. Review of dispersion relations

The linearised forms (non-linear terms dropped) of the 1D Boussinesq-type equations of Nwogu (1993) for constant depth can be expressed as

$$\eta_t + hu_{\alpha_x} + \left(\alpha + \tfrac{1}{3}\right)h^3 u_{\alpha_{xxx}} = 0 \tag{3.23}$$

$$u_{\alpha_t} + g\eta_x + \alpha h^2 u_{\alpha_{xxt}} = 0 \tag{3.24}$$

Consider a small amplitude, periodic wave with the angular frequency $\omega = 2\pi/T$ and the wave number $k = 2\pi/L$, where T = wave period and L = wave length, that is

$$\eta = \eta_a \exp[i(kx - \omega t)], \qquad u_\alpha = u_{\alpha a} \exp[i(kx - \omega t)] \tag{3.25}$$

in which η_a and $u_{\alpha a}$ are the amplitudes of the water surface elevation and of the horizontal velocity respectively. Substituting equations (3.25) into equations (3.23) and (3.24) gives the dispersion relation, which corresponds to a Padé [2,2] approximation in terms of (kh), that is.

$$(C_{[2,2]})^2 = gh\frac{1-\left(\alpha + \frac{1}{3}\right)(kh)^2}{1-\alpha(kh)^2} \tag{3.26}$$

where $C_{[2,2]}$ is the wave celerity corresponding to the linearised equations of Nwogu. The wave celerity $C_{[2,2]}$ is normalised by using the celerity C_{Airy} from Airy wave theory, where

$$(C_{Airy})^2 = \frac{g}{k}\tanh(kh) \tag{3.27}$$

Figure 3.2 shows that the normalised wave celerity for different values of α are plotted as a function of (kh). Shallow water depth corresponds to $kh < 0.1\pi$ (or $h/L < 1/20$) and deep water depth is $kh \geq \pi$ (or $h/L \geq ½$). An optimum value of α may be determined by minimising the wave celerity error over the entire range of $0 < kh < \pi$. Nwogu obtained a value of $\alpha = -0.390$ which corresponds to $z_\alpha = -0.531h$ with a maximum error of less than 1 % in $C_{[2,2]}/C_{Airy}$ over the entire range of $0 < kh < \pi$. This is in contrast to the standard form of the Boussinesq-type equations, which had a value of $\alpha = -1/3$ and resulted in a wave celerity error of 14 % when kh = 3.0. This confirms that the dispersion relation of Nwogu's equations depends strongly on the choice of the α value.

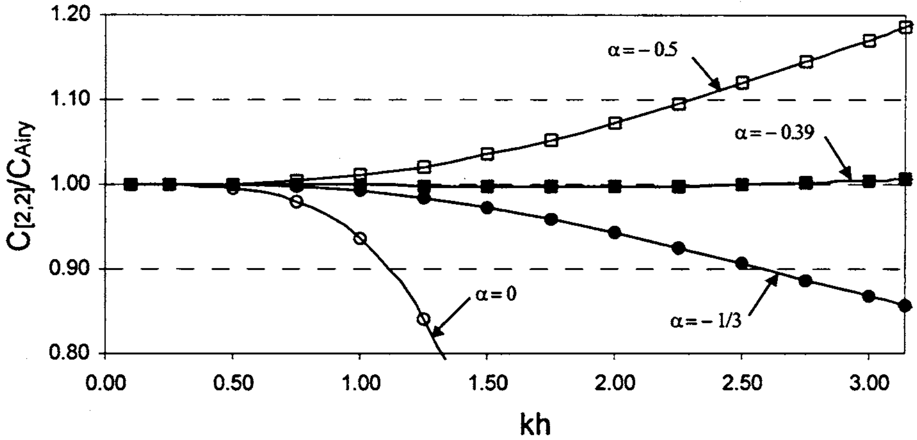

Figure 3.2. Effect of α ($-0.5 \le \alpha \le 0$) on the ratio of the wave celerity corresponding to the 1D linearised form of the equations of Nwogu (1993) over the wave celerity corresponding to Airy wave theory: $\alpha = -0.5$, $\alpha = 0$, $\alpha = -1/3$ (or equivalently the equations by Peregrine), and $\alpha = -0.390$ (obtained by Nwogu).

3.4. Numerical solution algorithm for the 1D basic model (1DBMW-1)

3.4.1. Solution method

The governing equations [(3.19) and (3.20)] are solved by the present author using a non-staggered finite difference method. The solution is advanced in time using the third-order Adams-Bashforth predictor and fourth-order Adams-Moulton corrector method. The first-order spatial derivatives are approximated by a fourth-order accurate finite difference scheme. However, the second-order accurate finite difference operators are employed to approximate the second- and third-order spatial derivatives (see Appendix B). The use of high order discretisation in space and time can avoid unwanted numerical diffusion errors, which are proportional to second-order spatial derivatives. The numerical technique adopted here follows the approach of Wei and Kirby (1995). Although the present model and Wei and Kirby's model are based on the same governing equations and numerical scheme, the present model is to be used as a basis for comparisons with other newly developed models in this thesis.

The *dimensional* Boussinesq-type continuity equation (3.19) can be written as

$$\eta_t = E(\eta, u_\alpha) \tag{3.28}$$

where

$$E(\eta, u_\alpha) = -[(h+\eta)u_\alpha]_x - \left(\tfrac{1}{2}z_\alpha^2 - \tfrac{1}{6}\right)(h^3 u_{\alpha_{xx}})_x - \left(z_\alpha + \tfrac{1}{2}\right)[h^2(hu_\alpha)_{xx}]_x \tag{3.29}$$

The *dimensional* Boussinesq-type momentum equation (3.20) can be expressed as

$$U_{\alpha_t} = F(\eta, u_\alpha) \tag{3.30}$$

where the variable groupings U_α and F are defined respectively as

$$U_\alpha = u_\alpha + z_\alpha\left[\tfrac{1}{2} z_\alpha\, u_{\alpha_{xx}} + (hu_\alpha)_{xx}\right] \tag{3.31}$$

$$F(\eta, u_\alpha) = -g\eta_x - u_\alpha u_{\alpha_x} \tag{3.32}$$

The steps in the model solutions process are:

- Values of η_i^{t+1} and the intermediate, velocity related variable $U_{\alpha_i}^{t+1}$ are calculated directly using the third-order explicit, Adams-Bashforth three-step predictor scheme applied to equations (3.28) and (3.30) respectively to give

$$\eta_i^{t+1} = \eta_i^t + \tfrac{1}{12}\Delta t[23E^t - 16E^{t-1} + 5E^{t-2}]_i + O(\Delta t^3) \tag{3.33}$$

$$U_{\alpha_i}^{t+1} = U_{\alpha_i}^t + \tfrac{1}{12}\Delta t[23F^t - 16F^{t-1} + 5F^{t-2}]_i + O(\Delta t^3) \tag{3.34}$$

where the time level t (superscript) refers to values at the present, known time level. All the terms on the right hand sides of equations (3.33) and (3.34) are known from previous calculations.

- The values of ${U_\alpha}_i^{t+1}$ are then used to predict the horizontal velocity at the new time level ${u_\alpha}_i^{t+1}$ using equation (3.31). This calculation requires the solution of a tridiagonal matrix system in which the coefficient matrix is constant in time as prescribed by equation (3.35). This equation is easily solved using Gaussian elimination.

$$\begin{bmatrix} \text{Coefficient} \\ \\ \text{matrix} \end{bmatrix} \left\{ u_\alpha \right\}^{t+1} = \left\{ U_\alpha \right\}^{t+1} \qquad (3.35)$$

- The newly predicted values of η_i^{t+1} and ${u_\alpha}_i^{t+1}$ are then used to calculate E_i^{t+1} and F_i^{t+1} using equations (3.29) and (3.32), respectively.

- In the next step, the fourth-order Adams-Moulton four-step corrector is employed to equations (3.28) and (3.30) respectively, which are written as

$$\eta_i^{t+1} = \eta_i^t + \tfrac{1}{24}\Delta t[9E^{t+1} + 19E^t - 5E^{t-1} + E^{t-2}]_i + O(\Delta t^5) \qquad (3.36)$$

$${U_\alpha}_i^{t+1} = {U_\alpha}_i^t + \tfrac{1}{24}\Delta t[9F^{t+1} + 19F^t - 5F^{t-1} + F^{t-2}]_i + O(\Delta t^5) \qquad (3.37)$$

- The corrector step is repeated if the misclose between two successive results exceeds a pre-set upper limit. The misclose in each of the two dependent variables η and u_α is calculated separately as defined below:

$$\Delta f = \frac{\sum_i \left| f_i^{t+1} - f_i^{(t+1)^*} \right|}{\sum_i \left| f_i^{t+1} \right|} \qquad (3.38)$$

where f denotes either η or u_α and $(\ )^*$ denotes the previous calculation. The corrector phase of the calculation is repeated if $\Delta f > 0.001$ or 0.1 % in either η or u_α.

The values of the free surface elevation and horizontal velocity determined above are for inside the fluid domain. At the boundaries, these values are determined using the boundary conditions explained below.

3.4.2. Boundary conditions

3.4.2.1. Incoming wave boundary conditions

The free surface elevation η at the incoming wave boundary is varied sinusoidally with time as

$$\eta = \tfrac{1}{2}H_i\cos(kx - \omega t) \qquad (3.39)$$

where H_i = incident wave height. For a locally constant depth, the continuity equation (3.19) simplifies to

$$\eta_t + u_\alpha\eta_x + (h+\eta)u_{\alpha_x} + \left(\alpha + \tfrac{1}{3}\right)h^3 u_{\alpha_{xxx}} = 0 \qquad (3.40)$$

The horizontal orbital velocity u_α at the incoming wave boundary can be obtained by substituting equations (3.25) into equation (3.40) and assuming that $\eta << h$ to give

$$u_\alpha = \frac{\omega\eta}{kh\left[1-\left(\alpha+\frac{1}{3}\right)(kh)^2\right]} \qquad (3.41)$$

Equation (3.41) automatically satisfies the Sommerfeld radiation condition (3.42) (see next section).

3.4.2.2. Outgoing wave boundary conditions

At the outgoing wave boundary, a 1D non-reflecting wave boundary condition is used to allow the passage and egress of the wave energy arriving from within the domain. An equation, which is equivalent to the Sommerfeld radiation condition, is applied to the present model, that is.

$$\eta_t + C\eta_x = 0 \tag{3.42}$$

where $C = \omega/k$. In practice, there will be some wave reflection from the boundary due to truncation errors, the initial transient, steep waves and the approximation of the wave celerity for irregular waves (Nwogu, 1993). Discretising the Sommerfeld radiation condition (3.42) explicitly gives the free surface elevation at the predictor stage in equation (3.43) and implicitly at the corrector stage in equation (3.44).

$$\eta_1^{t+1} = \eta_1^t - \frac{\Delta t}{\Delta x} C(3\eta_1 - 4\eta_2 + \eta_3)^t + O(\Delta x^2, \Delta t^2) \tag{3.43}$$

and

$$\eta_1^{t+1} = \frac{1}{3\left(1 + \frac{\Delta t}{\Delta x} C\right)} \left[4\eta_1^t - \eta_1^{t-1} + \frac{\Delta t}{\Delta x} C(4\eta_2 - \eta_3)^{t+1}\right] + O(\Delta x^2, \Delta t^2) \tag{3.44}$$

where the x-axis is as defined in Appendix A.

The corresponding horizontal orbital velocity at the outgoing wave boundary is obtained by substituting equations (3.25) and equation (3.42) into the continuity equation with a locally constant depth (3.40) to give an equation, which is exactly the same as equation (3.41). The set of boundary conditions for 1DBMWC-1 are displayed in Figure 3.3 for waves only case.

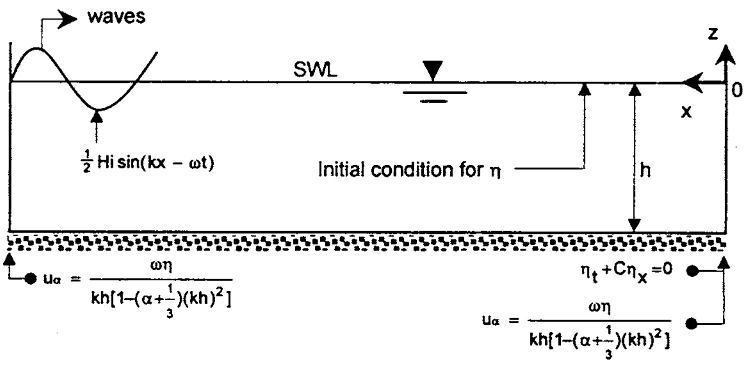

Figure 3.3. Boundary conditions for 1DBMW-1.

3.5. Model verification

3.5.1. Experimental set-up 1: Wave propagation up a slope

Solutions from the present numerical model (1DBMW-1) are compared with laboratory data collected by Nwogu (1993). The basin was 30 m wide, 20 m long and 3 m deep with a 1:25 constant slope beach with an impermeable concrete cover. The toe of the beach was located 4.6 m from the wave paddle and the water depth near the paddle was 0.56 m (Figure 3.4). Two tests are conducted with an incident deepwater wave ($h_i/L_o = 0.5$) and an intermediate depth water ($h_i/L_o = 0.36$).

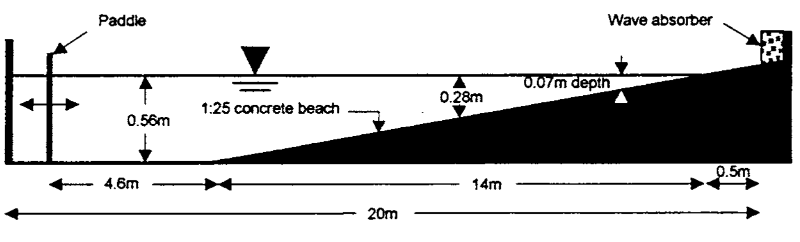

Figure 3.4. Experimental set-up 1 (Nwogu, 1993): the basin terminates with a 1:25 constant slope, concrete beach.

Test no. 1

In the first test with experimental set-up 1, an *incident deep water wave* ($T = 0.85$ s and $h_i/L_o = 0.5$) propagates from the incoming wave boundary where the depth is $h_i = 0.56$ m to the outgoing wave boundary at a depth of 0.07 m (rather than zero depth). The test conditions are: $H_i = 0.04$ m, $H_i/h_i = 0.071$, $k_ih_i = \pi$, $L_o/\Delta x = 28.2$, $T/\Delta t = 50.0$ and the Courant number, based on the incident wave depth, is given by

$$Cr_i = \sqrt{gh_i}\frac{\Delta t}{\Delta x} \tag{3.45}$$

$Cr_i = 1.00$ (in the first test)

Figures 3.5 and 3.6 show comparisons of the measured surface elevation with the predictions from the present numerical model at depths of 0.28 m and 0.07 m respectively. Both figures show that the results from the present numerical model underestimate the wave height by approximately 15 %. At the outgoing wave boundary however (see Figure 3.6), the water surface elevation in the computational model is flatter near the wave troughs compared to the measured waves.

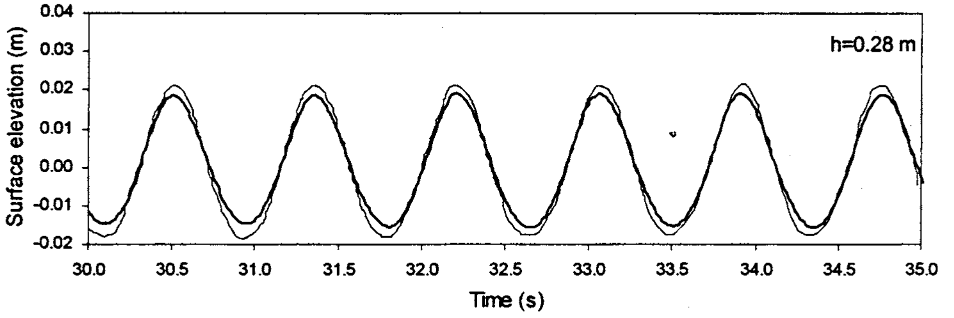

Figure 3.5. Incident deep water waves ($h_i/L_o = 0.5$): time series of the free surface elevation at 0.28 m depth predicted by the present model (bold line) and the laboratory measurements of Nwogu (thin line). Data: $T = 0.85$ s, $H_i = 0.04$ m, $H_i/h = 0.143$, $k_ih_i = \pi$ and $Cr_i = 1.00$.

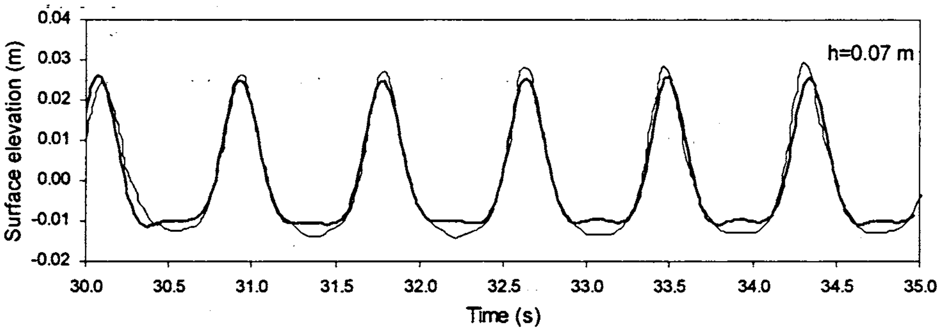

Figure 3.6. Incident deep water waves ($h_i/L_o = 0.5$): time series of the free surface elevation at the outgoing wave boundary (h = 0.07 m) predicted by the present model (bold line) and the laboratory measurements of Nwogu (thin line). Data: T = 0.85 s, $H_i = 0.04$ m, $H_i/h = 0.571$, $k_ih_i = \pi$ and $Cr_i = 1.00$.

Test no. 2

In the second test, also with experimental set-up 1, the shoaling of an *intermediate depth wave* (T = 1 s, $h_i = 0.56$ m and $h_i/L_o = 0.36$) is investigated. The test conditions are: $H_i = 0.066$ m, $H_i/h_i = 0.118$, $k_ih_i = 2.30$, $L_o/\Delta x = 39.0$, $T/\Delta t = 58.8$ and $Cr_i = 1.00$. The time series for the water surface elevation was measured at the outgoing wave boundary (h = 0.10 m) and at a water depth of 0.24 m. The results from the present Boussinesq-type numerical model and the laboratory data at 0.24 m depth agree well as shown in Figure 3.7. In Figure 3.8, the long wave troughs and peaked wave crests in the results of the present numerical model based on Nwogu's equations, is seen to capture the general form of the non-linear waves with the long flat troughs and the peaked wave crests.

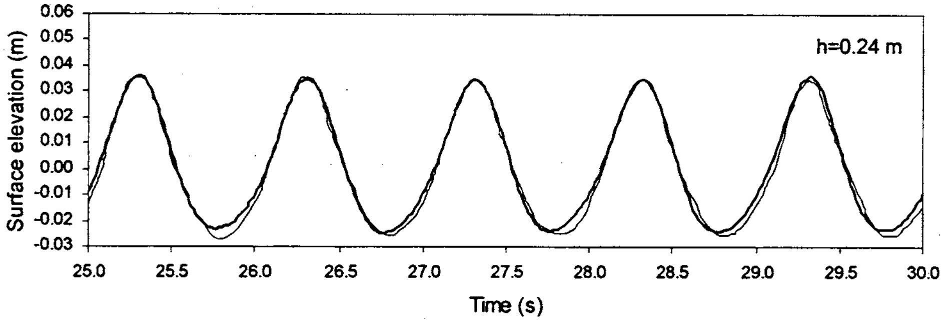

Figure 3.7. Intermediate depth water waves ($h_i/L_o = 0.36$): time series of the free surface elevation at 0.24 m depth predicted by the present model (bold line) and the laboratory measurements of Nwogu (thin line). Data: T = 1 s, $H_i = 0.066$ m, $H_i/h = 0.275$, $k_ih_i = 2.30$ and $C_{ri} = 1.00$.

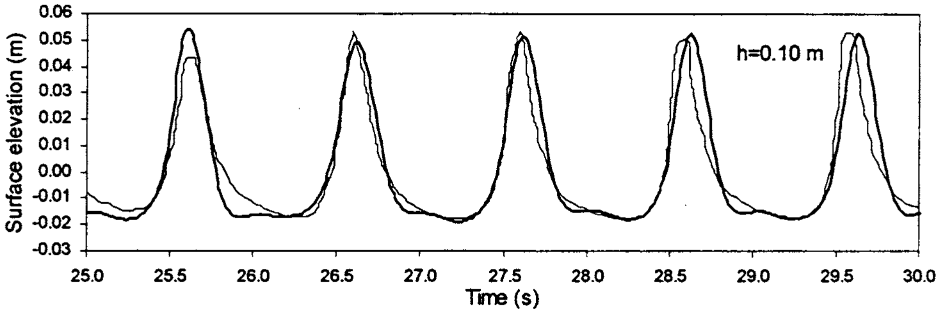

Figure 3.8. Intermediate depth water waves ($h_i/L_o = 0.36$): time series of the free surface elevation at the outgoing wave boundary (h = 0.10 m) predicted by the present model (bold line) and the laboratory measurements of Nwogu (thin line). Data: T = 1 s, $H_i = 0.066$ m, $H_i/h = 0.66$, $k_ih_i = 2.30$ and $C_{ri} = 1.00$.

3.5.2. Experimental set-up 2: Wave propagation in a channel with a submerged bar

The present author also applies the present numerical model to a different experimental set-up i.e. with waves propagating over a submerged bar in a channel. A sketch of the bathymetry is shown in Figure 3.9. The channel is 25 m long, 0.4 m deep on both sides of the bar and 0.1 m deep on top of the bar. The laboratory measurements of Luth *et al.* (1994) (see Borsboom *et al.*, 2000) are used to assess the performance of the present numerical model.

Two tests are conducted with two incident, intermediate waves $h_i/L_o = 0.063$ and $h_i/L_o = 0.251$

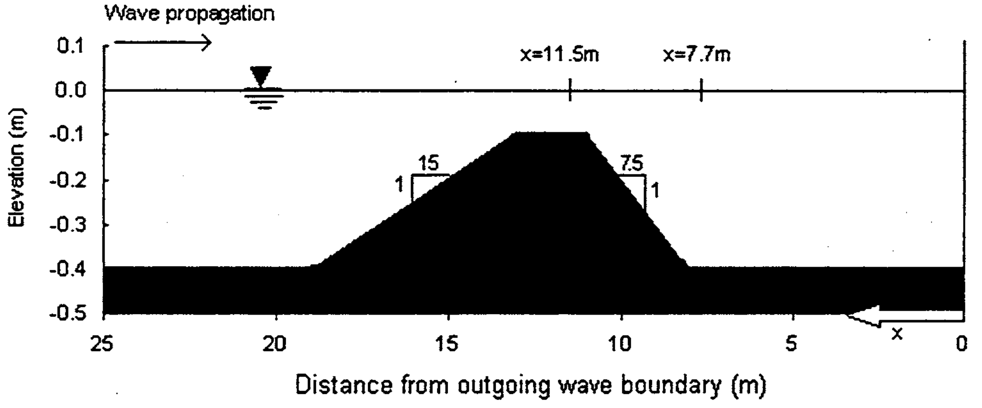

Figure 3.9. Experimental set-up 2 (Luth *et al.*, 1994): submerged bar topography with 25 m long channel, 0.4 m deep on both sides of the bar and 0.1 m deep on top of the bar.

Test no. 1

A train of waves with a period of 2.02 s and an incident wave height of 0.02 m propagates down the channel. The incident wave is an *intermediate depth wave* with $h_i/L_o = 0.63$. The computation is performed with a grid resolution of $L_o/\Delta x = 79.6$ and $T/\Delta t = 50.5$. The Courant number at the incoming wave boundary is 0.99. The time series for the free surface elevation was measured by Luth *et al.* on top of the bar (i.e. 11.5 m before the outgoing wave boundary) and behind the bar (i.e. 7.7 m before the outgoing wave boundary).

Figure 3.10 shows that the present numerical model results capture the main features of the free surface elevation time series at the top of the bar (at chainage $x = 11.5$ m). However, the numerical model is seen to slightly overestimate the highest wave crests, and underestimate the early portions of the lower wave crests. The lowest portions of the wave troughs are well represented by the numerical model.

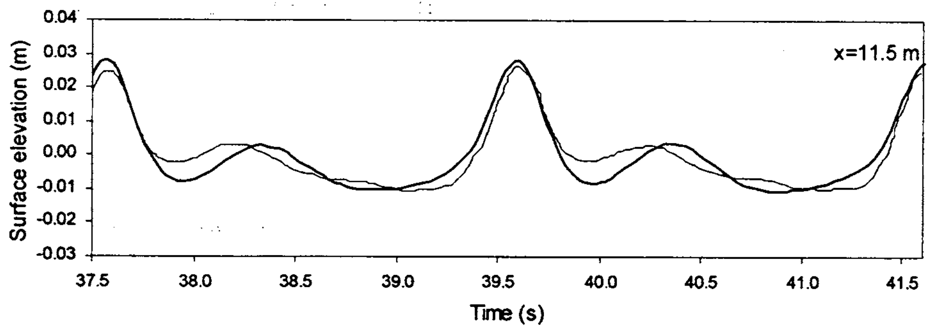

Figure 3.10. Top of the bar (i.e. 11.5 m before the outgoing wave boundary): time series of the water surface elevation predicted by the present model (bold line) and the laboratory measurements of Luth *et al.* (thin line). Data: $T = 2.02$ s, $H_i = 0.02$ m, $H_i/h = 0.2$, $k_ih_i = 0.67$, $h_i/L_o = 0.06$ and $Cr_i = 0.99$.

Figure 3.11 displays the numerical model results on the lee side of the bar at a chainage of $x = 7.7$ m from the outgoing boundary. The free surface elevation predicted by the numerical model marginally exceeds the measured wave crests but underestimates the wave troughs.

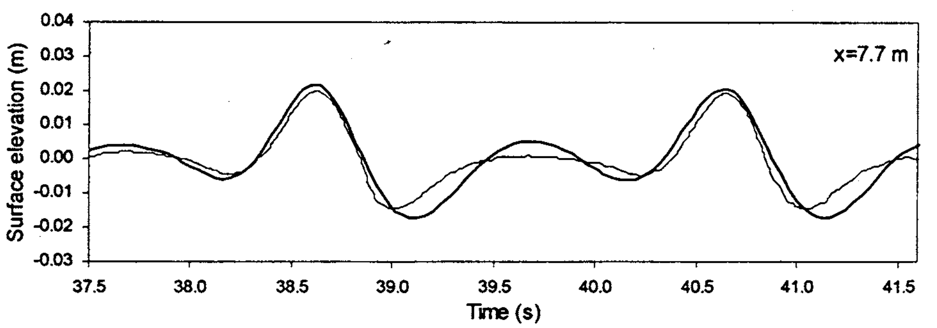

Figure 3.11. Behind the bar (i.e. 7.7 m before the outgoing wave boundary): time series of the water surface elevation predicted by the present model (bold line) and the laboratory measurements of Luth *et al.* (thin line). Data: $T = 2.02$ s, $H_i = 0.02$ m, $H_i/h = 0.05$, $k_ih_i = 0.67$, $h_i/L_o = 0.06$ and $Cr_i = 0.99$.

<u>Test no. 2</u>

The last test conditions for experimental set-up 2 consist of a wave train with 1.01 s period waves and 0.041 m incident wave height propagating over the same bathymetry as displayed in Figure 3.9. The incident wave is an *intermediate depth wave* with $h_i/L_o = 0.251$. The computation is performed with a grid resolution of $L_o/\Delta x = 19.9$ and $T/\Delta t = 33.7$. The Courant number at the incoming wave boundary is 0.74. As for the previous test, the time series for the free surface elevation was measured on top of and behind the submerged bar. Figures 3.12 and 3.13 show comparisons of the measured and predicted surface elevations. In Figure 3.12, the results from the numerical model and laboratory measurements show close agreement through the wave troughs but the numerical model overestimates the wave crests.

On the other hand, Figure 3.13 shows that the present Boussinesq-type numerical model slightly overestimates the wave crests but underestimates wave troughs on the lee side of the submerged bar. The waves in the numerical model are seen to be more symmetrical than the measured waves.

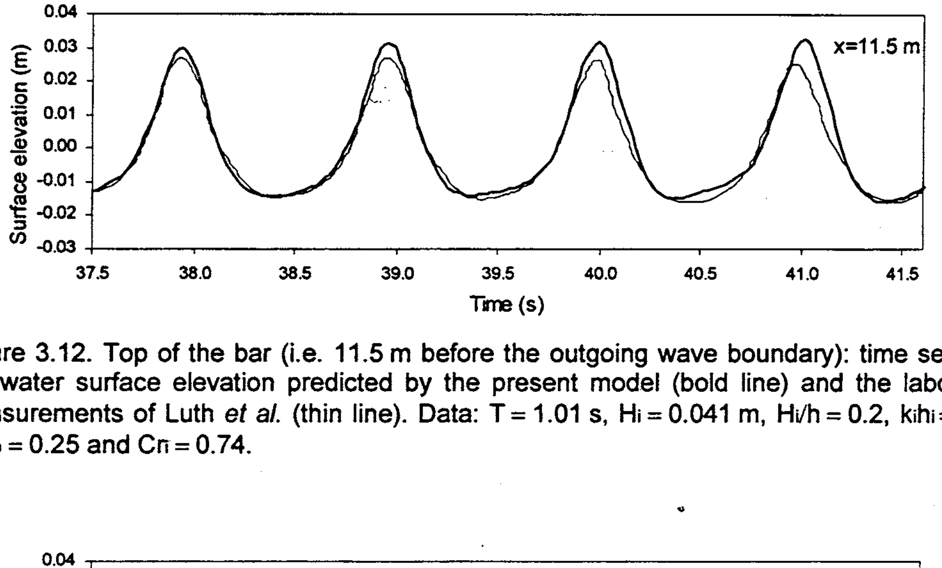

Figure 3.12. Top of the bar (i.e. 11.5 m before the outgoing wave boundary): time series of the water surface elevation predicted by the present model (bold line) and the laboratory measurements of Luth *et al.* (thin line). Data: T = 1.01 s, H_i = 0.041 m, H_i/h = 0.2, k_ih_i = 1.69, h_i/L_o = 0.25 and Cr_i = 0.74.

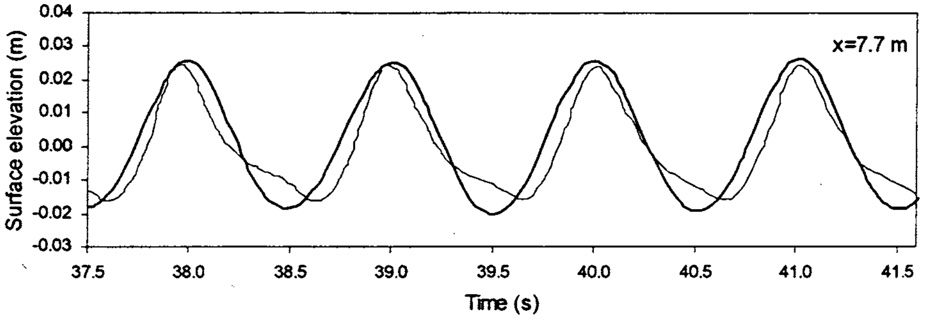

Figure 3.13. Behind the bar (i.e. 7.7 m before the outgoing wave boundary): time series of the water surface elevation predicted by the present model (bold line) and the laboratory measurements of Luth *et al.* (thin line). Data: T = 1.01 s, H_i = 0.041 m, H_i/h = 0.05, k_ih_i = 1.69, h_i/L_o = 0.25 and Cr_i = 0.74.

3.6. Conclusions

A new approach for deriving the Boussinesq-type momentum equation is introduced by the present author. This is done by applying the irrotationality condition to the horizontal Euler equation of motion. The present derivation is formulated directly at the arbitrary z-level velocity. In contrast, in the work of Nwogu (1993), the derivation was first directed through the bottom velocity, and then converted to the velocity at an arbitrary z-level. Although the present and Nwogu's derivations are different, the resulting Boussinesq-type equations are identical.

A 1D numerical model based on the resulting Boussinesq-type equations [i.e. the equations originally derived by Nwogu (1993)] is then developed by the present author as the basic numerical model in 1D. The present numerical model (1DBMW-1) is used to simulate incident monochromatic wave propagation from incident deep water (i.e. $kh = \pi$ or $h/L = ½$) to shallow water. This is confirmed by reasonable agreement between the present numerical model and laboratory data in the channel with a constant slope. The other tests show that the Boussinesq-type wave numerical model is capable of simulating a non-breaking wave transformation in a channel with a submerged bar. The effect of bottom friction is not included in the present numerical model. Comparisons of the results between the numerical model and the laboratory measurements seem to indicate that bottom friction is not a significant factor for the waves propagating over the physical model concrete beach and over the submerged bar used in these tests. However, while the numerical results from the model capture the general features of the waves over the bar, some disparities are noted in Figures 3.11 and 3.13.

The present numerical model is based on varying the incident free surface elevation sinusoidally. The horizontal velocity is then calculated by considering a periodic, small amplitude wave. At the outgoing wave boundary, the Sommerfeld radiation condition is discretised explicitly and implicitly to calculate predicted and corrected values (respectively) of the free surface elevation. The horizontal velocity is obtained by substituting a periodic, small amplitude wave into the continuity equation with a locally constant depth and satisfying the Sommerfeld radiation condition. The numerical model prediction of the water surface elevation at the outgoing wave boundary agrees well with measurements in the laboratory.

In the present numerical model, the numerical scheme, which was introduced by Wei and Kirby (1995), is used instead of the Crank-Nicholson numerical scheme applied to the previous numerical model by Nwogu (1993). The Sommerfeld radiation condition is applied to the present outgoing wave boundary instead of the scheme, which was introduced by Engquist and Majda (1997), used in the previous numerical model by Wei and Kirby (1995).

Chapter Four

1D Basic Model with an Improved Dispersion Relation

4.1. Introduction

It is well known that the major restriction of Boussinesq-type equations is their water depth limitation. Boussinesq-type equations have since been extended in order to obtain an improved dispersion relation in relative deeper water (e.g. by Witting, 1984; Murray, 1989; Madsen *et al.*, 1991; Madsen and Sørensen, 1992; Nwogu, 1993 and Schäffer and Madsen, 1995).

Schäffer and Madsen (1995) developed *two sets* of Boussinesq-type equations. Firstly, they generalised the Boussinesq-type equations of Madsen and Sørensen (1992) without the explicit restriction of small bottom slopes. However, the dispersion relation remained identical to that of Madsen and Sørensen. Secondly, they extended the Boussinesq-type equations of Nwogu (1993) by introducing four new free coefficients $(\beta_1,\beta_2,\gamma_1,\gamma_2) \leq O(1)$ while retaining Nwogu's free coefficient α in their *second set* of Boussinesq-type equations. Schäffer and Madsen's *second set* of Boussinesq-type equations had a dispersion relation, which corresponds to a Padé [4,4] expansion in terms of kh. By making an evaluation of the free coefficients optimised according to some error minimisation criterion, the *second set* of equations was capable of describing wave propagation in 'deeper water' with $h/L \leq 1$. Previously before extending the Boussinesq-type equations, they were only valid for $h/L \leq 0.5$. The differences in the wave celerity of various linearised Boussinesq-type equations relative to the wave celerity of Airy (linear) wave theory at three relative depths are presented in Table 4.1. The relative depth is defined as the ratio of the water depth h, to the deep water wave length L_o. (Note: in deep water i.e. $h/L \geq 0.5$, $L = L_o$).

	$\left(\frac{C_{\text{Boussinesq type equation}}}{C_{\text{Airy wave theory}}} - 1\right) \times 100\ \%$		
Dispersion relation corresponds to:	**at $h/L_o = 0.3$**	**at $h/L_o = 0.5$**	**at $h/L_o = 1.0$**
a Padé [0,2] approximation in kh, such as the equations of Peregrine (1967)	5 % slower	15 % slower	34 % slower
a Padé [2,2] approximation in kh, such as the equations of: Madsen *et. al.* (1991), Madsen and Sørensen (1992) and Nwogu (1993), Mera (Present study)	≈ 0 % faster	< 1 % faster	11.4 % faster
a Padé [4,4] approximation in kh, such as the equations of Schäffer and Madsen (1995)	≈ 0 % faster	≈ 0 % faster	< 1 % faster

Table 4.1. Wave celerity of various linearised Boussinesq-type equations relative to the wave celerity of Airy wave theory.

The aim of the present study is to numerically examine the effects of the additional terms in the *second set* of equations of Schäffer and Madsen (1995). These terms result in an improved dispersion relation. Therefore, a 1D numerical model for non-breaking waves based on the *second set* of Boussinesq-type equations derived by Schäffer and Madsen (1995)[1] is

[1] Throughout this thesis, the (set of Boussinesq-type) equations of Schäffer and Madsen (1995) refers to the *second* of two sets of Boussinesq-type equations in Schäffer and Madsen (1995)

developed by the present author. This numerical model is referred to 1DDBMW-2. At the incoming wave boundary, the free surface elevation is varied sinusoidally with time while the related horizontal velocity is determined from the continuity equation with a locally constant depth. At the outgoing wave boundary, the free surface elevation is obtained by employing the Sommerfeld radiation condition.

Finally, the present Boussinesq-type wave numerical model (1DDBMW-2) is applied to three experimental set-ups with incoming monochromatic waves. The experimental set-up are:

- a flat bottom channel,
- a channel with a sloping bottom and
- a channel with a submerged bar.

All scenarios numerically modelled exclude the effect of bottom friction. To assess the effects of the additional terms in the governing equations of 1DDBMW-2 for $h/L \leq 0.5$, the numerical solutions from 1DBMW-1 (i.e. the numerical model based on the governing equations without the additional terms) and 1DDBMW-2 are compared.

4.2. Derivation of the equations of Schäffer and Madsen (1995)

The frequency dispersion terms or μ^2 terms in the Boussinesq-type equations of Nwogu (1993) as shown in equations (3.16) and (3.17) can be further refined by introducing four new free coefficients $(\beta_1, \beta_2, \gamma_1, \gamma_2) \leq O(1)$. Following Schäffer and Madsen (1995), the operators $-\mu^2\beta_1 \nabla \bullet (h^2\nabla\ )$ and $\mu^2\beta_2 \nabla \bullet \nabla(h^2\ )$ are applied separately to the continuity equation (3.16) and terms up to $O(\varepsilon,\mu^2)$ are retained to yield the next two equations:

$$-\mu^2\beta_1\left\{\nabla \bullet (h^2\nabla\eta_t) + \nabla \bullet \left[h^2\nabla[\nabla \bullet (h\mathbf{u}_\alpha)]\right]\right\} = O(\varepsilon\mu^2, \mu^4) \qquad (4.1)$$

and

$$\mu^2\beta_2\{\nabla\bullet\nabla(h^2\eta_t)+\nabla\bullet\nabla[h^2\nabla\bullet(hu_\alpha)]\}=O(\varepsilon\mu^2,\mu^4) \tag{4.2}$$

Similarly, the operators $-\mu^2\gamma_1 h^2\nabla(\nabla\bullet\ )$ and $\mu^2\gamma_2 h\nabla(\nabla\bullet h\ )$ are applied separately to the momentum equation (3.17) to give the next two equations:

$$-\mu^2\gamma_1 h^2[\nabla(\nabla\bullet \mathbf{u}_{\alpha_t})+\nabla(\nabla\bullet\nabla\eta)]=O(\varepsilon\mu^2,\mu^4) \tag{4.3}$$

and

$$\mu^2\gamma_2 h\{\nabla[\nabla\bullet(h\mathbf{u}_{\alpha_t})]+\nabla[\nabla\bullet(h\nabla\eta)]\}=O(\varepsilon\mu^2,\mu^4) \tag{4.4}$$

Equations (4.1) and (4.2) are then added to the continuity equation (3.16), and equations (4.3) and (4.4) are added to the momentum equation (3.17) to obtain a set of 'deeper water' Boussinesq-type equations of Schäffer and Madsen (1995). The resulting Boussinesq-type equations are capable of describing wave transformation for relative depths (h/L_o) up to 1 (see Table 4.1). The resulting continuity and momentum equations are respectively

$$\eta_t+\nabla\bullet[(h+\varepsilon\eta)\mathbf{u}_\alpha]+\mu^2\nabla\bullet\{h\overline{\Gamma}-\beta_1 h^2\nabla[\nabla\bullet(h\mathbf{u}_\alpha)]+\beta_2\nabla[h^2\nabla\bullet(h\mathbf{u}_\alpha)]$$
$$-\beta_1 h^2\nabla\eta_t+\beta_2\nabla(h^2\eta_t)\}=O(\varepsilon\mu^2,\mu^4) \tag{4.5}$$

$$\mathbf{u}_{\alpha_t}+\nabla\eta+\varepsilon(\mathbf{u}_\alpha\bullet\nabla)\mathbf{u}_\alpha+\mu^2\{\Gamma_{\alpha_t}-\gamma_1 h^2\nabla(\nabla\bullet\mathbf{u}_{\alpha_t})+\gamma_2 h\nabla[\nabla\bullet(h\mathbf{u}_{\alpha_t})$$
$$-\gamma_1 h^2\nabla(\nabla\bullet\nabla\eta)+\gamma_2 h\nabla[\nabla\bullet(h\nabla\eta)]\}=O(\varepsilon\mu^2,\mu^4) \tag{4.6}$$

where Γ_α and $\overline{\Gamma}$ are defined by (3.11a) and (3.18) respectively.

An interesting phenomenon is found here, that is the dispersion or μ^2 terms in the equations of Nwogu (1993) [i.e. in equations (3.16) and (3.17)] have been refined. This results in an improved dispersion relation (see Table 4.1) and yet the order of the frequency dispersion and non-linearity retained in the resulting equations [(4.5) and (4.6)] remain identical to those of Nwogu (1993) and Peregrine (1967) i.e. up to $O(\varepsilon,\mu^2)$. Subsequently, equations (4.5) and (4.6) are only applicable to weakly non-linear waves with the lowest order frequency dispersion terms, i.e. $O(\varepsilon,\mu^2)$.

The 1D version of the continuity and momentum equations [(4.5) and (4.6)] can be expressed in *dimensional* form as

$$\eta_t + [(h+\eta)u_\alpha]_x + \left(\tfrac{1}{2}z_{c\alpha}{}^2 - \tfrac{1}{6}\right)(h^3 u_{\alpha_{xx}})_x + \left(z_{c\alpha} + \tfrac{1}{2} - \beta_1\right)[h^2(hu_\alpha)_{xx}]_x$$

$$+ \beta_2[h^2(hu_\alpha)_x]_{xx} - \beta_1(h^2\eta_{tx})_x + \beta_2(h^2\eta_t)_{xx} = 0 \qquad (4.7)$$

and

$$u_{\alpha_t} + g\eta_x + u_\alpha u_{\alpha_x} + \left(\tfrac{1}{2}z_{c\alpha}{}^2 - \gamma_1\right)h^2 u_{\alpha_{txx}} + (z_{c\alpha} + \gamma_2)h(hu_{\alpha_t})_{xx}$$

$$-\gamma_1 gh^2\eta_{xxx} + \gamma_2 gh(h\eta_x)_{xx} = 0 \qquad (4.8)$$

where α, β_1, β_2, γ_1, and γ_2, are 'free' coefficients. The method of determining these coefficients is explained in the next section. The definitions for z_α in equation (3.21) and α in equation (3.22) are still applicable here.

4.3. Dispersion relations

The 1D governing equations considered in the present Boussinesq-type numerical model [i.e. equations (4.7) and (4.8)] can be linearised (non-linear terms dropped) for constant depth, and are written as

$$\eta_t + hu_{\alpha_x} + \left(\alpha - \beta + \tfrac{1}{3}\right)h^3 u_{\alpha_{xxx}} - \beta h^2 \eta_{txx} = 0 \qquad (4.9)$$

$$u_{\alpha_t} + g\eta_x + (\alpha - \gamma)h^2 u_{\alpha_{xxt}} - g\gamma h^2 \eta_{xxx} = 0 \qquad (4.10)$$

where $\beta = \beta_1 - \beta_2$ and $\gamma = \gamma_1 - \gamma_2$ as defined by Schäffer and Madsen (1995). Substituting a periodic, small amplitude wave [i.e. equations (3.25)] into equations (4.9) and (4.10) gives the dispersion relation, which corresponds to a Padé [4,4] approximation in terms of kh:

$$(C_{[4,4]SM})^2 = gh\frac{[1+\gamma(kh)^2]\left[1-\left(\alpha-\beta+\tfrac{1}{3}\right)(kh)^2\right]}{[1+\beta(kh)^2][1-(\alpha-\gamma)(kh)^2]} \qquad (4.11)$$

where $C_{[4,4]SM}$ is the wave celerity corresponding to the equations of Schäffer and Madsen. The wave celerity expressed in equation (4.11) is an improved dispersion relation from the previous dispersion relation obtained from the equations of Nwogu [i.e. equation 3.3].

The dispersion relation equation (4.11) can be compared to the approximate celerity from Airy wave theory. This comparison is made easier by using a Padé [4,4] approximation of the dispersion relation from Airy wave theory. Witting (1984) found an approximate dispersion relation for Airy wave theory corresponding to a Padé [4,4] approximation in terms of kh for waves in an arbitrary depth, that is

$$(C_{[4,4]Airy})^2 = gh\frac{1+\frac{1}{9}(kh)^2+\frac{1}{945}(kh)^4}{1+\frac{4}{9}(kh)^2+\frac{1}{63}(kh)^4}+O[(kh)^{10}] \qquad (4.12)$$

Schäffer and Madsen determined the free coefficients (α, β, γ) by imposing

$$C_{[4,4]SM} = C_{[4,4]Airy} \qquad (4.13)$$

which yields the following four sets of solutions

$$\alpha,\beta,\gamma = \begin{cases} \dfrac{-3+\sqrt{\frac{684}{63}}+\sqrt{\frac{621}{945}}}{18}, \dfrac{4+\sqrt{\frac{684}{63}}}{18}, \dfrac{1+\sqrt{\frac{621}{945}}}{18} \approx 0.06143, 0.40528, 0.10059 & \text{(a)} \\ \dfrac{-3+\sqrt{\frac{684}{63}}-\sqrt{\frac{621}{945}}}{18}, \dfrac{4+\sqrt{\frac{684}{63}}}{18}, \dfrac{1-\sqrt{\frac{621}{945}}}{18} \approx -0.02865, 0.40528, 0.101052 & \text{(b)} \\ \dfrac{-3-\sqrt{\frac{684}{63}}+\sqrt{\frac{621}{945}}}{18}, \dfrac{4-\sqrt{\frac{684}{63}}}{18}, \dfrac{1+\sqrt{\frac{621}{945}}}{18} \approx -0.30469, 0.03917, 0.10059 & \text{(c)} \\ \dfrac{-3-\sqrt{\frac{684}{63}}-\sqrt{\frac{621}{945}}}{18}, \dfrac{4-\sqrt{\frac{684}{63}}}{18}, \dfrac{1-\sqrt{\frac{621}{945}}}{18} \approx -0.39476, 0.03917, 0.01052 & \text{(d)} \end{cases} \qquad (4.14)$$

The solution (4.14a) is inapplicable since $-0.5 \le \alpha \le 0$ in order to keep the level z_α inside the fluid i.e. $-h \le z_\alpha \le 0$. To determine the free coefficients β_1, β_2, γ_1, and γ_2, reference needs to be made to Schäffer and Madsen (1995).

In this study, the free coefficients are determined by imposing

$$C_{[4,4]SM} = C_{Airy} \qquad (4.15)$$

instead of equation (4.13), where the celerity C_{Airy} is from Airy wave theory, that is

$$(C_{Airy})^2 = \frac{g}{k}\tanh(kh) \tag{4.16}$$

A particular solution set for the free coefficients is found to be $\alpha = -0.39500$, $\beta = 0.03980$ and $\gamma = 0.01051$. This solution set is adopted in the present numerical model (1DDBMW-2).

The wave celerity $C_{[4,4]SM}$ corresponding to the particular solution ($\alpha = -0.39500$, $\beta = 0.03980$ and $\gamma = 0.01051$) and α, β, γ in equations (4.14b – d) are normalised with respect to the wave celerity of Airy wave theory C_{Airy} and compared. Figure 4.1 displays the errors in the normalised wave celerity as a function of the relative depth h/L_o. The comparison indicates that the particular solution $(\alpha,\beta,\gamma) = (-0.395, 0.0398, 0.01051)$ gives the best approximation to the celerity of Airy wave theory i.e. a celerity error less than 1 % faster with h/L_o up to 1, while the other solutions i.e. (4.14b – d) give a celerity error of just over 1 % faster at the same relative depth.

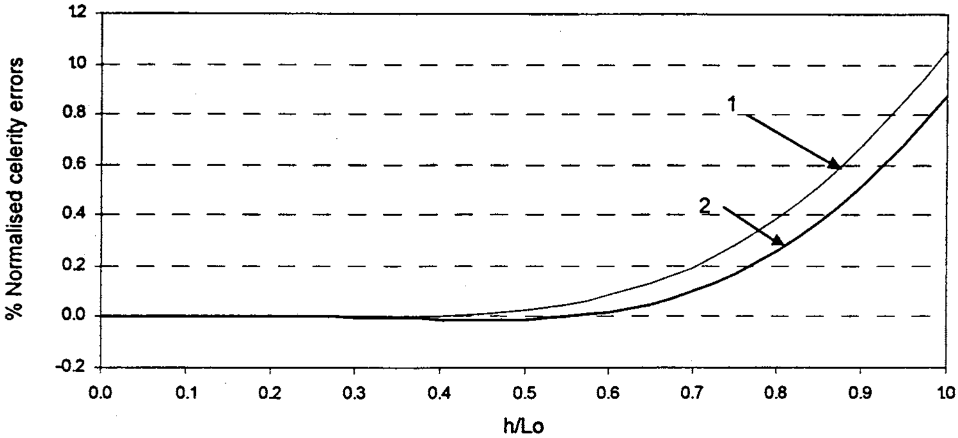

Figure 4.1. A comparison of normalised celerity errors of the linearised Boussinesq-type wave equations of Schäffer and Madsen (1995) for different values of the free coefficients (α,β,γ): (1) the three solutions (4.14b – d) which result in identical dispersion relations; and (2) the particular solution $(\alpha,\beta,\gamma) = (-0.395, 0.0398, 0.01051)$ adopted in this study (1DDBMW-2).

As shown in Figure 4.2, the linearised form of the Boussinesq-type equations derived by Schäffer and Madsen with a Padé [4,4] approximation to the dispersion relation, gives a celerity error less than that of other Boussinesq-type equations. However, the Boussinesq-type equations with a dispersion relation corresponding to a Padé [2,2] approximation in terms of kh (such as those of Madsen *et al.*, 1991; Madsen and Sørensen, 1992 and Nwogu, 1993) give a celerity error of 11.4 % faster than the wave celerity of Airy wave theory with $(h/L_o) \approx 1$. Conversely, the normalised celerity of Peregrine's (1967) formulation with a dispersion relation corresponding to a Padé [0,2] approximation in terms of kh give a celerity error of 33.4 % slower than the wave celerity of Airy wave theory at the same relative depth.

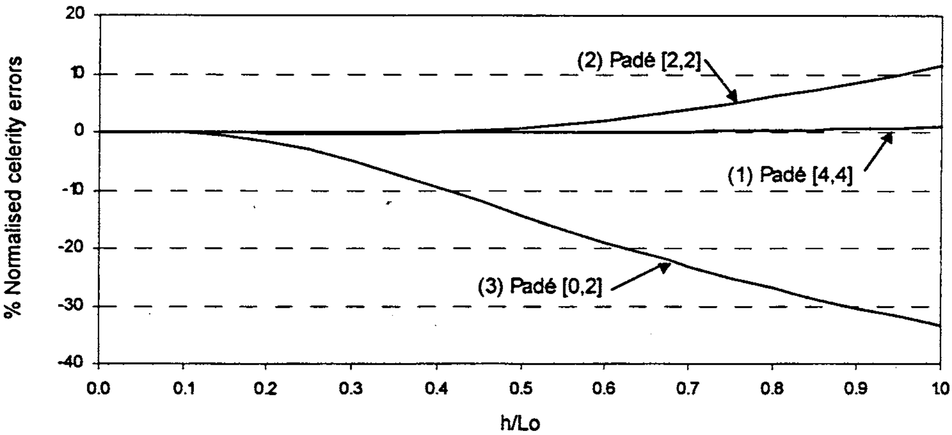

Figure 4.2. A comparison of normalised celerity errors of various linearised Boussinesq-type equations of: (1) Schäffer and Madsen (1995) with $(\alpha,\beta,\gamma) = (-0.395, 0.0398, 0.01051)$ (1DDBMW-2); (2) Madsen *et al.* (1991), Madsen and Sørensen (1992) and Nwogu (1993) or equivalently the equations of Schäffer and Madsen with $(\alpha,\beta,\gamma) = (-0.39,0,0)$; and (3) Peregrine (1967) or equivalently the equations by Schäffer and Madsen with $(\alpha,\beta,\gamma) = (-1/3,0,0)$.

4.4. Numerical solution algorithm for 1DDBMW-2

4.4.1. Solution method

A finite difference method with a non-staggered grid is used by the present author to solve the *dimensional* governing equations [(4.7) and (4.8)]. The numerical scheme used in Chapter Three is also applied in this chapter.

The *dimensional* continuity equation (4.7) can be expressed as

$$\Xi_t = E(\eta, u_\alpha) \tag{4.17}$$

where Ξ and E are the variable groupings defined as

$$\Xi = \eta - \beta_1 (h^2\eta_x)_x + \beta_2 (h^2\eta)_{xx} \tag{4.18}$$

$$E(\eta, u_\alpha) = -[(h+\eta)u_\alpha]_x - \left(\tfrac{1}{2} z_{c\alpha}^2 - \tfrac{1}{6}\right)(h^3 u_{\alpha_{xx}})_x$$
$$- \left(z_{c\alpha} + \tfrac{1}{2} - \beta_1\right)[h^2(hu_\alpha)_{xx}]_x - \beta_2 [h^2(hu_\alpha)_x]_{xx} \tag{4.19}$$

The continuity equation (4.17) is noted to be different to the corresponding continuity equation (3.28). This must result in a modification to how the governing equations in 1DDBMW-2 are implemented compared to 1DBMW-1 in Chapter Three. Following the procedure in Section 3.4.1, the *dimensional* momentum equation (4.8) can be written in the form of equation (3.30)

$$U_{\alpha_t} = F(\eta, u_\alpha) \tag{3.30}$$

where the variable groupings U_α and F become

$$U_\alpha = u_\alpha + \left(\tfrac{1}{2} z_{c\alpha}^2 - \gamma_1\right) h^2 u_{\alpha_{xx}} + (z_{c\alpha} - \gamma_2) h (hu_\alpha)_{xx} \tag{4.20}$$

$$F(\eta, u_\alpha) = -g\eta_x - u_\alpha u_{\alpha_x} + \gamma_1 g h^2 \eta_{xxx} - \gamma_2 g h (h\eta_x)_{xx} \tag{4.21}$$

The Adams-Bashforth predictor scheme (3.33) and the Adams-Moulton corrector scheme (3.36) become equations (4.22) and (4.23) respectively.

$$\Xi_i^{t+1} = \Xi_i^t + \tfrac{1}{12}\Delta t[23E^t - 16E^{t-1} + 5E^{t-2}]_i \qquad \text{(predictor)} \tag{4.22}$$

$$\Xi_i^{t+1} = \Xi_i^t + \tfrac{1}{24}\Delta t[9E^{t+1} + 19E^t - 5E^{t-1} + E^{t-2}]_i \text{ (corrector)} \tag{4.23}$$

To obtain the free surface elevation η at the new time level (t+1), further calculation is needed using the values of Ξ_i^{t+1} obtained from equation (4.22) for the predictor step and from equation (4.23) for the corrector step. The values of Ξ_i^{t+1} are then substituted into equation (4.18). Subsequently, equation (4.18) is arranged into a matrix form as shown in equation (4.24) to yield the new free surface elevation η_i^{t+1}.

$$\begin{bmatrix} \text{Coefficient} \\ \\ \text{Matrix} \end{bmatrix} \begin{Bmatrix} \\ \eta \\ \\ \end{Bmatrix}^{t+1} = \begin{Bmatrix} \\ \Xi \\ \\ \end{Bmatrix}^{t+1} \tag{4.24}$$

The horizontal velocities $u_{\alpha_i}^{t+1}$ are determined in the same way as set out in equation (3.35) of Section 3.4.1.

The values of the free surface elevation and horizontal velocity determined above are for inside the fluid domain. At the boundaries, these values are determined using the boundary conditions explained below.

4.4.2. Boundary conditions

4.4.2.1. Incoming wave boundary conditions

The model 1DDBMW-2 requires the surface elevation η and velocity u_α at the incoming wave boundary to be specified. At the incoming wave boundary, the free surface elevation is varied sinusoidally as shown in equation (3.39). The continuity equation (4.7) with a locally constant depth is

$$\eta_t + u_\alpha \eta_x + (h+\eta)u_{\alpha_x} + \left(\alpha - \beta + \tfrac{1}{3}\right)h^3 u_{\alpha_{xxx}} - \beta h^2 \eta_{txx} = 0 \tag{4.25}$$

Furthermore, the horizontal fluid velocity u_α at the incoming wave boundary is obtained by substituting equations (3.25) into (4.25) resulting in the expression below

$$u_\alpha = \frac{\omega\eta[1+\beta(kh)^2]}{kh\left[1-\left(\alpha-\beta+\frac{1}{3}\right)(kh)^2\right]} \tag{4.26}$$

The Sommerfeld radiation condition (3.42) is also automatically satisfied by equation (4.26).

4.4.2.2. Outgoing wave boundary conditions

(i) Free surface elevation:

The Sommerfeld radiation condition (3.42) i.e. $\eta_t + C\eta_x = 0$ is applied to the outgoing wave boundary of the present numerical model. For implementation, this boundary condition can be written in the same form as equation (4.17).

$$\Xi_t = E(\eta, u_\alpha) \tag{4.17}$$

where

$$\Xi = \eta \tag{4.27}$$

$$E(\eta, u_\alpha) = -C\eta_x \tag{4.28}$$

The finite difference approximation applied to η_x in equation (4.28) is

$$(\eta_x)_1^t = \frac{1}{2\Delta x}(3\eta_1 - 4\eta_2 + \eta_3)^t \tag{4.29}$$

(see Appendix A for the specification of the coordinate system).

(ii) Horizontal velocity:

While the boundary conditions for u_α are being explored, experimentation with the numerical models revealed that it is necessary to treat the cases of

(a) deep water and (b) transitional and shallow waters separately. In this study, no one boundary condition is successful in both cases.

(a) In deep water, the horizontal velocity u_α is determined by imposing

$$u_{\alpha_t} + Cu_{\alpha_x} = 0 \tag{4.30}$$

For implementation, equation (4.30) is transformed into the form of equation (3.30), U_α and F may be defined as

$$U_{\alpha_t} = F(\eta, u_\alpha) \tag{3.30}$$

where

$$U_\alpha = u_\alpha \tag{4.31}$$

$$F(\eta, u_\alpha) = -Cu_{\alpha_x} \tag{4.32}$$

The finite difference approximation applied to u_{α_x} in equation (4.32) is

$$(u_{\alpha_x})_1^t = \frac{1}{2\Delta x}(3u_{\alpha_1} - 4u_{\alpha_2} + u_{\alpha_3})^t \tag{4.33}$$

(b) In shallow water or intermediate depth water, the horizontal velocity is determined as follows. The Sommerfeld radiation condition (3.42) and the expression for a periodic, small amplitude wave are substituted into equation (4.25) to give an equation for u_α, which is identical to equation (4.26).

4.5. Model verification

4.5.1. Experimental set-up 1: Wave propagation in a constant depth channel

The standard form of the Boussinesq-type equations derived by Peregrine (1967) cannot simulate wave transformation in deep water with $h/L_o = 1$ since their dispersion relation gives a celerity error of 33.4 % slower than the wave celerity of Airy wave theory (Figure 4.2). A similar comment applies to the

Boussinesq-type equations with a dispersion relation corresponding to a Padé [2,2] approximation in terms of kh (e.g. Madsen *et al.*, 1991; Madsen and Sørensen, 1992 and Nwogu, 1993) since their dispersion relation gives a celerity error of 11.4 % faster than the wave celerity of Airy wave theory at the same relative depth (Figure 4.2).

Experimental set-up 1 (Figure 4.3) is aimed at testing the ability of the equations of Schäffer and Madsen to simulate the propagation of a monochromatic wave at $h/L_o = 1$. Consider, for example a train of waves with period T = 0.85 s, $L_o = 1.13$ and incoming wave height $H_i = 0.04$ m propagating in a channel with a flat bottom, 1.13 m deep and 16.84 m long. The intention of choosing these values is to obtain $h/L_o = 1$. The test conditions are: $\Delta x = 0.02$ m ($L_o/\Delta x = 56.4$) and $\Delta t = 0.01$ s ($T/\Delta t = 85.0$). The longitudinal profiles of the free surface along the channel are displayed in Figure 4.4 at times t = 15, 20 and 25 s. The outgoing wave boundary is located at x = 0 m.

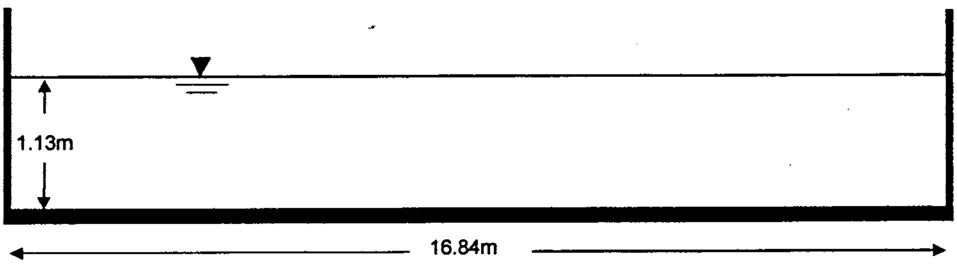

Figure 4.3. Experimental set-up 1: the channel with a flat bottom.

Figure 4.4 shows comparisons of the free surface elevation predicted by the present Boussinesq-type wave, numerical model (1DDBMW-2) and sinusoidal waves at different times. As shown in Figures 4.1 and 4.2, the wave celerity of 1DDBMW-2 propagates slightly faster than that of Airy wave theory (i.e. a purely sinusoidal wave moving without change of form at celerity C). Furthermore, the model results in Figure 4.4 show that the longitudinal profiles of the free surface elevation in deep water are seen to behave according to sinusoidal waves as expected. After 25 s, it is observed in the bottom plot of Figure 4.4 that some (unwanted) wave reflection is emanating from the downwave boundary with the transmitting boundary condition.

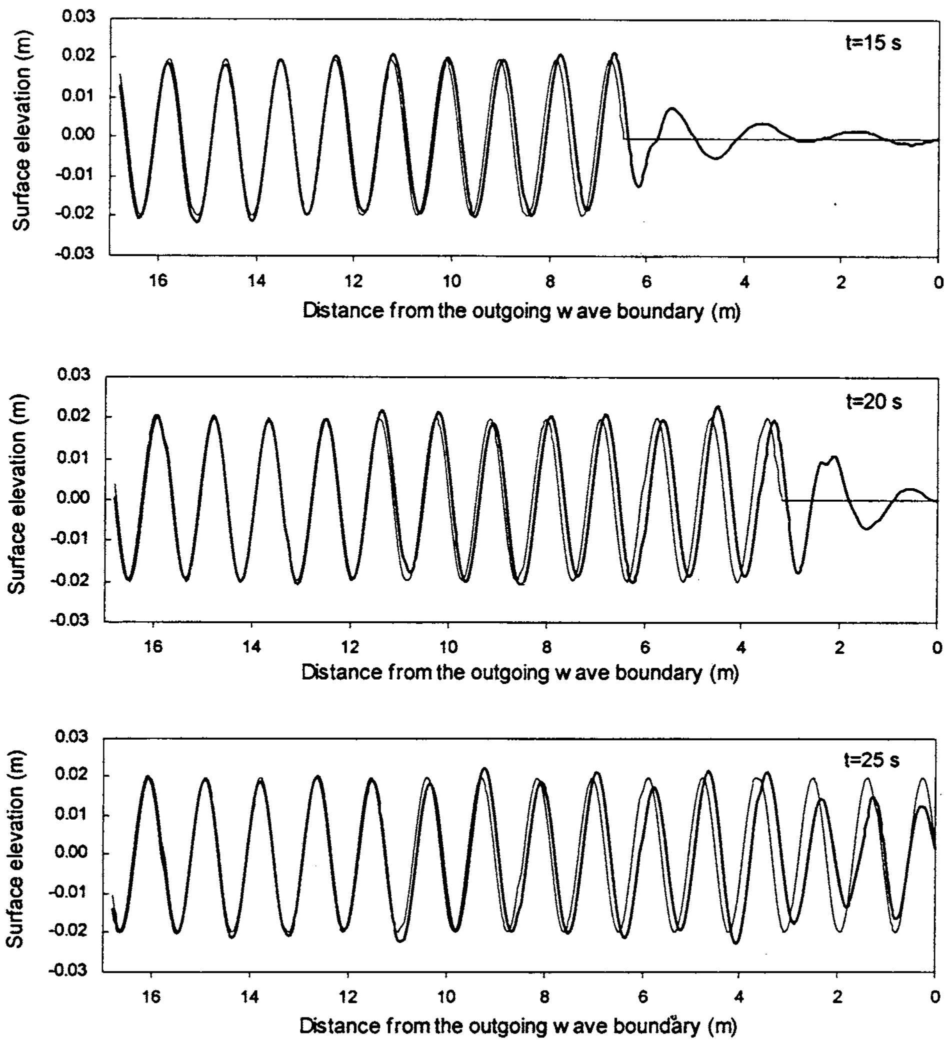

Figure 4.4. Deeper water ($h/L_o = 1.0$): the free surface elevation along the channel at t = 15, 20 and 25 s predicted by 1DDBMW-2 (bold lines) and Airy wave theory (thin lines). Data: $T = 0.85$ s, $H_i = 0.04$ m, $h = 1.13$ m, $\Delta x = 0.02$ m and $\Delta t = 0.01$ s.

4.5.2. Experimental set-up 2: Wave propagation up a slope

While 1DDBMW-2 is capable of simulating wave propagation in very deep water (i.e. h/L_o up to 1), it is still necessary to assess its performance in shallower water ($h/L_o \leq 0.5$), as is done for 1DBMW-1 in Chapter Three. Laboratory data collected by Nwogu (1993) are presented in Chapter Three and are used to assess the performance of 1DDBMW-2.

In the first test with experimental set-up 2 (Figure 3.4), an *incident deep water wave* ($h_i/L_o = 0.5$) propagates from the incoming wave boundary where the depth is 0.56 m, up a slope to the outgoing wave boundary where the depth is 0.07 m. The computation is carried out with the following wave and mesh parameters: $T = 0.85$ s, $H_i = 0.04$ m, $\Delta x = 0.02$ m ($L_o/\Delta x = 56.4$) and $\Delta t = 0.01$ s ($T/\Delta t = 85.0$). Comparisons of the time series for the water surface elevation predicted by 1DDBMW-2 (bold lines) and laboratory measurements (thin lines) at depths of 0.28 m and 0.07 m are shown in Figures 4.5 and 4.6 respectively.

For a depth of 0.28 m, the results predicted by 1DDBMW-2 agree well with laboratory measurements. At the outgoing wave boundary however, the surface elevation in the computational model is a little flatter through the wave troughs compared to those of measured waves. At both depths, the present numerical model (1DDBMW-2) is seen to perform better than the numerical model developed in Chapter Three (1DBMW-1).

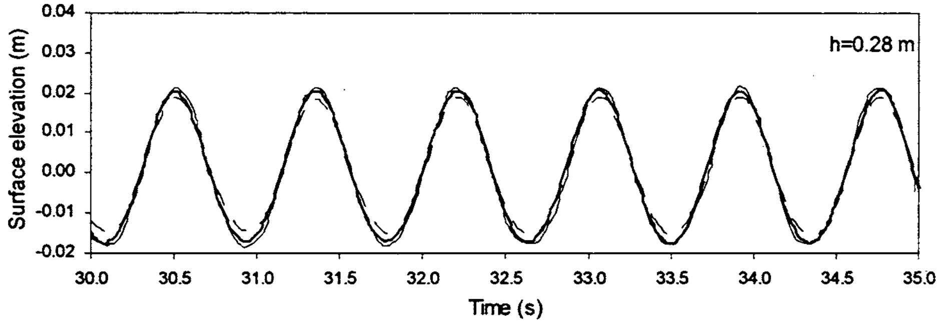

Figure 4.5. Incident deep water waves ($h_i/L_o = 0.5$): time series of the free surface elevation at 0.28 m depth predicted by 1DDBMW-2 (bold line), the laboratory measurements of Nwogu (thin line) and 1DBMW-1 (dashed line). Data: $T = 0.85$ s, $H_i = 0.04$ m, $h_i = 0.56$ m, $\Delta x = 0.02$ m and $\Delta t = 0.01$ s.

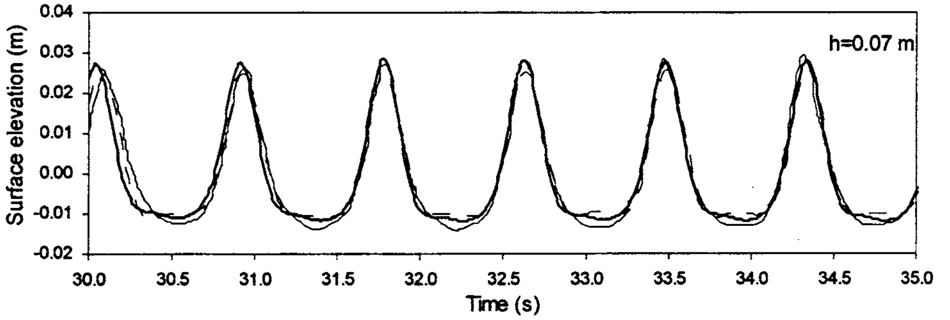

Figure 4.6. Incident deep water waves ($h_i/L_o = 0.5$): time series of the free surface elevation at the outgoing wave boundary ($h = 0.07$ m) predicted by 1DBMW-2 (bold line), the laboratory measurements of Nwogu (thin line) and 1DBMW-1 (dashed line). Data: $T = 0.85$ s, $H_i = 0.04$ m, $h_i = 0.56$, $\Delta x = 0.02$ m and $\Delta t = 0.01$ s.

Another test is carried out using the same experimental set-up 2 but this time with an *intermediate depth wave* ($h_i/L_o = 0.36$). The computation is performed with $T = 1$ s, $H_i = 0.066$ m, $h_i = 0.56$ m, $\Delta x = 0.02$ m ($L_o/\Delta x = 78.1$) and $\Delta t = 0.01$ s ($T/\Delta t = 100.0$). The time series for the water surface elevation was measured at the outgoing wave boundary ($h = 0.10$ m) and at a water depth of 0.24 m (Figures 4.7 and 4.8).

A comparison of the surface elevation at 0.24 m depth between the results of 1DDBMW-2 and the laboratory data shows that 1DDBMW-2 accurately predicts the shoaling waves as shown in Figure 4.7. Meanwhile, the performance of 1DDBMW-2 (bold line) is better than that of 1DBMW-1 (dashed lines) at 0.24 m depth.

The results for the water surface elevation at the outgoing wave boundary (h = 0.10 m) provide a more severe test of the performance of the numerical model. Figure 4.8 shows the formation of non-linear waves predicted by 1DBMW-1 and 1DDBMW-2 with the peaked wave crests and long low troughs. Interestingly, the results of each numerical model give different discrepancies against the laboratory measurements at h = 0.10 m, particularly around the wave crest.

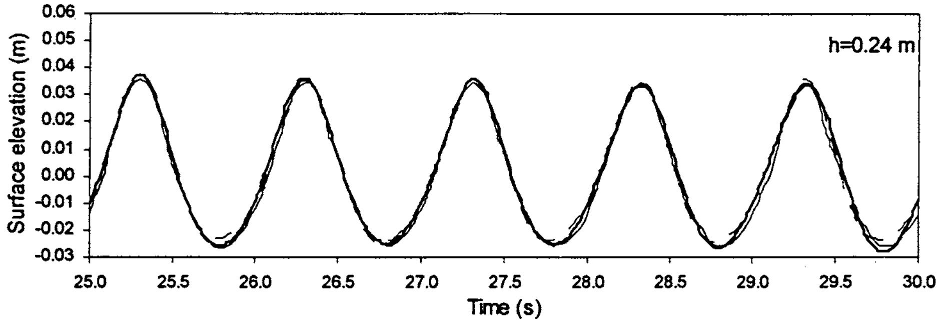

Figure 4.7. Intermediate depth water waves ($h_i/L_o = 0.36$): time series of the free surface elevation at 0.24 m depth predicted by 1DDBMW-2 (bold line), the laboratory measurements of Nwogu (thin line) and 1DBMW-1 (dashed line). Data: T = 1 s, $H_i = 0.066$ m, $h_i = 0.56$ m, $\Delta x = 0.02$ m and $\Delta t = 0.01$ s.

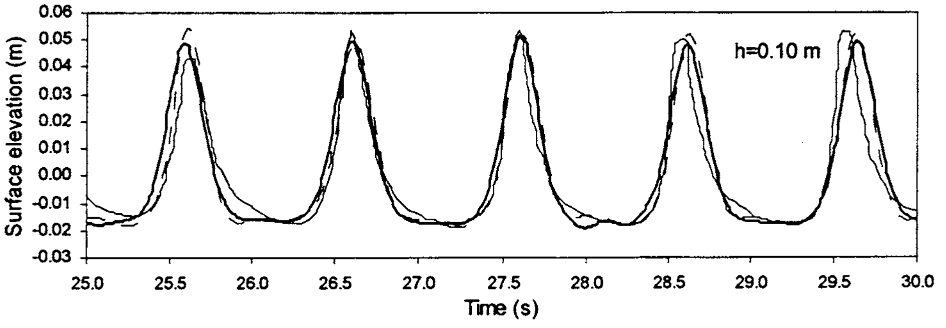

Figure 4.8. Intermediate depth water waves ($h_i/L_o = 0.36$): time series of the free surface elevation at the outgoing wave boundary (h = 0.10 m) predicted by 1DDBMW-2 (bold line), the laboratory measurements of Nwogu (thin line) and 1DBMW-1 (dashed line). Data: T = 1 s, $H_i = 0.066$ m, $h_i = 0.56$ m, $\Delta x = 0.02$ m and $\Delta t = 0.01$ s.

4.5.3. Experimental set-up 3: Wave propagation in a channel with a submerged bar

The last experimental set-up modelled (Figure 3.9) is one in which waves propagate over a submerged bar in a channel. The numerical set-up represented in Figure 3.9 follows the physical set-up of Luth *et al.* (1994) (see Borsboom *et al.*, 2000). The laboratory measurements of Luth *et al.* are also used to assess the accuracy of the numerical model results.

In the first test with the submerged shoal, a train of waves with a period of 2.02 s and an incoming wave height of 0.02 m propagates down a channel, which is 0.40 m deep. The computation is carried out with $\Delta x = 0.08$ m ($L_o/\Delta x = 79.6$) and $\Delta t = 0.02$ s ($T/\Delta t = 101.0$).

The results in Figure 4.9 show that 1DDBMW-2 captures the main features of the water surface time series at the top of the bar (x = 11.5 m). However, 1DDBMW-2 is seen to slightly overestimate the wave crests, and underestimate the early and late portions of the wave troughs. In Figure 4.10, a comparison of the water surface elevation on the lee side of the bar at a chainage of x = 7.7 m from the outgoing wave boundary shows that the results from 1DDBMW-2 marginally exceed the measured wave crests but more significantly underestimate the wave troughs.

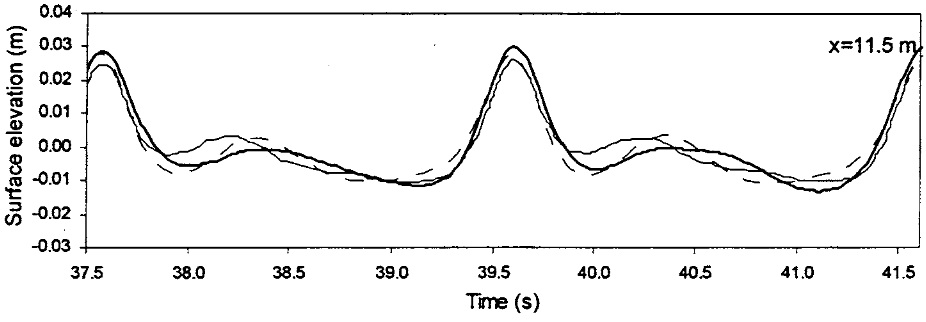

Figure 4.9. Top of the bar (i.e. 11.5 m before the outgoing wave boundary): time series of the water surface elevation predicted by 1DDBMW-2 (bold line), the laboratory measurements of Luth *et al.* (thin line) and 1DBMW-1 (dashed line). Data: $T = 2.02$ s, $H_i = 0.02$ m, $h_i = 0.4$ m, $h_i/L_o = 0.06$, $\Delta x = 0.08$ m and $\Delta t = 0.02$ s.

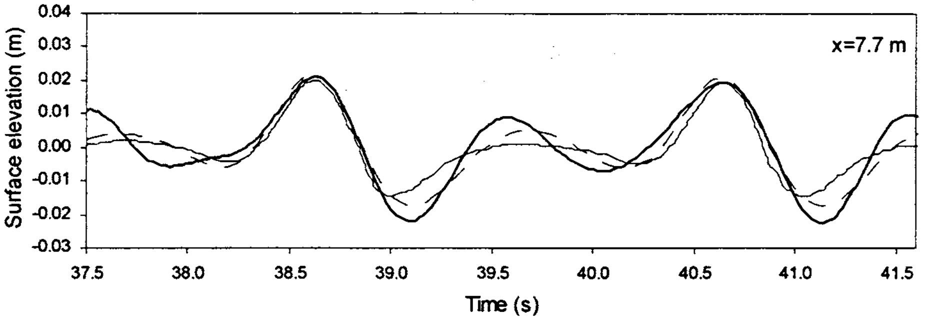

Figure 4.10. Behind the bar (i.e. 7.7 m before the outgoing wave boundary): time series of the water surface elevation predicted by 1DDBMW-2 (bold line), the laboratory measurements of Luth *et al.* (thin line) and 1DBMW-1 (dashed line). Data: $T = 2.02$ s, $H_i = 0.02$ m, $h_i = 0.4$ m, $h_i/L_o = 0.06$, $\Delta x = 0.08$ m and $\Delta t = 0.02$ s.

The last test investigated is of a train of steeper waves than the previous test i.e. with 1.01 s period and 0.041 m incoming wave height propagating over the same bathymetry as the previous test. The grid size and the time step are chosen to be 0.08 m ($L_o/\Delta x = 19.9$) and 0.02 s ($T/\Delta t = 50.5$) respectively. As for the previous test, the time series for water surface elevation was measured on top of and behind the submerged bar.

In Figure 4.11, a comparison of 1DDBMW-2 results with laboratory measurements of the water surface elevation on top of the bar show close agreement. On the outgoing wave side of the shoal at $x = 7.7$ m, Figure 4.12 shows that while 1DDBMW-2 slightly overestimates the wave crests, it significantly underestimates the wave troughs on the lee of the submerged bar. The waves in 1DDBMW-2 are seen to be more symmetrical than the measured waves (Figure 4.12).

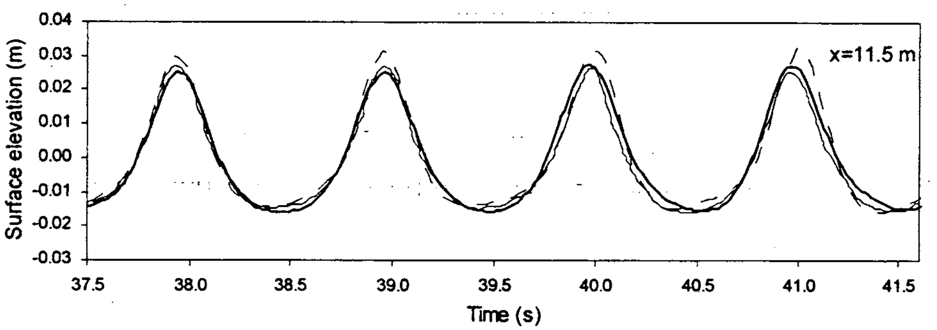

Figure 4.11. Top of the bar (i.e. 11.5 m before the outgoing wave boundary): time series of the water surface elevation predicted by 1DDBMW-2 (bold line), the laboratory measurements of Luth *et al.* (thin line) and 1DBMW-1 (dashed line). Data: $T = 1.01$ s, $H_i = 0.041$ m, $h_i = 0.4$ m, $h_i/L_o = 0.25$, $\Delta x = 0.08$ m and $\Delta t = 0.02$ s.

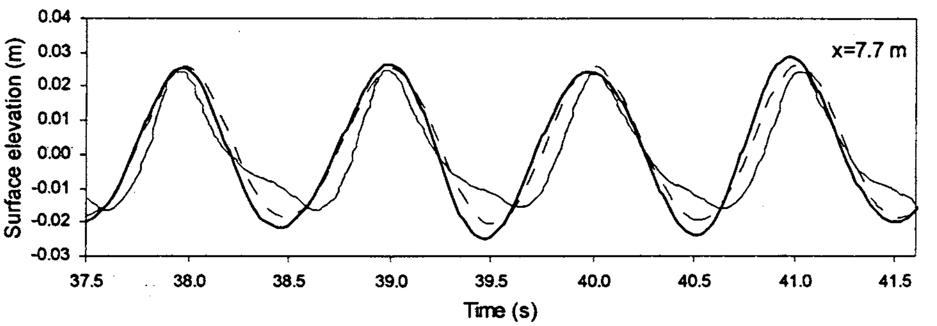

Figure 4.12. Behind the bar (i.e. 7.7 m before the outgoing wave boundary): time series of the water surface elevation predicted by 1DDBMW-2 (bold line), the laboratory measurements of Luth *et al.* (thin line) and 1DBMW-1 (dashed line). Data: $T = 1.01$ s, $H_i = 0.041$ m, $h_i = 0.4$ m, $h_i/L_o = 0.25$, $\Delta x = 0.08$ m and $\Delta t = 0.02$ s.

Although Figures 4.9, 4.10 and 4.12 show that 1DBMW-1 based on the equations of Nwogu (1993) presented in Chapter Three give generally slightly better results than 1DDBMW-2 based on the equations of Nwogu with the additional terms (i.e. the equations of Schäffer and Madsen, 1995), Figure 4.11 shows the opposite.

4.6. Conclusions

A 1D numerical model based on the Boussinesq-type equations derived by Schäffer and Madsen (1995) is developed by the present author. This numerical model is referred to 1DDBMW-2. At the incoming wave boundary, monochromatic, small amplitude waves are generated. At the outgoing wave boundary, a form of the Sommerfeld radiation condition is adopted to predict the free surface elevation and velocity.

The effects of the additional terms in the equations of Schäffer and Madsen (1995), which result in an improved dispersion relation, can be seen where the present Boussinesq-type wave numerical model (1DDBMW-2) is applicable to the simulation of the propagation of a monochromatic wave in channel with a flat bottom in very deep water ($h/L = 1$). The deep water criterion is taken to be $h/L \geq 0.5$. As predicted by the dispersion relation, the wave celerity associated with the governing equations in the present model is slightly faster than the wave celerity of Airy wave theory. The predicted free surface elevation in deep water compares well with Airy wave theory as expected.

1DDBMW-2 is capable of simulating non-breaking wave transformation in a channel with a slope. This is confirmed by good agreement between computed and measured free surface elevation. The other tests indicate that 1DDBMW-2 is also capable of simulating the propagation of a monochromatic wave in a channel with a submerged bar although 1DDBMW-2 performance on the downwave side of the bar is not as good as it is on the incoming wave side. As in 1DBMW-1, the effect of bottom friction is not included in 1DDBMW-2. Comparisons of 1DDBMW-2 results with the laboratory measurements indicate that bottom friction is not a significant factor for the waves propagating on the model concrete beach and over the submerged bar used in these tests.

Although 1DDBMW-2 is applicable to water depths up to $h/L = 1$ (compared with 1DBMW-1 developed in Chapter Three which is only valid up to $h/L = 0.5$), 1DBMW-1 seems to give generally better results than 1DDBMW-2 within the applicable range of 1DBMW-1 (i.e. $h/L \leq 0.5$).

It can be concluded that the additional terms in the governing equations of 1DDBMW-2, which result in an improved dispersion relation but with the same order of the frequency dispersion as 1DBMW-1 does not give a noticeably improved result. Based on the relative results of the 1D tests of 1DDBMW-2 and 1DBMW-1, the development of a 2D numerical model based on the equations of Schäffer and Madsen (1995) in this thesis is not considered necessary.

Chapter Five

1D Basic Model with Current Effects

5.1. Introduction

In the present study, a finite difference model based on the *second set* of partial differential equations of Chen *et al.* (1998) is coded up by the present author. This model, which is referred to 1DBMWC-3, is used to investigate numerically the effects of the dispersion terms associated with currents. That is, the results from 1DBMWC-3 are compared to the results from a model without currents [i.e. a model based on Nwogu's (1993) equations or 1DBMW-1].

5.2. Derivation of the equations of Chen *et al.* (1998)

5.2.1. Non-dimensionalisation based on wave scaling parameters

Following the approach of Chen *et al.* (1998), the *first set* of their equations is re-derived based on the depth-integrated continuity and momentum equations. In this study, the derivation here expands on the work of Chen *et al.* for greater clarity. The *wave* scaling parameters, which will be used here, are identical to those defined by equations (2.31) and (2.32) when deriving the equations of Peregrine, 1967 (Section 2.4), Nwogu, 1993 (Section 3.2) and Schäffer and Madsen, 1995 (Section 4.2) instead of the *wave* scaling parameters in the work of Chen *et al.* (1998). The dependent, *non-dimensional* variables defined by equations (2.32) for *waves* only can be written as

$$u = O(\varepsilon)\sqrt{gh_{ch}}\,u'\,,\;\; v = O(\varepsilon)\sqrt{gh_{ch}}\,v'\,,\;\; w = O(\varepsilon\mu)\sqrt{gh_{ch}}\,w' \qquad (5.1a)$$

$$\eta = O(\varepsilon)\,h_{ch}\,\eta'\,,\;\; p = O(\varepsilon)\,\rho g h_{ch}\,p' \qquad (5.1b)$$

where again the primes denote *non-dimensional* variables.

5.2.2. Non-dimensionalisation based on wave-current scaling parameters

Parameters ε, ν, δ and σ are introduced as explicit measures of the order of magnitude of each term in the equations, where $\varepsilon = a_{ch}/h_{ch}$, $\sigma = \varepsilon/\nu$ and $\delta = O(\varepsilon, \nu^2)$. To ensure the equations will be valid in the limit of vanishing current, it is necessary to specify $O(\varepsilon) \le \nu \le O(1)$. The extreme cases are: (i) $\nu = O(\varepsilon)$ meaning waves only and (ii) $\nu = O(1)$ meaning (waves interacting with) a strong current. The velocity variable is assumed to consist of two parts, a wave orbital velocity and a current velocity. In this derivation, the difference in horizontal scaling of ambient current and wave components is made. The current velocity is assumed to be steady, uniform over the depth and no greater than the shallow water wave celerity $C = \sqrt{gh}$. The spatial variation of the steady current is closely related to the variation of the bottom bathymetry. As reported by Madsen and Schäffer (1998), the horizontal length scales of the current variation and of the depth variation are assumed to be much longer than the characteristic wavelength. Consequently, strong currents [with $\nu = O(1)$] can be treated only on weakly varying bathymetry.

However, weak currents [with $\nu = O(\varepsilon)$] do not imply any restriction on the bathymetry variations.

It can be summarised that the *wave-scaling* parameters consist of two parts i.e. *wave* and *current* scaling parameters. Consequently, the dependent, *non-dimensional* variables for *waves and currents* can be written as

$$u = O(\varepsilon,\nu)\sqrt{gh_{ch}}\,u',\ \ v = O(\varepsilon,\nu)\sqrt{gh_{ch}}\,v',\ \ w = O(\varepsilon\mu,\sigma\nu\mu)\sqrt{gh_{ch}}\,w' \quad (5.2a)$$

$$\eta = O(\varepsilon,\nu^2)\,h_{ch}\,\eta',\ \ p = O(\varepsilon,\nu^2)\,\rho g h_{ch}\,p' \quad (5.2b)$$

Details of these scales can be found in Chen (1997) p27-32 and Chen *et al.* (1998) p16-20.

As a result, the *non-dimensional* equations (2.95a), (2.96), (3.1), (3.3) and (3.4), which are written in terms of *wave* scaling parameters (ε,μ), can be converted into those in terms of *wave-current* scaling parameters $(\varepsilon,\mu,\delta,\nu)$ to give

$$\mathbf{u}_z - \frac{\delta}{\nu}\nabla w = 0 \quad (5.3)$$

$$\eta_t + \nabla \bullet \int_{-h}^{\delta\eta} \mathbf{u}\,dz = 0 \quad (5.4)$$

$$\frac{\partial}{\partial t}\int_{-h}^{\delta\eta} \mathbf{u}\,dz + \nu(\mathbf{u}\bullet\nabla)\int_{-h}^{\delta\eta} \mathbf{u}\,dz + \nabla\int_{-h}^{\delta\eta} p\,dz - \delta p\big|_{z=-h}\nabla h = 0 \quad (5.5)$$

$$p(x,y,z,t) = \eta - \frac{z}{\delta} + \frac{\partial}{\partial t}\int_{z}^{\delta\eta} w\,dz + \nu(\mathbf{u}\bullet\nabla)\int_{z}^{\delta\eta} w\,dz - \frac{\nu}{\mu^2}w^2 \quad (5.6)$$

$$w = -\frac{\varepsilon}{\delta}\mu^2\nabla\bullet\int_{-h}^{z}\mathbf{u}\,dz \quad (5.7)$$

5.2.3. *First set* of equations of Chen et *al.* (1998)

The *first set* of Boussinesq-type equations of Chen *et al.* (1998) for wave-current interaction is presented in terms of the depth-averaged velocity $\overline{\mathbf{u}}$. The derivation of this set of partial differential equations can be demonstrated by following the approach of Chen *et al.*, although the *wave* scaling parameter used here differ from those used by Chen *et al.*.

The horizontal velocity of the fluid is expanded as a Taylor series with respect to the still water level, horizontal velocity $\tilde{\mathbf{u}} = \mathbf{u}(x,y,0,t)$.

$$\mathbf{u}(x,y,z,t) = \mathbf{u}(x,y,0,t) + z\mathbf{u}_z(x,y,0,t) + \tfrac{1}{2}z^2\mathbf{u}_{zz}(x,y,0,t) + \ldots$$

$$= \tilde{\mathbf{u}} + z\tilde{\mathbf{u}}_z + \tfrac{1}{2}z^2\tilde{\mathbf{u}}_{zz} + \ldots \tag{5.8}$$

Evaluating equations (3.7) for $\mathbf{u}_z$ and (3.8) for $\mathbf{u}_{zz}$ at $z = 0$, and substituting into equation (5.8) gives the horizontal velocity (written in terms of the *wave-current* scaling parameters, as explained in Section 5.2.2)

$$\mathbf{u} = \tilde{\mathbf{u}} - \frac{\varepsilon}{\nu}\mu^2\left\{\tfrac{1}{2}z^2\nabla(\nabla \bullet \tilde{\mathbf{u}}) + z\nabla[\nabla \bullet (h\tilde{\mathbf{u}})]\right\} + \text{truncation error} \tag{5.9}$$

Substituting equation (5.9) for $\mathbf{u}$ into (5.7) for w gives

$$w = -\frac{\varepsilon}{\delta}\mu^2[z\nabla \bullet \tilde{\mathbf{u}} + \nabla \bullet (h\tilde{\mathbf{u}})] + O\left(\frac{\varepsilon}{\delta}\mu^4\right) \tag{5.10}$$

Without stating as much, Chen *et al.* (1998) assumed that $\varepsilon \cong \nu$ in the vertical velocity or in other words, the vertical velocity due to the ambient current is very small compared to the orbital vertical velocity due to the waves. Now, the truncation error of equation (5.9) can be determined by integrating the irrotationality condition (5.3) from z to 0. This results in

$$\mathbf{u} - \tilde{\mathbf{u}} = -\frac{\delta}{\nu}\int_z^0 \nabla w \, dz \tag{5.11}$$

Inserting equation (5.10) for w into (5.11) leads to

$$\mathbf{u} = \tilde{\mathbf{u}} - \frac{\varepsilon}{\nu}\mu^2\left\{\tfrac{1}{2}z^2\nabla(\nabla\bullet\tilde{\mathbf{u}}) + z\nabla[\nabla\bullet(h\tilde{\mathbf{u}})]\right\} + O\left(\frac{\varepsilon}{\nu}\mu^4\right) \tag{5.12}$$

Substituting equation (5.12) into the definition of the depth-averaged velocity $\overline{\mathbf{u}} = \frac{1}{h+\delta\eta}\int_{-h}^{\delta\eta}\mathbf{u}\,dz$, and integrating leads to

$$\overline{\mathbf{u}} = \tilde{\mathbf{u}} - \frac{\varepsilon}{\nu}\mu^2\left\{\frac{1}{6}\frac{\delta^3\eta^3+h^3}{\delta\eta+h}\nabla(\nabla\bullet\tilde{\mathbf{u}}) + \frac{1}{2}\frac{\delta^2\eta^2-h^2}{\delta\eta+h}\nabla[\nabla\bullet(h\tilde{\mathbf{u}})]\right\} + O\left(\frac{\varepsilon}{\nu}\mu^4\right)$$

$$= \tilde{\mathbf{u}} - \frac{\varepsilon}{\nu}\mu^2\left\{\tfrac{1}{6}h^2\nabla(\nabla\bullet\tilde{\mathbf{u}}) - \tfrac{1}{2}h\nabla[\nabla\bullet(h\tilde{\mathbf{u}})]\right\}$$

$$+\delta\frac{\varepsilon}{\nu}\mu^2\eta\left\{\tfrac{1}{6}h\nabla(\nabla\bullet\tilde{\mathbf{u}}) - \tfrac{1}{2}\nabla[\nabla\bullet(h\tilde{\mathbf{u}})]\right\}$$

$$-\delta^2\frac{\varepsilon}{\nu}\mu^2\,\tfrac{1}{6}\eta^2\nabla(\nabla\bullet\tilde{\mathbf{u}}) + O\left(\frac{\varepsilon}{\nu}\mu^4\right) \tag{5.13}$$

Note: $(\delta^3\eta^3+h^3)/(\delta\eta+h) = \delta^2\eta^2+h^2-\delta\eta h$ and $(\delta^2\eta^2-h^2)/(\delta\eta+h) = \delta\eta-h$. Equation (5.12) can be expressed in terms of $\overline{\mathbf{u}}$ by subtracting equation (5.13) from (5.12) and substituting the terms $\tilde{\mathbf{u}} = \overline{\mathbf{u}} + O(\varepsilon\mu^2/\nu)$ [also from equation (5.13)] into the dispersive terms i.e. $O(\varepsilon\mu^2/\nu, \delta\varepsilon\mu^2/\nu, \delta^2\varepsilon\mu^2/\nu)$ gives

$$\mathbf{u} = \overline{\mathbf{u}} + \frac{\varepsilon}{\nu}\mu^2\left\{\left(\tfrac{1}{6}h^2 - \tfrac{1}{2}z^2\right)\nabla(\nabla\bullet\overline{\mathbf{u}}) - \left(z+\tfrac{1}{2}h\right)\nabla[\nabla\bullet(h\overline{\mathbf{u}})]\right\}$$

$$-\delta\frac{\varepsilon}{\nu}\mu^2\eta\left\{\tfrac{1}{6}h\nabla(\nabla\bullet\overline{\mathbf{u}}) - \tfrac{1}{2}\nabla[\nabla\bullet(h\overline{\mathbf{u}})]\right\}$$

$$+\delta^2\frac{\varepsilon}{\nu}\mu^2\,\tfrac{1}{6}\eta^2\nabla(\nabla\bullet\overline{\mathbf{u}}) + O\left(\frac{\varepsilon}{\nu}\mu^4\right) \tag{5.14}$$

In the expression for the horizontal velocity above, the vertical variation through the water column comes about through the presence of the vertical coordinate z. It will be noted that the coordinate z does not appear in the last two terms of equation (5.14) (unlike other Boussinesq-type equations to be developed in Appendix C) and in this sense, the vertical variation of **u** is somewhat more limited. The vertical velocity can be expressed in terms of $\overline{\mathbf{u}}$ by substitution of equation (5.14) for **u** into equation (5.7) for w:

$$w = -\frac{\varepsilon}{\delta}\mu^2\nabla\bullet[(z+h)\overline{\mathbf{u}}] + O\left(\frac{\varepsilon}{\delta}\mu^4\right) \tag{5.15}$$

Substitution of equation (5.14) for **u**, and equation (5.15) for w, into equation (5.6) for p leads to

$$\begin{aligned} p = {} & \left(\eta - \frac{z}{\delta}\right) + \frac{\varepsilon}{\delta}\mu^2\left[\tfrac{1}{2}z^2\nabla\bullet\overline{\mathbf{u}}_t + z\nabla\bullet(h\overline{\mathbf{u}}_t)\right] - \varepsilon\mu^2\left[\delta\tfrac{1}{2}\eta^2\nabla\bullet\overline{\mathbf{u}}_t + \eta\nabla\bullet(h\overline{\mathbf{u}}_t)\right] \\ & + \frac{\nu\varepsilon}{\delta}\mu^2\left\{\tfrac{1}{2}z^2\overline{\mathbf{u}}\bullet\nabla(\nabla\bullet\overline{\mathbf{u}}) + z\overline{\mathbf{u}}\bullet\nabla[\nabla\bullet(h\overline{\mathbf{u}})]\right\} \\ & - \nu\varepsilon\mu^2\left\{\delta\tfrac{1}{2}\eta^2\overline{\mathbf{u}}\bullet\nabla(\nabla\bullet\overline{\mathbf{u}}) + \eta\overline{\mathbf{u}}\bullet\nabla[\nabla\bullet(h\overline{\mathbf{u}})]\right\} \\ & + O\left(\frac{\varepsilon^2}{\delta}\mu^2, \frac{\varepsilon}{\delta}\mu^4\right) \end{aligned} \tag{5.16}$$

Use of the definition of the depth-averaged velocity in the depth-integrated continuity equation (5.4) leads to equation (5.17). Substitution of equations (5.14) for **u**, and equation (5.16) for p into the depth-integrated momentum equation (5.5) leads to equation (5.18). Equations (5.17) and (5.18) are the *first set* of Boussinesq-type equations of Chen *et al.* (1998) for wave-current interaction in shallow water.

$$\eta_t + \nabla\bullet(h\overline{\mathbf{u}}) + \delta\eta\nabla\bullet\overline{\mathbf{u}} + \nu\overline{\mathbf{u}}\bullet\nabla\eta = 0 \tag{5.17}$$

and

$$\begin{aligned} & \overline{\mathbf{u}}_t + \nu(\overline{\mathbf{u}}\bullet\nabla)\overline{\mathbf{u}} + \nabla\eta \\ & \quad + \mu^2[\Lambda_0^1 + \underbrace{\nu\Lambda_1^1 + \delta(\Lambda_2^1 + \nu\Lambda_3^1) + \delta^2(\Lambda_4^1 + \nu\Lambda_5^1)}_{\text{Dispersion terms associated with currents}}] = O(\varepsilon\mu^2, \mu^4) \end{aligned} \tag{5.18}$$

where

$$\Lambda_0^1 = h\Gamma_t \tag{5.18a}$$

$$\Lambda_1^1 = (\overline{\mathbf{u}} \bullet \nabla)(h\Gamma) \tag{5.18b}$$

$$\Lambda_2^1 = -\eta\{\Gamma_t + \nabla[\nabla \bullet (h\overline{\mathbf{u}}_t)]\} \tag{5.18c}$$

$$\Lambda_3^1 = -\eta(\overline{\mathbf{u}} \bullet \nabla)\{\Gamma + \nabla[\nabla \bullet (h\overline{\mathbf{u}})]\} \tag{5.18d}$$

$$\Lambda_4^1 = -\tfrac{1}{3}\eta^2\nabla(\nabla \bullet \overline{\mathbf{u}}_t) \tag{5.18e}$$

$$\Lambda_5^1 = -\tfrac{1}{3}\eta^2(\overline{\mathbf{u}} \bullet \nabla)[\nabla(\nabla \bullet \overline{\mathbf{u}})] \tag{5.18f}$$

in which

$$\Gamma = \tfrac{1}{6}h\nabla(\nabla \bullet \overline{\mathbf{u}}) - \tfrac{1}{2}\nabla[\nabla \bullet (h\overline{\mathbf{u}})] \tag{5.18g}$$

The dispersion relation corresponds to equations (5.17) and (5.18) is a Padé [0,2] expansion of the dispersion relation given by Airy wave theory. Only the dispersion terms Λ_i^1 $(i=2,3,4,5)$ include the free surface elevation η. When the ambient currents vanish, the dispersion terms associated with currents [i.e. Λ_i^1 $(i=1,2,3,4,5)$] become negligible as detailed by Chen (1997) p27-32 and Chen *et al.* (1998) p16-20. As a result, this set of equations reduces to the equations of Peregrine (1967) written below.

$$\eta_t + \nabla \bullet [(h + \varepsilon\eta)\overline{\mathbf{u}}] = 0 \tag{2.111}$$

$$\overline{\mathbf{u}}_t + \varepsilon(\overline{\mathbf{u}} \bullet \nabla)\overline{\mathbf{u}} + \nabla\eta = \mu^2\{\tfrac{1}{2}h\nabla[\nabla \bullet (h\overline{\mathbf{u}}_t)] - \tfrac{1}{6}h^2\nabla(\nabla \bullet \overline{\mathbf{u}}_t)\} + O(\varepsilon\mu^2, \mu^4) \tag{2.112}$$

5.2.4. *Second set* of equations of Chen et *al.* (1998)

The *second set* of partial differential equations of Chen *et al.* (1998) is presented in terms of the horizontal velocity at an arbitrary elevation $\mathbf{u}_\alpha$.

Evaluating $\mathbf{u} = \mathbf{u}_\alpha$ at $z = z_\alpha$, equation (5.14) leads to

$$\mathbf{u}_\alpha = \overline{\mathbf{u}} + \frac{\varepsilon}{\nu}\mu^2\left\{\left(\tfrac{1}{6}h^2 - \tfrac{1}{2}z_\alpha{}^2\right)\nabla(\nabla \bullet \overline{\mathbf{u}}) - \left(z_\alpha + \tfrac{1}{2}h\right)\nabla[\nabla \bullet (h\overline{\mathbf{u}})]\right\}$$

$$-\delta\frac{\varepsilon}{\nu}\mu^2\eta\left\{\tfrac{1}{6}h\nabla(\nabla \bullet \overline{\mathbf{u}}) - \tfrac{1}{2}\nabla[\nabla \bullet (h\overline{\mathbf{u}})]\right\}$$

$$+\delta^2\frac{\varepsilon}{\nu}\mu^2\tfrac{1}{6}\eta^2\nabla(\nabla \bullet \overline{\mathbf{u}}) + O\left(\frac{\varepsilon}{\nu}\mu^4\right) \qquad (5.19)$$

Re-arranging equation (5.19) to make $\overline{\mathbf{u}}$ the subject gives

$$\overline{\mathbf{u}} = \mathbf{u}_\alpha - \frac{\varepsilon}{\nu}\mu^2\left\{\left(\tfrac{1}{6}h^2 - \tfrac{1}{2}z_\alpha{}^2\right)\nabla(\nabla \bullet \overline{\mathbf{u}}) - \left(z_\alpha + \tfrac{1}{2}h\right)\nabla[\nabla \bullet (h\overline{\mathbf{u}})]\right\}$$

$$+\delta\frac{\varepsilon}{\nu}\mu^2\eta\left\{\tfrac{1}{6}h\nabla(\nabla \bullet \overline{\mathbf{u}}) - \tfrac{1}{2}\nabla[\nabla \bullet (h\overline{\mathbf{u}})]\right\}$$

$$-\delta^2\frac{\varepsilon}{\nu}\mu^2\tfrac{1}{6}\eta^2\nabla(\nabla \bullet \overline{\mathbf{u}}) + O\left(\frac{\varepsilon}{\nu}\mu^4\right) \qquad (5.20)$$

Substitution of the terms $\overline{\mathbf{u}} = \mathbf{u}_\alpha + O(\varepsilon\mu^2/\nu)$ into the second derivative terms of equation (5.20) leads to

$$\overline{\mathbf{u}} = \mathbf{u}_\alpha + \frac{\varepsilon}{\nu}\mu^2\left\{\left(\tfrac{1}{2}z_\alpha{}^2 - \tfrac{1}{6}h^2\right)\nabla(\nabla \bullet \mathbf{u}_\alpha) + (z_\alpha + \tfrac{1}{2}h)\nabla[\nabla \bullet (h\mathbf{u}_\alpha)]\right\}$$

$$+\delta\frac{\varepsilon}{\nu}\mu^2\eta\left\{\tfrac{1}{6}h\nabla(\nabla \bullet \mathbf{u}_\alpha) - \tfrac{1}{2}\nabla[\nabla \bullet (h\mathbf{u}_\alpha)]\right\}$$

$$-\delta^2\frac{\varepsilon}{\nu}\mu^2\tfrac{1}{6}\eta^2\nabla(\nabla \bullet \mathbf{u}_\alpha) + O\left(\frac{\varepsilon}{\nu}\mu^4\right) \qquad (5.21)$$

Since there is no mention of z in the above equation, there is no vertical variation of the current field. Substitution of equation (5.21) for $\overline{\mathbf{u}}$ into the *first* *set* of equations [(5.17) and (5.18)] gives the *second set* of Boussinesq-type equations of Chen *et al.*.

$$\eta_t + \nabla \bullet (h\mathbf{u}_\alpha) + \delta\eta\nabla \bullet \mathbf{u}_\alpha + \nu\mathbf{u}_\alpha \bullet \nabla\eta$$

$$+\mu^2(\Pi_0^2 + \underbrace{\delta\Pi_1^2 + \delta^2\Pi_2^2 + \delta^3\Pi_3^2}_{\text{Dispersion terms associated with currents}}) = O(\varepsilon\mu^2, \mu^4) \tag{5.22}$$

and

$$\mathbf{u}_{\alpha_t} + \nu(\mathbf{u}_\alpha \bullet \nabla)\,\mathbf{u}_\alpha + \nabla\eta$$

$$+\mu^2[\Lambda_0^2 + \underbrace{\nu\Lambda_1^2 + \delta(\Lambda_2^2 + \nu\Lambda_3^2) + \delta^2(\Lambda_4^2 + \nu\Lambda_5^2)}_{\text{Dispersion terms associated with currents}}] = O(\varepsilon\mu^2, \mu^4) \tag{5.23}$$

where

$$\Pi_0^2 = \nabla \bullet (h\overline{\Gamma}) \tag{5.22a}$$

$$\Pi_1^2 = \eta\nabla\Gamma_\alpha \tag{5.22b}$$

$$\Pi_2^2 = -\tfrac{1}{2}\eta^2\nabla^2[\nabla \bullet (h\mathbf{u}_\alpha)] \tag{5.22c}$$

$$\Pi_3^2 = -\tfrac{1}{6}\eta^3\nabla^2(\nabla \bullet \mathbf{u}_\alpha) \tag{5.22d}$$

$$\Lambda_0^2 = \Gamma_{\alpha_t} \tag{5.23a}$$

$$\Lambda_1^2 = (\mathbf{u}_\alpha \bullet \nabla)\Gamma_\alpha \tag{5.23b}$$

$$\Lambda_2^2 = -\eta\nabla[\nabla \bullet (h\mathbf{u}_{\alpha_t})] \tag{5.23c}$$

$$\Lambda_3^2 = -\eta(\mathbf{u}_\alpha \bullet \nabla)\nabla[\nabla \bullet (h\mathbf{u}_\alpha)] \tag{5.23d}$$

$$\Lambda_4^2 = -\tfrac{1}{2}\eta^2\nabla(\nabla \bullet \mathbf{u}_{\alpha_t}) \tag{5.23e}$$

$$\Lambda_5^2 = -\tfrac{1}{2}\eta^2(\mathbf{u}_\alpha \bullet \nabla)\nabla(\nabla \bullet \mathbf{u}_\alpha) \tag{5.23f}$$

in which Γ_α and $\overline{\Gamma}$ are defined by equations (3.11a) and (3.18) respectively, and $\nabla^2 = \nabla \bullet \nabla$. The equations (5.22) and (5.23) are applicable to the combined motion of waves and currents in the coastal zone but exclude bottom friction and wave breaking. The dispersion terms associated with currents [i.e. Π_i^2 $(i=1,2,3)$ in the continuity equation (5.22) and Λ_i^2 $(i=1,2,3,4,5)$ in the momentum equation (5.23)] become negligible when the ambient currents vanish as detailed by Chen (1997) p27-32 and Chen *et al.* (1998) p16-20. With no ambient currents, this *second set* of Chen *et al.*'s equations reduces to the Boussinesq-type equations of Nwogu (1993) written below.

$$\eta_t + \nabla \bullet [(h + \varepsilon\eta)\mathbf{u}_\alpha] + \mu^2 \nabla \bullet (h\bar{\Gamma}) = O(\varepsilon\mu^2, \mu^4) \tag{3.16}$$

$$\mathbf{u}_{\alpha_t} + \nabla\eta + \varepsilon(\mathbf{u}_\alpha \bullet \nabla)\mathbf{u}_\alpha + \mu^2 \Gamma_{\alpha_t} = O(\varepsilon\mu^2, \mu^4) \tag{3.17}$$

The terms associated with currents are parts of terms with non-linearity. The terms associated with currents do not affect the dispersion relation[1]. Consequently, the dispersion relation of the *second set* of equations of Chen *et al.* (1998) [(5.22) and (5.23)] is identical to the dispersion relation associated with the partial differential equations of Nwogu (1993) (i.e. a Padé [2,2] from Airy wave theory) (see also Table 1.1).

The *second set* of Boussinesq-type equations of Chen *et al.* (1998) [(5.22) and (5.23)] can be expressed in 1D *dimensional* form. The Boussinesq-type continuity equation (5.22) is

$$\eta_t + [(h + \eta)u_\alpha]_x + \Pi_{1D}^2 = 0 \tag{5.24}$$

where

$$\Pi_{1D}^2 = (h\Gamma_\alpha)_x - \left[\tfrac{1}{6}h^3 u_{\alpha_{xx}} - \tfrac{1}{2}h^2 (hu_\alpha)_{xx}\right]_x + \overbrace{\eta\Gamma_{\alpha_x} - \tfrac{1}{2}\eta^2 (hu_\alpha)_{xxx} - \tfrac{1}{6}\eta^3 u_{\alpha_{xxx}}}^{\text{Dispersive terms associated with currents}} \tag{5.24a}$$

$$\Gamma_\alpha = \tfrac{1}{2} z_\alpha^2 u_{\alpha_{xx}} + z_\alpha (hu_\alpha)_{xx} \tag{5.24b}$$

and the Boussinesq-type momentum equation (5.23) now with bottom friction included is

[1] The dispersion relation is obtained: (i) from the *non-dimensional* governing equations with terms with non-linearity ε dropped or (ii) from the *dimensional* governing equations with non-linear terms dropped (see Sections 3.3 and 4.3).

$$u_{\alpha_t} + g\eta_x + u_\alpha u_{\alpha_x} + \tfrac{1}{2} z_\alpha{}^2 u_{\alpha_{txx}} + z_\alpha (hu_\alpha)_{txx}$$

$$+ u_\alpha \left\{ \tfrac{1}{2} z_{c\alpha} (h^2 u_{\alpha_{xx}})_x + z_{c\alpha} \left[h (hu_\alpha)_{xx} \right]_x \right\}$$

$$- \eta (hu_{\alpha_t})_{xx} - \eta u_\alpha (hu_\alpha)_{xxx} - \tfrac{1}{2} \eta^2 u_{\alpha_{txx}} - \tfrac{1}{2} \eta^2 u_\alpha u_{\alpha_{xxx}} = R_c \qquad (5.25)$$

where

$$R_c = -\frac{g\,|\,u_\alpha\,|\,u_\alpha}{C_c{}^2\, h} \qquad (5.25a)$$

and R_c = bottom friction term, C_c = Chezy coefficient and free coefficient $\alpha = -0.39$ (see Section 3.3). For the frictionless case R_c is zero.

5.3. Boussinesq-type numerical model (1DBMWC-3)

5.3.1. Solution method

The 1D governing equations with bottom friction included [(5.24) and (5.25)] are solved by the present author in a similar fashion as the governing equations in Chapter Three. The continuity equation (5.24) can be then written as equation (3.28):

$$\eta_t = E(\eta, u_\alpha) \qquad (3.28)$$

where

$$E(\eta, u_\alpha) = -\left[(h+\eta)u_\alpha\right]_x - \Pi^2_{1D} \qquad (5.26)$$

The momentum equation (5.25) can also be expressed in the form of equation (3.30):

$$U_{\alpha_t} = F(\eta, u_\alpha) \qquad (3.30)$$

where

$$U_\alpha = u_\alpha + z_\alpha\left[\tfrac{1}{2} z_\alpha u_{\alpha_{xx}} + (hu_\alpha)_{xx}\right] - \eta\left[(hu_\alpha)_{xx} + \tfrac{1}{2}\eta u_{\alpha_{xx}}\right] \qquad (5.27)$$

and

$$F(\eta, u_\alpha) = -g\eta_x - u_\alpha u_{\alpha_x} - u_\alpha\left\{\tfrac{1}{2}z_{c\alpha}{}^2(h^2u_{\alpha_{xx}})_x + z_{c\alpha}[h(hu_\alpha)_{xx}]_x\right\}$$

$$+\eta u_\alpha[(hu_\alpha)_{xxx} + \tfrac{1}{2}\eta u_{\alpha_{xxx}}] + R_c \qquad (5.28)$$

The continuity and momentum equations, which are written in the form of equations (3.28) and (3.30) respectively, are then discretised on a 1D mesh and integrated using the Adams-Bashforth three-step predictor and Adams-Moulton four-step corrector schemes (similar to what is done in Chapter Three). This gives values of η and U_α at time level (t+1).

The velocities at the new time level $U_{\alpha_i}^{t+1}$ remain to be solved. In the next step of the solution process, equation (5.27) is arranged into a matrix form as shown in equation (5.29). It is noted that the resulting coefficient matrix for calculating values of u_α varies with time since it contains terms at time level (t+1). This is in contrast to 1DBMW-1 in Chapter Three, where the coefficient matrix is constant in time. Equation (5.29) is easily solved using Gaussian elimination.

$$\begin{bmatrix} \text{Coefficient} \\ \\ \text{Matrix} \end{bmatrix}^{t+1} \begin{Bmatrix} \\ u_\alpha \\ \\ \end{Bmatrix}^{t+1} = \begin{Bmatrix} \\ U_\alpha \\ \\ \end{Bmatrix}^{t+1} \qquad (5.29)$$

The values of the free surface elevation and horizontal velocity determined above are for inside the fluid domain. At the boundaries, these values are determined using the boundary conditions explained below.

5.3.2. Boundary conditions for waves only case

5.3.2.1. Incoming wave boundary conditions

For a locally constant depth, the continuity equation (5.24) reduces to

$$\eta_t + u_\alpha \eta_x + (h+\eta)u_{\alpha_x} + \left[(\alpha + \tfrac{1}{3})h^3 + \alpha h^2\eta - \tfrac{1}{2}h\eta^2 - \tfrac{1}{6}\eta^3\right]u_{\alpha_{xxx}} = 0 \quad (5.30)$$

If the incoming wave is prescribed as a periodic, small amplitude wave [i.e. $\eta = \frac{1}{2}H_i\cos(kx - \omega t)$], the corresponding horizontal velocity at an arbitrary level ($z = z_\alpha$) u_α can be obtained by substituting equations (3.25) i.e. $\eta = \eta_a \exp[i(kx - \omega t)]$ and $u_\alpha = u_{\alpha a} \exp[i(kx - \omega t)]$ into equation (5.30) giving

$$u_\alpha = \frac{\omega\eta}{k\left\{h - k^2\left[(\alpha + \frac{1}{3})h^3 + \alpha h^2\eta - \frac{1}{2}h\eta^2 - \frac{1}{6}\eta^3\right]\right\}} \quad (5.31)$$

The Sommerfeld radiation condition (3.42) (i.e. $\eta_t + C\eta_x = 0$) is automatically satisfied by equation (5.31).

5.3.2.2. Outgoing wave boundary conditions

The Sommerfeld radiation condition (3.42) can be used to predict the free surface elevation at the outgoing wave boundary.

The Boussinesq-type continuity equation in terms of the depth-averaged velocity $\overline{u}$ is

$$\eta_t + [(h+\eta)\overline{u}]_x = 0 \quad (5.32)$$

Equation (5.32) is substituted into the Sommerfeld radiation condition (3.42) to eliminate η_t giving

$$[(h+\eta)\overline{u}]_x = C\eta_x \quad (5.33)$$

For a locally constant depth, the horizontal velocity is then obtained by integrating equation (5.33) over the x-direction to yield

$$\overline{u} = C\frac{\eta}{(h+\eta)} \tag{5.34}$$

Having solved for $\overline{u}$ in equation (5.34), equation (5.19) is applied to determine u_α. The set of boundary conditions for 1DBMWC-3 are displayed in Figure 5.1 for waves only case.

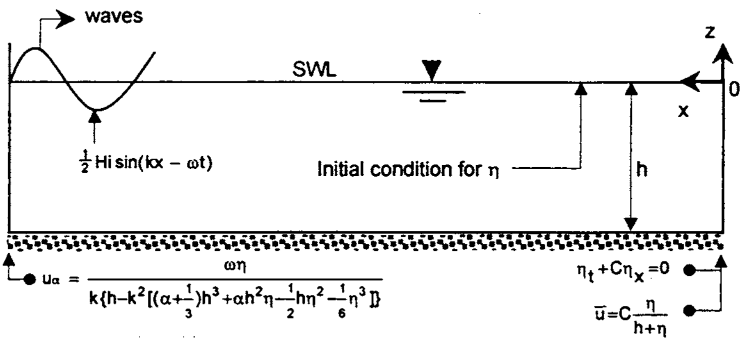

Figure 5.1. Waves only case: the free surface elevation η at the incoming wave boundary is varied sinusoidally with time.

5.3.3. Boundary conditions for current only case

Boundary conditions for the current only case have some similarities with the waves only case and are schematised in Figure 5.2.

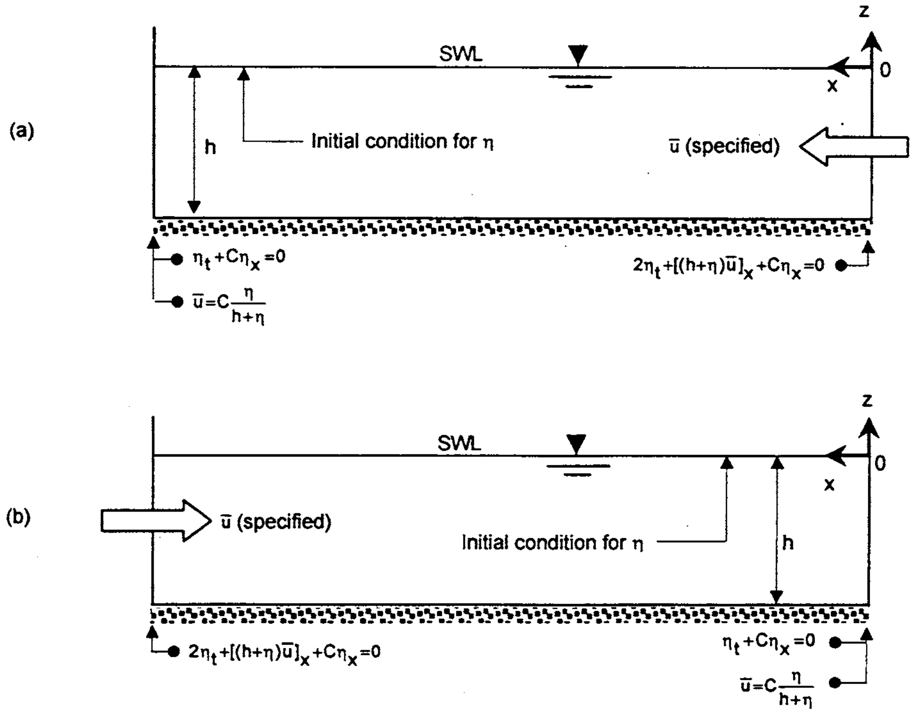

Figure 5.2. Current only case: (a) the imposed current flows from the right to the left hand boundaries; and (b) the imposed current flows from the left to the right hand boundaries. Note: $C=\sqrt{gh}$.

At the upstream end, the depth-averaged velocity is specified but the boundary condition also needs to involve η. One way of linking $\bar{u}$ and η at the upstream end is to combine the Sommerfeld radiation condition (3.42) and the continuity equation (5.32) to give

$$2\eta_t+[(h+\eta)\bar{u}]_x+C\eta_x=0 \tag{5.35}$$

5.3.4. Boundary conditions for wave-current interaction case

The governing equations considered in the present Boussinesq-type numerical model (1DBMWC-3) were derived based on a steady ambient current. In the model tests, the following procedure is adopted i.e.

- 1DBMWC-3 is run with current only from an arbitrary free surface elevation.
- The results from 1DBMWC-3 settle down to a steady state with η_c as the water level.
- After the steady state is reached, a sinusoidally varying surface elevation is imposed at the inflow or outflow boundary. This results in a wave train propagating into the computational domain.

Two boundary conditions applied at each end in the model for wave-current interaction are shown in Figure 5.3.

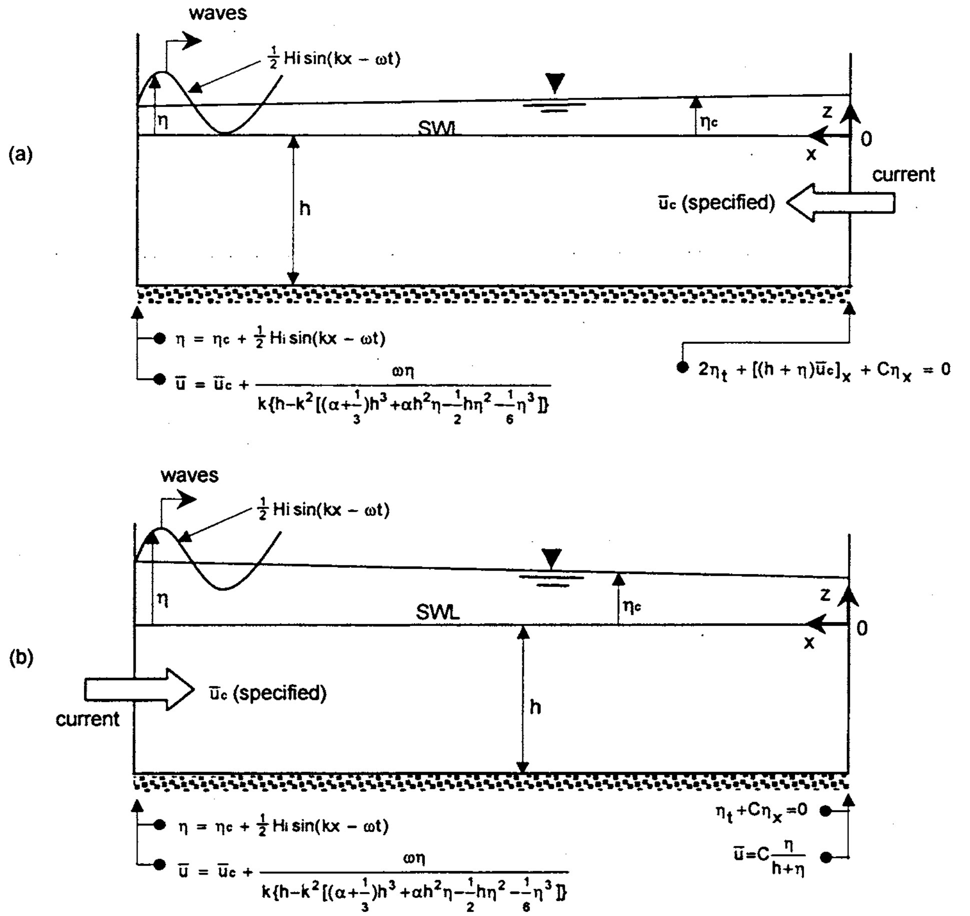

Figure 5.3. Wave-current interaction case: (a) waves and steady opposing current; and (b) waves and steady current in same direction.

The total velocity at the incoming wave boundary are specified by adding the steady current velocity to the orbital wave velocity as

$$\bar{u} = \bar{u}_c + \frac{\omega\eta}{k\left\{h - k^2\left[\left(\alpha + \frac{1}{3}\right)h^3 + \alpha h^2\eta - \frac{1}{2}h\eta^2 - \frac{1}{6}\eta^3\right]\right\}} \tag{5.36}$$

The same comment applies to the free surface elevation as

$$\eta = \eta_c + \tfrac{1}{2}H_i \sin(kx - \omega t) \tag{5.37}$$

5.4. 1D steady, non-linear shallow water numerical model (1DSSWM)

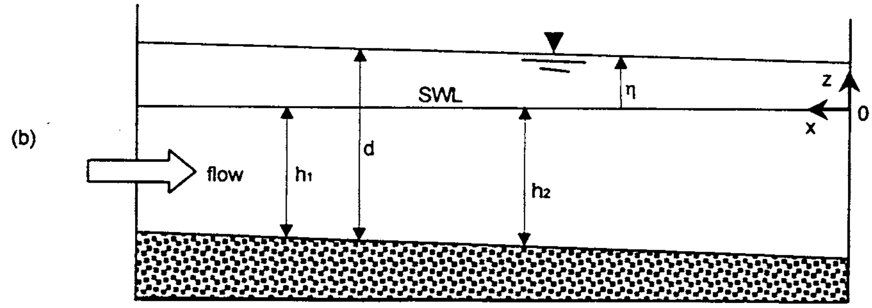

Figure 5.4. Definitions for d, h and η.

Referring to Figure 5.4, the 1D steady, non-linear shallow water equations with bottom friction included are

$$[(h+\eta)\bar{u}]_x = 0 \tag{5.38}$$

$$g\eta_x + \bar{u}\bar{u}_x = R_c \tag{5.39}$$

where

$$R_c = -g\frac{|\bar{u}|\bar{u}}{C_c^2 h} \tag{5.40}$$

where $\bar{u}$ is the depth-averaged horizontal velocity, R_c is the energy slope and C_c is the Chezy coefficient. A numerical model based on equations (5.38) and (5.39) can be used to predict the free surface elevation and velocity of a steady current in a wide channel (since the hydraulic radius has been approximated by the depth). It is noted that Chen (1997) also developed a numerical model based on the equations above for making comparisons with their 1D Boussinesq-type numerical model based on their third equations in the case of pure current motion. In the present study, the procedure of Chen (1997) is followed as far as equation (5.44).

Equations (5.38) and (5.39) can be expressed respectively as

$$(d\overline{u})_x = 0 \qquad (5.41)$$

$$gd_x + \overline{u}\,\overline{u}_x = gh_x + R_c \qquad (5.42)$$

where $d = h + \eta$ is the water depth from the free surface to the bottom and h_x is the bottom slope. Equation (5.42) is re-arranged as

$$\left(gd + \tfrac{1}{2}\overline{u}^2\right)_x = gh_x + R_c \qquad (5.43)$$

The momentum equation (5.43) may be discretised using a first-order accurate, finite difference operator to obtain

$$\left(gd + \tfrac{1}{2}\overline{u}^2\right)_{i-1} = \left(gd + \tfrac{1}{2}\overline{u}^2\right)_i + \tfrac{1}{2}\Delta x[(gh_x + R_c)_{i-1} + (gh_x + R_c)_i] \qquad (5.44)$$

where the unknowns are d_{i-1} and $\overline{u}_{i-1}$. (Note: The convention for the axes adopted here is shown in Figure 5.4). The unknown $\overline{u}_{i-1}$ in equation (5.44) is eliminated by substitution of the continuity equation $(d\overline{u})_i = (d\overline{u})_{i-1}$ and the definition of the friction term $R_c = -g\dfrac{|\overline{u}|\overline{u}}{C_c^2 h}$ into equation (5.44). The result of these operations is the cubic equation in the single unknown d_{i-1}.

$$g(d_{i-1})^3 - X_1(d_{i-1})^2 + X_2 = 0 \qquad (5.45)$$

where

$$X_1 = \left(gd + \tfrac{1}{2}\overline{u}^2\right)_i - \tfrac{1}{2}g\Delta x\left(\frac{|\overline{u}|\overline{u}}{C_c^2 h}\right)_i + g(h_{i-1} - h_i) \qquad (5.45a)$$

$$X_2 = \tfrac{1}{2}\overline{u}_i(d_i)^2\left[\overline{u}_i + g\Delta x\,\frac{|\overline{u}_i|}{(C_c^2 h)_{i-1}}\right] \qquad (5.45b)$$

Equation (5.45) is then solved for d_{i-1} using the Newton-Raphson technique to yield 3 solutions. These correspond to (i) a negative depth, (ii) a depth for subcritical flow and (iii) a depth for supercritical flow. The solution adopted corresponds to the subcritical flow. Free surface elevation due to a current η_{i-1} can be drawn using $d_{i-1} - h_{i-1}$.

5.5. 1D conservation of wave action numerical model (1DWACM)

As explained in Chapter Two, the Doppler shift for a wave train moving on a current can be expressed as

$$\omega_a - \hat{u}_c k = \sigma_i \tag{5.46}$$

or

$$(\omega_a - \hat{u}_c k)^2 - \sigma_i^2 = 0 \tag{5.47}$$

where ω_a is the absolute angular frequency, $\hat{u}_c$ is the horizontal ambient current velocity in the direction of wave propagation, k is the wave number, σ_i is the intrinsic or relative angular frequency. The Boussinesq-type equations [(5.22) and (5.23)] give rise to the Doppler shift (5.47) with a dispersion relation corresponding to a Padé [2,2] approximation in terms of kh, that is

$$\sigma_i^2 = gk^2h\frac{1-\left(\alpha+\frac{1}{3}\right)(kh)^2}{1-\alpha(kh)^2} \tag{5.48}$$

in which h is the water depth and the free coefficient α is used to defined z_α. Substitution of equation (5.48) for σ_i into equation (5.47) leads to

$$\omega_a^2 - 2\omega_a \hat{u}_c k + (\hat{u}_c k)^2 - gk^2h\frac{1-\left(\alpha+\frac{1}{3}\right)(kh)^2}{1-\alpha(kh)^2} = 0 \tag{5.49}$$

If the wave period $\omega_a = 2\pi/T$ and $\hat{u}_c$ are given, equation (5.49) can be solved for wave number k, using for example the Newton-Raphson method. The valid values for k are always positive and are then used to calculate the intrinsic angular frequency σ_i and the group velocity C_g as set out respectively below:

$$\sigma_i = \omega_a - \hat{u}_c k \tag{5.50}$$

$$C_g = nC \tag{5.51}$$

where $C = \dfrac{\omega_a}{k}$ and $n = \frac{1}{2}\left(1 + \dfrac{2kh}{\sinh(2kh)}\right)$

The principle of conservation of wave action equation is expressed as

$$(C_g A_w)_x = 0 \tag{5.52}$$

where $A_w = E/\sigma_i$ is the wave action, $E = \frac{1}{8}\rho g H^2$ is the wave energy, ρ is the fluid density and H is the wave height. Substituting the definition $A_w = E/\sigma_i$ into equation (5.52) and then discretising using a first-order accurate, finite difference operator gives

$$(H_{i-1})^2 = (H_i)^2 \frac{(C_g/\sigma_i)_i}{(C_g/\sigma_i)_{i-1}} \tag{5.53}$$

If H_i is given, a wave envelope can be drawn using $\eta_{i-1} \pm \frac{1}{2} H_{i-1}$, where η_{i-1} is the free surface elevation due to a steady current (without waves) at i – 1 (see Section 5.4). Although the conservation of wave action model (1DWACM) involves wave height, the results do not yield information on the propagation of individual waves, only on the spatial variation of wave height. This is in contrast to Boussinesq-type model models, which yield information on individual waves and how the water level varies within the wave period.

5.6. Experimental set-up 1: a slope

When the current vanishes, the governing equations of 1DBMWC-3 (i.e. the *second set* of equations of Chen *et al.*, 1998) mathematically reduce to the governing equations of 1DBMW-1 (i.e. the equations of Nwogu, 1993). Thus, 1DBMWC-3 is run for simulating wave propagation over a slope with the same numerical experiment set-up as used in 1DBMW-1 (Figure 3.4).

In the first test, 1DBMWC-3 is run with the same test conditions as 1DBMW-1 (i.e. $H_i/h_i = 0.071$, $k_ih_i = \pi$, $h_i/L_o = 0.5$, $L_o/\Delta x = 28.2$, $T/\Delta t = 50.0$) to simulate incident wave propagation from deep water (i.e. $h_i/L_o = 0.5$). The results in Figure 5.5 show that the numerical solutions of both models for the free surface elevation nearly coincide. The small discrepancy between the results of the two models is possibly due to the differences in the boundary conditions for the two models (see Figures 3.3 and 5.2). Comparisons on the model results versus the laboratory measurements are located in Chapter Three. This section focuses on 1DBMWC-3 compared with 1DBMW-1.

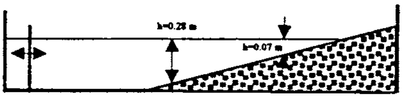

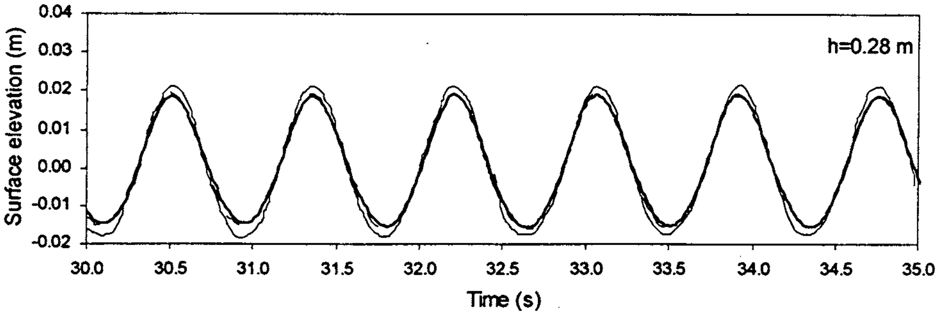

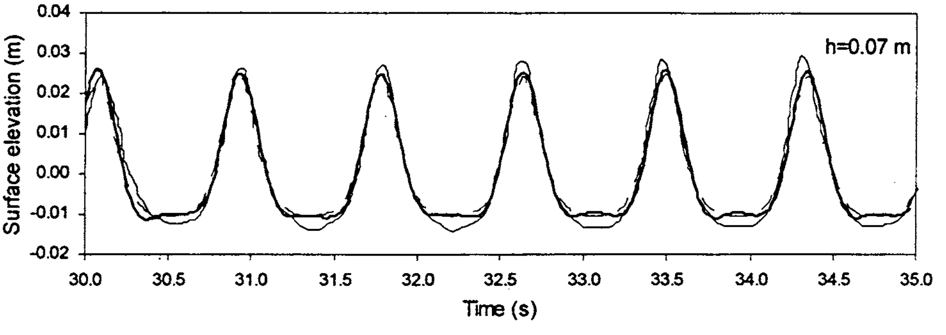

Figure 5.5. Incident deep water waves propagating over a slope: time series of the free surface elevation at 0.28 and 0.07 m depth predicted by 1DBMWC-3 (bold lines), the laboratory measurements (thin lines) and 1DBMW-1 (dashed lines). Test condition: $h_i = 0.56$ m, $H_i = 0.04$ m, $T = 0.85$ s, $\Delta x = 0.04$ m and $\Delta t = 0.017$ s.

The second test is to simulate the shoaling of an intermediate depth wave ($T = 1$ s, $H_i = 0.066$ m, $H_i/h_i = 0.118$, $k_i h_i = 2.30$, $h_i/L_o = 0.36$) with experimental set-up 1. With a grid resolution of $L_o/\Delta x = 39.0$ and $T/\Delta t = 58.8$, 1DBMW-1 (waves only) remains stable. However, 1DBMWC-3 (with the dispersion terms associated with currents included) but operated without currents being present does not remain stable. Consequently, the grid resolution for both models is made coarser to $L_o/\Delta x = 31.2$ and $T/\Delta t = 50.0$ with the result that the model remains stable. The predicted free surface elevation of both models is shown in Figure 5.6. As in the previous test, both numerical solutions are relatively close.

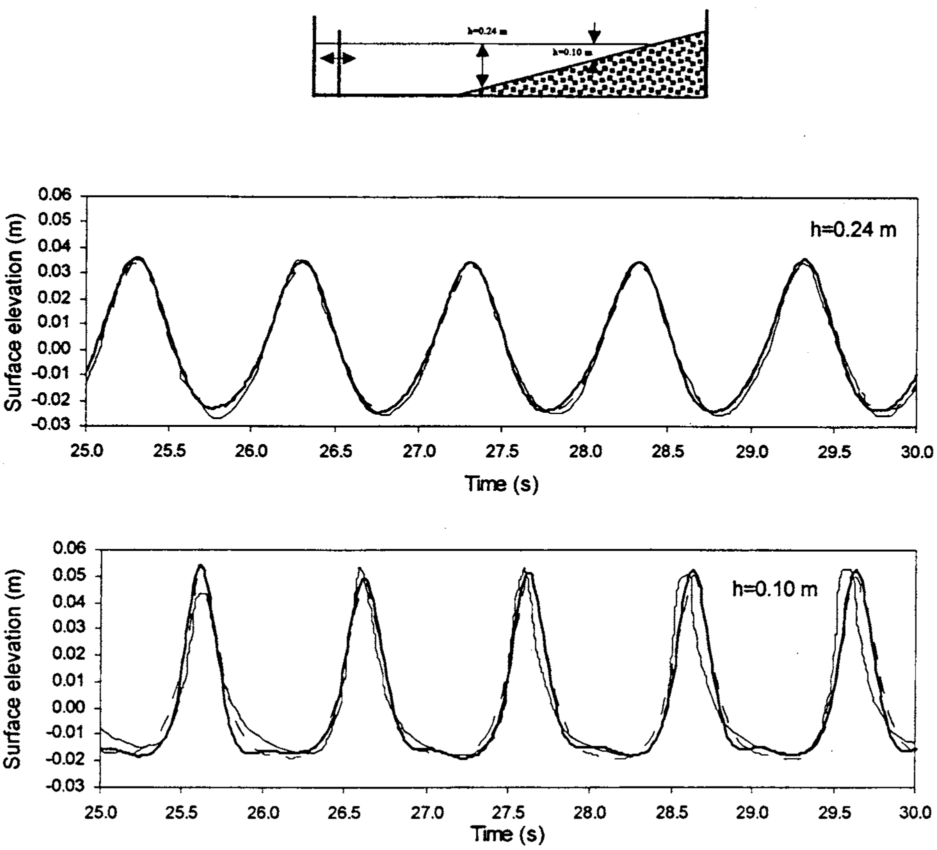

Figure 5.6. Incident intermediate depth water waves propagating over a slope: time series of the free surface elevation at 0.24 and 0.10 m depth predicted by 1DBMWC-3 (bold lines), the laboratory measurements (thin lines) and 1DBMW-1 (dashed lines). Test condition: $h_i = 0.56$ m, $H_i = 0.066$ m, $T = 1$ s, $\Delta x = 0.05$ m and $\Delta t = 0.02$ s.

5.7. Experimental set-up 2: a submerged bar

The second set-up for the numerical experiments consists of a channel with a submerged bar and is represented in Figure 5.7. The channel is 60 m long, 0.8 m deep on both sides of the bar and 0.2 m deep on top of the bar. The Chezy coefficient (C_c) is used to quantify the friction effects along the channel: between chainages 0 – 5 m, $C_c = 300\ m^{1/2}/s$; between chainages 5 – 23 m, $C_c = 30\ m^{1/2}/s$ and between chainages 23 – 60 m, $C_c = 300\ m^{1/2}/s$. This set-up follows that of Chen *et al.* (1998). As reported by Chen *et al.*, the use of the relatively strong bed friction between chainages 5 – 23 m serves to stabilise the flow simulation.

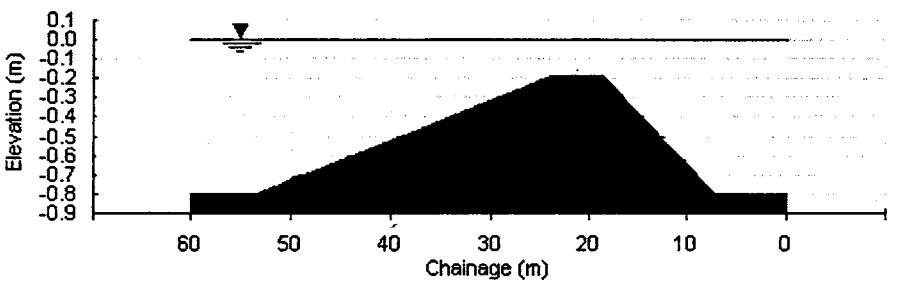

Figure 5.7. Channel with a submerged bar: the channel is 60 m long, 0.8 m deep on both sides of the bar and 0.2 m deep on top of the bar.

5.7.1. Test 1 with submerged bar (set-up 2): Steady current only case

Initially, a flat water surface and a constant inflow velocity of 0.17 m/s is imposed at the right hand boundary (x = 0 m) [see also Figure 5.2(a) for boundary conditions]. The imposed current flows from the right to the left hand boundaries, and reaches a steady state condition after about 120 s. The surface elevation increases to about 0.065 m at the right hand boundary and to approximately 0.052 m at the left hand boundary. Figures 5.8 and 5.8 show that the free surface elevation and velocity predicted by 1DBMWC-3 (bold lines) at $t = 120$ s agree well with the results of 1DSSWM (thin lines). The closeness of the results in Figures 5.8 and 5.9 indicate that the dispersion terms included in 1DBMWC-3 have only a slight effect on the free surface elevation. The biggest difference in the model results occurs where the water surface curvature is large upstream of the bar.

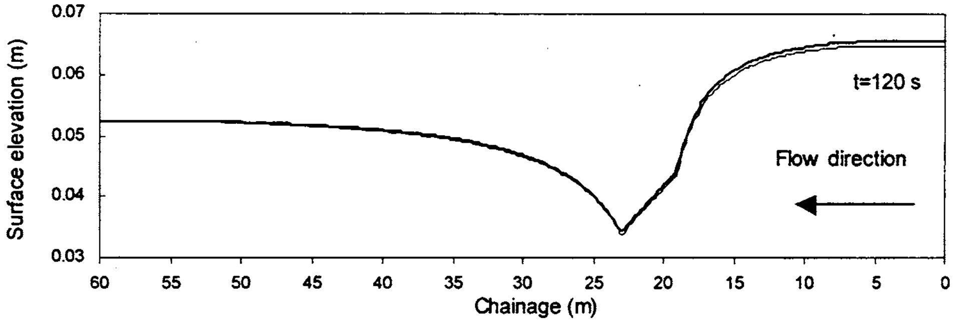

Figure 5.8. Steady flow in open channel with a submerged bar (Test 1): comparison of the free surface elevation predicted by 1DBMWC-3 (bold line) at $t = 120$ s and 1DSSWM (thin line). Test condition: $h_i = 0.8$ m, $\overline{u}_{c(x=0)} = 0.17$ m/s, $\Delta x = 0.2$ m and $\Delta t = 0.05$ s.

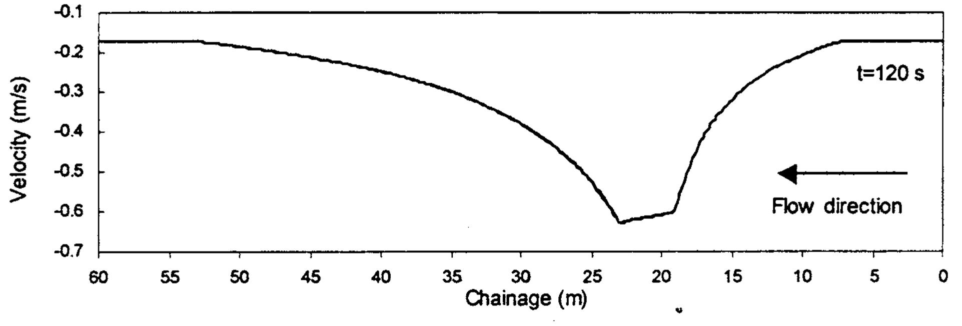

Figure 5.9. Steady flow in open channel with a submerged bar (Test 1): comparison of the horizontal velocity predicted by 1DBMWC-3 (bold line) at $t = 120$ s and 1DSSWM (thin line). Test condition: $h_i = 0.8$ m, $\overline{u}_{c(x=0)} = 0.17$ m/s, $\Delta x = 0.2$ m and $\Delta t = 0.05$ s.

5.7.2. Test 2 with submerged bar (set-up 2): Waves and steady strong opposing current

Once the currents through the channel reach a steady state at $t = 120$ s, the free surface elevation at the left hand boundary ($x = 60$ m) is varied sinusoidally with time [see also Figure 5.3(a) for boundary conditions]. The incoming wave has a period $T = 1.2$ s and an initial wave height of 0.02 m. This computation is performed with a grid resolution of $L_o/\Delta x = 22.5$ and $T/\Delta t = 48.0$ where $L_o = gT^2/(2\pi) = 2.25$ m.

Figure 5.10 shows the free surface elevation predicted by 1DBMWC-3 for combined wave-current motion at a time of $120 + 75 = 195$ s. The wave is blocked at about $x = 26.5$ m (Figure 5.11) when the local current velocity equals the opposing local group velocity. This phenomenon shows that the Boussinesq-type equations can permit an opposing current, which can exceed the group velocity. Figure 5.10 shows a comparison of an instantaneous solution from 1DBMWC-3 (bold line) and the results of 1DWACM (thin lines). They show good agreement from the left hand boundary ($x = 60$ m) to a chainage of about $x = 33$ m and then 1DWACM predicts increasingly higher and higher wave heights which go to infinity at the blocking point.

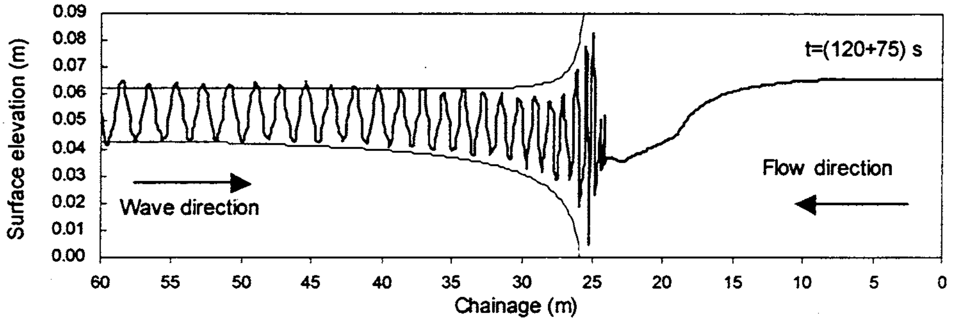

Figure 5.10. Waves propagating over a submerged bar against a steady, strong opposing current (Test 2). The bold line denotes the computed instantaneous solution by 1DBMWC-3 at $t = 120 + 75 = 195$ s. The thin lines defining the wave envelope denote the results of 1DWACM. Test condition: $h_i = 0.8$ m, $H_i = 0.02$ m, $T = 1.2$ s, $\overline{u}c_{(x=0)} = 0.17$ m/s, $\Delta x = 0.1$ m and $\Delta t = 0.025$ s.

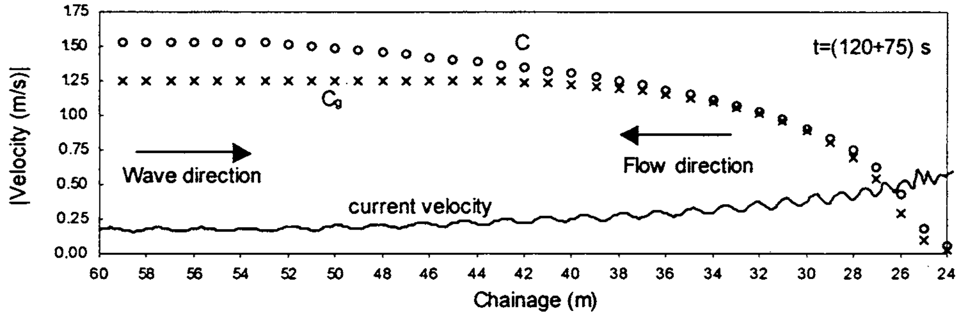

Figure 5.11. Waves propagating over a submerged bar against a steady, strong opposing current (Test 2): the relationship between the absolute local current velocity (bold line) and the local wave celerity (circles) and the local group velocity (crosses) predicted by 1DBMWC-3 at $t = 120 + 75 = 195$ s. Test condition: $h_i = 0.8$ m, $H_i = 0.02$ m, $T = 1.2$ s, $\bar{u}_{c(x=0)} = 0.17$ m/s, $\Delta x = 0.1$ m and $\Delta t = 0.025$ s.

5.7.3. Test 3 with submerged bar (set-up 2): Waves and steady weak opposing current

Test 3 is similar to the previous test, except that this time a wave period of 2.4 s is used instead of 1.2 s [see also Figure 5.3(a) for boundary conditions]. The computation is carried out with a grid resolution of $L_o/\Delta x = 45$ and $T/\Delta t = 96$. 1DBMWC-3 is run for a time of $t = 120 + 47.5 = 167.5$ s. Figure 5.12 shows that the current does not block the 2.4 s wave, which is able to propagate against the current. This is confirmed by Figure 5.13, where it is seen that the local current velocity does not exceed the local group velocity at any location in the channel (compare with the 1.2 s wave in Figure 5.11). In Figure 5.12, it is evident that there is good agreement between the results of 1DBMWC-3 and those of 1DWACM except between $x = 10$ m and $x = 26$ m. In this region of the channel, the wave heights predicted by 1DBMWC-3 are contained with the envelope of wave heights predicted by 1DWACM.

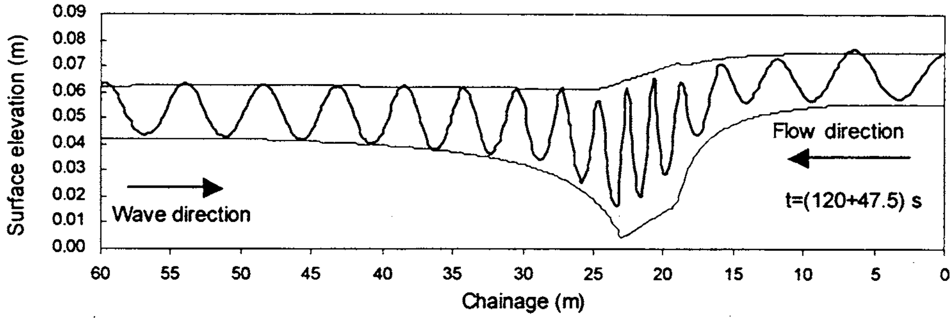

Figure 5.12. Waves propagating over a submerged bar against a steady, weak opposing current (Test 3). The oscillatory motion of the free surface elevation predicted 1DBMWC-3 at $t = 120 + 47.5 = 167.5$ s is enclosed by the wave envelope (thin lines) of the results of 1DWACM. Test condition: $h_i = 0.8$ m, $H_i = 0.02$ m, $T = 2.4$ s, $\bar{u}c_{(x=0)} = 0.17$ m/s, $\Delta x = 0.2$ m and $\Delta t = 0.025$ s.

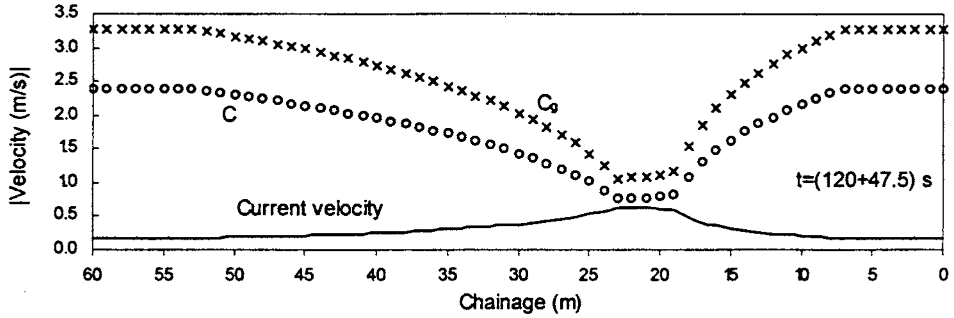

Figure 5.13. Waves propagating over a submerged bar against a steady, weak opposing current (Test 3): the relationship between the absolute local current velocity (line) and local wave celerity (circles) and local group velocity (crosses) predicted by 1DBMWC-3 at $t = 120 + 47.5 = 167.5$ s. Test condition: $h_i = 0.8$ m, $H_i = 0.02$ m, $T = 2.4$ s, $\bar{u}c_{(x=0)} = 0.17$ m/s, $\Delta x = 0.2$ m and $\Delta t = 0.025$ s.

5.7.4. Test 4 with submerged bar (set-up 2): Steady current only case

The fourth test considered here is similar to the first test, but now a constant inflow velocity of 0.17 m/s is imposed at the left hand boundary ($x = 60$ m) instead of at the right hand boundary [see also Figure 5.2(b) for boundary conditions]. The imposed current flows from the left to the right hand boundaries and reaches a steady state condition after about 120 s. This gives rise to a water surface, which varies from about 0.065 m at the left hand boundary ($x = 60$ m) to approximately 0.053 m at the right hand boundary ($x = 0$ m) at the steady state condition at $t = 120$ s. A comparison of the free surface elevation predicted by 1DBMWC-3 (bold line) with 1DSSWM (thin line) gives good agreement as shown in Figure 5.14. As in the first test, the dispersion terms incorporated in 1DBMWC-3 are seen to barely cause any discernible difference in the free surface elevation, even where the curvature of the water surface is large.

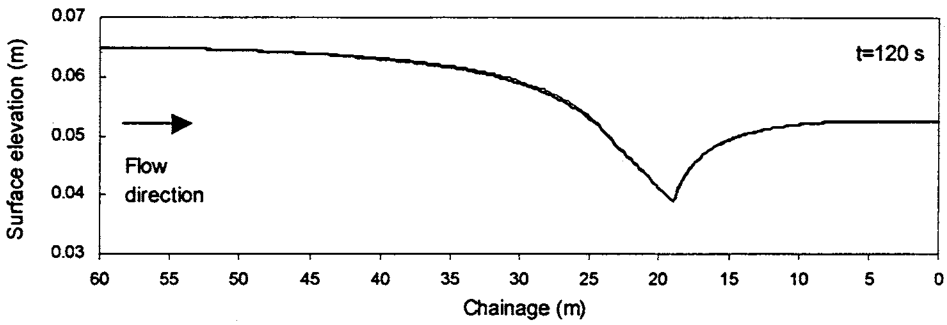

Figure 5.14. Steady flow in open channel with a submerged bar (Test 4): comparison of the free surface elevation predicted by 1DBMWC-3 (bold line) at $t = 120$ s and 1DSSWM (thin line). Test condition: $h_i = 0.8$ m, $\bar{u}_{c(x=60)} = 0.17$ m/s, $\Delta x = 0.2$ m and $\Delta t = 0.05$ s.

5.7.5. Test 5 with submerged bar (set-up 2): Waves and steady current in same direction

After the current reaches a steady state condition (Test 4), the free surface elevation at the left hand boundary ($x = 60$ m) is varied sinusoidally with time [see also Figure 5.3(b) for boundary conditions]. The wave period, incident wave height, grid resolution and time increment remain identical to the values used in the second test (i.e. $T = 1.2$ s, $H_i = 0.02$ m, $\Delta x = 0.2$ m, $L_o/\Delta x = 22.5$, $\Delta t = 0.025$ s and $T/\Delta t = 48.0$). The effects of a current on waves moving in the same direction lead to a noticeable stretching of the wavelengths compared to the case with waves and current in opposite directions (compare Figures 5.15 and 5.10). It can be seen in Figure 5.15 that except near the right hand boundary ($x = 0$ m), good agreement is obtained in a comparison of the free surface elevation from 1DBMWC-3 results (bold line) at $t = 120 + 75 = 195$ s and the results of 1DWACM (thin lines). The discrepancy between the two model results near the right hand boundary is due to boundary conditions, which are evidently not performing well.

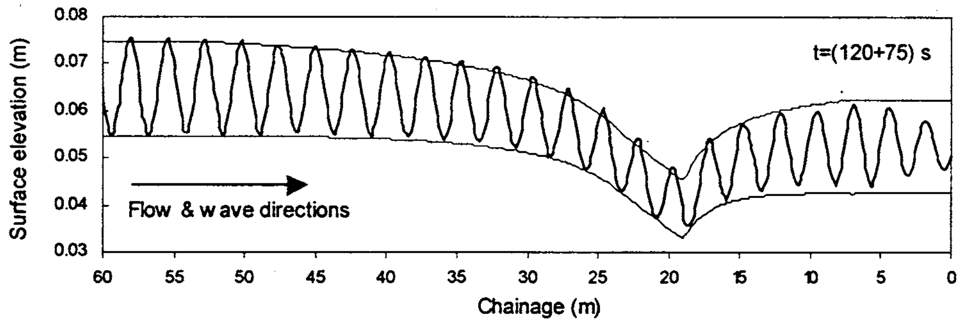

Figure 5.15. Waves and steady current in same direction moving over a submerged bar (Test 5): The bold line denotes the instantaneous water surface (with waves) from 1DBMWC-3 and the thin lines denote 1DWACM. Test condition: $h_i = 0.8$ m, $H_i = 0.02$ m, $T = 1.2$ s, $\overline{u}c_{(x=60)} = 0.17$ m/s, $\Delta x = 0.1$ m and $\Delta t = 0.025$ s.

5.8. Conclusions

A numerical model together with various boundary conditions for fully combined wave-current motion is developed by the present author. This numerical model is referred to as 1DBMWC-3. The governing equations are the 1D Boussinesq-type equations with a Doppler shift in which the dispersion relation corresponds to a Padé [2,2] expansion in terms of kh as derived by Chen *et al.* (1998). The boundary conditions for the present numerical model (1DBMWC-3) are determined for the particular cases of waves only, current only and wave-current interaction.

The governing equations of 1DBMWC-3 mathematically reduce to those of 1DBMW-1 in the absence of an ambient current. This is numerically confirmed by the close agreement between the numerical solutions from 1DBMWC-3 and 1DBMW-1. However, numerical corroboration is still required by extending this work into 2D, which is documented in Chapter Seven.

In the case of pure current motion, the results of 1DBMWC-3 are compared to those of 1DSSWM. Excellent agreement is obtained. When waves are present, the results from the 1DWACM are compared with those from 1DBMWC-3 in the case of fully coupled wave-current motion. The comparison indicates generally good agreement between the results.

Chapter Six

2D Basic Model

6.1. Introduction

One of the main difficulties in a 2D numerical wave model compared to a 1D numerical model is in the furnishing of a set of boundary conditions. Two-dimensional Boussinesq-type numerical models have been proposed; some examples are by Abbott *et al.* (1978), Hauguel (1980), Yoon and Liu (1989), Madsen *et al.* (1991), Madsen and Sørensen (1992), Wei and Kirby (1995), Nwogu (1996) and Sørensen *et al.* (1998). However, detailed consideration of the 2D boundary conditions was not usually included, with a notable exception being that of Wei and Kirby.

Wei and Kirby (1995) developed a 2D Boussinesq-type wave numerical model based on the equations of Nwogu (1993). Their numerical model included incoming, reflecting and outgoing wave boundary conditions. In the case of a monochromatic wave propagating over a shoal, the incoming wave specified was a small amplitude wave. The horizontal velocity at the incoming wave boundary was determined using Airy wave theory. At the reflecting wave boundary, the free surface elevation was obtained by setting the spatial derivative of the free surface elevation normal to an impermeable wall to zero (i.e. $\nabla\eta \bullet \mathbf{n} = 0$). The horizontal velocity at that boundary was obtained by imposing a no-shear condition for the flow along the boundary wall. At the outgoing wave boundary, an approximate radiation boundary condition proposed by Engquist and Majda (1977) was adopted to predict the free surface elevation. However, this boundary condition inevitably introduced some wave reflection along that boundary that led to instability. To reduce the reflection, damping terms were added to the momentum equations. The governing equations and boundary conditions were discretised using an implicit finite difference scheme and a non-staggered grid. Wei and Kirby applied their model: (i) to study wave evolution in a closed basin to verify the symmetry of the computed results and to test various boundary conditions and (ii) to simulate monochromatic wave propagation over an elliptic shoal. A comparison between the numerical model results and laboratory measurements showed that the numerical model was capable of providing a solution for wave propagation over a wide range of water depths.

The 1D numerical model based on the equations of Nwogu (1993) is detailed in Chapter Three (1DBMW-1). However, the aim of the present study is to simulate 2D wave propagation by developing a 2D numerical model based on the Boussinesq-type equations of Nwogu. This 2D numerical model is referred to 2DBMW-4. The numerical scheme applied by Wei and Kirby (1995) is employed by the present author in the model being developed. Three kinds of boundary conditions are incorporated into the numerical scheme:

(i) incoming wave boundary condition,

(ii) outgoing wave boundary condition and

(iii) reflecting wave boundary condition.

At the incoming wave boundary, monochromatic, small amplitude waves are generated. At the outgoing wave boundary, the 2D Sommerfeld radiation condition is applied to calculate both the free surface elevation and horizontal velocity. The reflecting wave boundary conditions are based on zero normal flux.

2DBMW-4 is tested using data from the physical experiments of Chawla and Kirby (1996) [see Chen *et al.* (2000)] and also Berkhoff *et al.* (1982). The main differences between the present work and the previous work of Wei and Kirby (1995) and Wei *et al.* (1999) are in the determination of the appropriate boundary conditions. See Table 6.1 for a summary of the various differences.

Investigators	**Wei and Kirby (1995)**	**Wei *et al.* (1999)**	**Mera (present study)**
Governing equations	Nwogu (1993)	Nwogu (1993)	Nwogu (1993)
Time integration in the numerical scheme	Wei and Kirby (1995) (Third-order predictor & fourth-order corrector schemes)	Wei and Kirby (1995) (Third-order predictor & fourth-order corrector schemes)	Wei and Kirby (1995) (Third-order predictor & fourth-order corrector schemes)
Incoming wave boundary condition	1) Monochromatic waves 2) Continuity equation and Sommerfeld radiation condition	1) Monochromatic and random waves 2) Source function method (Wei *et al.*, 1999)	1) Monochromatic and random waves 2) Continuity equation and Sommerfeld radiation condition
Reflecting wave boundary condition	Wei and Kirby (1995)	Wei and Kirby (1995)	Mera (Present study)
Outgoing wave boundary condition	Engquist and Majda (1977)	Engquist and Majda (1977)	Sommerfeld radiation condition
Other explanation relating to the outgoing wave boundary condition	Damping terms added to the momentum equation	Damping terms added to the momentum equation	Use a filter to reduce reflecting wave from boundary. (Mera, present study)
Test cases	1) Wave evolution in a closed basin. 2) Monochromatic wave propagation over a sloping bed with an elliptic shoal [Berkhoff *et al.*'s (1982) set-up	1) Monochromatic wave propagation over a sloping bed with an elliptic shoal [Berkhoff *et al.*'s (1982) set-up 2) 2D random wave.	1) Monochromatic wave propagation over a flat bottom with an elliptic shoal [Chawla and Kirby's (1996) set-up] 2) Monochromatic wave propagation over a sloping bed with an elliptic shoal [Berkhoff *et al.*'s (1982) set-up]

Table 6.1. Differences between the current and previous research.

6.2. Governing equations for 2D basic model (2DBMW-4)

The governing equations of 2DBMW-4 (the present Boussinesq-type numerical model) are the 2D equations of Nwogu (1993) [i.e. equations (3.16) and (3.17)], which are applicable to the horizontal propagation of regular or irregular, multi-directional waves in water of varying depth. The *dimensional* form of these equations is

$$\eta_t + \nabla \bullet [(h+\eta)\mathbf{u}_\alpha] + \nabla \bullet \left\{\left(\tfrac{1}{2}z_\alpha{}^2 - \tfrac{1}{6}h^2\right)h\nabla(\nabla \bullet \mathbf{u}_\alpha) + \left(z_\alpha + \tfrac{1}{2}h\right)h\nabla[\nabla \bullet (h\mathbf{u}_\alpha)]\right\} = 0 \tag{6.1}$$

$$\mathbf{u}_{\alpha_t} + g\nabla\eta + (\mathbf{u}_\alpha \bullet \nabla)\mathbf{u}_\alpha + z_\alpha\left\{\tfrac{1}{2}z_\alpha\nabla(\nabla \bullet \mathbf{u}_{\alpha_t}) + \nabla[\nabla \bullet (h\mathbf{u}_{\alpha_t})]\right\} = 0 \tag{6.2}$$

where $\mathbf{u}_\alpha = (u_\alpha, v_\alpha)$ = horizontal velocity vector at an arbitrary level ($z = z_\alpha$) below still water level. The definitions for z_α in equation (3.21) and α in equation (3.22) for 1D are also valid in 2D. The Boussinesq-type continuity equation (6.1) can be written as

$$\begin{aligned}\eta_t &+ [(h+\eta)u_\alpha]_x + [(h+\eta)v_\alpha]_y \\ &+ \left(\tfrac{1}{2}z_{c\alpha}{}^2 - \tfrac{1}{6}\right)[h^3(u_{\alpha_{xx}} + v_{\alpha_{xy}})]_x + \left(z_{c\alpha} + \tfrac{1}{2}\right)\{h^2[(hu_\alpha)_{xx} + (hv_\alpha)_{xy}]\}_x \\ &+ \left(\tfrac{1}{2}z_{c\alpha}{}^2 - \tfrac{1}{6}\right)[h^3(u_{\alpha_{xy}} + v_{\alpha_{yy}})]_y + \left(z_{c\alpha} + \tfrac{1}{2}\right)\{h^2[(hu_\alpha)_{xy} + (hv_\alpha)_{yy}]\}_y = 0\end{aligned} \tag{6.3}$$

where $z_{c\alpha} = z_\alpha/h$. Similarly, the Boussinesq-type momentum equation (6.2) in the x- and y-directions can be written as

$$u_{\alpha_t} + \tfrac{1}{2}z_\alpha{}^2(u_{\alpha_{txx}} + v_{\alpha_{txy}}) + z_\alpha[(hu_{\alpha_t})_{xx} + (hv_{\alpha_t})_{xy}] + g\eta_x + u_\alpha u_{\alpha_x} + v_\alpha u_{\alpha_y} = 0 \tag{6.4}$$

$$v_{\alpha_t} + \tfrac{1}{2}z_\alpha{}^2(u_{\alpha_{txy}} + v_{\alpha_{tyy}}) + z_\alpha[(hu_{\alpha_t})_{xy} + (hv_{\alpha_t})_{yy}] + g\eta_y + u_\alpha v_{\alpha_x} + v_\alpha v_{\alpha_y} = 0 \tag{6.5}$$

where the subscripts x and y denote partial differentiation with respect to the x- and y-directions respectively.

6.3. Numerical solution algorithm for 2DBMW-4

6.3.1. Solution method

The governing equations [(6.3) through to (6.5)] are discretised by the present author using the equivalent 2D form of the 1D implicit non-staggered finite difference method in Chapter Three.

- <u>Continuity equation</u>

The continuity equation (6.3) can be written as

$$\eta_t = E(\eta, u_\alpha, v_\alpha) \tag{6.6}$$

where

$$E(\eta,u_\alpha,v_\alpha) = -\left[(h+\eta)u_\alpha\right]_x - \left[(h+\eta)v_\alpha\right]_y$$
$$-\left(\tfrac{1}{2}z_{c\alpha}^2 - \tfrac{1}{6}\right)\left[h^3\left(u_{\alpha_{xx}} + v_{\alpha_{xy}}\right)\right]_x - \left(z_{c\alpha} + \tfrac{1}{2}\right)\left\{h^2\left[(hu_\alpha)_{xx} + (hv_\alpha)_{xy}\right]\right\}_x$$
$$-\left(\tfrac{1}{2}z_{c\alpha}^2 - \tfrac{1}{6}\right)\left[h^3\left(u_{\alpha_{xy}} + v_{\alpha_{yy}}\right)\right]_y - \left(z_{c\alpha} + \tfrac{1}{2}\right)\left\{h^2\left[(hu_\alpha)_{xy} + (hv_\alpha)_{yy}\right]\right\}_y = 0 \tag{6.7}$$

- <u>Momentum equations</u>

The momentum equations [(6.4) and (6.5)] can be expressed as

$$U_{\alpha_t} = F(\eta, u_\alpha, v_\alpha) + \left[F_1(v_\alpha)\right]_t \tag{6.8}$$

$$V_{\alpha_t} = G(\eta, u_\alpha, v_\alpha) + \left[G_1(u_\alpha)\right]_t \tag{6.9}$$

where U_α, V_α, F, G, F_1 and G_1 are the variable groupings defined below:

$$U_\alpha = u_\alpha + z_\alpha\left[\tfrac{1}{2}z_\alpha\, u_{\alpha_{xx}} + (hu_\alpha)_{xx}\right] \tag{6.10}$$

$$V_\alpha = v_\alpha + z_\alpha\left[\tfrac{1}{2}z_\alpha\, v_{\alpha_{yy}} + (hv_\alpha)_{yy}\right] \tag{6.11}$$

$$F(\eta, u_\alpha, v_\alpha) = -g\eta_x - u_\alpha u_{\alpha_x} - v_\alpha u_{\alpha_y} \tag{6.12}$$

$$G(\eta, u_\alpha, v_\alpha) = -g\eta_y - u_\alpha v_{\alpha_x} - v_\alpha v_{\alpha_y} \tag{6.13}$$

$$F_1(v_\alpha) = -z_\alpha\left[\tfrac{1}{2}z_\alpha\, v_{\alpha_{xy}} + (hv_\alpha)_{xy}\right] \tag{6.14}$$

$$G_1(u_\alpha) = -z_\alpha\left[\tfrac{1}{2}z_\alpha\, u_{\alpha_{xy}} + (hu_\alpha)_{xy}\right] \tag{6.15}$$

- <u>Predictor algorithm</u>

The predictor scheme adopted is the explicit third-order Adams-Bashforth method and is applied to the continuity equation (6.6) and the momentum equations [(6.8) and (6.9)] to give

$$\eta_{i,j}^{t+1} = \eta_{i,j}^{t} + \tfrac{1}{12}\Delta t[23E^{t} - 16E^{t-1} + 5E^{t-2}]_{i,j} \tag{6.16}$$

$$U_{\alpha_{i,j}}^{t+1} = U_{\alpha_{i,j}}^{t} + \tfrac{1}{12}\Delta t[23F^{t} - 16F^{t-1} + 5F^{t-2}]_{i,j} + [2F_1^{t} - 3F_1^{t-1} + F_1^{t-2}]_{i,j} \tag{6.17}$$

$$V_{\alpha_{i,j}}^{t+1} = V_{\alpha_{i,j}}^{t} + \tfrac{1}{12}\Delta t[23G^{t} - 16G^{t-1} + 5G^{t-2}]_{i,j} + [2G_1^{t} - 3G_1^{t-1} + G_1^{t-2}]_{i,j} \tag{6.18}$$

All the terms on the right hand sides of equations (6.16) to (6.18) are at the earlier time levels [(t-2) to t] and known from previous calculations.

As in the 1D version of the model (1DBMW-1), values of η_i^{t+1} are calculated directly. However, the horizontal velocity components (u_α,v_α) at the new time level (t+1) are calculated from the known intermediate variables (U_α,V_α) at the new time level (t+1) and defined in equations (6.10) and (6.11). In matrix form, these equations can be written in the form of equations (6.19). These equations require the solution of tridiagonal matrix systems, where the coefficient matrices are constant in time and equations (6.10) and (6.11) are solved using Gaussian elimination.

$$\begin{bmatrix} \text{Coefficient} \\ \\ \text{matrix} \end{bmatrix} \begin{Bmatrix} \\ u_\alpha \\ \\ \end{Bmatrix}^{t+1} = \begin{Bmatrix} \\ U_\alpha \\ \\ \end{Bmatrix}^{t+1} \tag{6.19a}$$

$$\begin{bmatrix} \text{Coefficient} \\ \\ \text{matrix} \end{bmatrix} \left\{ \begin{matrix} \\ v_\alpha \\ \\ \end{matrix} \right\}^{t+1} = \left\{ \begin{matrix} \\ V_\alpha \\ \\ \end{matrix} \right\}^{t+1} \tag{6.19b}$$

Equations (6.19) yield the (x,y) velocity components (u_α, v_α).

- <u>Corrector algorithm</u>

The newly predicted values of $\eta_{i,j}^{t+1}, u_{\alpha_{i,j}}^{t+1}$ and $v_{\alpha_{i,j}}^{t+1}$ are then substituted into equations (6.7), (6.12) to (6.15) to yield $E_{i,j}^{t+1}, F_{i,j}^{t+1}, G_{i,j}^{t+1}, (F_1)_{i,j}^{t+1}$ and $(G_1)_{i,j}^{t+1}$ respectively. These values of these parameters are then substituted into the continuity equation (6.6) and the momentum equations [(6.8) and (6.9)], which are converted to the form of the fourth-order Adams-Moulton corrector, that is

$$\eta_{i,j}^{t+1} = \eta_{i,j}^{t} + \tfrac{1}{24}\Delta t[9E^{t+1} + 19E^{t} - 5E^{t-1} + E^{t-2}]_{i,j} \tag{6.20}$$

$$U_{\alpha_{i,j}}^{t+1} = U_{\alpha_{i,j}}^{t} + \tfrac{1}{24}\Delta t[9F^{t+1} + 19F^{t} - 5F^{t-1} + F^{t-2}]_{i,j} + [F_1^{t+1} - F_1^{t}]_{i,j} \tag{6.21}$$

$$V_{\alpha_{i,j}}^{t+1} = V_{\alpha_{i,j}}^{t} + \tfrac{1}{24}\Delta t[9G^{t+1} + 19G^{t} - 5G^{t-1} + G^{t-2}]_{i,j} + [G_1^{t+1} - G_1^{t}]_{i,j} \tag{6.22}$$

The corrector step is repeated until the misclose between two successive results is less than a pre-set upper limit. The misclose in each of the three dependent variables η, u_α and v_α is calculated separately and defined below:

$$\Delta f = \frac{\sum_{i,j} \left| f_{i,j}^{t+1} - f_{i,j}^{(t+1)*} \right|}{\sum_{i,j} \left| f_{i,j}^{t+1} \right|} \tag{6.23}$$

where f denotes any one of the dependent variables and ( )* denotes the previous iteration values. The corrector step is repeated if $\Delta f > 0.001 = 0.1$ %.

The values of the free surface elevation and horizontal velocities determined above are for inside the fluid domain. At the boundaries, these values are determined using boundary conditions explained below.

6.3.2. Boundary conditions

6.3.2.1. Incoming wave boundary conditions in 2D

The free surface elevation η at the incoming wave boundary is varied sinusoidally as

$$\eta = \tfrac{1}{2}H_i \sin(\mathbf{k} \bullet \mathbf{x} - \omega t) \tag{6.24}$$

where H_i = incoming wave height, $\mathbf{k} \bullet \mathbf{x} = (k \cos \theta_i)\,x + (k \sin \theta_i)\,y$, $\mathbf{k}$ = wave number vector, $k = |\mathbf{k}|$ (see Appendix A for vector components), $\mathbf{x}$ = horizontal spatial vector and θ_i = incoming wave angle between the direction of propagation and the x-axis.

The velocity boundary condition is now considered. A periodic, small amplitude wave is now expressed in exponential form with angular frequency ω.

$$\eta = \eta_a \exp[i(\mathbf{k} \bullet \mathbf{x} - \omega t)], \qquad \mathbf{u}_\alpha = \mathbf{u}_{\alpha a} \exp[i(\mathbf{k} \bullet \mathbf{x} - \omega t)] \tag{6.25}$$

where η_a = amplitude of the water surface elevation and $\mathbf{u}_{\alpha a}$ = amplitude of the horizontal velocity. For a locally constant depth, the continuity equation (6.1) simplifies to

$$\eta_t + (h + \eta)(\nabla \bullet \mathbf{u}_\alpha) + \mathbf{u}_\alpha \bullet \nabla\eta + \left(\alpha + \tfrac{1}{3}\right)h^3 \nabla \bullet [\nabla(\nabla \bullet \mathbf{u}_\alpha)] = 0 \tag{6.26}$$

The horizontal velocity at the incoming wave boundary can be obtained by substituting equations (6.25) into equation (6.26) to eliminate the time and spatial derivatives to give

$$u_\alpha = \frac{\omega\eta}{kh\left[1-\left(\alpha+\frac{1}{3}\right)(kh)^2\right]} \tag{6.27}$$

where $\eta << h$ for a small amplitude wave. Equation (6.27) automatically satisfies the Sommerfeld radiation condition (6.30) in which $C = \omega/k$. Expressing equation (6.27) in the x- and y-directions gives

$$u_\alpha = \frac{\omega\eta}{kh\left[1-\left(\alpha+\frac{1}{3}\right)(kh)^2\right]}\cos\theta_i \tag{6.28}$$

$$v_\alpha = \frac{\omega\eta}{kh\left[1-\left(\alpha+\frac{1}{3}\right)(kh)^2\right]}\sin\theta_i \tag{6.29}$$

Hence at the incoming wave boundary, equation (6.24) specifies η while equations (6.28) and (6.29) yield the velocity components (u_α, v_α) respectively.

6.3.2.2. Outgoing wave boundary conditions in 2D

The boundary condition for η is considered first. At the outgoing wave boundary, the 2D Sommerfeld radiation condition is used to allow the passage and egress of the wave energy, that is

$$\eta_t + \mathbf{C} \bullet \nabla\eta = 0 \tag{6.30}$$

where

$$\mathbf{C} = |\,\mathbf{C}\,|\cos\theta\,\mathbf{i} + |\,\mathbf{C}\,|\sin\theta\,\mathbf{j} \tag{6.31}$$

in which $|\,\mathbf{C}\,| = \dfrac{\omega}{|\,\mathbf{k}\,|}$ and θ is the local wave propagation direction defined by

$$\theta = \tan^{-1}\left(\frac{\eta_y}{\eta_x}\right) \qquad \text{for} \quad \eta_x \neq 0 \tag{6.32}$$

(see Appendix A for a coordinate system). For implementation of the outgoing wave boundary condition into the code, equation (6.30) is transformed into the form of equation (6.6) giving

$$E(\eta, u_\alpha, v_\alpha) = -\left|\mathbf{C}\right|\cos\theta\,\eta_x - \left|\mathbf{C}\right|\sin\theta\,\eta_y \tag{6.33}$$

where the derivatives are discretised as

$$(\eta_x)^t_{i,j} = \frac{1}{2\Delta x}(3\eta_i - 4\eta_{i+1} + \eta_{i+2})^t_j \tag{6.34}$$

$$(\eta_y)^t_{i,j} = \frac{1}{2\Delta y}(\eta_{j+1} - \eta_{j-1})^t_i \tag{6.35}$$

The boundary condition for the velocity components is considered next. The depth-integrated continuity equation (2.36) can be expressed in terms of the depth-averaged horizontal velocity as

$$\eta_t + \nabla \bullet [(h+\eta)\overline{\mathbf{u}}] = 0 \tag{6.36}$$

Equation (6.36) is the exact continuity equation and is identical to the Boussinesq-type continuity equation in terms of the depth-averaged velocity as the velocity variable. Equation (6.36) is then substituted into equation (6.30) to eliminate η_t giving

$$\nabla \bullet [(h+\eta)\overline{\mathbf{u}}] = \mathbf{C} \bullet \nabla\eta \tag{6.37}$$

For a locally constant depth, equation (6.37) may be integrated over the fluid domain to obtain the horizontal velocities

$$\overline{u} = C\frac{\eta}{h+\eta}\cos\theta \tag{6.38}$$

$$\overline{v} = C\frac{\eta}{h+\eta}\sin\theta \tag{6.39}$$

where $C = \left|\mathbf{C}\right|$. Having solved for $\overline{u}$, $\overline{v}$ in equations (6.38) and (6.39), equation (5.19) is applied to determined u_α, v_α.

The formulations for determining the free surface elevation and horizontal velocity in the present numerical model (2DBMW-4) are different to those in the work of Wei and Kirby (1995). These investigators predicted the free surface elevation at a boundary (parallel to the y-axis) using the approximation (6.40) proposed by Engquist and Majda (1977) instead of equation (6.30).

$$\eta_{tt} + C\eta_{xt} - \tfrac{1}{2}C^2\eta_{yy} = 0 \tag{6.40}$$

where $C = \sqrt{gh}$.

Wei and Kirby then calculated the horizontal velocity using the momentum equations with damping terms included instead of equations (6.38) and (6.39). The damping terms were analogous to linear viscous terms in the Navier-Stokes equations (Israeli and Orszag, 1981). More information about the damping terms used in the momentum equations can be found in Wei and Kirby (1995).

Hence the boundary condition for η at the outgoing wave boundary is specified by equation (6.30) and for (u_α, v_α), the boundary conditions are equations (6.38) and (6.39).

6.3.2.3. Reflecting wave boundary conditions in 2D

Boundary condition for v_α

The kinematic boundary condition at an impermeable wall can be stated as

$$\mathbf{u}_\alpha \bullet \mathbf{n} = 0 \qquad \mathbf{x} \in \partial\Omega \tag{6.41}$$

where $\mathbf{n}$ is an outward normal vector, Ω is the fluid domain, $\partial\Omega$ is the boundary and $\mathbf{x}$ is a position in the boundary. Consider, for example, the case of an impermeable wall being parallel to the x-axis. Equation (6.41) is a boundary condition and can be written as

$$v_\alpha = 0 \qquad \mathbf{x} \in \partial\Omega \tag{6.42}$$

<u>Boundary condition for η</u>

The slope and the curvature of v_α normal to the impermeable wall is assumed to be zero and expressed respectively as

$$v_{\alpha_y} = 0 \quad \text{and} \quad v_{\alpha_{yy}} = 0 \qquad \mathbf{x} \in \partial\Omega \tag{6.43}$$

The continuity equation (6.1) can be expressed in terms of the volume flux vector **Q** as

$$\eta_t + \nabla \bullet \mathbf{Q} = 0 \tag{6.44}$$

where

$$\mathbf{Q} = (h+\eta)\mathbf{u}_\alpha + \left(\tfrac{1}{2}z_\alpha^2 - \tfrac{1}{6}h^2\right)h\nabla(\nabla \bullet \mathbf{u}_\alpha) + \left(z_\alpha + \tfrac{1}{2}h\right)h\nabla[\nabla \bullet (h\mathbf{u}_\alpha)] \tag{6.45}$$

Once again, the kinematic boundary can be expressed in terms of the volume flux vector at an impermeable wall as

$$\mathbf{Q} \bullet \mathbf{n} = 0 \qquad \mathbf{x} \in \partial\Omega \tag{6.46}$$

For the case of the impermeable wall being parallel to the x-axis, the volume flux in the y-direction at the boundary becomes zero or

$$(h+\eta)v_\alpha + \left(\tfrac{1}{2}z_\alpha^2 - \tfrac{1}{6}h^2\right)h(u_{\alpha_{xy}} + v_{\alpha_{yy}}) + \left(z_\alpha + \tfrac{1}{2}h\right)h[(hu_\alpha)_{xy} + (hv_\alpha)_{yy}] = 0$$
$$\mathbf{x} \in \partial\Omega \tag{6.47}$$

Substituting equation (6.47) into equation (6.3) gives a reflecting wave boundary condition for calculating the free surface elevation at the boundary wall as set out below:

$$\eta_t + [(h+\eta)u_\alpha]_x + \left(\tfrac{1}{2}z_{c\alpha}^2 - \tfrac{1}{6}\right)[h^3(u_{\alpha_{xx}} + v_{\alpha_{xy}})]_x$$
$$+ \left(z_{c\alpha} + \tfrac{1}{2}\right)\{h^2[(hu_\alpha)_{xx} + (hv_\alpha)_{xy}]\}_x = 0 \qquad \mathbf{x} \in \partial\Omega \tag{6.48}$$

The present approach differs from that of Wei and Kirby, who predicted the free surface elevation at the reflecting wave boundary by imposing

$$\nabla\eta \bullet \mathbf{n} = 0 \qquad \mathbf{x} \in \partial\Omega \tag{6.49}$$

Boundary condition for u_α

For a locally constant depth, the horizontal velocity in the x-direction may be obtained by substituting equations (6.42) and (6.43) into equation (6.47) giving

$$u_{\alpha_{xy}} = 0 \qquad \mathbf{x} \in \partial\Omega \qquad (6.50)$$

The last condition is also different to the work of Wei and Kirby, who imposed a condition of zero shear stress along the boundary wall to estimate u_α.

For a boundary parallel to the x-axis, the boundary conditions are equations (6.48), (6.50) and (6.42) for η, u_α and v_α respectively.

6.3.3. Filter

To enhance the stability of the computation, two three-point filters are applied to $\eta_{i,j}^{t+1}$, $u_{\alpha_{i,j}}^{t+1}$ and $v_{\alpha_{i,j}}^{t+1}$. The filters take the form:

$$f_{i,j}^{t+1} = \frac{1}{r_x + 2}\left(f_{i+1,j}^{*} + r_x \cdot f_{i,j}^{*} + f_{i-1,j}^{*}\right)^{t+1} \qquad (6.51)$$

and

$$f_{i,j}^{t+1} = \frac{1}{r_y + 2}\left(f_{i,j-1}^{*} + r_y \cdot f_{i,j}^{*} + f_{i,j+1}^{*}\right)^{t+1} \qquad (6.52)$$

where f^* denotes η, u_α and v_α, and f denotes the new values of η, u_α and v_α. r_x and r_y are constant smoothing coefficients which are determined empirically.

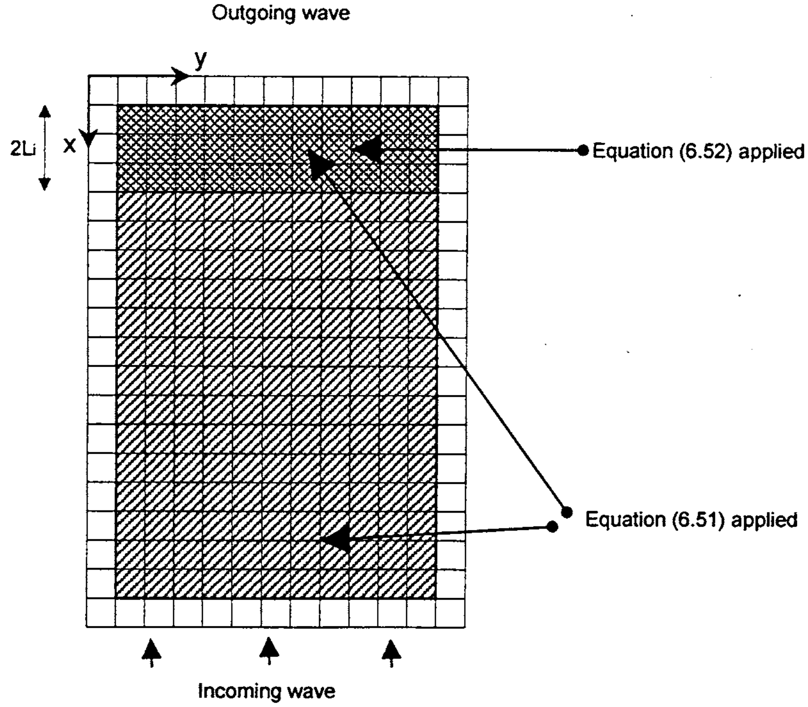

Figure 6.1. Filter.

From Figure 6.1 can be seen that equation (6.51) is applied to all points in the fluid domain excluding the boundaries. Equation (6.52) however, is only applied to a strip of the fluid domain, which is about two times the incoming wavelength in width and is adjacent to the outgoing wave boundary. Consequently, equations (6.7), (6.12) through to (6.15) and (6.20) through to (6.22) are re-calculated after the results have been filtered.

The filters are said to be 'soft' filters because the effects on the results at a particular point are small. To achieve this, the values of the coefficients r_x and r_y should be large numbers. In these computations, for example, r_x and r_y are set to 2000 and 100, respectively. However, small values for r_x and r_y result in large effects on the filtered dependent variables ($f_{i,j}^{t+1}$), which may be followed by spurious attenuation of the wave heights. The values for r_x and r_y are obtained by trial and error. As the values of the coefficients are relatively large numbers and the filtered variables are re-calculated, this will probably not have much effect on the order of the truncation error retained of the governing equations.

6.4. Model verification

6.4.1. Scenario 1: Wave propagation over a circular shoal on a flat bottom basin

As reported by Chen *et al.* (2000), Chawla and Kirby (1996) conducted laboratory experiments of non-breaking wave propagation over a submerged shoal. The physical wave basin was approximately 18 m long and 18.2 m wide. The numerical representation of this wave basin is in Figure 6.2. The centre of the shoal was located at (x,y) = (13,9.22) m with the perimeter given by

$$(x-13)^2+(y-9.22)^2=(2.57)^2 \tag{6.53}$$

The water depth over the circular shoal was given by

$$h=h_{even}+8.73-\sqrt{82.81-(x-13)^2-(y-9.22)^2} \tag{6.54}$$

in which h_{even} was the constant depth of the wave basin while the rest of the basin bathymetry was flat. The incoming wave boundary is located at $x = 18$ m, the outgoing wave boundary is at $x = 0$ m and the reflecting wave boundaries are situated at $y = 0$ m and $y = 18.2$ m.

Chen *et al.* (2000) also used the laboratory set-up of Chawla and Kirby to verify their numerical model, which was based on the Boussinesq-type equations proposed by Wei *et al.* (1995). As noted by Chen *et al.*, the wave height at the incoming wave boundary was 0.0118 m, the wave period was 1.0 s, the depth h_{even} in equation (6.54) was 0.45 m and the top of the shoal had a depth of 0.08 m.

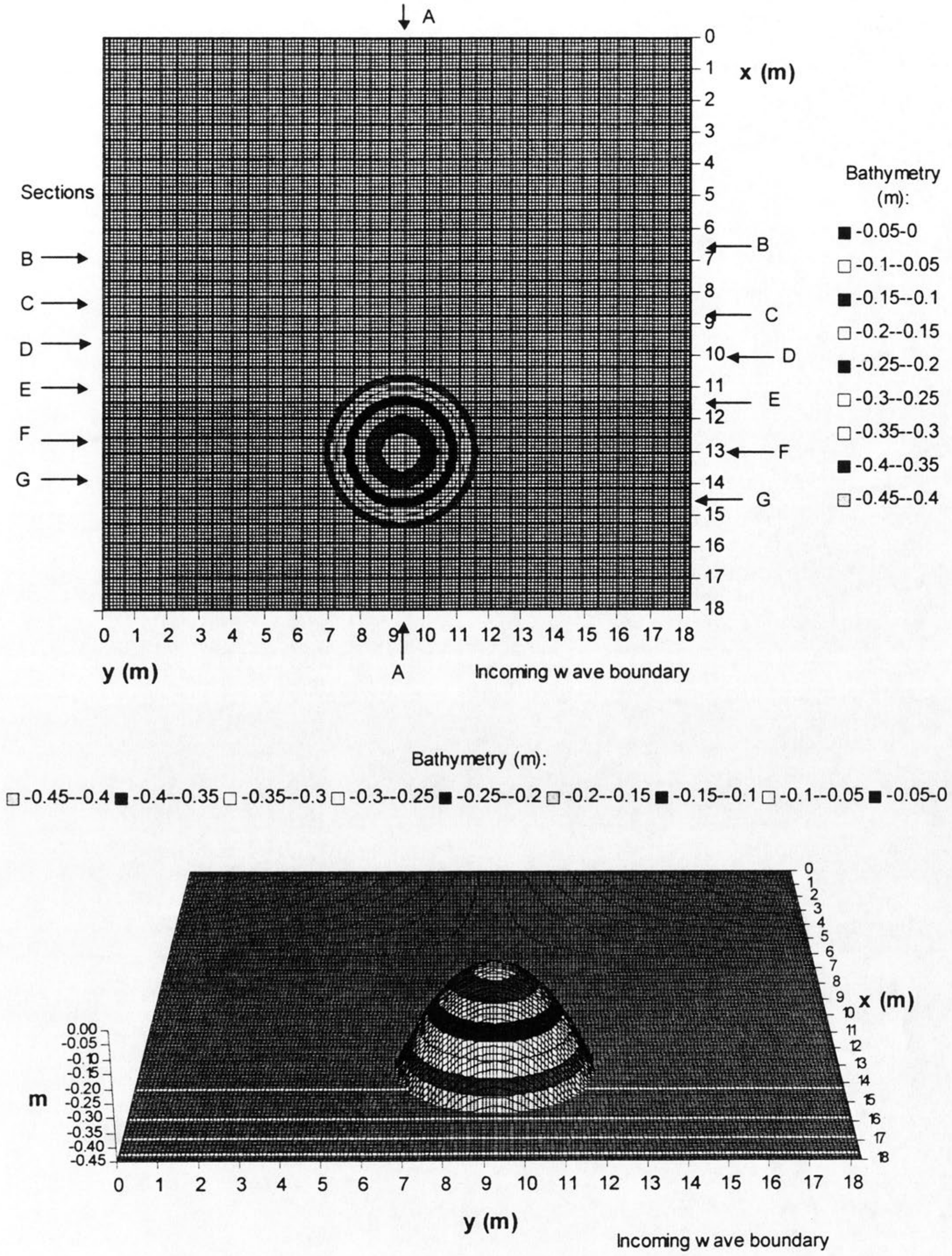

Figure 6.2. Plan (top) and perspective (bottom) views of numerical bathymetry following Chawla and Kirby's (1996) laboratory set-up. Basin size is 18 m long and 18.2 m wide. Side walls are at y = 0 and 18.2 m. Centre of the circular shoal is located at (x,y) = (13,9.22) m. Transects of wave gauge locations: Sections A–A at y = 9.22 m, B–B at x = 6.88 m, C–C at x = 8.35 m, D–D at x = 10.005 m, E–E at x = 11.5 m, F–F at x = 13 m and G–G at x = 14.5 m.

The computation is performed with $\Delta x = 0.05$ m, $\Delta y = 0.1$ m and $\Delta t = 0.01$ s. The initial conditions for 2DBMW-4 runs are a flat water surface at still water level. A monochromatic wave is generated at the incoming wave boundary.

After running 2DBMW-4, the computed free surface elevation is collected during the last 10 s of the 40 s simulation and transformed to the root-mean-square wave height (H_{rms}). The H_{rms} values are normalised by the incoming wave height and represented by solid lines. The computed values for the normalised H_{rms} are compared to the physical data, which are plotted as small circles in Figure 6.3.

The data in Figure 6.3 shows how the waves shoal as they pass over the circular shoal. The wave height is seen to increase sharply by a factor of more than two and half times on top of the shoal, and decrease dramatically behind the shoal. These phenomena are shown along Section A–A. The results of 2DBMW-4 are seen to capture the effects of the combined refraction-diffraction wave field as shown along Sections B–B to G–G. Although the computational shoal is not quite symmetrically located (centred at $y = 9.22$ m instead of $y = 9.10$ m), 2DBMW-4 is still able to accurately simulate the wave field. Perspective views of the shoaling, refracting and diffracting asymmetrical waves can be seen in Figure 6.4.

In addition, 2DBMW-4 is based on the weakly non-linear Boussinesq-type equations. However, when the results from 2DBMW-4 are qualitatively compared with those from fully non-linear model of Chen *et al.* (2000), the accuracy of both models is seen to be comparable.

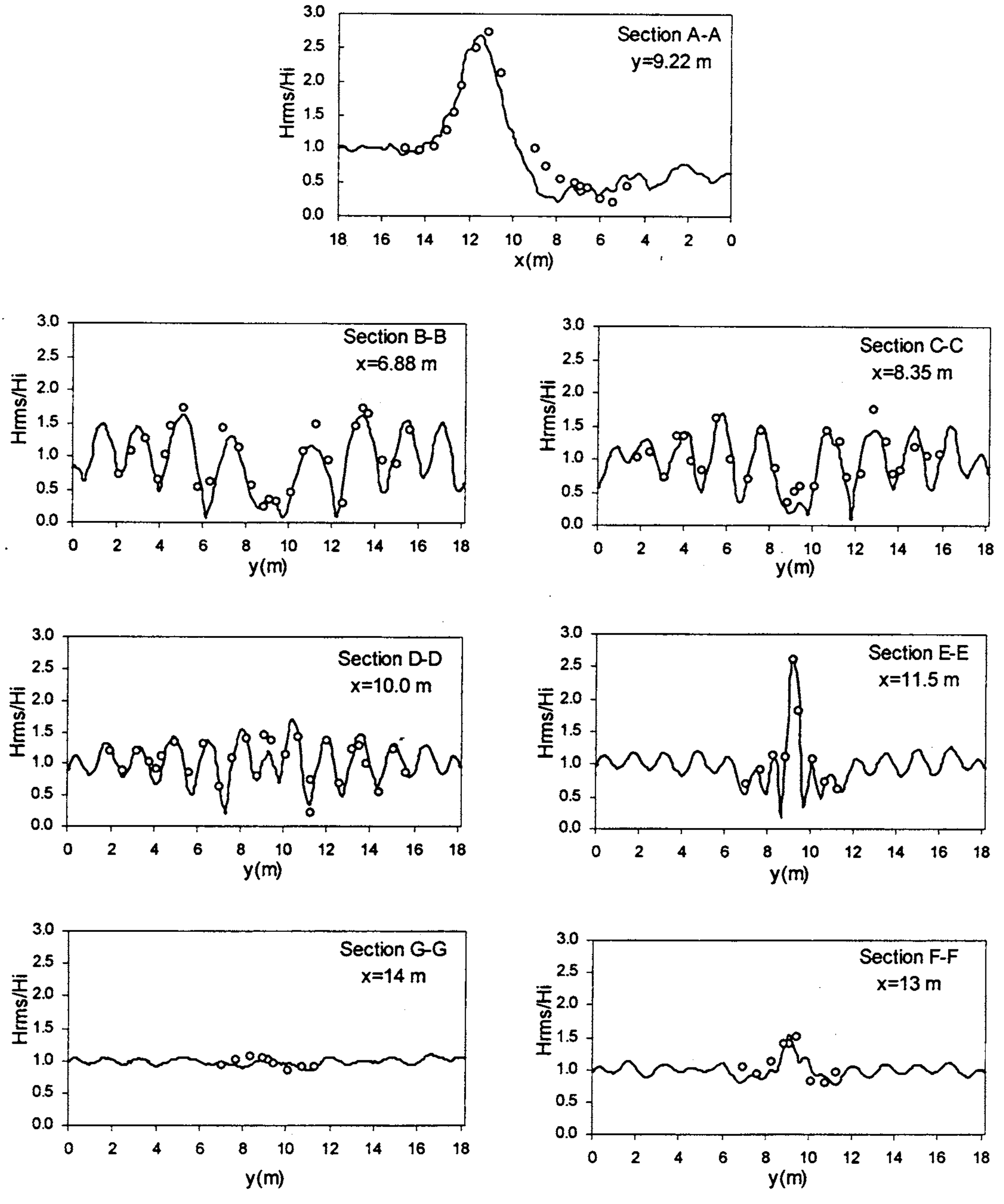

Figure 6.3. Wave heights (H_{rms}) normalised with respect to the incoming wave height: comparisons between 2DBMW-4 (——) and laboratory data (∘∘∘) along various transects for the experiment of Chawla and Kirby (1996). Data: $T = 1.0$ s, $H_i = 0.0118$ m, $\theta_i = 0^\circ$, $h_{even} = 0.45$ m, $\Delta x = 0.05$ m, $\Delta y = 0.10$ m and $\Delta t = 0.01$ s.

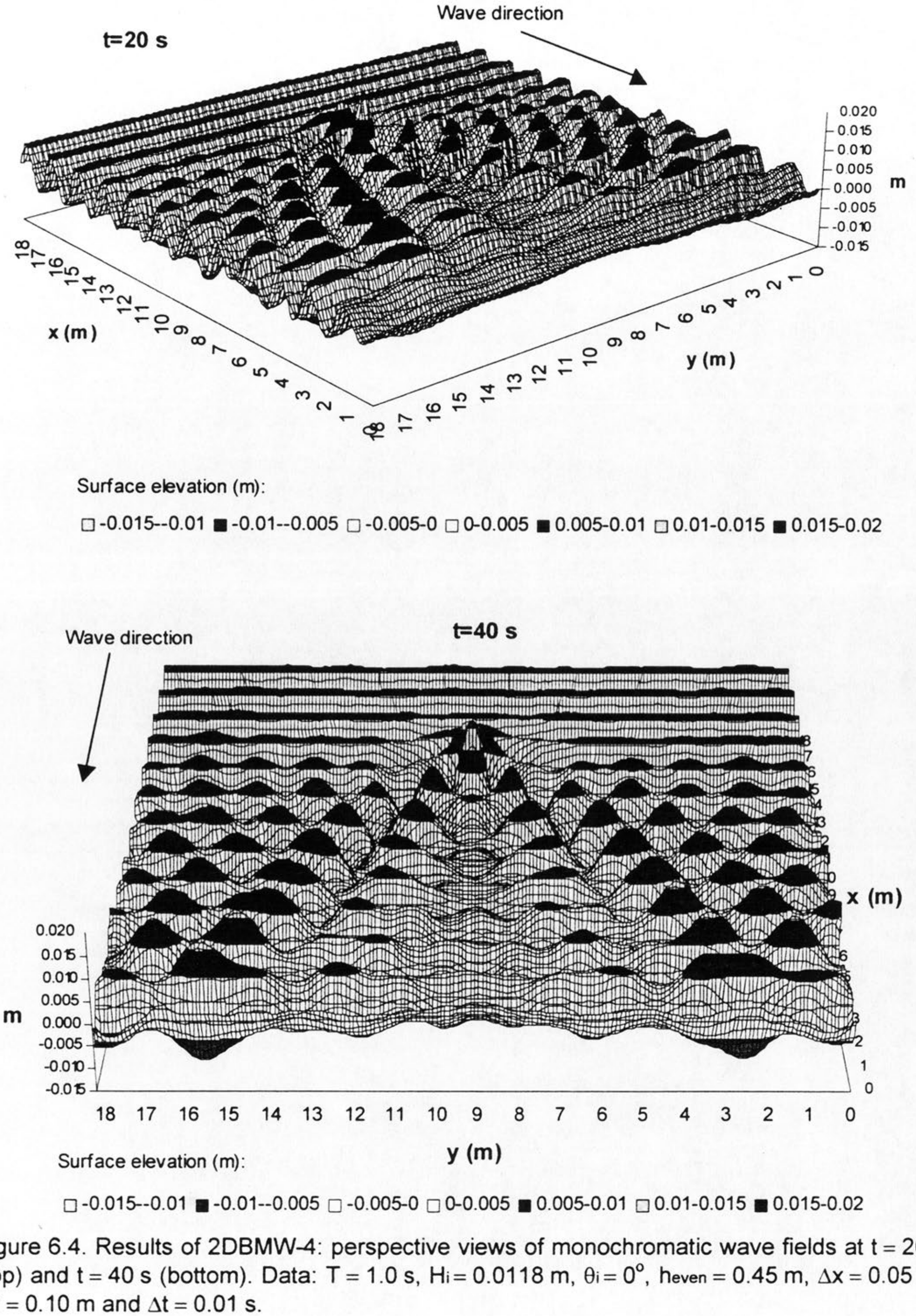

Figure 6.4. Results of 2DBMW-4: perspective views of monochromatic wave fields at t = 20 s (top) and t = 40 s (bottom). Data: T = 1.0 s, H_i = 0.0118 m, $\theta_i = 0^o$, h_{even} = 0.45 m, Δx = 0.05 m, Δy = 0.10 m and Δt = 0.01 s.

6.4.2. Scenario 2: Wave propagation over an elliptic shoal on a sloping bottom basin

Berkhoff *et al.* (1982) conducted some laboratory experiments of wave refraction and diffraction as an incoming monochromatic wave propagated over complex bathymetry. The experimental bathymetry consisted of an elliptic shoal lying on a plane sloping bottom with a slope of 1:50 (the numerical wave basin is shown in Figure 6.5). The bathymetry had the same centre point as the shoal. The depth contours were inclined at an angle of 20^0 to a straight wave paddle. The physical wave basin was approximately 25 m long and 20 m wide. At one side of the basin, waves were generated and at the opposite side, the wave energy was nearly totally dissipated by a breaking process at a gravel beach. At the incoming wave boundary, a monochromatic wave was generated with a period T = 1.0 s and amplitude $\eta_i = 0.0232$ m. For the initial conditions, the water surface is set to still water level. More information about the physical experiment can be found in Berkhoff *et al.* (1982).

Because 2DBMW-4 only applies to non-breaking waves, the numerical wave basin is truncated to be 3 m shorter than the physical one. Consequently, the numerical basin becomes 22 m long and 20 m wide. The incoming wave boundary is located at the same position as in the laboratory (i.e. x = 22 m) and the outgoing wave boundary is at the opposite side at x = 0 m. Meanwhile, the reflecting wave boundaries remain in the same location i.e. at y = 0 m and y = 20 m, and the depth over the flat bottom is 0.45 m.

The computation is performed with $\Delta x = \Delta y = 0.1$ m and $\Delta t = 0.02$ m. The computed free surface elevation is recorded during the last 6 s of the 32 s simulation and transformed to the root-mean-square wave height (H_{rms}). As for the first scenario tested, the H_{rms} wave heights are then normalised by the incoming wave height.

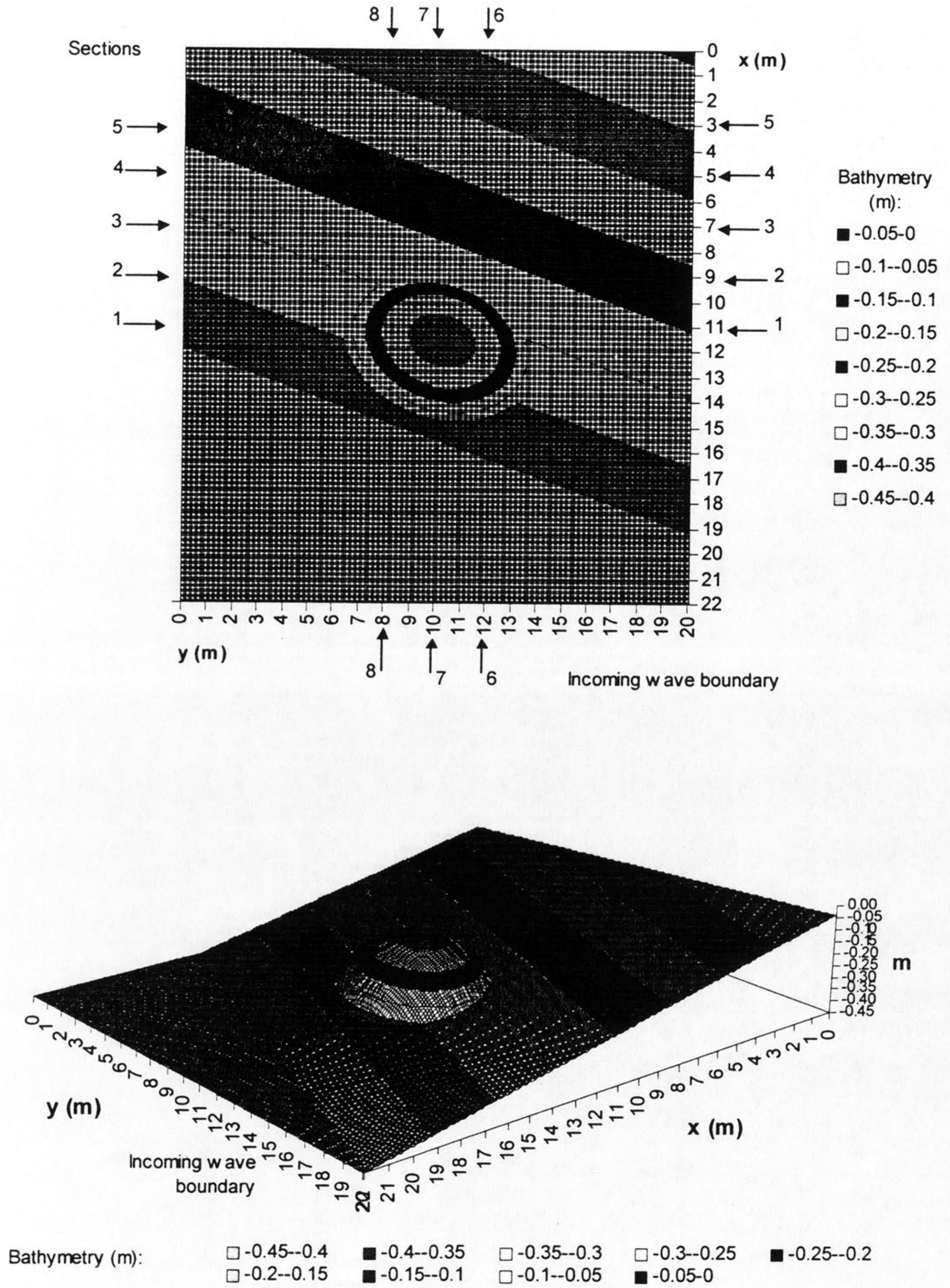

Figure 6.5. Plan (top) and perspective (bottom) views of numerical bathymetry following Berkhoff *et al.*'s (1982) laboratory set-up. Basin size is 22 m long and 20 m wide. Side walls are at y = 0 and 20 m. Centre of the elliptic shoal is located at (x,y) = (12,10) m. Transects of wave gauge locations: Sections 1–1 at x = 11 m, 2–2 at x = 9 m, 3–3 at x = 7 m, 4–4 at x = 5 m, 5–5 at x = 3 m, 6–6 at y = 12 m, 7–7 at y = 10 m and 8–8 at y = 8 m, h_{even} = 0.45 m.

Figure 6.6 shows comparisons of the normalised wave height between the numerical model (lines) and laboratory data (circles). In this scenario, the reflection and diffraction effects are stronger than for the first scenario. It is evident from the results however, that 2DBMW-4 is capable of reasonably simulating the transverse variation of the wave field as shown along Sections 1–1 to 5–5 except for Section 2–2. Here it is noted that the model significantly overestimates the wave height. Wave shoaling can be seen in the longitudinal Sections 6–6 to 8–8 of Figure 6.6. Along the central Section 7–7 it is evident that the model overestimates the wave height significantly in the vicinity of $x = 7$–9 m. 2DBMW-4 simulates the wave shoaling beyond the shoal over the slope reasonably well. Perspective views of these phenomena can be seen in Figure 6.7.

Wei and Kirby (1995) and Wei *et al.* (1999) also used the laboratory data of Berkhoff *et al.* (1982) to compare against the results of their numerical models. The numerical models of both of these groups of investigators and 2DBMW-4 (the present numerical model) are all based on the Boussinesq-type equations proposed by Nwogu (1993). The numerical models differ however, in the different formulations of the boundary conditions. Although based on limited comparisons of laboratory data and numerical model predictions, some general conclusions on the quality of the numerical model solutions can be made. Comparisons show that the wave fields predicted by 2DBMW-4 are generally better than those of Wei and Kirby (1995) but not as good as those of Wei *et al.* (1999).

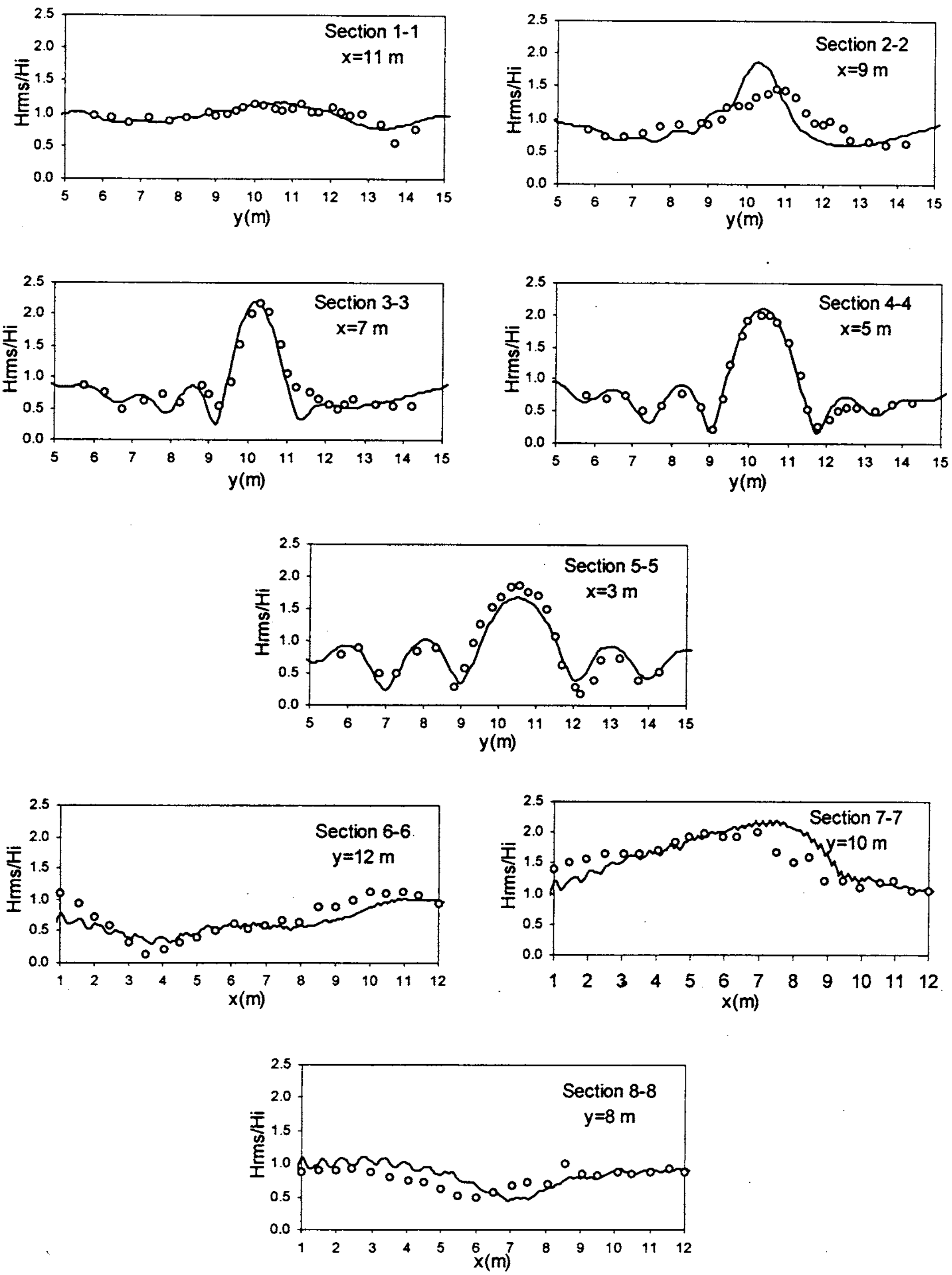

Figure 6.6. Wave height (H_{rms}) normalised with respect to the incoming wave height: comparisons between 2DBMW-4 (——) and laboratory data (∘ ∘ ∘) along various Sections for the experiment of Berkhoff *et al.* (1982). Data: $T = 1.0$ s, $\eta_i = 0.0232$ m, $\theta_i = 0°$, $h_{even} = 0.45$ m, $\Delta x = \Delta y = 0.10$ m and $\Delta t = 0.02$ s.

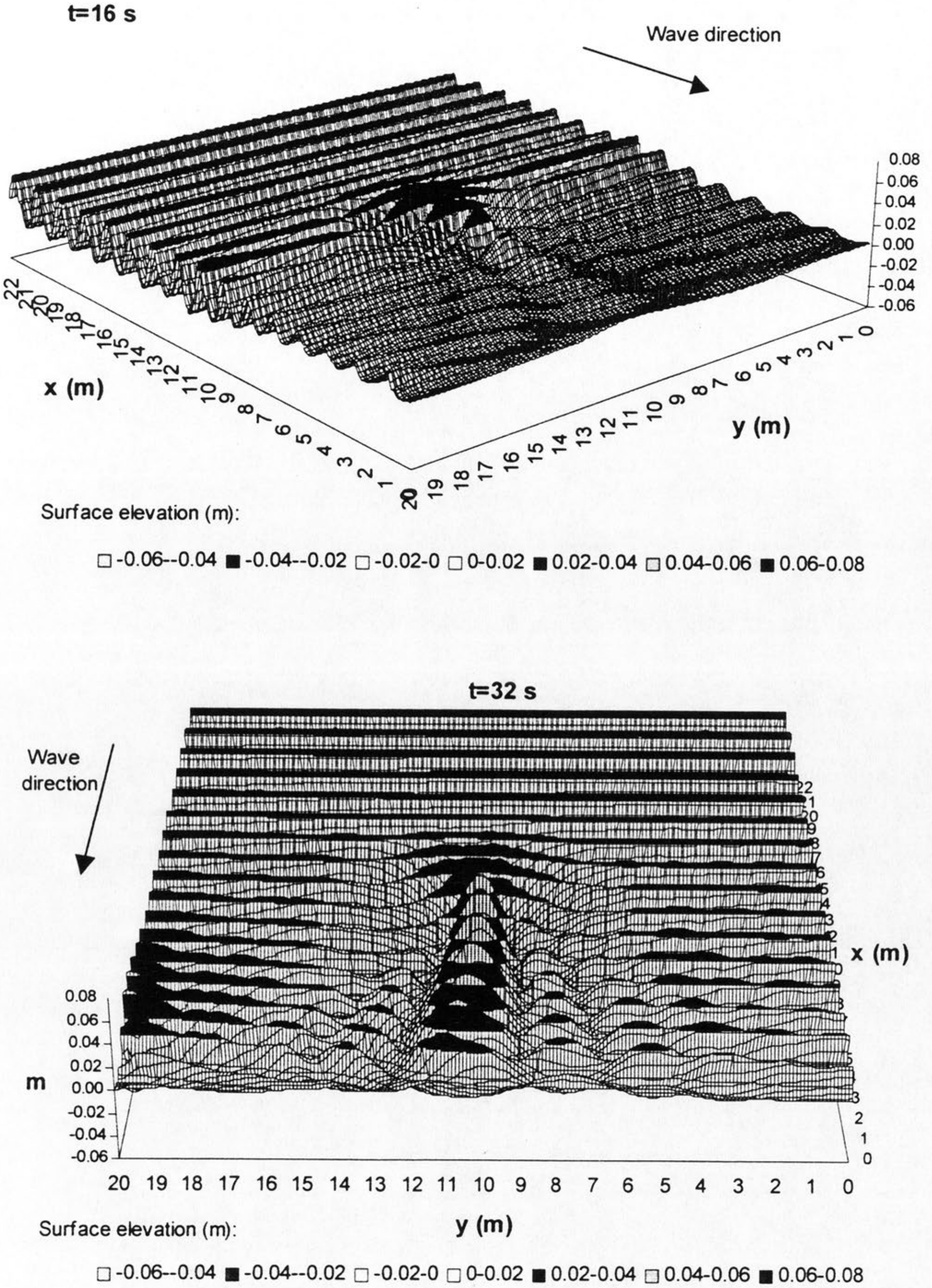

Figure 6.7. Results of 2DBMW-4: perspective views of monochromatic wave fields at t = 16 s (top) and t = 32 s (bottom). Data: T = 1.0 s, $\eta_i = 0.0232$ m, $\theta_i = 0^\circ$, $h_{even} = 0.45$ m, $\Delta x = \Delta y = 0.10$ m and $\Delta t = 0.02$ s.

6.5. Conclusions

A 2D numerical model based on the Boussinesq-type equations proposed by Nwogu (1993) is developed by the present author as the basic numerical model in studying the effects of 2D dispersion terms associated with currents in the next chapter. In the present Boussinesq-type numerical model (2DBMW-4), a monochromatic, small amplitude wave is generated at the incoming wave boundary by varying the free surface elevation sinusoidally. The 2D Sommerfeld radiation condition is employed at the outgoing wave boundary to predict all dependent variables. The reflecting wave boundary conditions are based on zero normal flux. 2DBMW-4 results are compared to the laboratory data for monochromatic wave transformations over a submerged circular shoal lying on a flat bottom basin (Chawla and Kirby, 1996) and over a submerged elliptic shoal resting on a sloping bottom basin (Berkhoff *et al.*, 1982). Comparisons of the results of 2DBMW-4 with laboratory measurements show that it is capable of simulating a non-breaking wave field over a variable bathymetry.

In the previous models by Wei and Kirby (1995) and Wei *et al.* (1999), the absorbing wave boundary introduced by Engquist and Majda (1977) was applied to the outgoing wave boundary instead of the Sommerfeld radiation condition as used in 2DBMW-4. Meanwhile the differences between the previous models themselves were:

- Wei *et al.*'s model employed a source function method at the incoming wave boundary.
- Wei and Kirby's model used a combination of the Boussinesq-type continuity equation and Sommerfeld radiation condition at the incoming wave boundary.

Chapter Seven

2D Basic Model with Current Effects

7.1. Introduction

The effects of wave-current interaction in a 1D Boussinesq-type, numerical model formulation have been reported by the present author in Chapter Five. This formulation is based on the *second set* of equations of Chen *et al.* (1998) (1DBMWC-3). A similar but different model was also proposed by Chen *et al.* (1998) but based on their *third set* of equations.

As mentioned in Chapter Five, the main goal of the present study is to investigate numerically the effects of the dispersion terms associated with currents, which are not included in the equations of Nwogu (1993). The effects of the dispersion terms associated with currents in a 1D numerical model (1DBMWC-3) have been investigated in Chapter Five. Here, the investigation is extended to 2D. Several 2D Boussinesq-type numerical models have already been developed by Yoon and Liu (1989) and Prüser and Zielke (1990).

A 2D numerical model based on the *second set* of Boussinesq-type equations derived by Chen *et al.* (1998) is developed by the present author.

This 2D numerical model is referred to 2DBMWC-5. The *second set* of equations of Chen *et al.* is equivalent to the equations of Nwogu extended to include a current. The governing equations in 2DBMWC-5 are solved by the present author using the non-staggered finite difference method detailed in Chapter Six. A suitable set of boundary conditions is determined by the present author for the three cases of waves only, current only and combined wave-current motion.

The experimental set-up consists of a circular shoal lying on a flat bottom basin. The tests modelled are waves only case, currents only case, waves and opposing current, and waves and current in same direction. To reduce the computational instability believed to be due to the small reflected waves from the outgoing wave boundary, a three-point filter introduced by the present author is applied in the x- and y-directions.

For comparison purposes, laboratory data are only available for the case of wave motion only. Consequently, a 2D numerical model based on the unsteady, non-linear shallow water equations is also developed by the present author. This 2D numerical model is referred to 2DUSWM-6 and is compared with the present Boussinesq-type numerical model (2DBMWC-5) for the currents only case.

7.2. 2D Boussinesq-type numerical model (2DBMWC-5)

7.2.1. Governing equations

The governing equations considered in 2DBMWC-5 are the *second set* of Boussinesq-type equations for fully coupled wave-current motion derived by Chen *et al.* (1998) [i.e. equations (5.22) and (5.23)]. The *dimensional* form of the continuity equation (5.22) is

$$\eta_t + \nabla \bullet [(h+\eta)\mathbf{u}_\alpha] + \Pi^2 = 0 \qquad (7.1)$$

where

$$\Pi^2 = \nabla \bullet (h\Gamma_\alpha) - \nabla \bullet \left\{\tfrac{1}{6}h^3\nabla(\nabla \bullet \mathbf{u}_\alpha) - \tfrac{1}{2}h^2[\nabla \bullet (h\mathbf{u}_\alpha)]\right\} + \eta(\nabla \bullet \Gamma_\alpha)$$

$$-\tfrac{1}{2}\eta^2\nabla \bullet \left\{\nabla[\nabla \bullet (h\mathbf{u}_\alpha)]\right\} - \tfrac{1}{6}\eta^3\nabla \bullet [\nabla(\nabla \bullet \mathbf{u}_\alpha)] \tag{7.1a}$$

Again Γ_α is defined by equation (3.11a). The *dimensional* momentum equation (5.23) is expressed as

$$\mathbf{u}_{\alpha_t} + g\nabla\eta + (\mathbf{u}_\alpha \bullet \nabla)\mathbf{u}_\alpha + \Lambda^{2t} + \Lambda^{2s} = 0 \tag{7.2}$$

where

$$\Lambda^{2t} = \Gamma_{\alpha_t} - \eta\nabla[\nabla \bullet (h\mathbf{u}_{\alpha_t})] - \tfrac{1}{2}\eta^2\nabla(\nabla \bullet \mathbf{u}_{\alpha_t}) \tag{7.2a}$$

$$\Lambda^{2s} = (\mathbf{u}_\alpha \bullet \nabla)\Gamma_\alpha - \eta(\mathbf{u}_\alpha \bullet \nabla)[\nabla \bullet (h\mathbf{u}_\alpha)] - \tfrac{1}{2}\eta^2(\mathbf{u}_\alpha \bullet \nabla)[\nabla(\nabla \bullet \mathbf{u}_\alpha)] \tag{7.2b}$$

The *dimensional* continuity equation (7.1) can be written as

$$\eta_t + [(h+\eta)u_\alpha]_x + [(h+\eta)v_\alpha]_y + \Pi^{2x} + \Pi^{2y} = 0 \tag{7.3}$$

where

$$\Pi^{2x} = \left(\tfrac{1}{2}z_{c\alpha}^2 - \tfrac{1}{6}\right)[h^3(u_{\alpha_{xx}} + v_{\alpha_{xy}})]_x + \left(z_{c\alpha} + \tfrac{1}{2}\right)\left\{h^2[(hu_\alpha)_{xx} + (hv_\alpha)_{xy}]\right\}_x$$

$$+\eta\tfrac{1}{2}z_{c\alpha}^2[h^2(u_{\alpha_{xx}} + v_{\alpha_{xy}})]_x + \eta z_{c\alpha}\left\{h[(hu_\alpha)_{xx} + (hv_\alpha)_{xy}]\right\}_x$$

$$-\tfrac{1}{2}\eta^2[(hu_\alpha)_{xxx} + (hv_\alpha)_{xxy}] - \tfrac{1}{6}\eta^3(u_{\alpha_{xxx}} + v_{\alpha_{xxy}}) \tag{7.3a}$$

$$\Pi^{2y} = \left(\tfrac{1}{2}z_{c\alpha}^2 - \tfrac{1}{6}\right)[h^3(u_{\alpha_{xy}} + v_{\alpha_{yy}})]_y + \left(z_{c\alpha} + \tfrac{1}{2}\right)\left\{h^2[(hu_\alpha)_{xy} + (hv_\alpha)_{yy}]\right\}_y$$

$$+\eta\tfrac{1}{2}z_{c\alpha}^2[h^2(u_{\alpha_{xy}} + v_{\alpha_{yy}})]_y + \eta z_{c\alpha}\left\{h[(hu_\alpha)_{xy} + (hv_\alpha)_{yy}]\right\}_y$$

$$-\tfrac{1}{2}\eta^2[(hu_\alpha)_{xyy} + (hv_\alpha)_{yyy}] - \tfrac{1}{6}\eta^3(u_{\alpha_{xyy}} + v_{\alpha_{yyy}}) \tag{7.3b}$$

The *dimensional* momentum equation (7.2) can be expressed in the x- and y-directions respectively as

$$u_{\alpha_t} + \Lambda^{2tx} + g\eta_x + u_\alpha u_{\alpha_x} + v_\alpha u_{\alpha_y} + \Lambda^{2sx} = 0 \tag{7.4}$$

$$v_{\alpha_t} + \Lambda^{2ty} + g\eta_y + u_\alpha v_{\alpha_x} + v_\alpha v_{\alpha_y} + \Lambda^{2sy} = 0 \qquad (7.5)$$

where

$$\Lambda^{2tx} = \tfrac{1}{2} z_\alpha{}^2 (u_{\alpha_{txx}} + v_{\alpha_{txy}}) + z_\alpha[(hu_\alpha)_{txx} + (hv_\alpha)_{txy}] - \eta[(hu_{\alpha_t})_{xx} + (hv_{\alpha_t})_{xy}]$$

$$- \tfrac{1}{2}\eta^2 (u_{\alpha_{txx}} + v_{\alpha_{txy}}) \qquad (7.4a)$$

$$\Lambda^{2sx} = u_\alpha z_{c\alpha}\left\{\tfrac{1}{2} z_{c\alpha}[h^2(u_{\alpha_{xx}} + v_{\alpha_{xy}})]_x + \{h[(hu_\alpha)_{xx} + (hv_\alpha)_{xy}]\}_x\right\}$$

$$+ v_\alpha z_{c\alpha}\left\{\tfrac{1}{2} z_{c\alpha}[h^2(u_{\alpha_{xx}} + v_{\alpha_{xy}})]_y + \{h[(hu_\alpha)_{xx} + (hv_\alpha)_{xy}]\}_y\right\}$$

$$- \eta\{u_\alpha[(hu_\alpha)_{xxx} + (hv_\alpha)_{xxy}] + v_\alpha[(hu_\alpha)_{xxy} + (hv_\alpha)_{xyy}]\}$$

$$- \tfrac{1}{2}\eta^2[u_\alpha(u_{\alpha_{xxx}} + v_{\alpha_{xxy}}) + v_\alpha(u_{\alpha_{xxy}} + v_{\alpha_{xyy}})] \qquad (7.4b)$$

$$\Lambda^{2ty} = \tfrac{1}{2} z_\alpha{}^2 (u_{\alpha_{txy}} + v_{\alpha_{tyy}}) + z_\alpha[(hu_\alpha)_{txy} + (hu_\alpha)_{tyy}] - \eta[(hu_{\alpha_t})_{xy} + (hv_{\alpha_t})_{yy}]$$

$$- \tfrac{1}{2}\eta^2 (u_{\alpha_{txy}} + v_{\alpha_{tyy}}) \qquad (7.5a)$$

$$\Lambda^{2sy} = u_\alpha z_{c\alpha}\left\{\tfrac{1}{2} z_{c\alpha}[h^2(u_{\alpha_{xy}} + v_{\alpha_{yy}})]_x + \{h[(hu_\alpha)_{xy} + (hv_\alpha)_{yy}]\}_x\right\}$$

$$+ v_\alpha z_{c\alpha}\left\{\tfrac{1}{2} z_{c\alpha}[h^2(u_{\alpha_{xy}} + v_{\alpha_{yy}})]_y + \{h[(hu_\alpha)_{xy} + (hv_\alpha)_{yy}]\}_y\right\}$$

$$- \eta\{u_\alpha[(hu_\alpha)_{xxy} + (hv_\alpha)_{xyy}] + v_\alpha[(hu_\alpha)_{xyy} + (hv_\alpha)_{yyy}]\}$$

$$- \tfrac{1}{2}\eta^2[u_\alpha(u_{\alpha_{xxy}} + v_{\alpha_{xyy}}) + v_\alpha(u_{\alpha_{xyy}} + v_{\alpha_{yyy}})] \qquad (7.5b)$$

7.2.2. Numerical solution algorithm for 2DBMWC-5

7.2.2.1. Solution method

In the present work, the governing equations [(7.3), (7.4) and (7.5)] are solved using an implicit, non-staggered finite difference method. The numerical technique adopted here follows that in Chapter Six and is not repeated here but rather a brief outline of the equations solved is given.

The *dimensional* continuity equation (7.3) can be written in the form of equation (6.6), that is

$$\eta_t = E(\eta, u_\alpha, v_\alpha) \tag{6.6}$$

where

$$E(\eta, u_\alpha, v_\alpha) = -[(h+\eta)u_\alpha]_x - [(h+\eta)v_\alpha]_y - \Pi^{2x} - \Pi^{2y} \tag{7.6}$$

The *dimensional* momentum equations (7.4) and (7.5) can be expressed in the form of equations (6.8) and (6.9) respectively, that is

$$U_{\alpha_t} = F(\eta, u_\alpha, v_\alpha) + [F_1(v_\alpha)]_t \tag{6.8}$$

$$V_{\alpha_t} = G(\eta, u_\alpha, v_\alpha) + [G_1(u_\alpha)]_t \tag{6.9}$$

where U_α, V_α, F, G, F_1 and G_1 are

$$U_\alpha = u_\alpha + \tfrac{1}{2}(z_\alpha^2 - \eta^2)u_{\alpha_{xx}} + (z_\alpha - \eta)(hu_\alpha)_{xx} \tag{7.7}$$

$$V_\alpha = v_\alpha + \tfrac{1}{2}(z_\alpha^2 - \eta^2)v_{\alpha_{yy}} + (z_\alpha - \eta)(hv_\alpha)_{yy} \tag{7.8}$$

$$F(\eta, u_\alpha, v_\alpha) = -g\eta_x - u_\alpha u_{\alpha_x} - v_\alpha u_{\alpha_y} - \Lambda^{2sx} \tag{7.9}$$

$$G(\eta, u_\alpha, v_\alpha) = -g\eta_y - u_\alpha v_{\alpha_x} - v_\alpha v_{\alpha_y} - \Lambda^{2sy} \tag{7.10}$$

$$F_1(v_\alpha) = -\tfrac{1}{2}(z_\alpha^2 - \eta^2)v_{\alpha_{xy}} - (z_\alpha - \eta)(hv_\alpha)_{xy} \tag{7.11}$$

$$G_1(u_\alpha) = -\tfrac{1}{2}(z_\alpha^2 - \eta^2)u_{\alpha_{xy}} - (z_\alpha - \eta)(hu_\alpha)_{xy} \tag{7.12}$$

Equations (7.7) and (7.8) can be arranged into matrix form as shown in equations (7.13). It is noted that all matrices are at the time level (t+1) with the coefficient matrix varying with time. (This is in contrast to those in Chapter Six, which are constant in time). Equations (7.13) are solved using Gaussian elimination.

$$\begin{bmatrix} \text{Coefficient} \\ \\ \text{matrix} \end{bmatrix}^{t+1} \begin{Bmatrix} \\ u_\alpha \\ \\ \end{Bmatrix}^{t+1} = \begin{Bmatrix} \\ U_\alpha \\ \\ \end{Bmatrix}^{t+1} \tag{7.13a}$$

$$\begin{bmatrix} \text{Coefficient} \\ \\ \text{matrix} \end{bmatrix}^{t+1} \begin{Bmatrix} \\ v_\alpha \\ \\ \end{Bmatrix}^{t+1} = \begin{Bmatrix} \\ V_\alpha \\ \\ \end{Bmatrix}^{t+1} \tag{7.13b}$$

7.2.2.2. Boundary conditions for waves only case in 2D

The set of boundary conditions for the waves only case is discussed first. (In subsequent subsection, the other cases of currents only and waves plus currents will be considered).

7.2.2.2.1. Incoming wave boundary conditions in 2D

For a locally constant depth, the continuity equation (7.1) reduces to

$$\eta_t + (h+\eta)(\nabla \bullet \mathbf{u}_\alpha) + \mathbf{u}_\alpha \bullet \nabla\eta$$
$$+ \left[\left(\alpha + \tfrac{1}{3}\right)h^3 + \alpha h^2\eta - \tfrac{1}{2}h\eta^2 - \tfrac{1}{6}\eta^3\right] \nabla \bullet [\nabla(\nabla \bullet \mathbf{u}_\alpha)] = 0 \tag{7.14}$$

If the prescribed incoming wave is a periodic, small amplitude wave defined by equations (6.25), the horizontal velocity at the incoming wave boundary can be obtained by substituting equations (6.25) into equation (7.14) giving

$$u_\alpha = \frac{\omega\eta}{k\left\{h - k^2\left[\left(\alpha + \frac{1}{3}\right)h^3 + \alpha h^2\eta - \frac{1}{2}h\eta^2 - \frac{1}{6}\eta^3\right]\right\}} \tag{7.15}$$

It is noted that the Sommerfeld radiation condition (6.30) i.e. $\eta_t + \mathbf{C} \bullet \nabla\eta = 0$ (in which $\mathbf{C} = \omega/k$) is automatically satisfied by equation (7.15). If equation (7.15) is expressed in the x- and y-directions the result is

$$u_\alpha = \frac{\omega\eta}{k\left\{h - k^2\left[\left(\alpha + \frac{1}{3}\right)h^3 + \alpha h^2\eta - \frac{1}{2}h\eta^2 - \frac{1}{6}\eta^3\right]\right\}}\cos\theta_i \tag{7.16}$$

$$v_\alpha = \frac{\omega\eta}{k\left\{h - k^2\left[\left(\alpha + \frac{1}{3}\right)h^3 + \alpha h^2\eta - \frac{1}{2}h\eta^2 - \frac{1}{6}\eta^3\right]\right\}}\sin\theta_i \tag{7.17}$$

7.2.2.2.2. Outgoing wave boundary conditions in 2D

As in Chapter Six, the 2D Sommerfeld radiation condition (6.30) is applied at the outgoing wave boundary to predict the free surface elevation. The horizontal velocities are determined based on the depth-integrated continuity equation. As a result, equations (6.38) and (6.39) for $\bar{u}$ and $\bar{v}$ respectively are also valid here, that is

$$\bar{u} = C\frac{\eta}{h+\eta}\cos\theta \tag{6.38}$$

$$\bar{v} = C\frac{\eta}{h+\eta}\sin\theta \tag{6.39}$$

Having solved for $\bar{u}$, $\bar{v}$ in equations (6.38) and (6.39), equation (5.19) is applied to determined u_α, v_α.

7.2.2.2.3. Reflecting wave boundary conditions in 2D

The reflecting wave boundary conditions in 2DBMWC-5 are similarly derived as for 2DBMW-4 in Chapter Six. Using the conditions specified in equations (6.41) through to (6.43), the continuity equation (7.1) can be expressed in terms of the volume flux vector **Q** as in equation (6.44)

$$\eta_t + \nabla \bullet \mathbf{Q} = 0 \tag{6.44}$$

where

$$\mathbf{Q} = (h+\eta)(\mathbf{u}_\alpha + \Gamma_\alpha) - \tfrac{1}{6}(h^3+\eta^3)\nabla(\nabla \bullet \mathbf{u}_\alpha) + \tfrac{1}{2}(h^2-\eta^2)\nabla[\nabla \bullet (h\mathbf{u}_\alpha)] \tag{7.18}$$

Applying the kinematic boundary condition in terms of the volume flux vector at an impermeable wall as shown in equation (6.46), the volume flux in the y-direction (i.e. for the case of the impermeable wall being parallel to the x-axis) at the boundary, is zero

$$\mathbf{Q}_y = 0 \qquad \mathbf{x} \in \partial\Omega \tag{7.19}$$

i.e.

$$(h+\eta)v_\alpha + \left[\tfrac{1}{2}z_\alpha^2(h+\eta) - \tfrac{1}{6}(h^3+\eta^3)\right](u_{\alpha_{xy}} + v_{\alpha_{yy}})$$
$$+\left[z_\alpha(h+\eta) + \tfrac{1}{2}(h^2+\eta^2)\right]\left[(hu_\alpha)_{xy} + (hv_\alpha)_{yy}\right] = 0 \qquad \mathbf{x} \in \partial\Omega \tag{7.20}$$

Following the procedures in Chapter Six, the continuity equation (6.48) for predicting the free surface elevation and $u_{\alpha_{xy}} = 0$ i.e. equation (6.50) for the horizontal velocity at the reflecting wave boundary become equations (7.21) and (7.22) respectively.

$$\eta_t + [(h+\eta)u_\alpha]_x + \Pi^{2x} = 0 \qquad \mathbf{x} \in \partial\Omega \tag{7.21}$$

$$u_{\alpha_{xy}} = 0 \qquad \mathbf{x} \in \partial\Omega \tag{7.22}$$

where equation (7.22) remains identical to equation (6.50).

For a boundary parallel to the x-axis, the boundary conditions are equations (7.21), (7.22) and (5.23) for η, u_α and v_α respectively. Two set of boundary conditions for 2DBMWC-5 are deployed in Figure 7.1 for the waves only case.

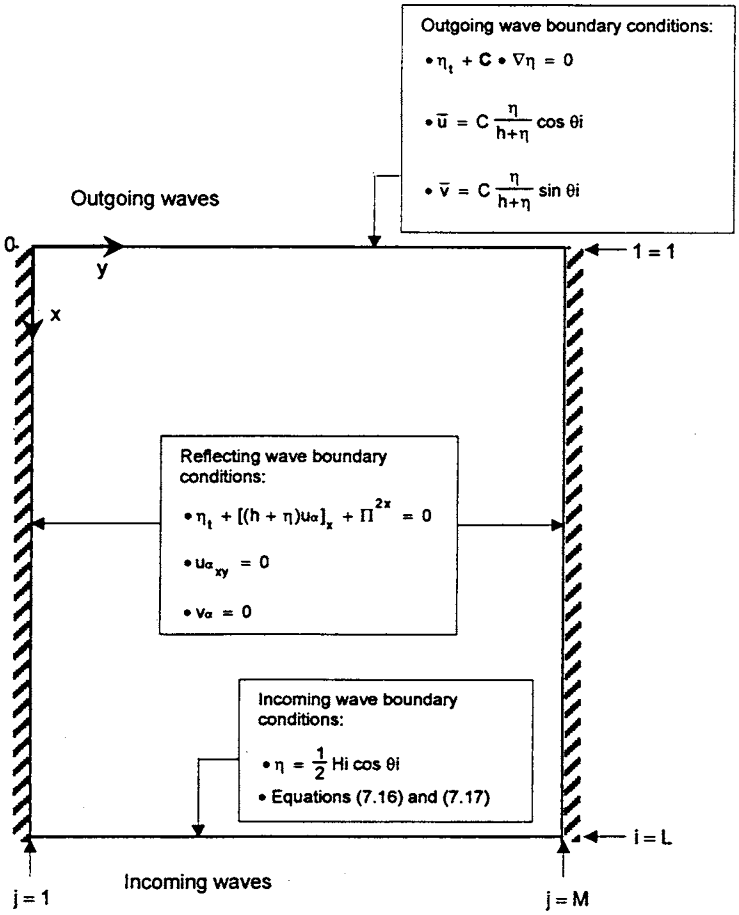

Figure 7.1. Boundary conditions for wave only case. The imposed monochromatic wave propagates from $i = L$ to $i = 1$. Side walls are located at $j = 1$ and $j = M$. Note: $i = 1,2,3,\ldots L$ and $j = 1,2,3,\ldots,M$.

7.2.2.3. Boundary conditions for current only case in 2D

Boundary conditions for current only case are carried over from Section 5.3.3 (for η and $\bar{u}$ at inflow and outflow boundaries) and Subsection 7.2.2.2 (for no-flow boundary conditions i.e. equivalent to the reflecting wave boundary conditions). These boundary conditions are schematised in Figure 7.2.

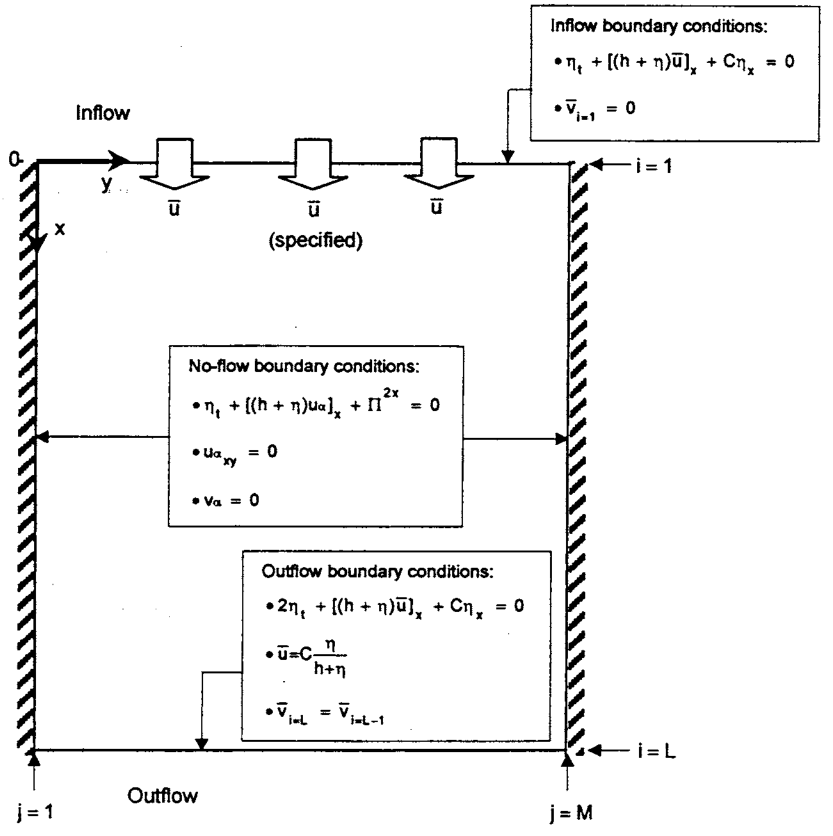

Figure 7.2. Boundary conditions for current only case. The imposed current flows from i = 1 to i = L. Side walls are located at j = 1 and j = M. Note: i = 1,2,3,...L.; j = 1,2,3,...,M and $C = \sqrt{gh}$. Explanations for equations to determine η and $\bar{u}$ at inflow and outflow boundaries can be found in Section 5.3.3.

7.2.2.4. Boundary conditions for wave-current interaction case in 2D

As in the 1D model tests (Chapter Five), the following procedure is again adopted i.e.

- Model is run with current only from an arbitrary free surface elevation (see Figure 7.2).
- The results from the model settle down to a steady state.
- After the steady state is reached, a sinusoidally varying surface elevation is imposed at the inflow or outflow boundary. This results in a wave train propagating into the computational domain (see Figure 7.3).

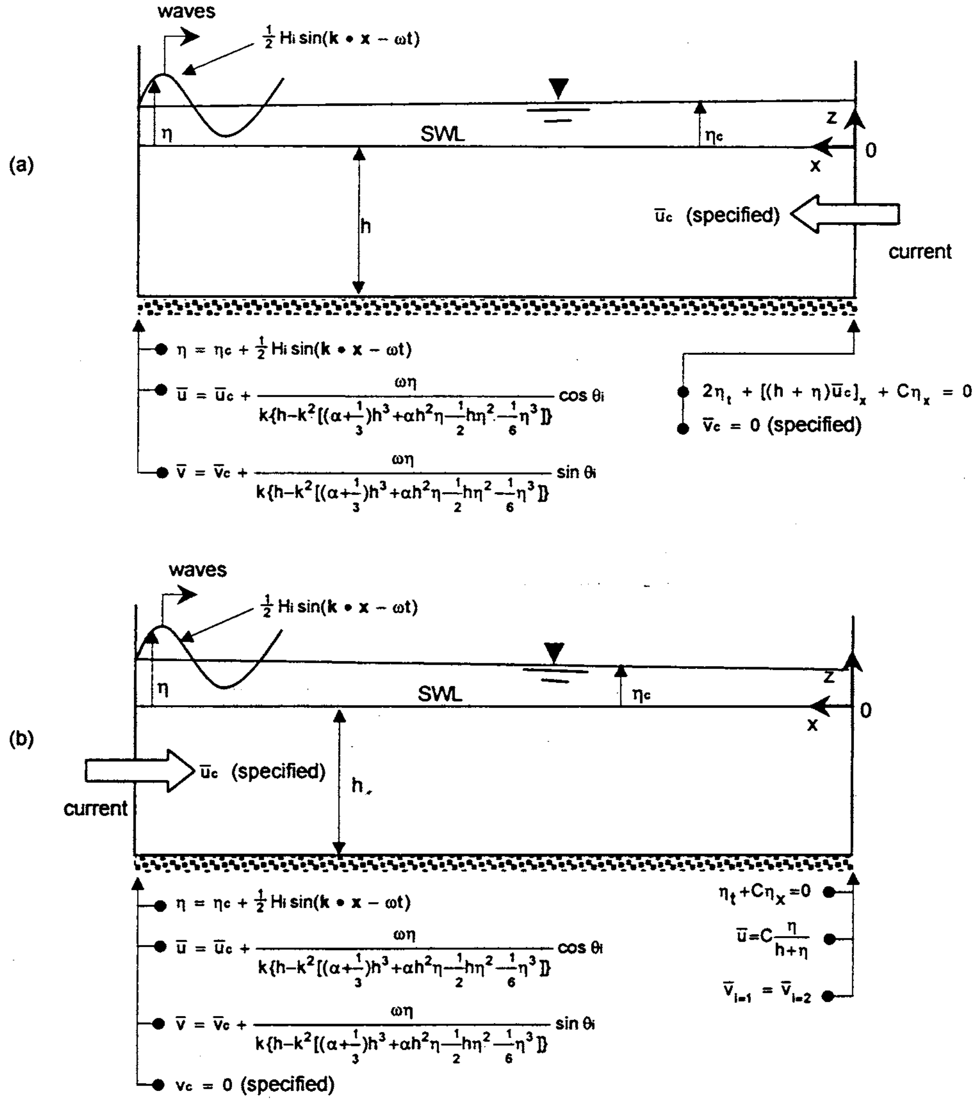

Figure 7.3. Boundary conditions for wave-current interaction case: (a) waves and steady opposing current; and (b) waves and steady current in same direction. Note: no-flow boundary conditions are same as those for waves or current only (see Figure 7.2). Explanations for equations to determine η and $\bar{u}$ at inflow and outflow boundaries can be found in Section 5.3.3.

7.3. 2D unsteady, non-linear shallow water numerical model (2DUSWM-6)

The model 2DUSWM-6 is developed in order to enable comparisons to be made between it and the Boussinesq-type wave-current interaction model 2DBMWC-5 run with currents only.

7.3.1. Governing equations

The *dimensional* unsteady, non-linear shallow water equations are

$$\eta_t + \nabla \bullet [(h+\eta)\overline{u}] = 0 \tag{7.23}$$

and

$$\overline{\mathbf{u}}_t + g\nabla\eta + (\overline{\mathbf{u}} \bullet \nabla)\overline{\mathbf{u}} = 0 \tag{7.24}$$

where friction is not included. The *dimensional* continuity equation (7.23) can be written as

$$\eta_t + [(h+\eta)\overline{u}]_x + [(h+\eta)\overline{v}]_y = 0 \tag{7.25}$$

and the (frictionless) *dimensional* momentum equation (7.24) can be decomposed into the x- and y-directions respectively as

$$\overline{u}_t + g\eta_x + \overline{u}\,\overline{u}_x + \overline{v}\,\overline{u}_y = 0 \tag{7.26}$$

$$\overline{v}_t + g\eta_y + \overline{u}\,\overline{v}_x + \overline{v}\,\overline{v}_y = 0 \tag{7.27}$$

7.3.2. Numerical solution algorithm for 2DUSWM-6

7.3.2.1. Solution method

Equations (7.25) through to (7.27) are solved by the present author in a similar way as the governing equations in 2DBMWC-5. The *dimensional* continuity equation (7.25) can be written as

$$\eta_t = E(\eta, \bar{u}, \bar{v}) \tag{7.28}$$

where

$$E(\eta, \bar{u}, \bar{v}) = -[(h+\eta)\bar{u}]_x - [(h+\eta)\bar{v}]_y \tag{7.29}$$

The *dimensional* momentum equations (7.26) and (7.27) can be expressed respectively as

$$u_t = F(\eta, \bar{u}, \bar{v}) \tag{7.30}$$

$$v_t = G(\eta, \bar{u}, \bar{v}) \tag{7.31}$$

where

$$F(\eta, \bar{u}, \bar{v}) = -g\eta_x - \bar{u}\bar{u}_x - \bar{v}\bar{u}_y \tag{7.32}$$

$$G(\eta, \bar{u}, \bar{v}) = -g\eta_y - \bar{u}\bar{v}_x - \bar{v}\bar{v}_y \tag{7.33}$$

The third-order explicit, Adams-Bashforth predictor scheme is applied to the continuity equation (7.28) and the momentum equations [(7.30) and (7.31)] to give

$$\eta_{i,j}^{t+1} = \eta_{i,j}^{t} + \tfrac{1}{12}\Delta t[23E^t - 16E^{t-1} + 5E^{t-2}]_{i,j} \tag{7.34}$$

$$\bar{u}_{i,j}^{t+1} = \bar{u}_{i,j}^{t} + \tfrac{1}{12}\Delta t[23F^t - 16F^{t-1} + 5F^{t-2}]_{i,j} \tag{7.35}$$

$$\bar{v}_{i,j}^{t+1} = \bar{v}_{i,j}^{t} + \tfrac{1}{12}\Delta t[23G^t - 16G^{t-1} + 5G^{t-2}]_{i,j} \tag{7.36}$$

where the right hand sides only involve terms at the earlier time levels of t, t–1 and t–2. Values of η_{i}^{t+1}, $\bar{u}_{i,j}^{t+1}$ and $\bar{v}_{i,j}^{t+1}$ are calculated directly. (This is in contrast to 2DBMWC-5 in which the intermediate variables U, V are first computed and from which the horizontal velocity components u_α, v_α can be determined).

The newly predicted values of $\eta_{i,j}^{t+1}$, $\bar{u}_{i,j}^{t+1}$ and $\bar{v}_{i,j}^{t+1}$ are then used to calculate estimates of $E_{i,j}^{t+1}, F_{i,j}^{t+1}$ and $G_{i,j}^{t+1}$ using equations (7.29), (7.32) and

(7.33) respectively. Employing the fourth-order Adams-Moulton corrector to the continuity and momentum equations leads to

$$\eta_{i,j}^{t+1} = \eta_{i,j}^{t} + \tfrac{1}{24}\Delta t[9E^{t+1} + 19E^{t} - 5E^{t-1} + E^{t-2}]_{i,j} \tag{7.37}$$

$$\overline{u}_{i,j}^{t+1} = \overline{u}_{i,j}^{t} + \tfrac{1}{24}\Delta t[9F^{t+1} + 19F^{t} - 5F^{t-1} + F^{t-2}]_{i,j} \tag{7.38}$$

$$\overline{v}_{i,j}^{t+1} = \overline{v}_{i,j}^{t} + \tfrac{1}{24}\Delta t[9G^{t+1} + 19G^{t} - 5G^{t-1} + G^{t-2}]_{i,j} \tag{7.39}$$

where the right hand sides involve terms at the time levels of t+1, t, t–1 and t–2. Note that equations (7.34) and (7.37) remain identical to equations (6.16) and (6.20) respectively. The corrector step is repeated if the error between two successive results exceeds a pre-set upper limit. The relative error in each of the three dependent variables η, $\overline{u}$ and $\overline{v}$ is calculated separately and defined according to equation (6.23).

7.3.2.2. Boundary conditions for current only case in 2D

The free surface elevation and the horizontal velocity at the inflow and outflow boundary conditions for 2DUSWM-6 are derived in the same way as those for the Boussinesq-type numerical model (2DBMWC-5). The resulting boundary conditions for 2DUSWM-6 are identical to those for 2DBMWC-5 (compare Figures 7.2 and 7.4).

A no-flow boundary, parallel to the x-axis (say) is considered. At a no-flow boundary however, the formulations in 2DUSWM-6 are slightly different from those in 2DBMWC-5. As there is no Π^{2x} terms in 2DUSWM-6 and $\overline{u}$ is used instead of u_α, equation (7.21) is utilised to estimate the free surface elevation and is re-written as

$$\eta_t + [(h+\eta)\overline{u}]_x = 0 \qquad \mathbf{x} \in \partial\Omega \tag{7.40}$$

Equation (7.40) is solved using the same method as in Section 7.3.2.1. To determine the horizontal velocity (say in the x-direction) parallel to an impermeable wall, a condition of zero shear is imposed on the flow along the boundary wall. This can be mathematically stated as

$$\bar{u}_y = 0 \qquad \mathbf{x} \in \partial\Omega \tag{7.41}$$

Then, the horizontal velocity in the y-direction (i.e. perpendicular to the impermeable wall) is

$$\bar{v} = 0 \qquad \mathbf{x} \in \partial\Omega \tag{7.42}$$

The set of boundary conditions for 2DUSWM-6 are displayed in Figure 7.4 for the currents only case.

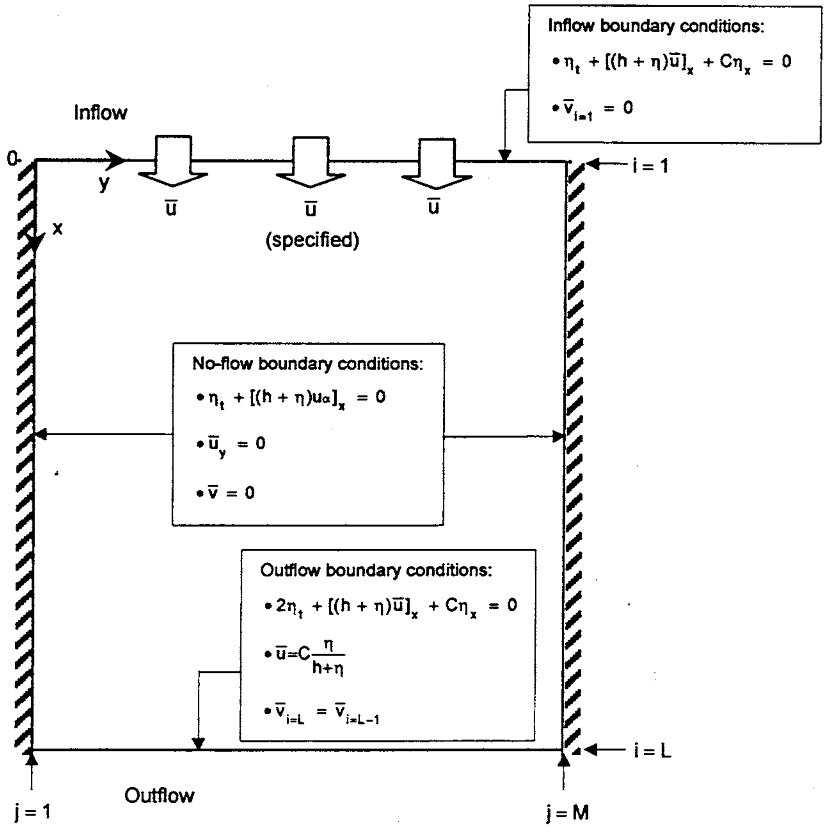

Figure 7.4. Boundary conditions for current only case. The imposed current flows from $i = 1$ to $i = L$. Side walls are located at $j = 1$ and $j = M$. Note: $i = 1,2,3,\dots L$; $j = 1,2,3,\dots,M$ and $C = \sqrt{gh}$.

7.4. Experimental set-up

The numerical set-up is the same as that in scenario 1 depicted in Figure 6.2 and follows the physical set-up in a laboratory of Chawla and Kirby (1996) (see Chen *et al.*, 2000).

7.4.1. Test 1: Waves only case

As noted by Chen *et al.* (2000), the wave height at the incident wave boundary was 0.0118 m, the wave period was 1.0 s, the depth h_{even} was 0.45 m and the depth of water above the top of the shoal was 0.08 m. In this test, with $\Delta x = 0.05$, $\Delta y = 0.10$ m and $\Delta t = 0.01$ s, 2DBMW-4 (waves only) remains stable. However, 2DBMWC-5 (with the dispersion terms associated with currents included) but operated without currents being presented does not remain stable. Consequently, the computational mesh for both models is coarsened to $\Delta x = \Delta y = 0.1$ m and $\Delta t = 0.02$ s. This coarsening of the computational mesh results in an increase in the Courant number by 58 % where in 2D, the Courant number is defined by

$$Cr = \sqrt{gh}\frac{\Delta t}{\sqrt{\Delta x^2 + \Delta y^2}} \tag{7.43}$$

Then, the free surface elevation at the incoming wave boundary ($x = 18$ m in Figure 6.2) is varied sinusoidally. The initial conditions for the model runs are a flat water surface at still water level. The computed free surface elevation over the numerical basin is stored for the last 10 s of the 40 s simulation period and the results processed to find the root-mean-square wave height (H_{rms}). The results from 2DBMWC-5 and 2DBMW-4 as well as the measured values in the laboratory are presented in Figure 7.5.

The results for Sections A-A through to G-G reveal that the results of 2DBMWC-5 and 2DBMW-4 nearly coincide. The governing equations for 2DBMW-4 (waves only) and 2DBMWC-5 (waves + currents) are different but since in this particular scenario, no currents are present, the results from both models should be the same and almost coincide. This seems to confirm that the more general model 2DBMWC-5 collapses down to 2DBMW-4 in the waves only case. Plan and perspective views of shoaling, refracting and diffracting asymmetrical waves at $t = 40$ s by 2DBMWC-5 can be seen in Figure 7.6.

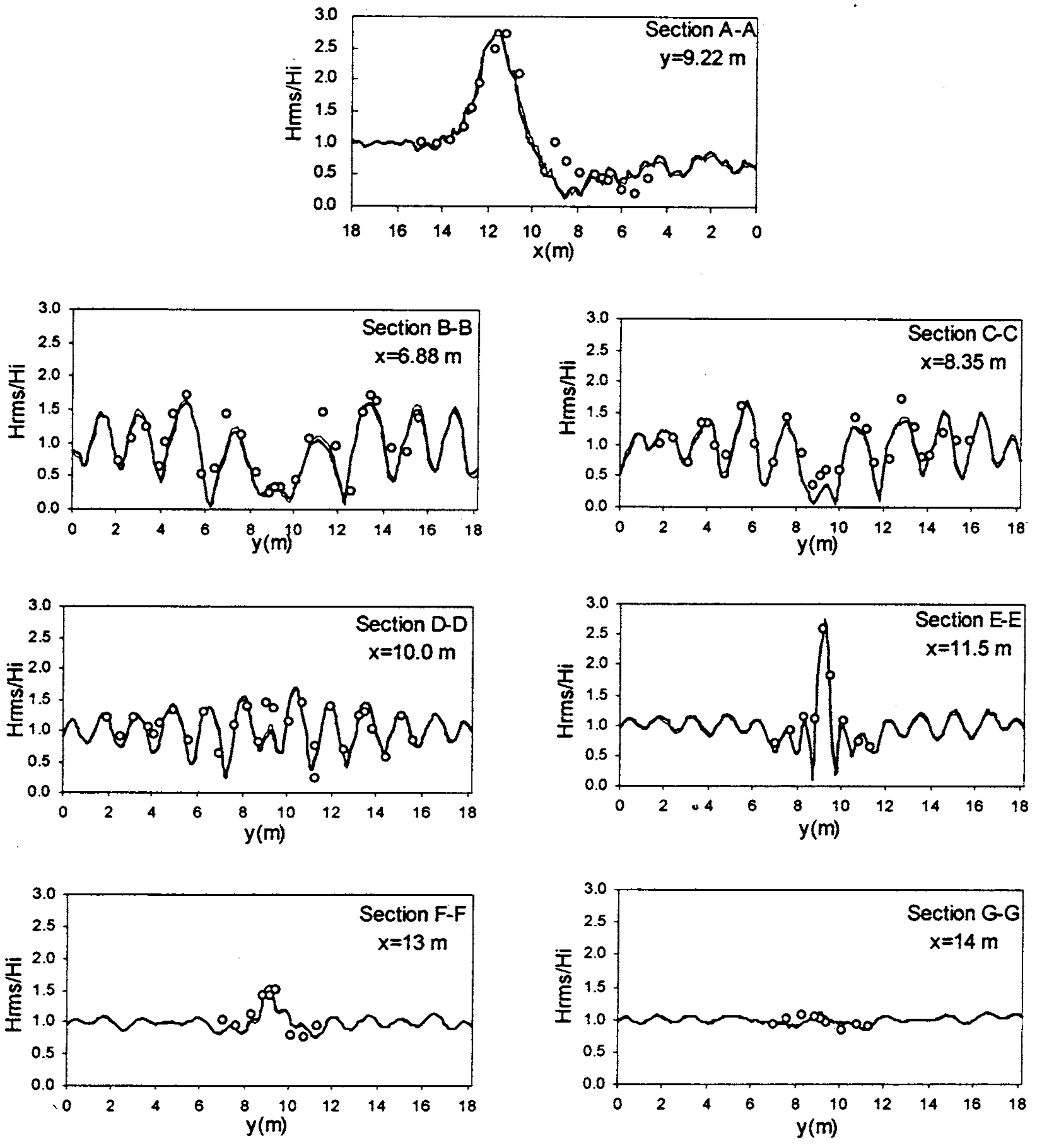

Figure 7.5. Wave heights (H_{rms}) normalised with respect to the incoming wave height in the case of pure wave motion: comparisons between the results of 2DBMWC-5 (bold lines), 2DBMW-4 (thin lines) and laboratory data (circles) along various sections for the experiment of Chawla and Kirby (1996). Data: $T = 1.0$ s, $H_i = 0.0118$ m, $\theta_i = 0°$, $h_{even} = 0.45$ m, $\Delta x = \Delta y = 0.10$ m and $\Delta t = 0.02$ s.

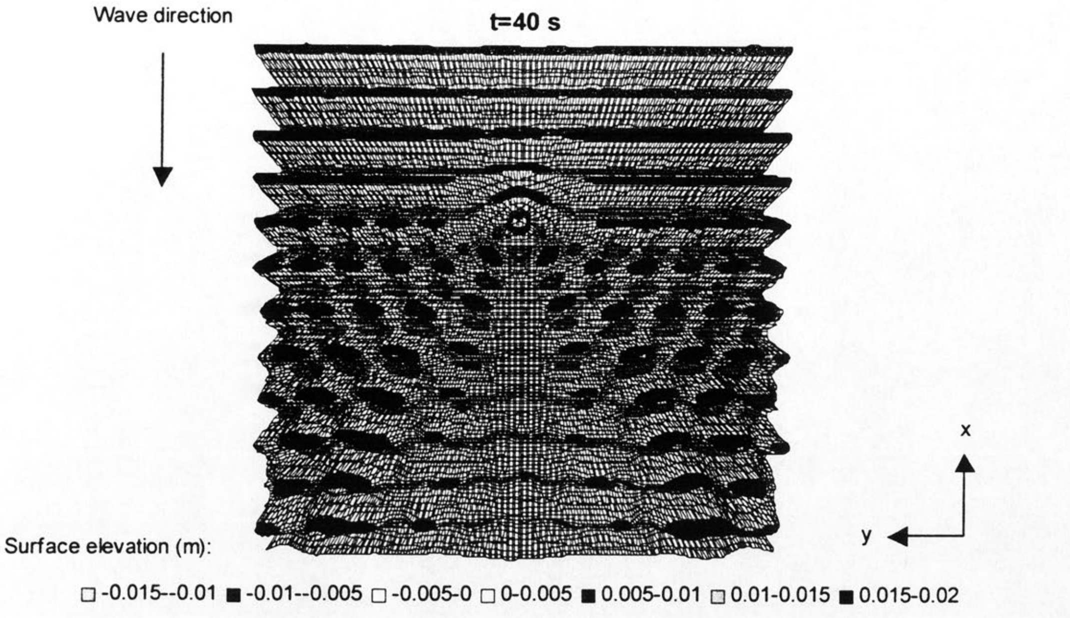

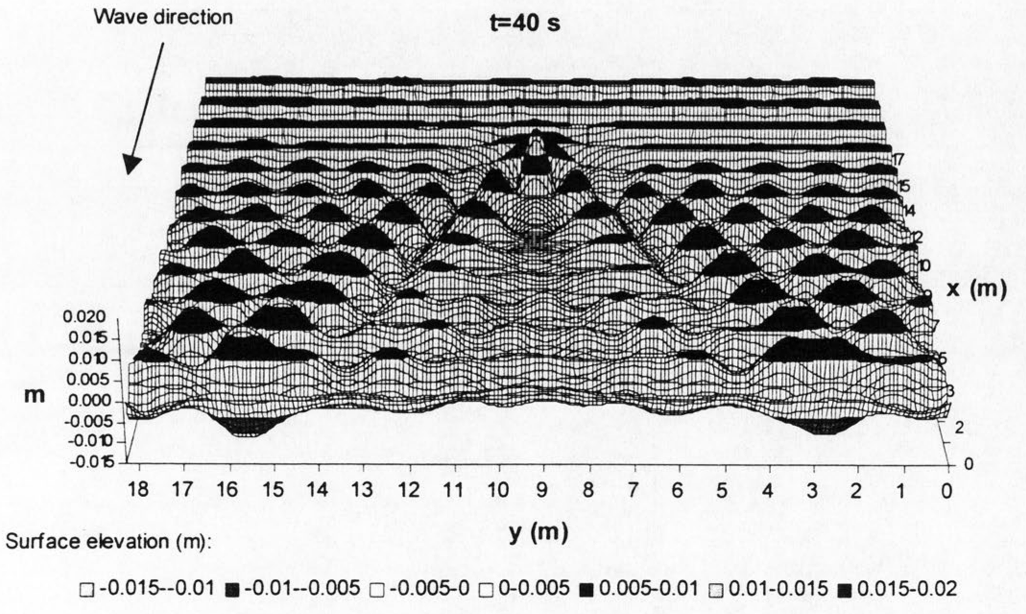

Figure 7.6. Wave only case: plan (top) and perspective (bottom) views of the free surface elevation at $t = 40$ s predicted by 2DBMWC-5. Data: $T = 1.0$ s, $H_i = 0.0118$ m, $\theta_i = 0^o$, $h_{even} = 0.45$ m, $\Delta x = \Delta y = 0.10$ m and $\Delta t = 0.02$ s.

7.4.2. Test 2: Current only case

In this test, the same bathymetry is used as for Test 1. A flat water surface and a steady velocity of 0.10 m/s is imposed at the northern boundary (x = 0 m) (see also Figure 7.2). The computation is carried out with the same mesh as in the first test. This test is applied to both 2DBMWC-5 and 2DUSWM-6. The imposed current flows from x = 0 m to x = 18 m, and reaches a steady state condition after about t = 65 s. Figures 7.7 shows some significant differences in the free surface elevation over the circular shoal (at x = 11 and 15 m and y = 9 m). It is evident from the model results in Figure 7.7 that 2DBMWC-5 produced generally flatter water surface than 2DUSWM-6. Interestingly, the two sets of numerical model results agree well along the centreline of the shoal (at x = 13 m).

Figures 7.8 and 7.9 show comparisons of the magnitude of the x- and y-velocity components predicted by both numerical models. Unlike the surface elevation, the two sets of velocity components generally coincide but there is a notable exception near the incident current boundary for the y-component of velocity (Figure 7.9 at y = 2, 5 and 7 m) where there is a series of oscillations. The maximum magnitude of the x-velocity occurs over the centre of the shoal as illustrated in Figure 7.8 (at x = 13 and y = 9 m). Additionally, the results in Figure 7.9 (at x = 11 and 15 m and y = 7 m) show that the maximum magnitude of the y-velocity occurs near the centre of the shoal. Perspective views of the surface elevations at t = 65 s predicted by both numerical models are shown in Figure 7.10. Moreover, Figure 7.11 shows the velocity vectors predicted by both numerical models at t = 65 s.

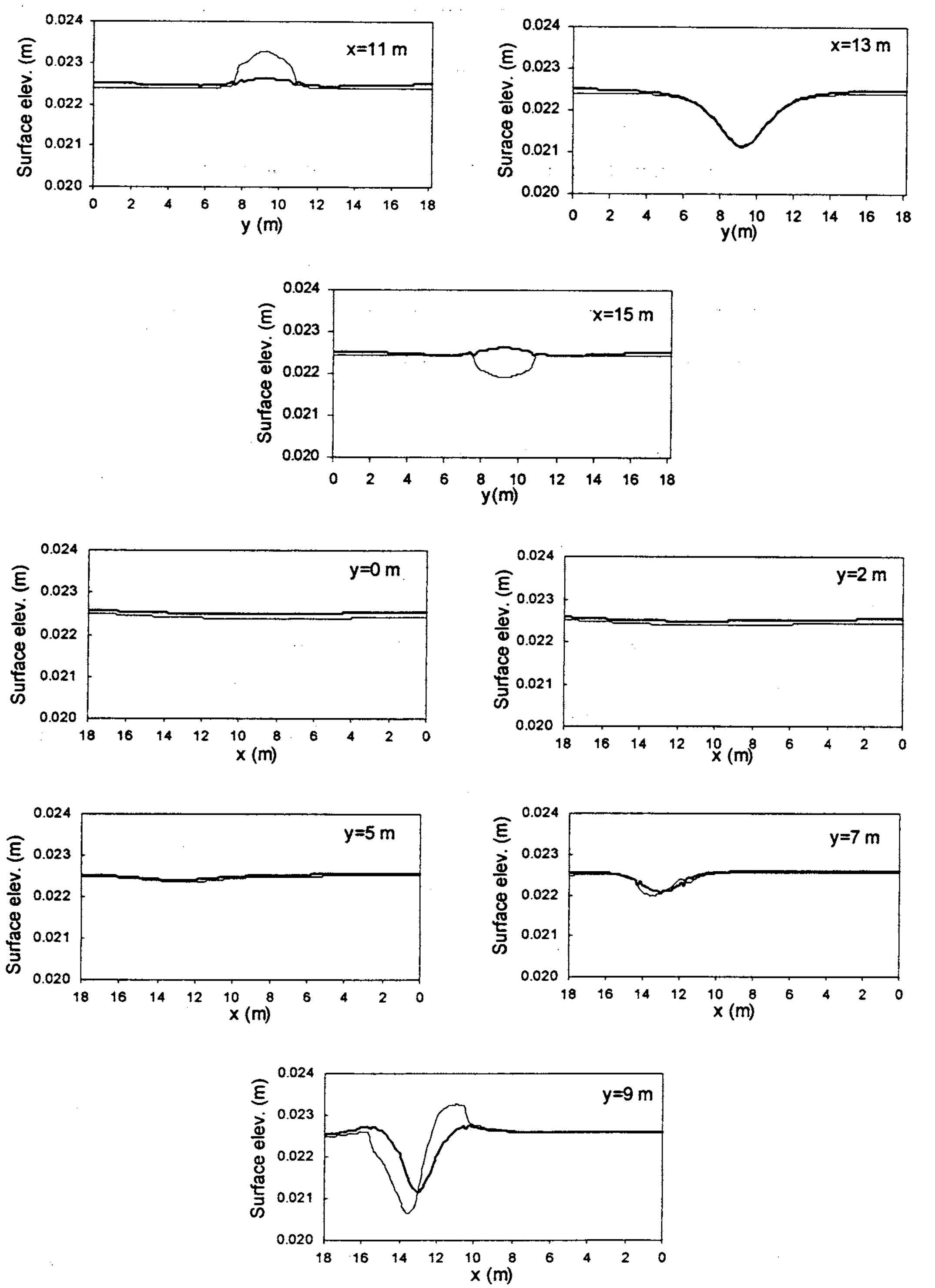

Figure 7.7. Current only case (flow from $x = 0$ to $x = 18$ m): comparisons of the free surface elevation at $t = 65$ s between results of 2DBMWC-5 (bold lines) and 2DUSWM-6 (thin lines) for $x = 11$, 13 and 15 m and for $y = 0$, 2, 5, 7 and 9 m. Data: $\theta_i = 0^\circ$, $h_{even} = 0.45$ m, $\overline{u}c_{(x=0)} = 0.10$ m/s, $\overline{v}c_{(x=0)} = 0$ m/s, $\Delta x = \Delta y = 0.10$ m and $\Delta t = 0.02$ s.

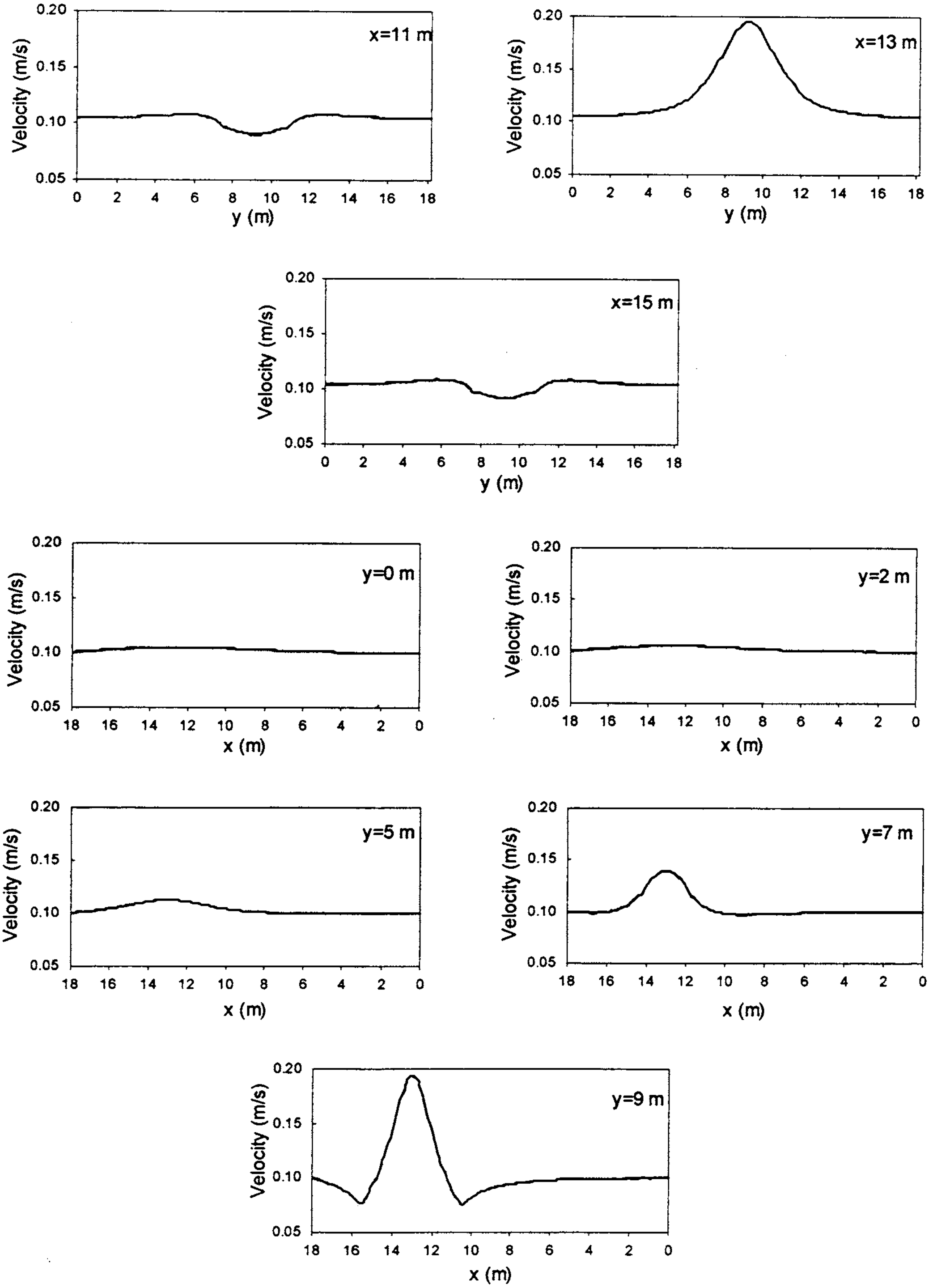

Figure 7.8. Current only case (flow from $x = 0$ to $x = 18$ m): comparisons of the magnitude of the x-component of velocity at $t = 65$ s between results of 2DBMWC-5 (bold lines) and 2DUSWM-6 (thin lines) for $x = 11$, 13 and 15 m and for $y = 0$, 2, 5, 7 and 9 m. Data: $\theta_i = 0^\circ$, $h_{even} = 0.45$ m, $\overline{u}_{c(x=0)} = 0.10$ m/s, $\overline{v}_{c(x=0)} = 0$ m/s, $\Delta x = \Delta y = 0.10$ m and $\Delta t = 0.02$ s.

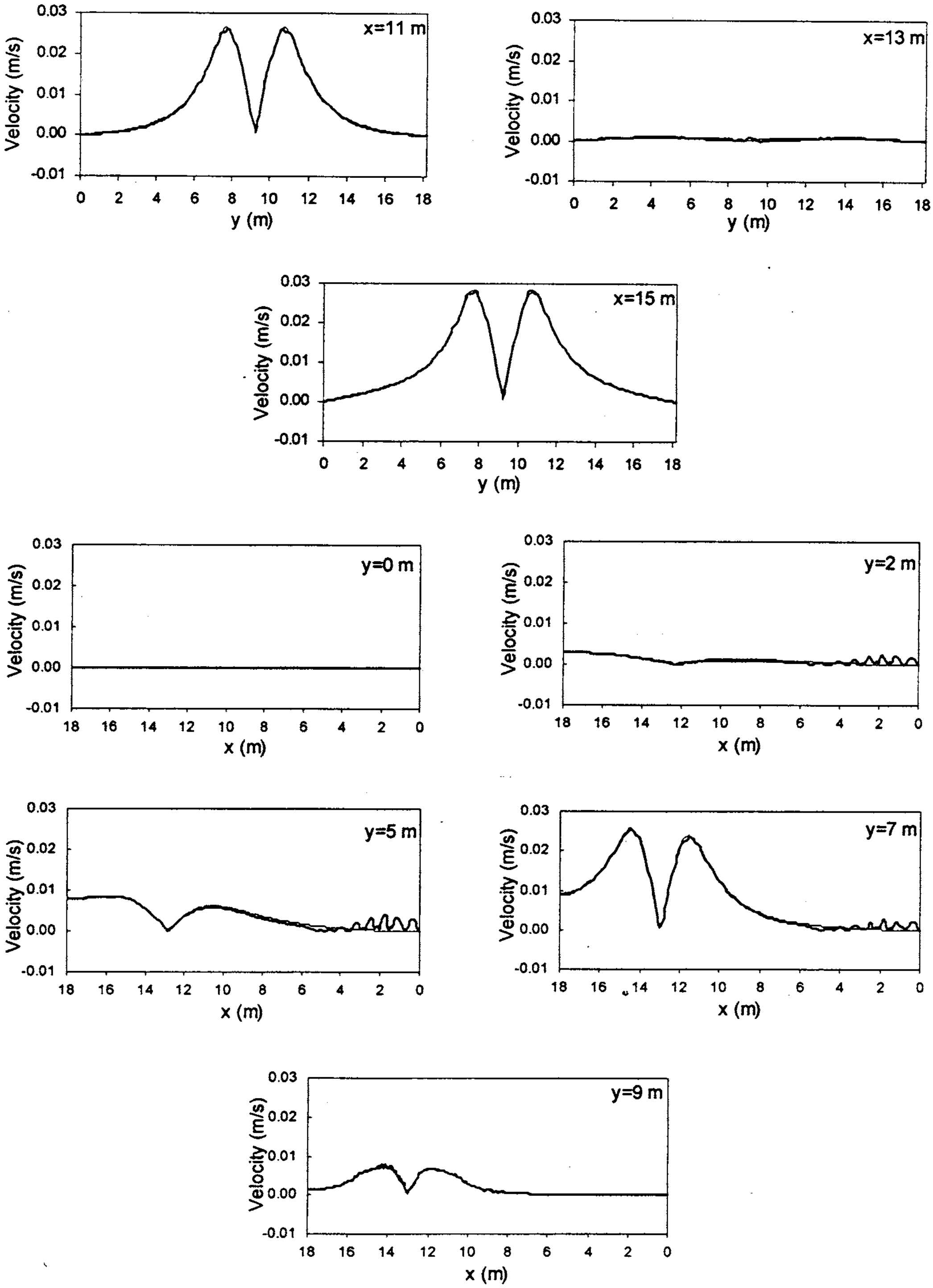

Figure 7.9. Current only case (flow from $x = 0$ to $x = 18$ m): comparisons of the magnitude of the y-component of velocity at $t = 65$ s between results of 2DBMWC-5 (bold lines) and 2DUSWM-6 (thin lines) for $x = 11$, 13 and 15 m and for $y = 0$, 2, 5, 7 and 9 m. Data: $\theta_i = 0^o$, $h_{even} = 0.45$ m, $\overline{u}c_{(x=0)} = 0.10$ m/s, $\overline{v}c_{(x=0)} = 0$ m/s, $\Delta x = \Delta y = 0.10$ m and $\Delta t = 0.02$ s.

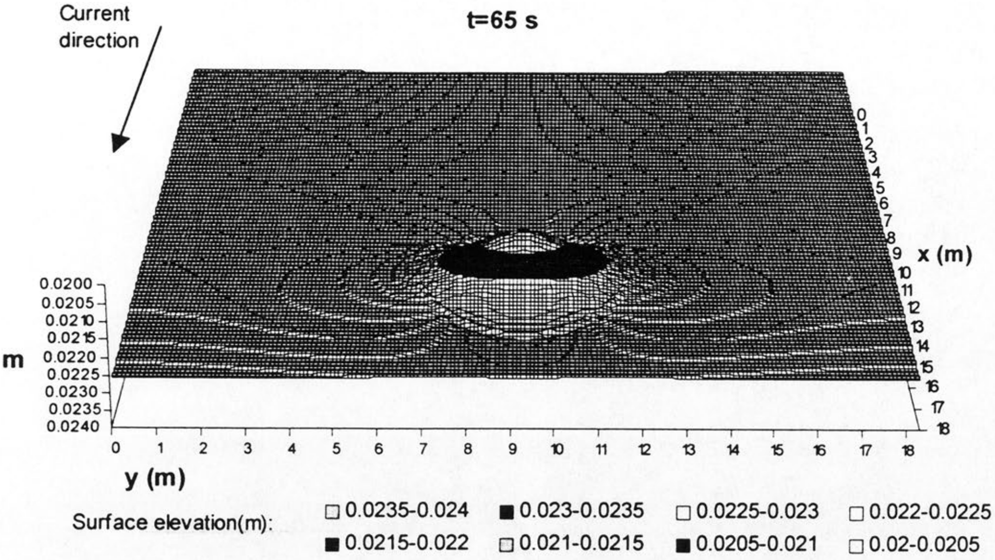

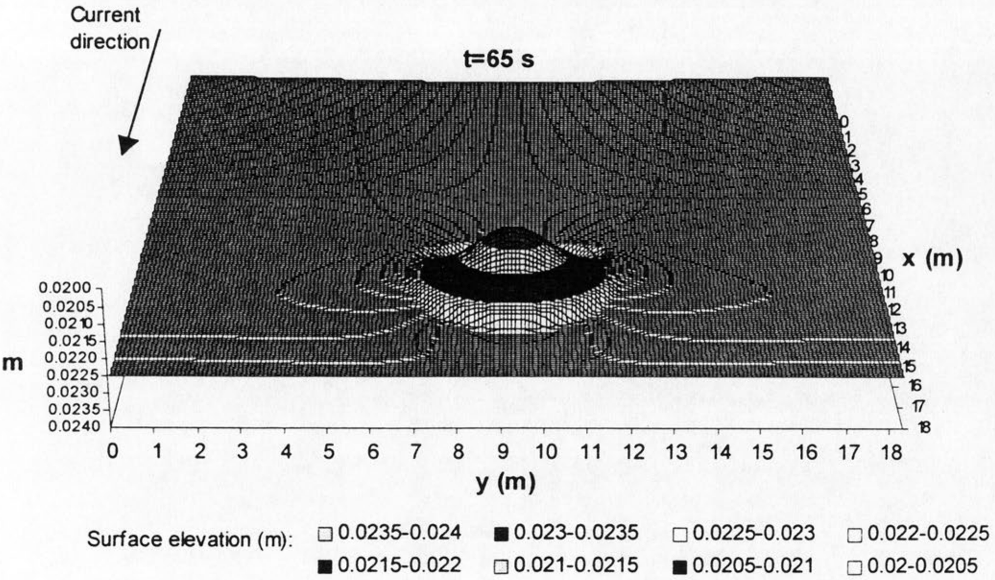

Figure 7.10. Current only case (flow from x = 0 to x = 18 m): perspective views of the free surface elevation (upside down) at t = 65 s predicted by 2DBMWC-5 (top) and by 2DUSWM-6 (bottom). Data: $\theta_i = 0^{o}$, $h_{even} = 0.45$ m, $\overline{u}c_{(x=0)} = 0.10$ m/s, $\overline{v}c_{(x=0)} = 0$ m/s, $\Delta x = \Delta y = 0.10$ m and $\Delta t = 0.02$ s.

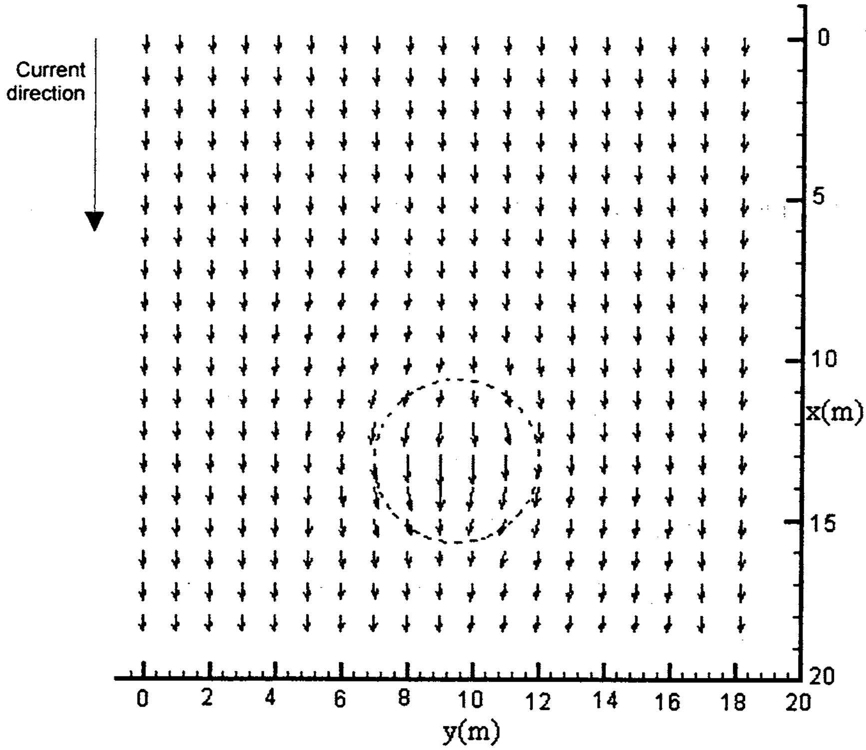

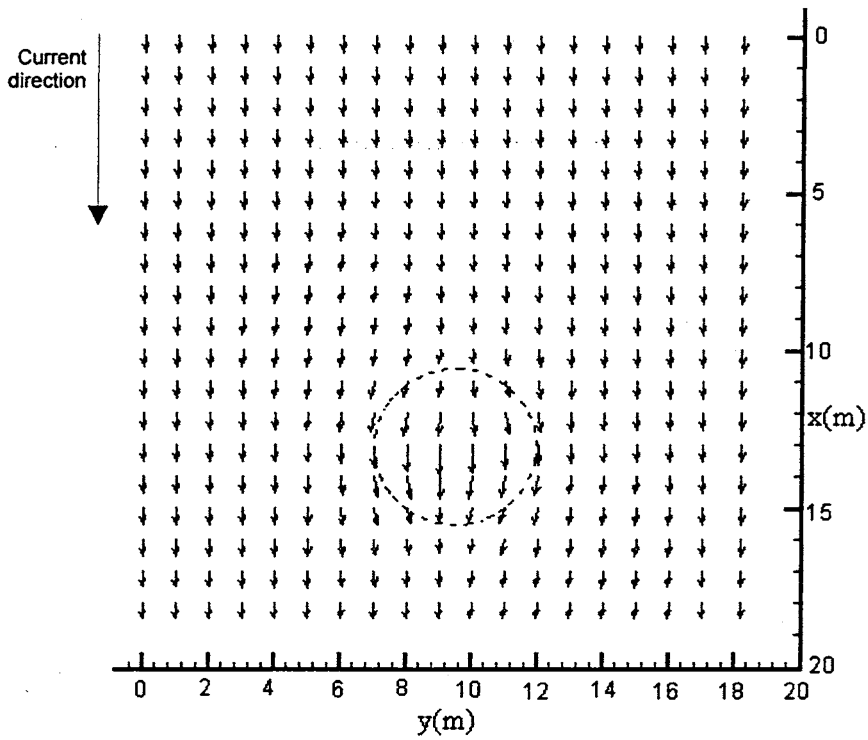

Figure 7.11. Current only case (flow from x = 0 to x = 18 m): the velocity vectors at t = 65 s predicted by 2DBMWC-5 (top) and by 2DUSWM-6 (bottom). Data: $\theta_i = 0°$, $h_{even} = 0.45$ m, $\overline{u}c_{(x=0)} = 0.10$ m/s, $\overline{v}c_{(x=0)} = 0$ m/s, $\Delta x = \Delta y = 0.10$ m and $\Delta t = 0.02$ s.

7.4.3. Test 3: Waves and opposing current

Once the currents in the basin reach a steady state (after about $t = 65$ s), the free surface elevation at the southern boundary ($x = 18$ m) is sinusoidally varied with time to generate an incident wave [see also Figure 7.3(a)]. The incoming wave specifications and the grid resolution remain the same as is used in the first test i.e. $T = 1.0$ s, $H_i = 0.0118$ m, $\Delta x = \Delta y = 0.1$ m and $\Delta t = 0.02$ s. At the incoming wave boundary ($x = 18$ m), the ambient current is allowed to pass through, leaving the flow domain. The wavelengths due to the waves propagating against a steady opposing current are slightly shorter than those due to the pure wave motion. This is evident in Figure 7.12, where the bold lines represent the waves with an opposing current and the thin lines denote the waves without a current. In Figure 7.12, the surface elevation with a current present is raised by about 0.0225 m (see also Figure 7.7). Perspective views of the surface elevation predicted by 2DBMWC-5 at $t = 20$ s and at $t = 40$ s are shown in Figure 7.13. Figure 7.14 shows the corresponding velocity vectors predicted by 2DBMWC-5.

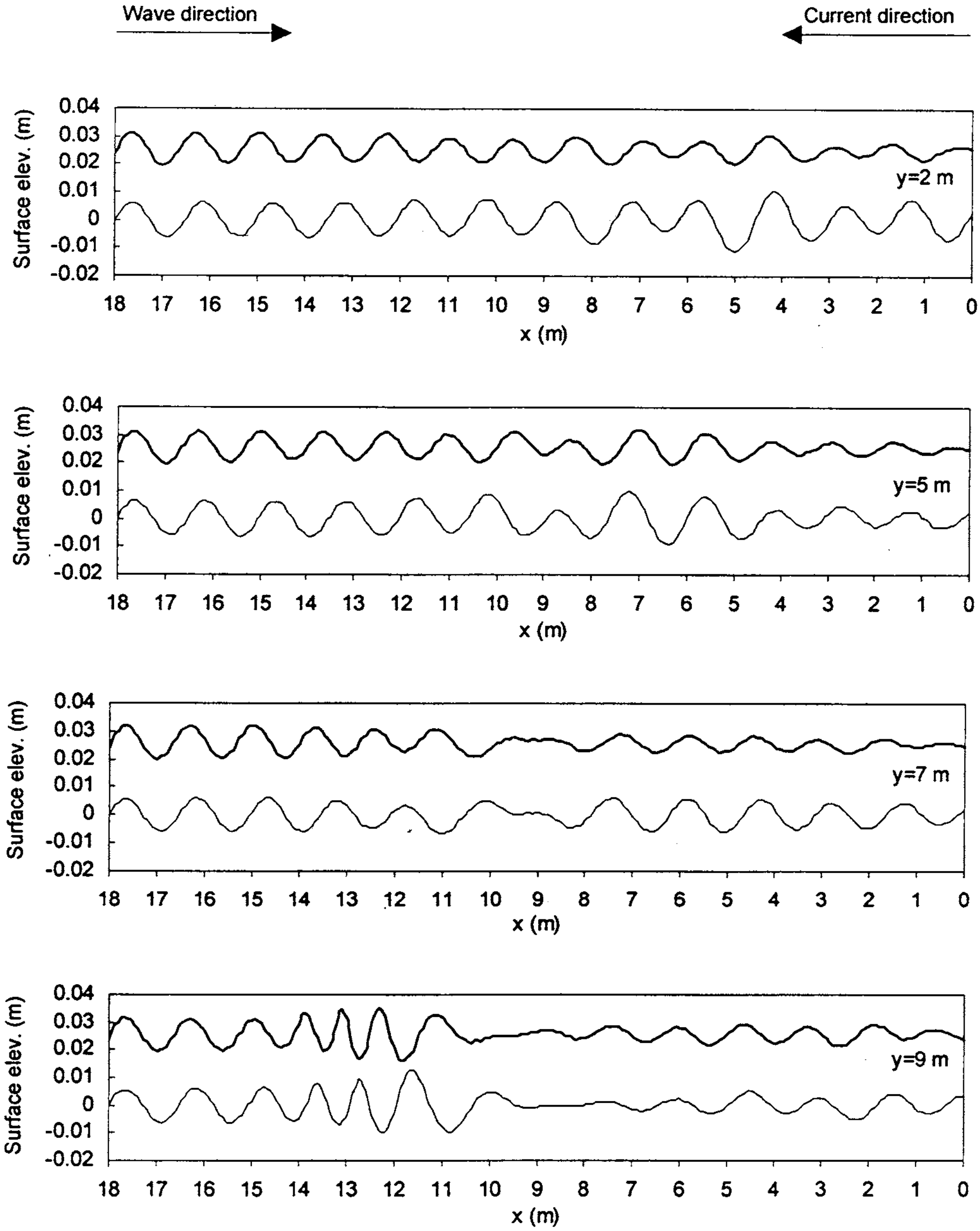

Figure 7.12. Waves with period T = 1 s propagating against a steady, opposing current with steady inflow velocity of 0.1 m/s along the x = 0 boundary. Both free surface elevation predicted by 2DBMWC-5 at t = 40 s. The waves with (bold lines) and without (thin lines) the presence of the ambient current for y = 2, 5, 7 and 9 m. Data: T = 1 s, $H_i = 0.0118$ m, $\theta_i = 0^{\circ}$, $h_{even} = 0.45$ m, $\Delta x = \Delta y = 0.10$ m and $\Delta t = 0.02$ s.

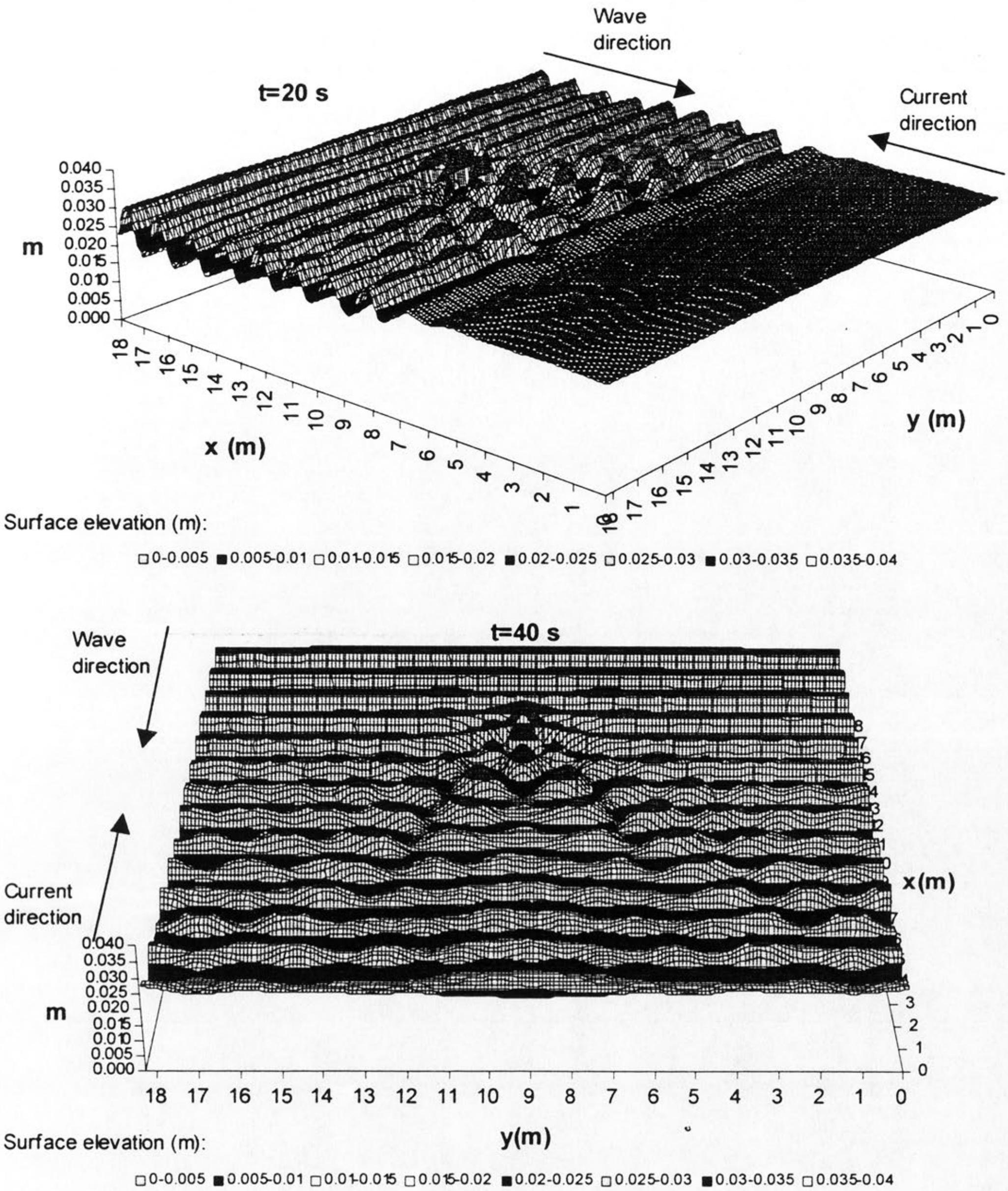

Figure 7.13. Waves with period T = 1 s propagating against a steady, opposing current with steady inflow velocity of 0.1 m/s along the x = 0 boundary. Perspective views of the free surface elevation predicted by 2DBMWC-5 at t = 20 s (top) and at t = 40 s (bottom). Data: $T = 1$ s, $H_i = 0.0118$ m, $\theta_i = 0^{\circ}$, $h_{even} = 0.45$ m, $\Delta x = \Delta y = 0.10$ m and $\Delta t = 0.02$ s.

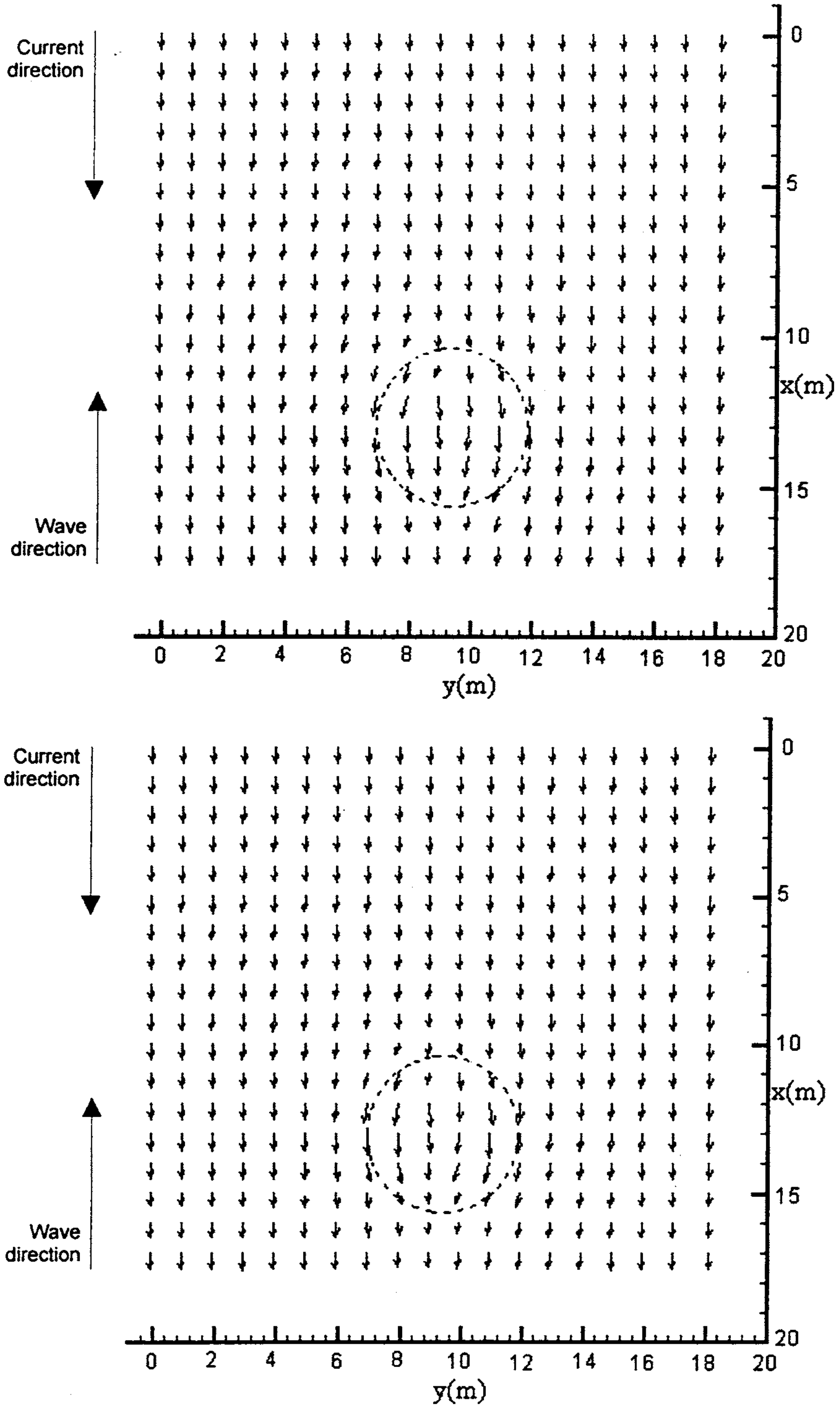

Figure 7.14. Waves with period T = 1 s propagating against a steady, opposing current with steady inflow velocity of 0.1 m/s along the x = 0 boundary. The velocity vectors predicted by 2DBMWC-5 at t = 20 s (top) and at t = 40 s (bottom). The velocities shown in figures above are the total velocity (i.e. combined orbital waves and ambient current velocities at the particular times. Data: T = 1 s, $H_i = 0.0118$ m, $\theta_i = 0°$, $h_{even} = 0.45$ m, $\Delta x = \Delta y = 0.10$ m and $\Delta t = 0.02$ s.

7.4.4. Test 4: Current only case

In this test, a flat water surface and a constant inflowing velocity of 0.10 m/s is imposed in the opposite direction to that in Test 2, i.e. at the southern boundary ($x = 18$ m) instead of at the northern boundary. This leads to a steady currents flowing from $x = 18$ m to $x = 0$ m of the basin (not presented here).

7.4.5. Test 5: Waves and current in same direction

On top of the steady current field (Test 4), a sinusoidal wave train with a period of 1.0 s and a wave height of 0.0118 m is imposed at $x = 18$ m [see also Figure 7.3(b)]. The incoming wave period and wave height are same as is used in Test 1.

The results in Figure 7.15 show that the waves propagating with a co-flowing steady current (bold lines) have slightly increased wavelengths compared to the case with only wave propagation (thin lines) at $t = 40$ s. Perspective views of the free surface elevation predicted by 2DBMWC-5 at $t = 20$ s and at $t = 40$ s are shown in Figure 7.16 and the predicted velocity vectors are illustrated in Figure 7.17.

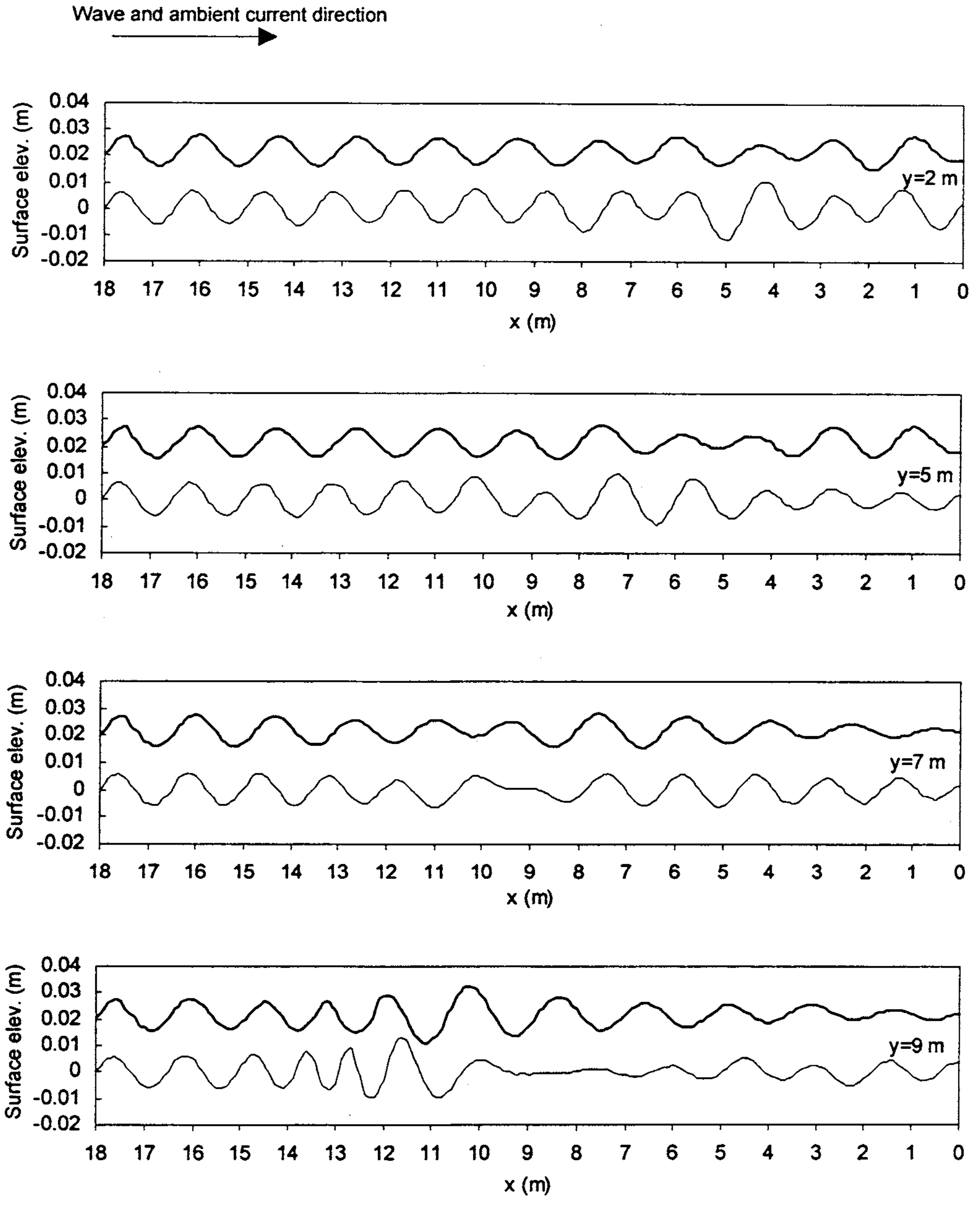

Figure 7.15. Waves with period T = 1 s propagating with a co-flowing steady current with steady inflow velocity of 0.1 m/s along the x = 18 m boundary. The free surface elevation predicted by 2DBMWC-5 at t = 40 s. The waves with (bold lines) and without (thin lines) the presence of the ambient current for y = 2, 5, 7 and 9 m. Data: T = 1 s, H_i = 0.0118 m, θ_i = 0°, h_{even} = 0.45 m, $\Delta x = \Delta y$ = 0.10 m and Δt = 0.02 s.

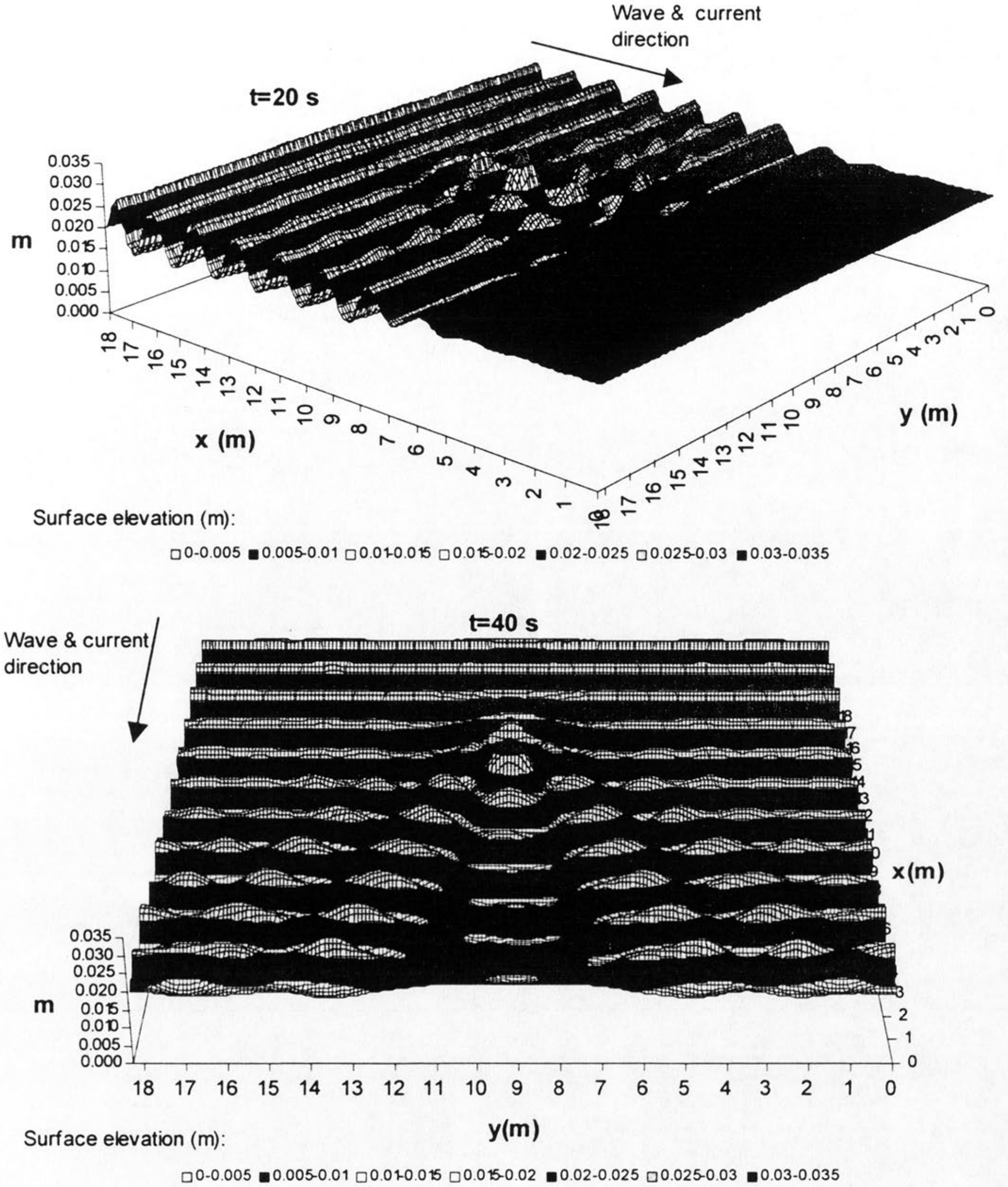

Figure 7.16. Waves with period T = 1 s propagating with a co-flowing steady current with steady inflow velocity of 0.1 m/s along the x = 18 m boundary. Perspective views of the free surface elevation predicted by 2DBMWC-5 at t = 20 s (top) and at t = 40 s (bottom). Data: T = 1 s, H_i = 0.0118 m, θ_i = 0°, h_{even} = 0.45 m, $\Delta x = \Delta y$ = 0.10 m and Δt = 0.02 s.

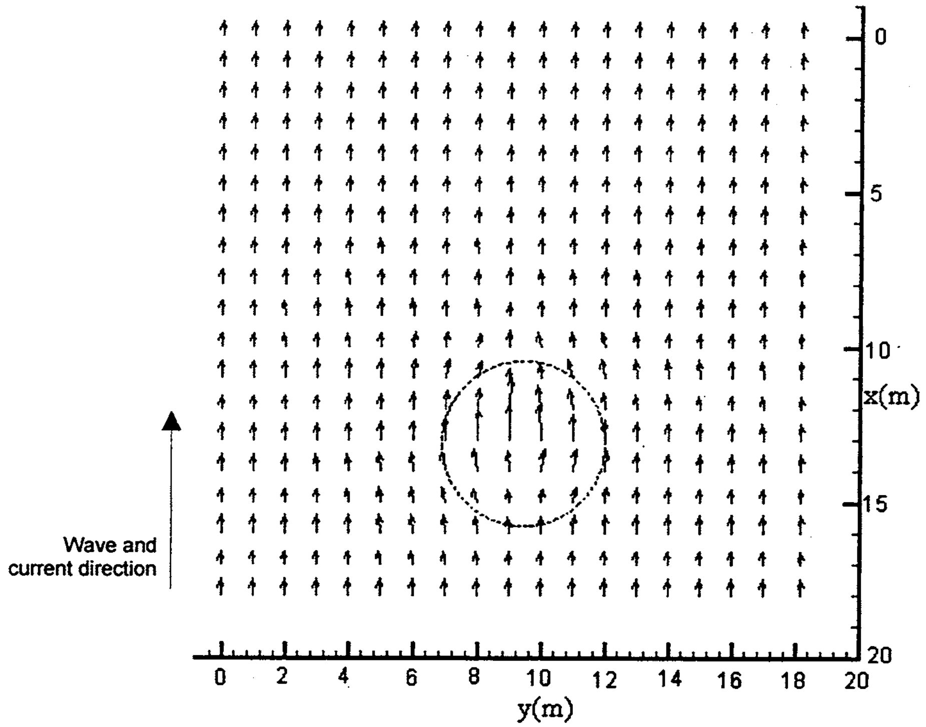

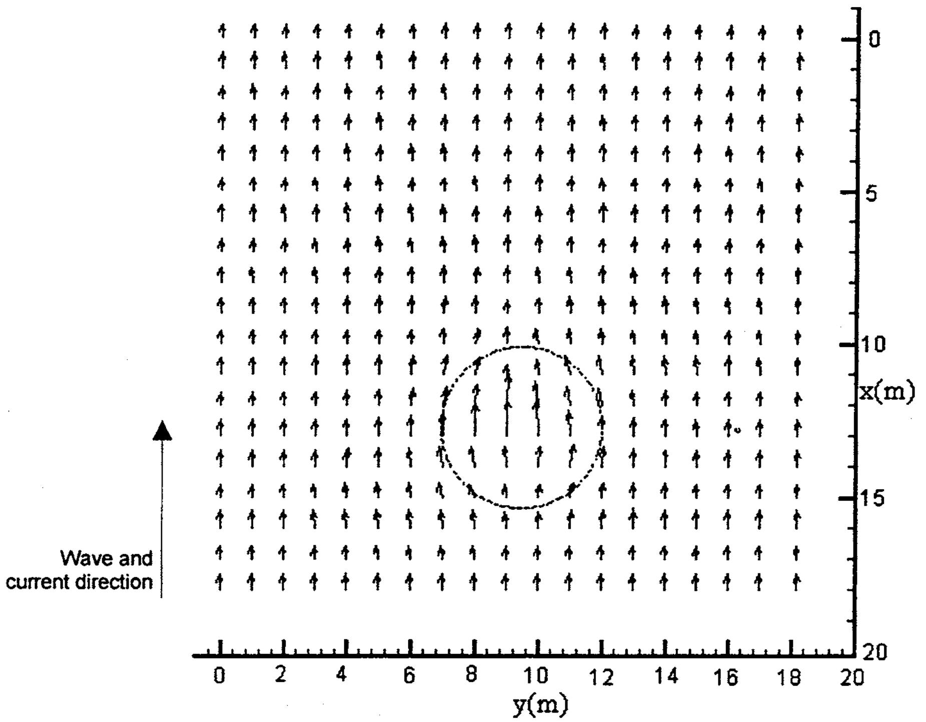

Figure 7.17. Waves with period $T = 1$ s propagating with a co-flowing steady current with steady inflow velocity of 0.1 m/s along the $x = 18$ m boundary. The velocity vectors predicted by 2DBMWC-5 at $t = 20$ s (top) and at $t = 40$ s (bottom). The velocities shown in figures above are the total velocity (i.e. combined orbital waves and ambient current velocities at the particular times. Data: $T = 1$ s, $H_i = 0.0118$ m, $\theta_i = 0°$, $h_{even} = 0.45$ m, $\Delta x = \Delta y = 0.10$ m and $\Delta t = 0.02$ s.

7.5. Conclusions

Two 2D numerical models, one based on the Boussinesq-type equations for full wave-current interaction (2DBMWC-5) and the other based on the unsteady, non-linear shallow water equations (2DUSWM-6) are developed by the present author. The governing equations of both numerical models are solved using an implicit finite difference method with a non-staggered grid. For the Boussinesq-type numerical model (2DBMWC-5), the boundary conditions are determined on the basis of particular cases i.e. waves only, currents only and combined wave-current motion. For the unsteady, non-linear shallow water numerical model (2DUSWM-6) however, the boundary conditions correspond to the currents only case. This is due to 2DUSWM-6 being developed for comparison purposes in the current only case.

The results of 2DBMWC-5 agree reasonably well with those of 2DBMW-4 (the numerical model, which is developed in Chapter Six, with the dispersion terms associated with currents excluded) and the available laboratory data in the case of pure wave motion. This reinforces the fact that 2DBMWC-5 reduces to 2DBMW-4 when the currents vanish.

2DBMWC-5 and 2DUSWM-6 give similar results except near the shoal and this is where it can be expected that the higher order derivatives (i.e. the dispersion terms) representing the effects of non-hydrostatic pressure become more important.

The effects of including depth uniform currents in the *second set* of equations of Chen *et al.* (1998) are seen to be the effects on wavelength: in the case of waves and opposing current, the wavelengths become shorter and in the case of waves propagating with a co-flowing current, the wavelengths become longer. Due to a lack of laboratory and field data, the effects of current on a 2D wave field are only examined quantitatively. Consequently, the suitable laboratory data for verification of the observed behaviour will be worth exploring for the future research.

Chapter Eight

Summary, Conclusions and Recommendations

8.1. Summary

Three new Boussinesq-type numerical models are developed by the present author:

(i) 1DDBMW-2 based on the existing partial differential equations of Schäffer and Madsen (1995), and

(ii) 1DBMWC-3 and 2DBMWC-5 based on the existing partial differential equations of Chen *et al.* (1998)

The numerical performance of the above three new models has not been previously assessed. The governing (partial differential) equations corresponding to the three models (1DDBMW-2, 1DBMWC-3, 2DBMWC-5) are extensions (comprising additional terms) to what is referred to here as the basic partial differential equations of Nwogu (1993). The present author develops two basic numerical models in 1D (1DBMW-1) and 2D (2DBMW-4) based on Nwogu's partial differential equations. By comparing the results from the three new models with the results from the basic numerical models, it is possible to assess the effects of the additional terms in the three new models.

More specifically, the research is focused on:

- numerically studying the effects of the additional terms in the governing partial differential equations of 1DDBMW-2 which improve the dispersion relation in deeper water. At the same time, the order of the frequency dispersion and non-linearity in Schäffer and Madsen's (1995) partial differential equations are the same as in the basic partial differential equations of Nwogu (1993).
- numerically investigating the effects of the additional dispersion terms associated with currents in the governing partial differential equations of 1DBMWC-3 and 2DBMWC-5. While the basic partial differential equations of Nwogu are not applicable to wave-current interaction, Chen *et al.*'s partial differential equations with the additional terms permit the interaction of ambient currents and waves.

Three additional ancillary (simplified case) models are developed by the present author to assist in the validation of the more complex Boussinesq-type equations

(a) 1DSSWM based on the 1D steady, non-linear shallow water equations,

(b) 1DWACM based on the 1D conservation of wave action equation and

(c) 2DUSWM-6 based on the 2D unsteady, non-linear shallow water equations.

8.2. Conclusions

The specific conclusions for this study are:

(i) the additional terms in the governing equations of 1DDBMW-2 result in this model being applicable in deeper water (i.e. $h/L \leq 1$). This conclusion is based on the fact that while the basic models (1DBMW-1 and 2DBMW-4) run satisfactorily in shallower water (i.e. $h/L \leq ½$), they are unstable in deeper water (i.e. $h/L > ½$). This result is obtained in spite of the fact that the finite difference operator is implicit. On the other hand, the new model (1DDBMW-2) works well in the depth $h/L = 1$.

(ii) the additional terms in the governing equations of 1DBMWC-3 and 2DBMWC-5 lead to both models capable of simulating wave-current interaction. Although no laboratory data are available, this conclusion is based on the 1D results of the new model (1DBMWC-3) operated in a scenario in which the waves are blocked by an opposing current with a velocity equal to the group velocity of the oncoming waves.

The study also gives emphasis to the determination of the appropriate boundary conditions in connection with the governing equations and numerical scheme considered. When both waves and currents are present, the appropriate boundary conditions depend on whether the waves and currents are co-flowing or counter flowing. With one exception, the boundary conditions reasonably work well.

With the new models, the scenario simulated includes waves with and without currents. If a boundary condition in a numerical model is not functioning well, this can show itself in one or two ways:

- at the boundary, model results with a sudden change in wave height are indicative of an unsatisfactory boundary condition.
- within the modelling domain, disagreement between the measured and simulated results could also indicate an unsatisfactory boundary

condition. The generally good agreement between the results of the new models and laboratory data or the results from one of the ancillary models indicates that the boundary conditions must have been functioning reasonably well.

The one exception is in the case where the waves and currents are co-flowing. At the downstream boundary, it is noted that unwanted wave attenuation occurs. [It is interesting to note that Wei *et al.* (1999) published the results for a waves-only scenario and experienced significant unwanted attenuation].

New sets of Boussinesq-type partial differential equations are also developed by the present author. They consist of:

(i) Boussinesq-type (ε,μ^2) equations with an ambient current included and presented in terms of:

 (a) the arbitrary z-level horizontal velocity (BEWCAV-A),

 (b) the bottom velocity (BEWCBV-B) and

 (c) the still water level velocity (BEWCSV-C);

(ii) Boussinesq-type (ε,μ^2) equations for weakly non-linear waves presented in terms of the bottom velocity (BEWBV-D);

(iii) Boussinesq-type $(\mu^2,\varepsilon^3\mu^2)$ equations in terms of the horizontal velocity at an arbitrary z-elevation (FBE2O-E).

The present author also successfully re-derives a number of the existing Boussinesq-type partial differential equations in a new and systematic methodology. They are:

(a) the (ε,μ^2) equations of Boussinesq (1872),

(b) the (ε,μ^2) equations of Peregrine (1967) (in terms of the still water level horizontal velocity),

(c) the (ε,μ^2) equations of Nwogu (1993),

(d) the $(\mu^2,\varepsilon^3\mu^2)$ equations of Wei *et al.* (1995) and

(e) the $(\mu^4,\varepsilon^5\mu^4)$ equations of Madsen and Schäffer (1998)

Although the above partial differential equations in (a) – (e) are not new, they are significantly different from existing derivations.

8.3. Recommendations

Recommendations for future research related to and arising from this study include:

(i) Laboratory work needs to be undertaken to provide free surface elevation and velocity measurements in the case of full interaction between waves and ambient currents. These data are urgently required as verification of the Boussinesq-type numerical models and particularly for 2D wave and ambient current fields.

(ii) Improvement in the capabilities of the boundary conditions in the present numerical models, so that the resulting numerical models are applicable to regular and irregular waves with and without current effects. One boundary condition needing to be improved is the downstream boundary in the case of co-flowing waves and currents (see Figure 5.15).

(iii) Develop some numerical models based on an unstructured grid. Such a facility would significantly expand the region of applicability of the Boussinesq-type numerical models in coastal regions.

(iv) Five new sets of Boussinesq-type partial differential equations have been developed by the present author in Appendix C. These partial differential equations need to be discretised into numerical models and their performance assessed to uncover any advantages or disadvantages over other formulations.

References

Abbott, M.B., McCowan, A.D. and Warren, I.R., 1984. Accuracy of short-wave numerical models. *J. Hydraulic Engineering*, **110**(10), 1287-1301.

Abbott, M.B., Petersen, H.M. and Skovgaard, O., 1978. On the numerical modelling of short waves in shallow water. *J. Hydraulic Research* **16**(3), 173-204.

Beji, S. and Battjes, J.A., 1994. Numerical simulation of nonlinear wave propagation over a bar, *Coastal Engineering* **23**, 1-16.

Berkhoff, J.C.W., Booy, N. and Radder, A.C., 1982. Verification of numerical wave propagation models for simple harmonic linear water waves. *Coastal Engineering* **6**, 255-279.

Borsboom, M., Doorn, N., Groeneweg, J. and Van Gent, M., 2000. A Boussinesq-type wave model that conserves both mass and momentum, *Intl. Conf. Coastal Eng.* (full paper not yet available), Sydney.

Boussinesq, J., 1871. Théorie de l'intumescence liquide appellee onde solitaire ou de translation se propagent dans un canal rectangulaire. *Des Comptes Rendus Des Séances De L'Académie Des Sciences*, 755-759

Boussinesq, J., 1872. Théorie des ondes et des ramous qui se propagent le long d'un canal rectangulaire horizontal, en communi quant au liquide contenu dans ce canal des vitesses sensiblement pareilles de la surface au fond. *J. Math. Pures Appl.* 2^{nd} *Series* **17**, 55-108.

Chen, Q., 1997. *The study of wave blocking and current effects on nonlinear interactions of shallow water waves using advanced Boussinesq models.* PhD thesis at Old Dominion University, Norfolk, Virginia, USA.

Chen, Q., Kirby, J.T., Dalrymple, R.A., Kennedy, A.B. and Chawla, A., 2000. Boussinesq modeling of wave transformation, breaking, and runup. II: 2D. *J. Waterway, Port, Coastal, and Ocean Eng. ASCE* **126**(1), 48-56.

Chen, Q, Madsen, P.A., Schäffer, H.A. and Basco, D.R., 1998. Wave-current interaction based on an enhanced Boussinesq approach. *Coastal Engineering* **33**, 11-39.

Chen, Y. and Liu, P.L.-F., 1995. Modified Boussinesq equations and associated parabolic models for water wave propagation, *J. Fluid Mechanics* **288**, 351-381.

Dean, R.G., 1965. Stream function representation of nonlinear ocean waves, *J. Geophysical Research* **70**(18), 4561-4572.

Dean, R.G. and Dalrymple, R.A., 1984. *Water wave mechanics for engineers and scientists,* Englewood Cliffs, New Jersey, Prentice-Hall, Inc., 353p.

Dingemans, M.W., 1997. *Water wave propagation an uneven bottoms,* Advanced Series on Ocean Engineering **13**, World Scientific, Singapore, 967p.

Elgar, S. and Guza, R.T., 1985. Shoaling gravity waves: comparisons between field observations, linear theory and a nonlinear model. *J. Fluid Mechanics* **158**, 47-70.

Elgar, S., Freilich, M.H. and Guza, R.T., 1990. Model-data comparisons of moments of nonbreaking shoaling surface gravity waves. *J. Geophysical Research* **95**(C9), 16055-16063.

Engquist, B. and Majda, A., 1997. Absorbing boundary conditions for the numerical simulation. *Math. Comp.* **31**(139), 629-651.

Faires, J.D. and Burden, R., 2003. *Numerical method*, 3rd edition, Thomson, Brooks/Cole.

Freilich, M.H. and Guza, R.T., 1984. Nonlinear effects on shoaling surface gravity waves. *Philos. Trans. Roy. Soc. London Ser. A* **311**, 1-41.

Grilli, S.T. Skourup, J. and Svendsen, I.A., 1989. An efficient boundary element method for nonlinear water waves. *Eng. Anal. With Boundary Elements* **6**, 97-107.

Hauguel, A., 1980. A numerical model of storm waves in shallow water waves. *Proc., 17th Intl. Conf. Coastal Eng.*, Sydney, Australia, 746-762.

Israeli, M. and Orszag, S. A., 1981. Approximation of radiation boundary conditions. *J. Comp. Phys.* **41**(1), 115-135.

Kaihatu, J.M. and Kirby, J.T., 1998. Two-dimensional parabolic modeling of extended Boussinesq equations. *J. Waterway, Port, Coastal, and Ocean Eng. ASCE* **124**(2), 57-67.

Larsen, J. and Dancy, H., 1983. Open boundaries in short wave simulations - A new approach. *Coastal Engineering* **7**(3), 285-297.

Liu, P.L-F., Yoon, S.B. and Kirby, J.T., 1985. Nonlinear refraction-diffraction of waves in shallow water. *J. Fluid Mechanics* **153**, 185-201.

Longuet-Higgins, M.S. and Stewart, R.W., 1961. The changes in amplitude of short gravity waves on steady non-uniform currents. *J. Fluid Mechanics* **10**, 529-549.

Madsen, P.A., Murray, R. and Sørensen, O.R., 1991. A new form of the Boussinesq equations with improved linear dispersion characteristics. *Coastal Engineering* **15**, 371-388.

Madsen, P.A. and Schäffer, H.A., 1998. Higher-order Boussinesq-type equations for surface gravity waves: derivation and analysis. *Philos. Trans. Roy. Soc. London Ser. A* **356**, 3123-3184.

Madsen, P.A. and Sørensen, O.R., 1992. A new form of the Boussinesq equations with improved linear dispersion characteristics (Part 2). *Coastal Engineering* **18**, 183-204.

Madsen, P.A. and Sørensen, O.R., 1993. Bound waves and triad interactions in shallow water. *Coastal Engineering* **20**, 359-388.

Madsen, P.A. and Warren, I.R., 1984. Performance of a numerical short-wave model. *Coastal Engineering* **8**, 73-93.

McCowan, J., 1894. On the highest wave of permanent type. *Philos. Mag. J. Science* **38**, 351-358.

Mei, C.C., 1992. *The applied dynamics of ocean surface waves*. Advanced Series on Ocean Engineering **1**, World Scientific, Singapore, 740p.

Mei, C.C. and LeMéhauté, B., 1966. Note on the equations of long waves over an uneven bottom. *J. Geophysical Research* **71**, 393-400.

Murray, R.J., 1989. Short wave modelling using new equations of Boussinesq type, *Proc., 9th Austr. Conf. Coastal and Ocean Eng.*, Adelaide, Australia, 331-336.

Nwogu, O., 1993. Alternative form of Boussinesq equations for nearshore wave propagation. *J. Waterway, Port, Coastal, and Ocean Eng. ASCE* **119**(6), 618-638.

Nwogu, O.G., 1996. Numerical prediction of breaking waves and currents with a Boussinesq model. *Proc. 25th Intl. Conf. Coastal Eng.*, Orlando, Florida, 4807-4820.

Peregrine, D.H., 1967. Long waves on a beach. *J. Fluid Mechanics* **27**(4), 815-827.

Phillips, O.M., 1977. *Dynamics of the upper ocean*, Cambridge Univ. Press, London, England.

Prüser, H.-H. and Zielke, W., 1990. Irregular waves on a current, *Proc. 22nd Intl. Conf. Coastal Eng.*, Delft, The Netherlands, 1088-1101.

Schäffer, H.A. and Madsen, P.A., 1995. Further enhancements of Boussinesq-type equations. *Coastal Engineering* **26**, 1-14.

Schaper, H. and Zielke, W., 1984. A numerical solution of Boussinesq-type equations, *Proc. 19nd Intl. Conf. Coastal Eng.*, Houston, Texas, 1057-1072.

Serre, P.F., 1953. *Contribution á l'étude des écoulements permanents et variables dans les canaux*, 374-388 & 830-872. Paris: La Houille Blanche.

Skjelbreia, L. and Hendrickson, J., 1960. Fifth order gravity wave theory, *Proc. 7th Intl Conf. Coastal Eng.* **1**(10), 184-196.

Sørensen, O.R., Schäffer, H.A. and Madsen, P.A., 1998. Surf zone dynamics simulated by a Boussinesq type model. III. Wave-induced horizontal nearshore circulations. *Coastal Engineering* **33**, 155-176.

Wei, G. and Kirby, J.T., 1995. Time-dependent numerical code for extended Boussinesq equations, *J. Waterway, Port, Coastal, and Ocean Eng. ASCE* **121**(5), 251-261.

Wei, G., Kirby, J.T., Grilli, S.T. and Subrayama, R., 1995. A fully nonlinear Boussinesq model for surface waves. Part 1. Highly nonlinear unsteady waves. *J. Fluid Mechanics* **294**, 71-92.

Wei, G., Kirby, J.T. and Sinha, A., 1999, Generation of waves in Boussinesq models using a source function method. *Coastal Engineering* **36**, 271-299.

Witting, J.M., 1984. A unified model for the evolution of nonlinear water waves, *J. Comp. Phys.* **56**, 203-236.

Yoon, S.B. and Liu, P.L.-F., 1989. Interactions of currents and weakly nonlinear water waves in shallow water. *J. Fluid Mechanics* **205**, 397-419.

Appendix A

Coordinate Systems and Orientations

The coordinate system and the convention adopted for the positive directions of various parameters and variables used in this thesis are defined in the figures below. This particular selection is made in order to maintain a correspondence with the x-,y-axes normally chosen as Cartesian coordinates. This can be easily seen by rotating Figure A.3 through 90° in anticlockwise direction.

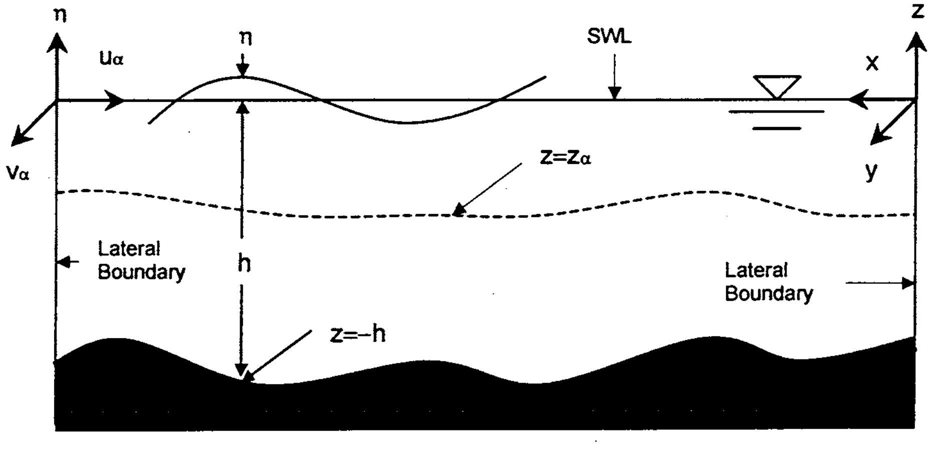

Figure A.1. Definition for η, u_α, v_α, z, z_α, x, y and their positive directions.

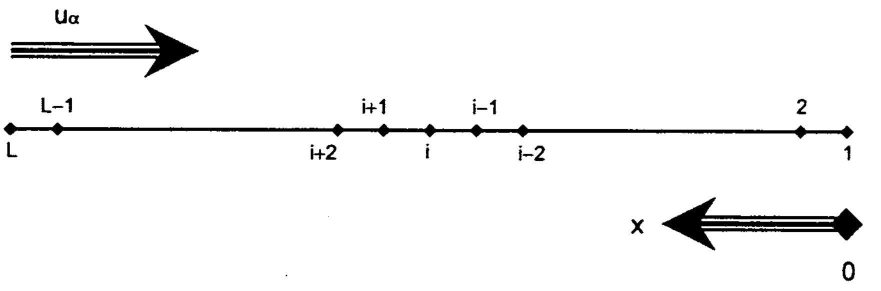

Figure A.2. 1D Cartesian coordinate system and the positive direction for u_α.

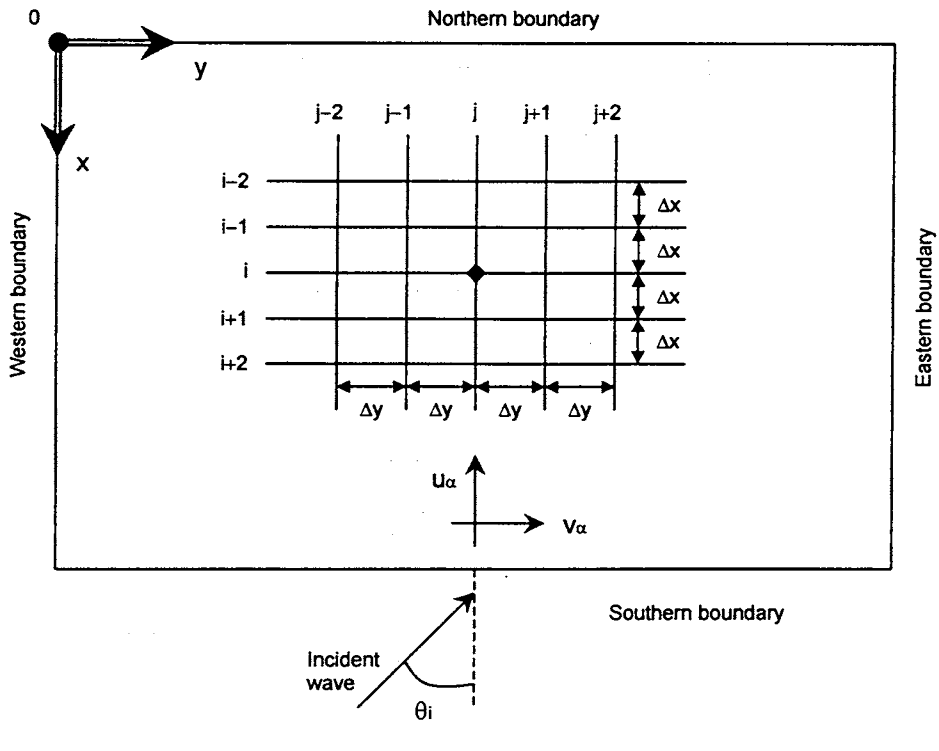

Figure A.3. 2D Cartesian coordinate system and the positive directions for the velocity components u_α, v_α and the incident wave direction θ_i.

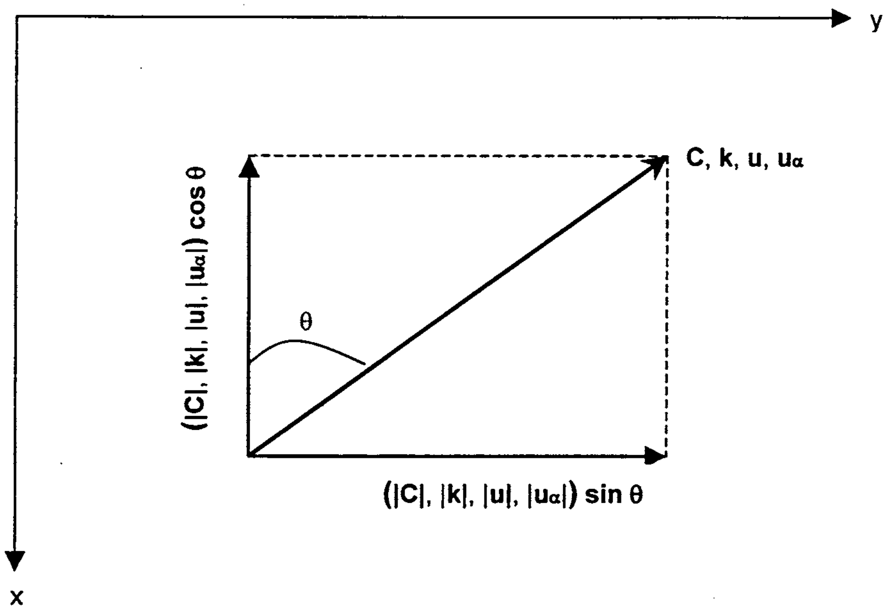

Figure A.4. Vector components and the positive directions for **C**, **k**, **u** and $\mathbf{u}_\alpha$.

Appendix B

Central, Finite Difference Operators

All the Boussinesq-type equations and the 2D unsteady, non-linear shallow water equations considered in this thesis are discretised using fourth-order accurate finite difference operators for the first-order spatial derivatives and second-order accurate finite difference operators for the second- and third-order spatial derivatives. Derivatives with mixed order spatial derivatives are discretised using second-order accurate finite difference operators. This selection of finite difference forms retains up to five points in the computational stencil. The present finite difference operators are derived based on the convention for positive slopes shown in Figure B.1.

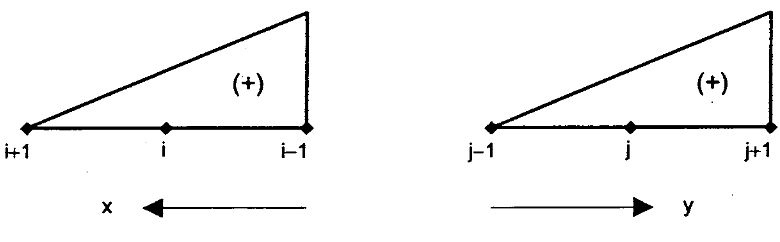

Figure B.1. Convention adopted for positive slopes.

Although this convention is unusual, it follows the Cartesian coordinate system used in this thesis (see Appendix A).

As examples, spatial derivatives of variable P, are discretised as

$$\left.\frac{\partial P}{\partial x}\right|_{i,j} = \frac{-1}{12\Delta x}\left(P_{i-2} - 8\,P_{i-1} + 8\,P_{i+1} - P_{i+2}\right)_j + O(\Delta x)^4 \tag{B.1}$$

$$\left.\frac{\partial P}{\partial y}\right|_{i,j} = \frac{1}{12\Delta y}\left(P_{j-2} - 8\,P_{j-1} + 8\,P_{j+1} - P_{j+2}\right)_i + O(\Delta y)^4 \tag{B.2}$$

$$\left.\frac{\partial P}{\partial x}\right|_{i,j} = \frac{-1}{2\Delta x}\left(P_{i+1} - P_{i-1}\right)_j + O(\Delta x)^2 \tag{B.3}$$

$$\left.\frac{\partial P}{\partial y}\right|_{i,j} = \frac{1}{2\Delta y}\left(P_{j+1} - P_{j-1}\right)_i + O(\Delta y)^2 \tag{B.4}$$

$$\left.\frac{\partial^2 P}{\partial x^2}\right|_{i,j} = \frac{1}{(\Delta x)^2}\left(P_{i-1} - 2\,P_i + P_{i+1}\right)_j + O(\Delta x)^2 \tag{B.5}$$

$$\left.\frac{\partial^2 P}{\partial y^2}\right|_{i,j} = \frac{1}{(\Delta y)^2}\left(P_{j-1} - 2\,P_j + P_{j+1}\right)_i + O(\Delta y)^2 \tag{B.6}$$

$$\left.\frac{\partial^3 P}{\partial x^3}\right|_{i,j} = \frac{-1}{2(\Delta x)^3}\left(-P_{i-2} + 2\,P_{i-1} - 2\,P_{i+1} + P_{i+2}\right)_j + O(\Delta x)^2 \tag{B.7}$$

$$\left.\frac{\partial^3 P}{\partial y^3}\right|_{i,j} = \frac{1}{2(\Delta y)^3}\left(-P_{j-2} + 2\,P_{j-1} - 2\,P_{j+1} + P_{j+2}\right)_i + O(\Delta y)^2 \tag{B.8}$$

Derivatives with mixed order spatial derivatives for h and u are discretised as

$$\left.\frac{\partial^2}{\partial x^2}\left(h\frac{\partial u}{\partial x}\right)\right|_{i,j} = \frac{-\left[h_{i-1}\left(u_i - u_{i-2}\right) - 2\,h_i\left(u_{i+1} - u_{i-1}\right) + h_{i+1}\left(u_{i+2} - u_i\right)\right]_j}{2(\Delta x)^3} + O(\Delta x)^2 \tag{B.9}$$

$$\left.\frac{\partial}{\partial x}\left(h\frac{\partial^2 u}{\partial x^2}\right)\right|_{i,j} = \frac{-\left[h_{i+1}\left(u_i - 2\,u_{i+1} + u_{i+2}\right) - h_{i-1}\left(u_{i-2} - 2\,u_{i-1} + u_i\right)\right]_j}{2(\Delta x)^3} + O(\Delta x)^2 \tag{B.10}$$

Appendix C

Alternative 2D Boussinesq-Type Equations

C.1. Introduction

It is generally agreed by investigators, who developed Boussinesq-type equations, that a Boussinesq-type continuity equation was an expression of the form of the depth-integrated continuity equation (2.96) [see e.g. Peregrine (1967), Nwogu (1993), Wei *et al.* (1995), Chen *et al.* (1998) and Madsen and Schäffer (1998)].

$$\eta_t + \nabla \bullet \int_{-h}^{\varepsilon\eta} \mathbf{u}\, dz = 0 \tag{2.96}$$

Equation (2.96) is written in *dimensionless* form based on the wave scaling parameters (ε,μ) (where the primes have been dropped) as defined by equations (2.31) and (2.32). The investigators differed however, in their determination of a Boussinesq-type momentum equation.

In this appendix, the present author:

(i) derives four new sets of Boussinesq-type (ε,μ^2) equations;

(ii) derives a new set of fully non-linear Boussinesq-type (Serre-type) equations and

(iii) demonstrates new alternative derivations of the two existing sets of fully non-linear Boussinesq-type equations of:

 (a) Wei *et al.* (1995) and

 (b) Madsen and Schäffer (1998).

C.1.1. Existing derivations of existing Boussinesq-type equations

As explained in Section 3.2, the Boussinesq-type momentum equations in the work of Nwogu (1993) and Chen *et al.* (1998) were obtained from the depth-integrated momentum equation. This equation was obtained by integrating the horizontal Euler equation of motion and applying the dynamic free surface and kinematic seabed boundary conditions.

Conversely, Wei *et al.* (1995) introduced a series expansion for ϕ (the velocity potential) at $z = -h$, and then converted it to $z = z_\alpha$. The approximate expression for ϕ (at $z = z_\alpha$) was then substituted into equation (C.1), the free surface, dynamic boundary condition (i.e. the Bernoulli equation applied at the free surface) with pressure $p = 0$, to form a Boussinesq-type momentum equation.

$$\Phi_t + \tfrac{1}{2}[\varepsilon(\nabla\Phi)^2 + \frac{\varepsilon}{\mu^2}(\Phi_z)^2] + \eta = 0 \qquad \text{at } z = \varepsilon\eta(x,y,t) \qquad \text{(C.1)}$$

Madsen and Schäffer (1998) introduced an expansion of the velocity potential as a power series in the vertical coordinate to form the horizontal and vertical velocities and then utilised equation (C.1) for the free surface, dynamic boundary condition to develop a Boussinesq-type momentum equation.

Interestingly, since the free surface, dynamic boundary condition i.e. equation (C.1) was used instead of the governing equation (for example the horizontal Euler equation of motion), the expression for the pressure through the water column was not required in the work of both groups of investigators (Wei *et al.*, 1995 and Madsen and Schäffer, 1998).

C.1.2. Four new sets of Boussinesq-type (ε,μ^2) equations

Three of the four new sets of Boussinesq-type equations with the lowest order of frequency dispersion and non-linearity [i.e. including terms up to $O(\varepsilon,\mu^2)$] derived by the present author are the Boussinesq-type equations with ambient current included. They are presented in terms of:

(a) the horizontal velocity at an arbitrary z-level, $\mathbf{u}_\alpha$ (BEWCAV-A);

(b) the bottom velocity, $\mathbf{u}_b$ (BEWCBV-B); and

(c) the still water level velocity, $\tilde{\mathbf{u}}$ (BEWCSV-C).

Since the non-linearity parameter ε is neglected in the dispersion terms of BEWCAV-A, BEWCBV-B and BEWCSV-C, the problem of wave-current interaction[1] in these sets of equations is then treated explicitly[2]. All scaling assumptions for combined wave-current motion are based on those in the work of Chen *et al.* (1998). The details of the scaling are not explained here but can be found in Chen *et al.* p16-20 and Chen (1997) p27-32. A short explanation is given in Section 5.2.2. In the work of Chen *et al.*, the horizontal velocity was considered uniform over the depth. In the present study however, vertical variation of the horizontal velocity is allowed.

[1] See Section C.6.
[2] The word 'explicit' is used here in the sense that there are extra terms in the governing equations, which are dispersion terms associated with the ambient current, even though the velocity **u** includes orbital velocity and ambient current.

If the dispersion terms associated with currents are removed from BEWCBV-B, another set of Boussinesq-type equations (BEWBV-D) arises. To the author's knowledge, BEWBV-D are a new set of Boussinesq-type equations for weakly non-linear waves.

C.1.3. New set of Serre-type equations

A new set of Serre-type equations in which all terms of $O(\mu^2)$ are included and ε is allowed to be arbitrary (FBE2O-E), is also developed by the present author. These new equations are an alternative set of fully non-linear Boussinesq-type equations [including terms up to $O(\mu^2,\varepsilon^3\mu^2)$] to the equations derived by Wei *et al.* (1995). The momentum equation in FBE2O-E is derived by the present author from a depth-integrated form of the horizontal Euler equation of motion together with the irrotationality condition.

C.1.4. New derivation of existing fully non-linear Boussinesq-type equations

New derivations for two existing sets of fully non-linear Boussinesq-type equations of:

(i) Wei *et al.* (1995) [including terms up to $O(\mu^2,\varepsilon^3\mu^2)$] and

(ii) Madsen and Schäffer (1998) [including terms up to $O(\mu^4,\varepsilon^5\mu^4)$]

are also presented by the present author. The momentum equations in both sets of fully non-linear Boussinesq-type equations are derived here from the horizontal Euler equation of motion together with the irrotationality condition.

C.2. Derivation of four new sets of (ε,μ^2) equations

The procedure developed by the present author for deriving: (i) four new momentum equations (in BEWCAV-A, BEWCBV-B, BEWCSV-C and BEWBV-D), and (ii) three existing momentum equations [in Nwogu's (1993), Boussinesq's (1872) and Peregrine's (1967) equations] is illustrated in Figure C.1 (and Figure 1.4).

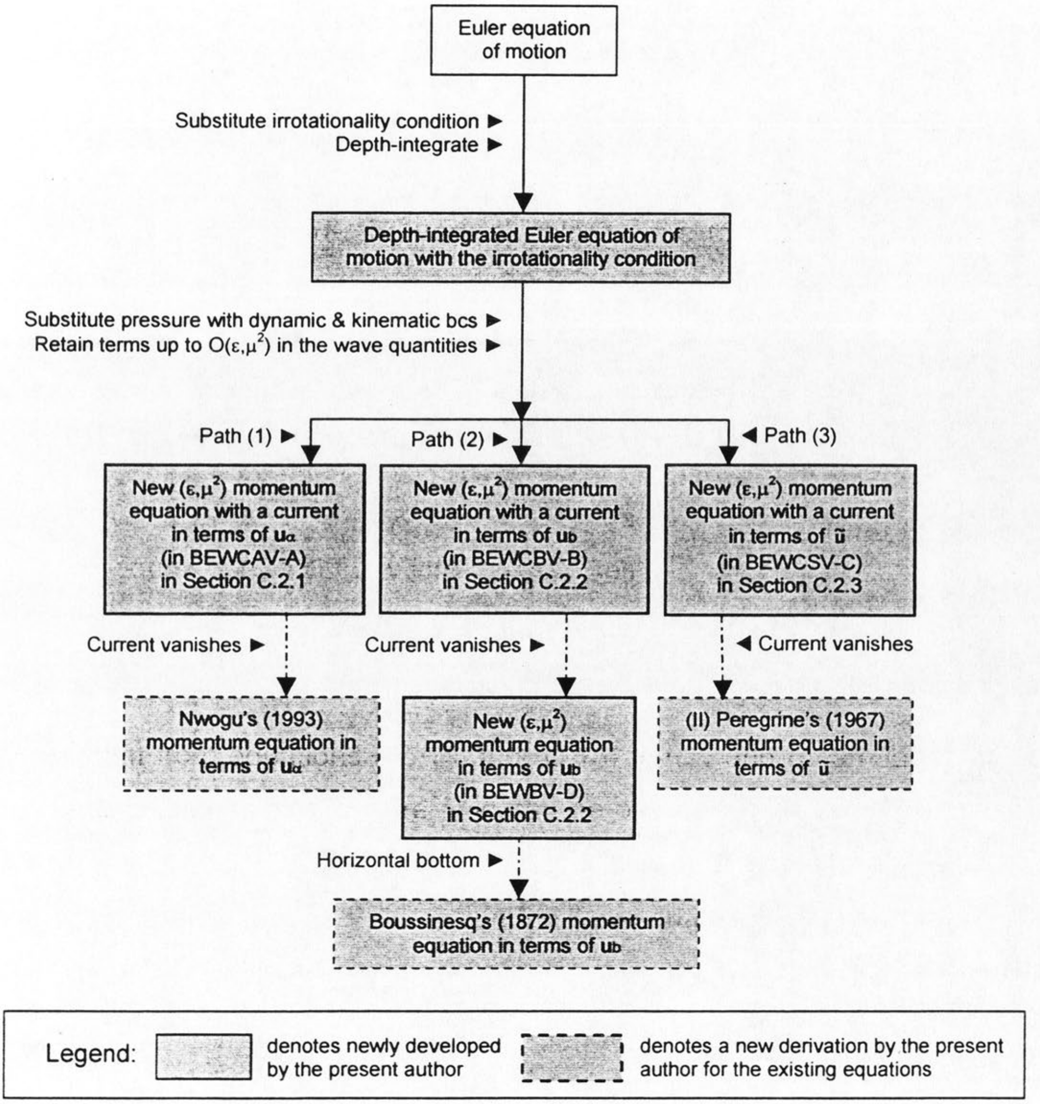

Figure C.1. New derivations of four new and three existing (ε,μ^2) momentum equations.

A new depth-integrated momentum equation can be obtained by integrating the horizontal Euler equation of motion with the irrotationality condition included [i.e. equation (3.2)]. This results in

$$\int_{-h}^{\varepsilon\eta}\left[\mathbf{u}_t+\varepsilon(\mathbf{u}\bullet\nabla)\mathbf{u}+\frac{\varepsilon}{\mu^2}w\nabla w+\nabla p\right]dz=0 \qquad (C.2)$$

A pressure distribution in the equation above can be obtained by integrating the vertical Euler equation of motion [i.e. equation (2.91)] from z to $\varepsilon\eta$, and then applying the free surface, dynamic boundary condition [i.e. equation (2.92)] to give

$$p=\eta-\frac{z}{\varepsilon}+\int_z^{\varepsilon\eta}[w_t+\varepsilon(\mathbf{u}\bullet\nabla)w]\,dz+\frac{\varepsilon}{\mu^2}\frac{1}{2}\left[w^2\Big|^{z=\varepsilon\eta}-w^2\Big|_{z=z}\right] \qquad (C.3)$$

The above expression for pressure i.e. equation (C.3) only satisfies the free surface, dynamic boundary condition. It can be compared to the pressure expression presented in equation (3.3) in which the dynamic and kinematic boundary conditions at the free surface are both satisfied.

$$p=\eta-\frac{z}{\varepsilon}+\frac{\partial}{\partial t}\int_z^{\varepsilon\eta}w\,dz+\varepsilon(\mathbf{u}\bullet\nabla)\int_z^{\varepsilon\eta}w\,dz-\frac{\varepsilon}{\mu^2}w^2 \qquad (3.3)$$

Equation (C.3) is an alternative to equation (3.3).

C.2.1. New (ε,μ^2) equations in terms of the velocity at an arbitrary z-elevation, $\mathbf{u}_\alpha$

Path (1) in Figure C.1:

Equations (2.96), (C.2), (C.3) and (3.3) above are written in terms of *wave* scaling parameters (ε,μ). These equations will now be re-written in terms of a different set of scaling parameters i.e. the *wave-current* scaling parameters ($\varepsilon,\mu,\delta,\nu$). The details can be found in Section 5.2.2 and Chen (1997) p27-32 and Chen *et al.* (1998) p16-20. This results in the following four equations respectively.

$$\eta_t + \nabla \bullet \int_{-h}^{\delta\eta} \mathbf{u}\, dz = 0 \tag{5.4}$$

$$\int_{-h}^{\delta\eta} \left[\mathbf{u}_t + \nu(\mathbf{u} \bullet \nabla)\mathbf{u} + \frac{\nu}{\mu^2} w\nabla w + \nabla p\right] dz = 0 \tag{C.4}$$

$$p = \eta - \frac{z}{\delta} + \int_{z}^{\delta\eta} [w_t + \nu(\mathbf{u} \bullet \nabla)w]\, dz + \frac{\nu}{\mu^2}\frac{1}{2}\left[w^2\Big|^{z=\delta\eta} - w^2\Big|_{z=z}\right] \tag{C.5}$$

$$p = \eta - \frac{z}{\delta} + \frac{\partial}{\partial t}\int_{z}^{\delta\eta} w\, dz + \nu(\mathbf{u} \bullet \nabla)\int_{z}^{\delta\eta} w\, dz - \frac{\nu}{\mu^2} w^2 \tag{5.6}$$

Similarly, equations (2.95a) for the irrotationality condition, (3.4) and (3.12) for w and (3.14) for **u** can be written as

$$\mathbf{u}_z - \frac{\delta}{\nu}\nabla w = 0 \tag{5.3}$$

$$w = -\frac{\varepsilon}{\delta}\mu^2 \nabla \bullet \int_{-h}^{z} \mathbf{u}\, dz \tag{5.7}$$

$$w = -\frac{\varepsilon}{\delta}\mu^2[z\nabla \bullet \mathbf{u}_\alpha + \nabla \bullet (h\mathbf{u}_\alpha)] + O\left(\frac{\varepsilon}{\delta}\mu^4\right) \tag{C.6}$$

$$\mathbf{u} = \mathbf{u}_\alpha + \frac{\varepsilon}{\nu}\mu^2\left\{\Gamma_\alpha - \tfrac{1}{2}z^2\nabla(\nabla \bullet \mathbf{u}_\alpha) - z\nabla[\nabla \bullet (h\mathbf{u}_\alpha)]\right\} + O\left(\frac{\varepsilon}{\nu}\mu^4\right) \tag{C.7}$$

Due to the presence of the elevation z in equations (C.6) and (C.7), it is clear that the vertical and horizontal velocities are permitted to vary through the water column. Inserting equations (C.6) for w and (C.7) for **u** into either (C.5) or (5.6) for p, integrating and retaining terms up to $O(\varepsilon)$ and $O(\mu^2)$ in the wave quantities gives

$$p = \eta - \frac{z}{\delta} + \frac{\varepsilon}{\delta}\mu^2\left[\tfrac{1}{2}z^2(\nabla \bullet \mathbf{u}_{\alpha_t}) + z\nabla \bullet (h\mathbf{u}_{\alpha_t})\right]$$

$$+ \varepsilon\mu^2\left[-\tfrac{1}{2}\delta\eta^2(\nabla \bullet \mathbf{u}_{\alpha_t}) - \eta\nabla \bullet (h\mathbf{u}_{\alpha_t})\right]$$

$$+ \nu\frac{\varepsilon}{\delta}\mu^2\left\{\tfrac{1}{2}z^2(\mathbf{u}_\alpha \bullet \nabla)(\nabla \bullet \mathbf{u}_\alpha) + z(\mathbf{u}_\alpha \bullet \nabla)[\nabla \bullet (h\mathbf{u}_\alpha)]\right\}$$

$$+ \nu\varepsilon\mu^2\left\{-\tfrac{1}{2}\delta\eta^2(\mathbf{u}_\alpha \bullet \nabla)(\nabla \bullet \mathbf{u}_\alpha) - \eta(\mathbf{u}_\alpha \bullet \nabla)[\nabla \bullet (h\mathbf{u}_\alpha)]\right\}$$

$$+ O\left(\frac{\varepsilon^2}{\delta}\mu^2, \frac{\varepsilon}{\delta}\mu^4\right) \qquad \text{(C.8)}$$

Substituting equation (C.7) for **u** into the depth-integrated continuity equation (5.4) and retaining terms up to $O(\varepsilon)$ and $O(\mu^2)$ in the wave quantities leads to equation (C.9). Substituting equations (C.6) for w, (C.7) for **u** and (C.8) for p into (C.4) for the depth-integrated momentum equation, integrating and retaining terms up to $O(\varepsilon)$ and $O(\mu^2)$ in the wave quantities leads to equation (C.10).

$$\eta_t + \nabla \bullet (h\mathbf{u}_\alpha) + \delta\eta\nabla \bullet \mathbf{u}_\alpha + \nu\mathbf{u}_\alpha \bullet \nabla\eta$$

$$+ \mu^2(\Pi_0^3 + \underbrace{\delta\Pi_1^3 + \delta^2\Pi_2^3 + \delta^3\Pi_3^3}_{\text{Dispersion terms associated with currents}}) = O(\varepsilon\mu^2, \mu^4) \qquad \text{(C.9)}$$

$$\mathbf{u}_{\alpha_t} + \nu(\mathbf{u}_\alpha \bullet \nabla)\mathbf{u}_\alpha + \nabla\eta$$

$$+ \mu^2[\Lambda_0^3 + \underbrace{\nu\Lambda_1^3 + \delta(\Lambda_2^3 + \nu\Lambda_3^3) + \delta^2(\Lambda_4^3 + \nu\Lambda_5^3)}_{\text{Dispersion terms associated with currents}}] = O(\varepsilon\mu^2, \mu^4) \qquad \text{(C.10)}$$

where

$$\Pi_0^3 = \Pi_0^2,\ \Pi_1^3 = \Pi_1^2,\ \Pi_2^3 = \Pi_2^2,\ \Pi_3^3 = \Pi_3^2 \qquad \text{(C.9a)}$$

$$\Lambda_0^3 = \Lambda_0^2,\ \Lambda_2^3 = \Lambda_2^2,\ \Lambda_4^3 = \Lambda_4^2 \qquad \text{(C.10a)}$$

$$\Lambda_1^3 = \nabla(\mathbf{u}_\alpha \bullet \Gamma_\alpha) + \tfrac{1}{6}h^2\nabla(\nabla \bullet \mathbf{u}_\alpha)^2 - \tfrac{1}{2}h[(\nabla \bullet \mathbf{u}_\alpha)\nabla \bullet (h\mathbf{u}_\alpha)] + \tfrac{1}{2}[\nabla \bullet (h\mathbf{u}_\alpha)]^2 \qquad \text{(C.10b)}$$

$$\Lambda_3^3 = -\eta\nabla\left\{(\mathbf{u}_\alpha \bullet \nabla)[\nabla \bullet (h\mathbf{u}_\alpha)]\right\} - \tfrac{1}{6}\eta h\nabla(\nabla \bullet \mathbf{u}_\alpha)^2 + \tfrac{1}{2}\eta\nabla[(\nabla \bullet \mathbf{u}_\alpha)\nabla \bullet (h\mathbf{u}_\alpha)] \qquad \text{(C.10c)}$$

$$\Lambda_5^3 = -\tfrac{1}{2}\eta^2\nabla[(\mathbf{u}_\alpha \bullet \nabla)(\nabla \bullet \mathbf{u}_\alpha)] + \tfrac{1}{6}\eta^2\nabla(\nabla \bullet \mathbf{u}_\alpha)^2 \qquad \text{(C.10d)}$$

The particular dispersion terms Π_i^2 $(i=0,1,2,3)$ and Λ_i^2 $(i=0,2,4)$ are defined by equations (5.22) and (5.23) respectively. Again Γ_α is defined by equations (3.11a). Equations (C.9) and (C.10) are a new set of Boussinesq-type (ε,μ^2) equations with an ambient current. To avoid confusion with the analysis in Sections C.5 and C.6, the new set of Boussinesq-type equations [(C.9) and (C.10)] is referred to as BEWCAV-A (see Figure C.1). It appears that the continuity equation (C.9) remains identical to the continuity equation (5.22) in the *second set* of equations of Chen *et al.* (1998).

When the ambient current vanishes, the dispersion terms associated with currents [i.e. Π_i^3 $(i=1,2,3)$ and Λ_i^3 $(i=1,2,3,4,5)$] become negligible as detailed by Chen *et al.* (1998) p16-20. As a result, BEWCAV-A reduce to the equations of Nwogu (1993) written below.

$$\eta_t + \nabla \bullet [(h+\varepsilon\eta)\mathbf{u}_\alpha] + \mu^2\nabla \bullet (h\overline{\Gamma}) = O(\varepsilon\mu^2,\mu^4) \qquad (3.16)$$

$$\mathbf{u}_{\alpha_t} + \nabla\eta + \varepsilon(\mathbf{u}_\alpha \bullet \nabla)\mathbf{u}_\alpha + \mu^2\Gamma_{\alpha_t} = O(\varepsilon\mu^2,\mu^4) \qquad (3.17)$$

C.2.2. New (ε,μ^2) equations in terms of the velocity at the seabed, $\mathbf{u}_b$

Path (2) in Figure C.1:

The *dimensional* horizontal velocity of the fluid at elevation z is expanded as a Taylor series with respect to the velocity $\mathbf{u}_b = \mathbf{u}(x,y,-h,t)$ at $z=-h$. This results in

$$\mathbf{u}(x,y,z,t) = \mathbf{u}(x,y,-h,t) + (z+h)\mathbf{u}_z(x,y,-h,t) + \frac{(z+h)^2}{2}\mathbf{u}_{zz}(x,y,-h,t) + \ldots$$

$$= \mathbf{u}_b + (z+h)\,\mathbf{u}_{b_z} + \frac{(z+h)^2}{2}\mathbf{u}_{b_{zz}} + \ldots \qquad \text{(C.11)}$$

Evaluating equations (3.7) for $\mathbf{u}_z$ and (3.8) for $\mathbf{u}_{zz}$ at $z = -h$, and substituting into (C.11) gives the *non-dimensional* horizontal velocity (written in the *wave-current* scaling parameters) as

$$\mathbf{u} = \mathbf{u}_b + \frac{\varepsilon}{\nu}\mu^2\left\{\tfrac{1}{2}(h^2 - z^2)\nabla(\nabla \bullet \mathbf{u}_b) - (h+z)\nabla[\nabla \bullet (h\mathbf{u}_b)]\right\} + \text{truncation error} \tag{C.12}$$

Substitution of equation (C.12) for $\mathbf{u}$ into (5.7) for w and retaining terms up to $O(\varepsilon\mu^2/\delta)$ gives the vertical velocity

$$w = -\frac{\varepsilon}{\delta}\mu^2[z\nabla \bullet \mathbf{u}_b + \nabla \bullet (h\mathbf{u}_b)] + O\left(\frac{\varepsilon}{\delta}\mu^4\right) \tag{C.13}$$

Without stating as much, Chen *et al.* (1998) assumed that $\varepsilon \cong \nu$ in the vertical velocity or in other words the vertical velocity due to the ambient current is very small compared to the orbital vertical velocity due to the waves. The truncation error of equation (C.12) can be determined by integrating the irrotationality condition (5.3) from –h to z. This results in

$$\mathbf{u} - \mathbf{u}_b = \frac{\delta}{\nu}\int_{-h}^{z}\nabla w \, dz \tag{C.14}$$

Inserting equation (C.13) for w into (C.14) gives

$$\mathbf{u} = \mathbf{u}_b + \frac{\varepsilon}{\nu}\mu^2\left\{\tfrac{1}{2}(h^2 - z^2)\nabla(\nabla \bullet \mathbf{u}_b) - (h+z)\nabla[\nabla \bullet (h\mathbf{u}_b)]\right\} + O\left(\frac{\varepsilon}{\nu}\mu^4\right) \tag{C.15}$$

It is evident from equations (C.13) and (C.15) that w and $\mathbf{u}$ can vary through the water column. The pressure field can be obtained by inserting equations (C.13) for w and (C.15) for $\mathbf{u}$ into either (C.5) or (5.6) for p, integrating and retaining terms up to $O(\varepsilon)$ and $O(\mu^2)$ in the wave quantities to give

$$p=\eta-\frac{z}{\delta}+\frac{\varepsilon}{\delta}\mu^2\left[\tfrac{1}{2}z^2(\nabla\bullet\mathbf{u}_{b_t})+z\nabla\bullet(h\mathbf{u}_{b_t})\right]$$

$$+\varepsilon\mu^2\left[-\tfrac{1}{2}\delta\eta^2(\nabla\bullet\mathbf{u}_{b_t})-\eta\nabla\bullet(h\mathbf{u}_{b_t})\right]$$

$$+\nu\frac{\varepsilon}{\delta}\mu^2\left\{\tfrac{1}{2}z^2(\mathbf{u}_b\bullet\nabla)(\nabla\bullet\mathbf{u}_b)+z(\mathbf{u}_b\bullet\nabla)[\nabla\bullet(h\mathbf{u}_b)]\right\}$$

$$+\nu\varepsilon\mu^2\left\{-\tfrac{1}{2}\delta\eta^2(\mathbf{u}_b\bullet\nabla)(\nabla\bullet\mathbf{u}_b)-\eta(\mathbf{u}_b\bullet\nabla)[\nabla\bullet(h\mathbf{u}_b)]\right\}$$

$$+O\left(\frac{\varepsilon^2}{\delta}\mu^2,\frac{\varepsilon}{\delta}\mu^4\right) \tag{C.16}$$

In a similar way to the development of BEWCAV-A in Section C.2.1, equations (C.13) for w, (C.15) for **u** and (C.16) for p are utilised [instead of equations (C.6) for w, (C.7) for **u** and (C.8) for p respectively]. As a result, the equivalent of equations (C.9) (continuity equation) and (C.10) (momentum equation) become equations (C.17) and (C.18) respectively.

$$\eta_t+\nabla\bullet(h\mathbf{u}_b)+\delta\eta\nabla\bullet\mathbf{u}_b+\nu\mathbf{u}_b\bullet\nabla\eta$$

$$+\mu^2(\Pi_0^4+\underbrace{\delta\Pi_1^4+\delta^2\Pi_2^4+\delta^3\Pi_3^4}_{\text{Dispersion terms associated with currents}})=O(\varepsilon\mu^2,\mu^4) \tag{C.17}$$

$$\mathbf{u}_{b_t}+\nu(\mathbf{u}_b\bullet\nabla)\mathbf{u}_b+\nabla\eta$$

$$+\mu^2[\Lambda_0^4+\underbrace{\nu\Lambda_1^4+\delta(\Lambda_2^4+\nu\Lambda_3^4)+\delta^2(\Lambda_4^4+\nu\Lambda_5^4)}_{\text{Dispersion terms associated with currents}}]=O(\varepsilon\mu^2,\mu^4) \tag{C.18}$$

where

$$\Pi_0^4=\nabla\bullet\left\{\tfrac{1}{2}h^3\nabla(\nabla\bullet\mathbf{u}_b)-h^2\nabla[\nabla\bullet(h\mathbf{u}_b)]\right\}-\tfrac{1}{6}h^3\nabla^2(\nabla\bullet\mathbf{u}_b)+\tfrac{1}{2}h^2\nabla^2[\nabla\bullet(h\mathbf{u}_b)] \tag{C.17a}$$

$$\Pi_1^4=\eta\nabla\bullet\left\{\tfrac{1}{2}h^2\nabla(\nabla\bullet\mathbf{u}_b)-h\nabla[\nabla\bullet(h\mathbf{u}_b)]\right\} \tag{C.17b}$$

$$\Pi_2^4=-\tfrac{1}{2}\eta^2\nabla^2[\nabla\bullet(h\mathbf{u}_b)] \tag{C.17c}$$

$$\Pi_3^4=-\tfrac{1}{6}\eta^3\nabla^2(\nabla\bullet\mathbf{u}_b) \tag{C.17d}$$

$$\Lambda_0^4=\tfrac{1}{2}h^2\nabla(\nabla\bullet\mathbf{u}_{b_t})-h\nabla[\nabla\bullet(h\mathbf{u}_{b_t})] \tag{C.18a}$$

$$\Lambda_1^4 = \nabla\left\{(\mathbf{u}_b \bullet \nabla)\left[\tfrac{1}{2}h^2(\nabla \bullet \mathbf{u}_b)\right] - (\mathbf{u}_b \bullet \nabla)[h\nabla \bullet (h\mathbf{u}_b)] + [\nabla \bullet (h\mathbf{u}_b)]^2\right\}$$

$$+\tfrac{1}{6}h^2\nabla(\nabla \bullet \mathbf{u}_b)^2 - \tfrac{1}{2}h\nabla[(\nabla \bullet \mathbf{u}_b)\nabla \bullet (h\mathbf{u}_b)] \qquad \text{(C.18b)}$$

$$\Lambda_2^4 = -\eta\nabla[\nabla \bullet (h\mathbf{u}_{b_t})] \qquad \text{(C.18c)}$$

$$\Lambda_3^4 = -\eta\nabla\left\{(\mathbf{u}_b \bullet \nabla)[\nabla \bullet (h\mathbf{u}_b)]\right\} - \tfrac{1}{6}\eta h\nabla(\nabla \bullet \mathbf{u}_b)^2 + \tfrac{1}{2}\eta\nabla[(\nabla \bullet \mathbf{u}_b)\nabla \bullet (h\mathbf{u}_b)]$$

(C.18d)

$$\Lambda_4^4 = -\tfrac{1}{2}\eta^2\nabla(\nabla \bullet \mathbf{u}_{b_t}) \qquad \text{(C.18e)}$$

$$\Lambda_5^4 = -\tfrac{1}{2}\eta^2[(\mathbf{u}_b \bullet \nabla)(\nabla \bullet \mathbf{u}_b)] + \tfrac{1}{6}\eta^2\nabla(\nabla \bullet \mathbf{u}_b)^2 \qquad \text{(C.18f)}$$

Equations (C.17) and (C.18) are a new set of Boussinesq-type equations [including terms up to $O(\varepsilon,\mu^2)$ in the wave quantities] with an ambient current in terms of the horizontal bottom velocity. This new set of Boussinesq-type equations is then referred to as BEWCBV-B (see Figure C.1). When the ambient current vanishes, the dispersion terms Π_i^4 $(i=1,2,3)$ in equation (C.17) and Λ_i^4 $(i=1,2,3,4,5)$ in equation (C.18), which are associated with currents, become negligible as detailed by Chen *et al.* (1998) p16-20. Consequently, BEWCBV-B reduce to the new set of Boussinesq-type equations (BEWBV-D) (Figure C.1) written below.

$$\eta_t + \nabla \bullet [(h+\varepsilon\eta)\mathbf{u}_b] + \mu^2\Pi_0^4 = O(\varepsilon\mu^2,\mu^4) \qquad \text{(C.19)}$$

$$\mathbf{u}_{\alpha_t} + \varepsilon(\mathbf{u}_b \bullet \nabla)\mathbf{u}_b + \nabla\eta + \mu^2\Lambda_0^4 = O(\varepsilon\mu^2,\mu^4) \qquad \text{(C.20)}$$

If the water depth is assumed to be constant, BEWBV-D i.e. equations (C.19) and (C.20) reduce to the equations of Boussinesq (1872) written below.

$$\eta_t + \varepsilon\mathbf{u}_b \bullet \nabla\eta + (\varepsilon\eta + h)(\nabla \bullet \mathbf{u}_b) - \mu^2\tfrac{1}{6}h^3\nabla^2(\nabla \bullet \mathbf{u}_b) = O(\varepsilon\mu^2,\mu^4) \qquad \text{(2.29)}$$

$$\mathbf{u}_{b_t} + \varepsilon(\mathbf{u}_b \bullet \nabla)\mathbf{u}_b + \nabla\eta - \mu^2\tfrac{1}{2}h^2\nabla(\nabla \bullet \mathbf{u}_{b_t}) = O(\varepsilon\mu^2,\mu^4) \qquad \text{(2.30)}$$

C.2.3. New (ε,μ^2) equations in terms of the velocity at still water level, $\tilde{u}$

Path (3) in Figure C.1:

In a similar procedure to that in Section C.2.2 but with $z=0$, expressions for the vertical and horizontal velocities as well as pressure field are

$$w=-\frac{\varepsilon}{\delta}\mu^2[z\nabla\bullet\tilde{\mathbf{u}}+\nabla\bullet(h\tilde{\mathbf{u}})]+O\left(\frac{\varepsilon}{\delta}\mu^4\right) \tag{C.21}$$

$$\mathbf{u}=\tilde{\mathbf{u}}-\frac{\varepsilon}{\nu}\mu^2\{\tfrac{1}{2}z^2\nabla(\nabla\bullet\tilde{\mathbf{u}})+z\nabla[\nabla\bullet(h\tilde{\mathbf{u}})]\}+O\left(\frac{\varepsilon}{\nu}\mu^4\right) \tag{C.22}$$

$$\begin{aligned}p=\eta-\frac{z}{\delta}&+\frac{\varepsilon}{\delta}\mu^2[\tfrac{1}{2}z^2(\nabla\bullet\tilde{\mathbf{u}}_t)+z\nabla\bullet(h\tilde{\mathbf{u}}_t)]\\&+\varepsilon\mu^2[-\tfrac{1}{2}\delta\eta^2(\nabla\bullet\tilde{\mathbf{u}}_t)-\eta\nabla\bullet(h\tilde{\mathbf{u}}_t)]\\&+\nu\frac{\varepsilon}{\delta}\mu^2\{\tfrac{1}{2}z^2(\tilde{\mathbf{u}}\bullet\nabla)(\nabla\bullet\tilde{\mathbf{u}})+z(\tilde{\mathbf{u}}\bullet\nabla)[\nabla\bullet(h\tilde{\mathbf{u}})]\}\\&+\nu\varepsilon\mu^2\{-\tfrac{1}{2}\delta\eta^2(\tilde{\mathbf{u}}\bullet\nabla)(\nabla\bullet\tilde{\mathbf{u}})-\eta(\tilde{\mathbf{u}}\bullet\nabla)[\nabla\bullet(h\tilde{\mathbf{u}})]\}+O\left(\frac{\varepsilon^2}{\delta}\mu^2,\frac{\varepsilon}{\delta}\mu^4\right)\end{aligned} \tag{C.23}$$

In the expressions for the vertical and horizontal velocities above, vertical variation through the water column is allowed. Utilising equations (C.21) to (C.23) for w, **u** and p [instead of (C.6), (C.7) and (C.8) respectively], equations (C.17) and (C.18) become (C.24) and (C.25) respectively, (which are newly developed by the present author).

$$\eta_t+\nabla\bullet(h\tilde{\mathbf{u}})+\delta\eta\nabla\bullet\tilde{\mathbf{u}}+\nu\tilde{\mathbf{u}}\bullet\nabla\eta+\mu^2(\Pi_0^5+\underbrace{\delta^2\Pi_2^5+\delta^3\Pi_3^5}_{\text{Dispersion terms associated with currents}})=O(\varepsilon\mu^2,\mu^4) \tag{C.24}$$

$$\tilde{\mathbf{u}}_t+\nu(\tilde{\mathbf{u}}\bullet\nabla)\tilde{\mathbf{u}}+\nabla\eta+\mu^2\underbrace{[\nu\Lambda_1^5+\delta(\Lambda_2^5+\nu\Lambda_3^5)+\delta^2(\Lambda_4^5+\nu\Lambda_5^5)]}_{\text{Dispersion terms associated with currents}}=O(\varepsilon\mu^2,\mu^4) \tag{C.25}$$

where

$$\Pi_0^5 = -\nabla \bullet \left\{ \tfrac{1}{6} h^3 \nabla(\nabla \bullet \tilde{\mathbf{u}}) - \tfrac{1}{2} h^2 \nabla[\nabla \bullet (h\tilde{\mathbf{u}})] \right\} \tag{C.24a}$$

$$\Pi_2^5 = -\tfrac{1}{2} \eta^2 \nabla^2 [\nabla \bullet (h\tilde{\mathbf{u}})] \tag{C.24b}$$

$$\Pi_3^5 = -\tfrac{1}{6} \eta^3 \nabla^2 (\nabla \bullet \tilde{\mathbf{u}}) \tag{C.24c}$$

$$\Lambda_1^5 = \tfrac{1}{6} h^2 \nabla(\nabla \bullet \tilde{\mathbf{u}})^2 - \tfrac{1}{2} h \nabla[(\nabla \bullet \tilde{\mathbf{u}}) \nabla \bullet (h\tilde{\mathbf{u}})] + \tfrac{1}{2} \nabla[\nabla \bullet (h\tilde{\mathbf{u}})]^2 \tag{C.25a}$$

$$\Lambda_2^5 = -\eta \nabla[\nabla \bullet (h\tilde{\mathbf{u}}_t)] \tag{C.25b}$$

$$\Lambda_3^5 = -\eta \nabla \left\{ (\tilde{\mathbf{u}} \bullet \nabla)[\nabla \bullet (h\tilde{\mathbf{u}})] \right\} - \tfrac{1}{6} \eta h \nabla(\nabla \bullet \tilde{\mathbf{u}})^2 + \tfrac{1}{2} \eta \nabla[(\nabla \bullet \tilde{\mathbf{u}}) \nabla \bullet (h\tilde{\mathbf{u}})] \tag{C.25c}$$

$$\Lambda_4^5 = -\tfrac{1}{2} \eta^2 \nabla(\nabla \bullet \tilde{\mathbf{u}}_t) \tag{C.25d}$$

$$\Lambda_5^5 = -\tfrac{1}{2} \eta^2 [(\tilde{\mathbf{u}} \bullet \nabla)(\nabla \bullet \tilde{\mathbf{u}})] + \tfrac{1}{6} \eta^2 \nabla(\nabla \bullet \tilde{\mathbf{u}})^2 \tag{C.25e}$$

Equations (C.24) and (C.25) are a new set of Boussinesq-type equations [including terms up to $O(\varepsilon,\mu^2)$ in the wave quantities] with an ambient current in terms of the horizontal velocity at still water level. This new set of Boussinesq-type equations is referred to as BEWCSV-C (Figure C.1). When the ambient current vanishes, all the dispersion terms associated with currents (i.e. the Π and Λ terms above except for Π_0^5) will become negligible as detailed by Chen *et al.* (1998) p16-20. The resulting equations then reduce to the equations of Peregrine (1967) in terms of $\tilde{\mathbf{u}}$ and are written below.

$$\eta_t + \nabla \bullet [(h + \varepsilon\eta)\tilde{\mathbf{u}}] = -\mu^2 \nabla \left\{ \tfrac{1}{2} h^2 \nabla[\nabla \bullet (h\tilde{\mathbf{u}})] - \tfrac{1}{6} h^3 \nabla(\nabla \bullet \tilde{\mathbf{u}}) \right\} + O(\varepsilon\mu^2, \mu^4) \tag{2.105}$$

$$\tilde{\mathbf{u}}_t + \varepsilon(\tilde{\mathbf{u}} \bullet \nabla)\tilde{\mathbf{u}} + \nabla\eta = O(\varepsilon\mu^2, \mu^4) \tag{2.106}$$

C.3. New derivation for new and existing $(\mu^2,\varepsilon^3\mu^2)$ equations

In this new derivation by the present author, the current is no longer treated explicitly (as in Section C.2) but implicitly. Consequently, the next derivation is similar to the derivation for pure wave motion (in Chapter Three). An illustration of the steps involved in this derivation is shown in Figure C.2 (and Figure 1.4).

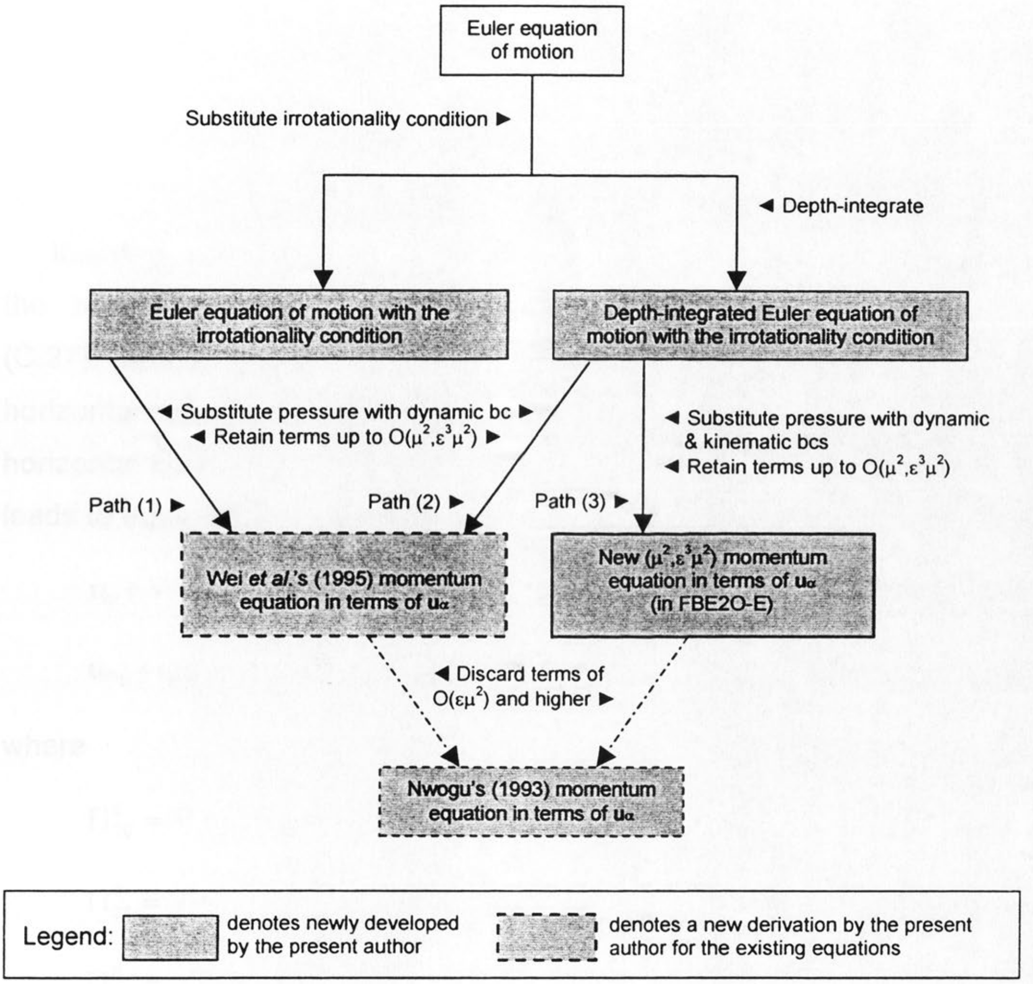

Figure C.2. New derivations of Wei *et al.*'s (1993) and new $(\mu^2,\varepsilon^3\mu^2)$ momentum equations.

Path (1) in Figure C.2:

Substitution of equation (3.12) for w and (3.14) for **u** into (C.3) for p and integrating leads to the pressure distribution

$$p = \eta - \frac{z}{\varepsilon} + \mu^2\left[\tfrac{1}{2}z^2(\nabla \bullet \mathbf{u}_{\alpha_t}) + z\nabla \bullet (h\mathbf{u}_{\alpha_t})\right]$$

$$+\varepsilon\mu^2\Big\{-\eta\nabla \bullet (h\mathbf{u}_{\alpha_t}) + \tfrac{1}{2}z^2[(\mathbf{u}_\alpha \bullet \nabla)(\nabla \bullet \mathbf{u}_\alpha) - (\nabla \bullet \mathbf{u}_\alpha)^2]$$

$$+ z\{(\mathbf{u}_\alpha \bullet \nabla)[\nabla \bullet (h\mathbf{u}_\alpha)] - (\nabla \bullet \mathbf{u}_\alpha)\nabla \bullet (h\mathbf{u}_\alpha)\}\Big\}$$

$$+\varepsilon^2\mu^2\Big\{-\tfrac{1}{2}\eta^2(\nabla \bullet \mathbf{u}_{\alpha_t}) + \eta\{(\nabla \bullet \mathbf{u}_\alpha)\nabla \bullet (h\mathbf{u}_\alpha) - (\mathbf{u}_\alpha \bullet \nabla)[\nabla \bullet (h\mathbf{u}_\alpha)]\}\Big\}$$

$$+\varepsilon^3\mu^2\{\tfrac{1}{2}\eta^2[(\nabla \bullet \mathbf{u}_\alpha)^2 - (\mathbf{u}_\alpha \bullet \nabla)(\nabla \bullet \mathbf{u}_\alpha)]\} + O(\mu^4) \qquad \text{(C.26)}$$

Inserting equation (3.14) for the horizontal velocity into equation (2.96) for the depth-integrated continuity equation and integrating leads to equation (C.27). Inserting equation (3.12) for the vertical velocity, (3.14) for the horizontal velocity and (C.26) for the pressure into equation (3.2) i.e. the horizontal Euler equation of motion combined with the irrotationality condition, leads to equation (C.28).

$$\eta_t + \nabla \bullet [(\varepsilon\eta + h)\mathbf{u}_\alpha] + \mu^2(\Pi_{20}^6 + \varepsilon\Pi_{21}^6 + \varepsilon^2\Pi_{22}^6 + \varepsilon^3\Pi_{23}^6) = O(\mu^4) \qquad \text{(C.27)}$$

$$\mathbf{u}_{\alpha_t} + \varepsilon(\mathbf{u}_\alpha \bullet \nabla)\mathbf{u}_\alpha + \nabla\eta + \mu^2(\Lambda_{20}^6 + \varepsilon\Lambda_{21}^6 + \varepsilon^2\Lambda_{22}^6 + \varepsilon^3\Lambda_{23}^6) = O(\mu^4) \qquad \text{(C.28)}$$

where

$$\Pi_{20}^6 = \nabla \bullet (h\overline{\Gamma}) \qquad \text{(C.27a)}$$

$$\Pi_{21}^6 = \nabla \bullet (\eta\Gamma_\alpha) \qquad \text{(C.27b)}$$

$$\Pi_{22}^6 = -\nabla \bullet \{-\tfrac{1}{2}\eta^2\nabla[\nabla \bullet (h\mathbf{u}_\alpha)]\} \qquad \text{(C.27c)}$$

$$\Pi_{23}^6 = -\nabla \bullet [\tfrac{1}{6}\eta^3\nabla(\nabla \bullet \mathbf{u}_\alpha)] \qquad \text{(C.27d)}$$

$$\Lambda_{20}^6 = \Gamma_{\alpha_t} \qquad \text{(C.28a)}$$

$$\Lambda_{21}^{6} = \nabla\{\mathbf{u}_\alpha \bullet \Gamma_\alpha - \eta\nabla \bullet (h\mathbf{u}_{\alpha_t}) + \tfrac{1}{2}[\nabla \bullet (h\mathbf{u}_\alpha)]^2\} \tag{C.28b}$$

$$\Lambda_{22}^{6} = \nabla\{-\tfrac{1}{2}\eta^2(\nabla \bullet \mathbf{u}_{\alpha_t}) + \eta\{(\nabla \bullet \mathbf{u}_\alpha)\nabla \bullet (h\mathbf{u}_\alpha) - (\mathbf{u}_\alpha \bullet \nabla)[\nabla \bullet (h\mathbf{u}_\alpha)]\}\} \tag{C.28c}$$

$$\Lambda_{23}^{6} = \nabla\{\tfrac{1}{2}\eta^2[(\nabla \bullet \mathbf{u}_\alpha)^2 - (\mathbf{u}_\alpha \bullet \nabla)(\nabla \bullet \mathbf{u}_\alpha)]\} \tag{C.28d}$$

in which Γ_α and $\overline{\Gamma}$ are defined by equations (3.11a) and (3.18) respectively. Equations (C.27) and (C.28) are a set of fully non-linear Boussinesq-type (Serre-type) equations, and are, as it turns out, exactly the same as that of Wei *et al.* (1995).

Although the present derivation is significantly different from the derivation in the work of Wei *et al.* (1995), the resulting equations are identical. Interestingly, because the free surface, kinematic boundary condition is not incorporated in the present derivation for Wei *et al.*'s momentum equation, the free surface, kinematic boundary condition is not satisfied. Consequently, there is scope to develop a new set of fully non-linear Boussinesq-type equations, which include the free surface, kinematic boundary condition (see Path (3) in Figure C.2).

Path (2) in Figure C.2:

Similar to Path (1), but equation (C.2) is used instead of equation (3.2) to develop a Boussinesq-type momentum equation. The resulting equation is exactly the same as that in Path (1) i.e. equation (C.28).

Path (3) in Figure C.2:

A procedure to develop a new set of Boussinesq-type equations is as follows. The free surface, kinematic boundary condition defined by equation (2.93) is inserted into the momentum equation by utilising the pressure field defined by equation (3.3) instead of being defined by equation (C.3). This results in a new expression for the pressure field as

$$p=\eta-\frac{z}{\varepsilon}+\mu^2\left[\tfrac{1}{2}z^2(\nabla\bullet\mathbf{u}_{\alpha_t})+z\nabla\bullet(h\mathbf{u}_{\alpha_t})\right]$$

$$+\varepsilon\mu^2\Big\{-\eta\nabla\bullet(h\mathbf{u}_{\alpha_t})-\eta_t\nabla\bullet(h\mathbf{u}_\alpha)-[\nabla\bullet(h\mathbf{u}_\alpha)]^2$$

$$+\tfrac{1}{2}z^2[(\mathbf{u}_\alpha\bullet\nabla)(\nabla\bullet\mathbf{u}_\alpha)-2(\nabla\bullet\mathbf{u}_\alpha)^2]$$

$$+z\big\{(\mathbf{u}_\alpha\bullet\nabla)[\nabla\bullet(h\mathbf{u}_\alpha)]-2(\nabla\bullet\mathbf{u}_\alpha)\nabla\bullet(h\mathbf{u}_\alpha)\big\}\Big\}$$

$$+\varepsilon^2\mu^2\big\{-\tfrac{1}{2}\eta^2(\nabla\bullet\mathbf{u}_{\alpha_t})-\eta\eta_t(\nabla\bullet\mathbf{u}_\alpha)-(\mathbf{u}_\alpha\bullet\nabla)[\eta\nabla\bullet(h\mathbf{u}_\alpha)]\big\}$$

$$-\varepsilon^3\mu^2(\mathbf{u}_\alpha\bullet\nabla)\left[\tfrac{1}{2}\eta^2(\nabla\bullet\mathbf{u}_\alpha)\right]+O(\mu^4) \qquad \text{(C.29)}$$

The above expression for the pressure is substituted into equation (C.2) for the depth-integrated momentum equation to yield the following new momentum equation.

$$\mathbf{u}_{\alpha_t}+\varepsilon(\mathbf{u}_\alpha\bullet\nabla)\mathbf{u}_\alpha+\nabla\eta+\mu^2(\Lambda_{20}^7+\varepsilon\Lambda_{21}^7+\varepsilon^2\Lambda_{22}^7+\varepsilon^3\Lambda_{23}^7)=O(\mu^4) \qquad \text{(C.30)}$$

where

$$\Lambda_{20}^7=\Lambda_{20}^6 \qquad \text{(C.30a)}$$

$$\Lambda_{21}^7=\nabla\big\{\mathbf{u}_\alpha\bullet\Gamma_\alpha-\eta\nabla\bullet(h\mathbf{u}_{\alpha_t})-\eta_t\nabla\bullet(h\mathbf{u}_\alpha)-\tfrac{1}{2}[\nabla\bullet(h\mathbf{u}_\alpha)]^2\big\}$$

$$-\tfrac{1}{6}h^2\nabla(\nabla\bullet\mathbf{u}_\alpha)^2+\tfrac{1}{2}h\nabla[(\nabla\bullet\mathbf{u}_\alpha)\nabla\bullet(h\mathbf{u}_\alpha)] \qquad \text{(C.30b)}$$

$$\Lambda_{22}^7=\nabla\big\{-\tfrac{1}{2}\eta^2(\nabla\bullet\mathbf{u}_{\alpha_t})-\eta\eta_t(\nabla\bullet\mathbf{u}_\alpha)-(\mathbf{u}_\alpha\bullet\nabla)[\eta\nabla\bullet(h\mathbf{u}_\alpha)]\big\}$$

$$+\tfrac{1}{6}\eta h\nabla(\nabla\bullet\mathbf{u}_\alpha)^2-\tfrac{1}{2}\eta\nabla[(\nabla\bullet\mathbf{u}_\alpha)\nabla\bullet(h\mathbf{u}_\alpha)] \qquad \text{(C.30c)}$$

$$\Lambda_{23}^7=-\nabla\big\{(\mathbf{u}_\alpha\bullet\nabla)\left[\tfrac{1}{2}\eta^2(\nabla\bullet\mathbf{u}_\alpha)\right]\big\}-\tfrac{1}{6}\eta^2\nabla(\nabla\bullet\mathbf{u}_\alpha)^2 \qquad \text{(C.30d)}$$

The new set of equations, which consists of the continuity equation (C.27) and momentum equation (C.30), is referred to as FBE2O-E (see Figure C.2). FBE2O-E satisfy all boundary conditions (i.e. the kinematic and dynamic free surface boundary conditions and the kinematic bottom boundary condition). FBE2O-E are an alternative set to equations (C.27) and (C.28).

Furthermore, no relation between ε and μ has been assumed in either set of equations. If terms of $O(\varepsilon) = O(\mu^2)$ is assumed, both sets of equations [(C.27) and (C.28); and (C.27) and (C.30)] reduce to the equations of Nwogu (1993).

C.4. New derivation of new and existing $(\mu^4, \varepsilon^5\mu^4)$ equations

Figure C.3 shows the steps in the derivations of two $(\mu^4, \varepsilon^5\mu^4)$ momentum equations.

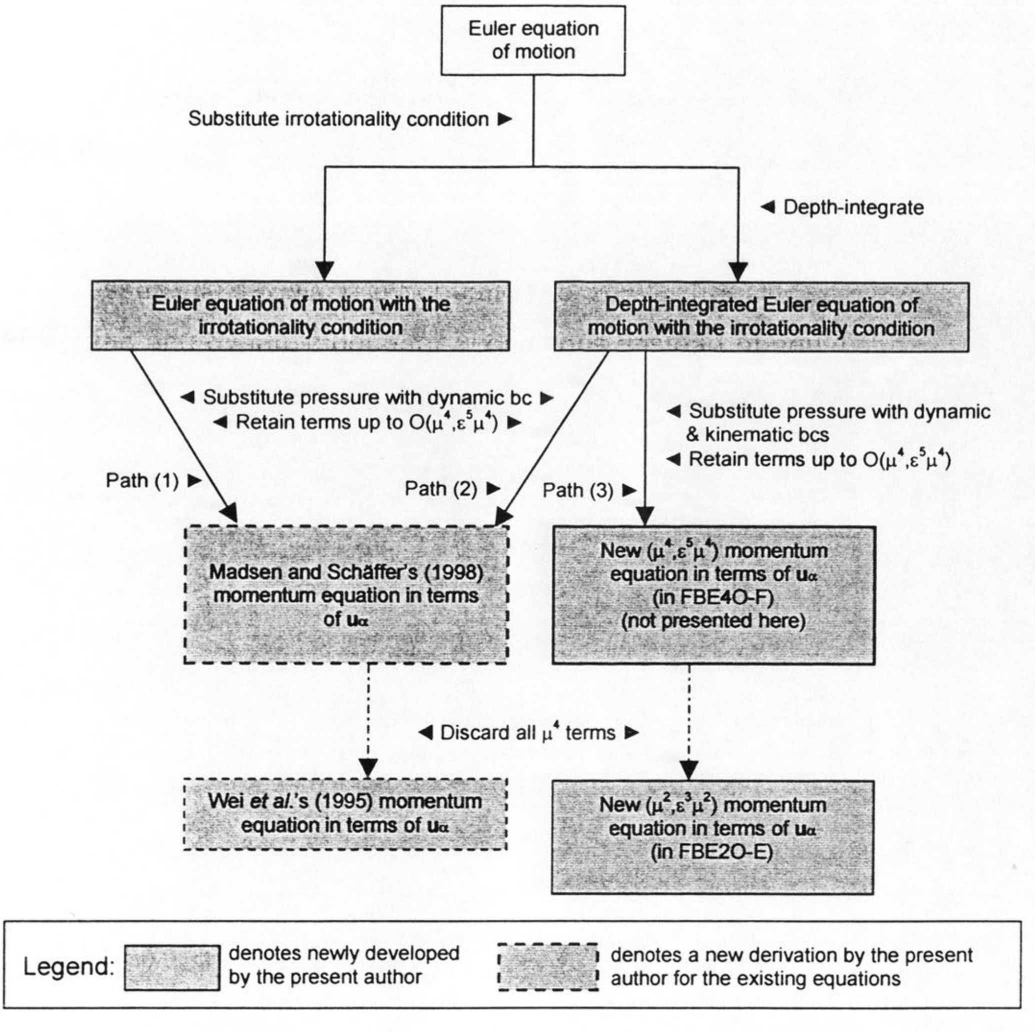

Figure C.3. New derivations of Madsen and Schäffer's (1998) and new $(\mu^4, \varepsilon^5\mu^4)$ momentum equations.

The second-order accurate vertical and horizontal velocities [(3.12) and (3.14)] [i.e. $O(\mu^2)$] can be extended to the fourth-order (truncating at the sixth-order) using the same procedure as in Chapter Three. This results in

$$w = -\mu^2[z\nabla \bullet \mathbf{u}_\alpha + \nabla \bullet (h\mathbf{u}_\alpha)]$$
$$+\mu^4\left\{\tfrac{1}{6}z^3\nabla^2(\nabla \bullet \mathbf{u}_\alpha) + \tfrac{1}{2}z^2\nabla^2[\nabla \bullet (h\mathbf{u}_\alpha)] - z(\nabla \bullet \Gamma_\alpha) - \nabla \bullet (h\overline{\Gamma})\right\} + O(\mu^6) \tag{C.31}$$

$$\mathbf{u} = \mathbf{u}_\alpha + \mu^2\left\{\Gamma_\alpha - \tfrac{1}{2}z^2\nabla(\nabla \bullet \mathbf{u}_\alpha) - z\nabla[\nabla \bullet (h\mathbf{u}_\alpha)]\right\}$$
$$+\mu^4\left\{\tfrac{1}{24}(z^4 - z_\alpha{}^4)\nabla[\nabla^2(\nabla \bullet \mathbf{u}_\alpha)] + \tfrac{1}{6}(z^3 - z_\alpha{}^3)\nabla\{\nabla^2[\nabla \bullet (h\mathbf{u}_\alpha)]\}\right.$$
$$\left.+\tfrac{1}{2}(z_\alpha{}^2 - z^2)\nabla(\nabla \bullet \Gamma_\alpha) + (z_\alpha - z)\nabla[\nabla \bullet (h\overline{\Gamma}_\alpha)]\right\} + O(\mu^6) \tag{C.32}$$

Again, Γ_α and $\overline{\Gamma}$ are defined by (3.11a) and (3.18) respectively.

Path (1) in Figure C.3:

Substituting equation (C.31) for w and (C.32) for **u** into equation (C.3) for p and integrating leads to the pressure distribution

$$p = \eta - \frac{z}{\varepsilon} + \mu^2[\tfrac{1}{2}z^2(\nabla \bullet \mathbf{u}_{\alpha_t}) + z\nabla \bullet (h\mathbf{u}_{\alpha_t})]$$
$$+\varepsilon\mu^2\left\{-\eta\nabla \bullet (h\mathbf{u}_{\alpha_t}) + \tfrac{1}{2}z^2[(\mathbf{u}_\alpha \bullet \nabla)(\nabla \bullet \mathbf{u}_\alpha) - (\nabla \bullet \mathbf{u}_\alpha)^2]\right.$$
$$\left.+z\{(\mathbf{u}_\alpha \bullet \nabla)[\nabla \bullet (h\mathbf{u}_\alpha)] - (\nabla \bullet \mathbf{u}_\alpha)\nabla \bullet (h\mathbf{u}_\alpha)\}\right\}$$
$$+\varepsilon^2\mu^2\left\{-\tfrac{1}{2}\eta^2(\nabla \bullet \mathbf{u}_{\alpha_t}) + \eta\{(\nabla \bullet \mathbf{u}_\alpha)\nabla \bullet (h\mathbf{u}_\alpha) - (\mathbf{u}_\alpha \bullet \nabla)[\nabla \bullet (h\mathbf{u}_\alpha)]\}\right\}$$
$$+\varepsilon^3\mu^2\left\{\tfrac{1}{2}\eta^2[(\nabla \bullet \mathbf{u}_\alpha)^2 - (\mathbf{u}_\alpha \bullet \nabla)(\nabla \bullet \mathbf{u}_\alpha)]\right\}$$
$$+\mu^4\left\{-\tfrac{1}{24}z^4\nabla^2(\nabla \bullet \mathbf{u}_{\alpha_t}) - \tfrac{1}{6}z^3\nabla^2[\nabla \bullet (h\mathbf{u}_{\alpha_t})] + \tfrac{1}{2}z^2(\nabla \bullet \Gamma_{\alpha_t})\right.$$
$$\left.+z\nabla \bullet (h\overline{\Gamma}_t)\right\}$$
$$+\varepsilon\mu^4\left\{-\eta\nabla \bullet (h\overline{\Gamma}_t) + \tfrac{1}{24}z^4[4(\nabla \bullet \mathbf{u}_\alpha)\nabla^2(\nabla \bullet \mathbf{u}_\alpha)\right.$$

$$
\begin{aligned}
&-(\mathbf{u}_\alpha \bullet \nabla)\nabla^2(\nabla \bullet \mathbf{u}_\alpha) - 3\nabla(\nabla \bullet \mathbf{u}_\alpha) \bullet \nabla(\nabla \bullet \mathbf{u}_\alpha)] \\
&+ \tfrac{1}{6} z^3 \{3(\nabla \bullet \mathbf{u}_\alpha)\nabla^2[\nabla \bullet (h\mathbf{u}_\alpha)] - 3\nabla(\nabla \bullet \mathbf{u}_\alpha) \bullet \nabla[\nabla \bullet (h\mathbf{u}_\alpha)] \\
&+ \nabla \bullet (h\mathbf{u}_\alpha)\nabla^2(\nabla \bullet \mathbf{u}_\alpha) - (\mathbf{u}_\alpha \bullet \nabla)\nabla^2[\nabla \bullet (h\mathbf{u}_\alpha)]\} \\
&+ \tfrac{1}{2} z^2 \{(\mathbf{u}_\alpha \bullet \nabla)(\nabla \bullet \Gamma_\alpha) + (\Gamma_\alpha \bullet \nabla)(\nabla \bullet \mathbf{u}_\alpha) - 2(\nabla \bullet \mathbf{u}_\alpha)(\nabla \bullet \Gamma_\alpha) \\
&+ \nabla \bullet (h\mathbf{u}_\alpha)\nabla^2[\nabla \bullet (h\mathbf{u}_\alpha)] - \nabla[\nabla \bullet (h\mathbf{u}_\alpha)] \bullet \nabla[\nabla \bullet (h\mathbf{u}_\alpha)]\} \\
&+ z\{((\mathbf{u}_\alpha \bullet \nabla)[\nabla \bullet (h\overline{\Gamma})] - (\nabla \bullet \mathbf{u}_\alpha)\nabla \bullet (h\overline{\Gamma}) \\
&+ (\Gamma_\alpha \bullet \nabla)[\nabla \bullet (h\mathbf{u}_\alpha)] - (\nabla \bullet \Gamma_\alpha)\nabla \bullet (h\mathbf{u}_\alpha)\}\} \\
&+ \varepsilon^2\mu^4 \{-\tfrac{1}{2}\eta^2(\nabla \bullet \Gamma_{\alpha_t}) + \eta\{(\nabla \bullet \mathbf{u}_\alpha)\nabla \bullet (h\overline{\Gamma}) - (\mathbf{u}_\alpha \bullet \nabla)[\nabla \bullet (h\overline{\Gamma})] \\
&+ (\nabla \bullet \Gamma_\alpha)\nabla \bullet (h\mathbf{u}_\alpha) - (\Gamma_\alpha \bullet \nabla)[\nabla \bullet (h\mathbf{u}_\alpha)]\}\} \\
&+ \varepsilon^3\mu^4 \{\tfrac{1}{6}\eta^3\nabla^2[\nabla \bullet (h\mathbf{u}_{\alpha_t})] + \tfrac{1}{2}\eta^2\{\{\nabla[\nabla \bullet (h\mathbf{u}_\alpha)]\}^2 \\
&- \nabla \bullet (h\mathbf{u}_\alpha)\nabla^2[\nabla \bullet (h\mathbf{u}_\alpha)] + 2(\nabla \bullet \mathbf{u}_\alpha)(\nabla \bullet \Gamma_\alpha) \\
&- (\mathbf{u}_\alpha \bullet \nabla)(\nabla \bullet \Gamma_\alpha) - (\Gamma_\alpha \bullet \nabla)(\nabla \bullet \mathbf{u}_\alpha)\}\} \\
&+ \varepsilon^4\mu^4 \{\tfrac{1}{24}\eta^4\nabla^2(\nabla \bullet \mathbf{u}_{\alpha_t}) + \tfrac{1}{6}\eta^3\{(\mathbf{u}_\alpha \bullet \nabla)\nabla^2[\nabla \bullet (h\mathbf{u}_\alpha)] \\
&- \nabla \bullet (h\mathbf{u}_\alpha)\nabla^2(\nabla \bullet \mathbf{u}_\alpha) + 3\nabla(\nabla \bullet \mathbf{u}_\alpha) \bullet \nabla[\nabla \bullet (h\mathbf{u}_\alpha)] \\
&- 3(\nabla \bullet \mathbf{u}_\alpha)\nabla^2[\nabla \bullet (h\mathbf{u}_\alpha)]\}\} \\
&+ \varepsilon^5\mu^4 \{\tfrac{1}{24}\eta^4\{(\mathbf{u}_\alpha \bullet \nabla)\nabla^2(\nabla \bullet \mathbf{u}_\alpha) + 3[\nabla(\nabla \bullet \mathbf{u}_\alpha)]^2 \\
&- 4(\nabla \bullet \mathbf{u}_\alpha)\nabla^2(\nabla \bullet \mathbf{u}_\alpha)\}\} + O(\mu^6) \qquad \text{(C.33)}
\end{aligned}
$$

Inserting equation (C.32) for the vertically varied horizontal velocity into equation (2.96) for the depth-integrated continuity equation gives equation (C.34). Inserting the vertically varied velocities [(C.31) and (C.32)] and pressure distribution (C.33) into equation (3.2) gives equation (C.35).

$$\eta_t + \nabla \bullet [(\varepsilon\eta + h)\mathbf{u}_\alpha] + \mu^2(\Pi_{20}^8 + \varepsilon\Pi_{21}^8 + \varepsilon^2\Pi_{22}^8 + \varepsilon^3\Pi_{23}^8)$$

$$\mu^4(\Pi_{40}^8 + \varepsilon\Pi_{41}^8 + \varepsilon^2\Pi_{42}^8 + \varepsilon^3\Pi_{43}^8 + \varepsilon^4\Pi_{44}^8 + \varepsilon^5\Pi_{45}^8) = O(\mu^6) \qquad \text{(C.34)}$$

$$\mathbf{u}_{\alpha_t} + \varepsilon(\mathbf{u}_\alpha \bullet \nabla)\mathbf{u}_\alpha + \nabla\eta + \mu^2(\Lambda_{20}^8 + \varepsilon\Lambda_{21}^8 + \varepsilon^2\Lambda_{22}^8 + \varepsilon^3\Lambda_{23}^8)$$

$$\mu^4(\Lambda_{40}^8 + \varepsilon\Lambda_{41}^8 + \varepsilon^2\Lambda_{42}^8 + \varepsilon^3\Lambda_{43}^8 + \varepsilon^4\Lambda_{44}^8 + \varepsilon^5\Lambda_{45}^8) = O(\mu^6) \qquad \text{(C.35)}$$

where

$$\Pi_{20}^8 = \Pi_{20}^6,\ \Pi_{21}^8 = \Pi_{22}^6,\ \Pi_{22}^8 = \Pi_{22}^6,\ \Pi_{23}^8 = \Pi_{23}^6, \qquad \text{(C.34a)}$$

$$\Pi_{40}^8 = \nabla \bullet \Big\{\big(\tfrac{1}{120}h^4 - \tfrac{1}{24}z_\alpha{}^4\big)h\nabla[\nabla^2(\nabla \bullet \mathbf{u}_\alpha)]$$

$$+\big(\tfrac{1}{24}h^3 - \tfrac{1}{6}z_\alpha{}^3\big)h\nabla\big(\nabla^2[\nabla \bullet (h\mathbf{u}_\alpha)]\big)$$

$$+\big(\tfrac{1}{2}z_\alpha{}^2 - \tfrac{1}{6}h^2\big)h\nabla(\nabla \bullet \Gamma_\alpha) + \big(z_\alpha + \tfrac{1}{2}h\big)h\nabla[\nabla \bullet (h\overline{\Gamma})]\Big\} \qquad \text{(C.34b)}$$

$$\Pi_{41}^8 = \nabla \bullet \Big\{-\tfrac{1}{24}z_\alpha{}^4\eta\nabla[\nabla^2(\nabla \bullet \mathbf{u}_\alpha)] - \tfrac{1}{6}z_\alpha{}^3\eta\nabla\{\nabla^2[\nabla \bullet (h\mathbf{u}_\alpha)]\}$$

$$+\tfrac{1}{2}z_\alpha{}^2\eta\nabla(\nabla \bullet \Gamma_\alpha) + z_\alpha\,\eta\nabla[\nabla \bullet (h\overline{\Gamma})]\Big\} \qquad \text{(C.34c)}$$

$$\Pi_{42}^8 = -\nabla \bullet \{-\tfrac{1}{2}\eta^2\nabla[\nabla \bullet (h\overline{\Gamma})]\} \qquad \text{(C.34d)}$$

$$\Pi_{43}^8 = -\nabla \bullet [\tfrac{1}{6}\eta^3\nabla(\nabla \bullet \Gamma_\alpha)] \qquad \text{(C.34e)}$$

$$\Pi_{44}^8 = \nabla \bullet \{\tfrac{1}{24}\eta^4\nabla\{\nabla^2[\nabla \bullet (h\mathbf{u}_\alpha)]\}\} \qquad \text{(C.34f)}$$

$$\Pi_{45}^8 = \nabla \bullet \{\tfrac{1}{120}\eta^5\nabla[\nabla^2(\nabla \bullet \mathbf{u}_\alpha)]\} \qquad \text{(C.34g)}$$

$$\Lambda_{20}^8 = \Lambda_{20}^6,\ \Lambda_{21}^8 = \Lambda_{21}^6,\ \Lambda_{22}^8 = \Lambda_{22}^6,\ \Lambda_{23}^8 = \Lambda_{23}^6, \qquad \text{(C.35a)}$$

$$\Lambda^8_{40} = -\tfrac{1}{24} z_\alpha{}^4 \nabla[\nabla^2(\nabla \bullet \mathbf{u}_{\alpha_t})] - \tfrac{1}{6} z_\alpha{}^3 \nabla\{\nabla^2[\nabla \bullet (h\mathbf{u}_{\alpha_t})]\}$$

$$+\tfrac{1}{2} z_\alpha{}^2 \nabla(\nabla \bullet \Gamma_{\alpha_t}) + z_\alpha \nabla[\nabla \bullet (h\overline{\Gamma}_t)] \qquad \text{(C.35b)}$$

$$\Lambda^8_{41} = \nabla\Big\{\tfrac{1}{2}\Gamma_\alpha{}^2 + (\nabla \bullet \mathbf{u}_\alpha)\nabla \bullet (h\overline{\Gamma}) - \eta \nabla \bullet (h\overline{\Gamma}_t)$$

$$+\mathbf{u}_\alpha \bullet \Big\{-\tfrac{1}{24} z_\alpha{}^4 \nabla[\nabla^2(\nabla \bullet \mathbf{u}_\alpha)] - \tfrac{1}{6} z_\alpha{}^3 \nabla\{\nabla^2[\nabla \bullet (h\mathbf{u}_\alpha)]\}$$

$$+\tfrac{1}{2} z_\alpha{}^2 \nabla(\nabla \bullet \Gamma_\alpha) + z_\alpha \nabla[\nabla \bullet (h\overline{\Gamma})]\Big\}\Big\} \qquad \text{(C.35c)}$$

$$\Lambda^8_{42} = \nabla\Big\{-\tfrac{1}{2}\eta^2(\nabla \bullet \Gamma_{\alpha_t}) + \eta\big\{(\nabla \bullet \mathbf{u}_\alpha)\nabla \bullet (h\overline{\Gamma}) - (\mathbf{u}_\alpha \bullet \nabla)[\nabla \bullet (h\overline{\Gamma})]$$

$$+(\nabla \bullet \Gamma_\alpha)\nabla \bullet (h\mathbf{u}_\alpha) - (\Gamma_\alpha \bullet \nabla)[\nabla \bullet (h\mathbf{u}_\alpha)]\big\}\Big\} \qquad \text{(C.35d)}$$

$$\Lambda^8_{43} = \nabla\Big\{\tfrac{1}{6}\eta^3\nabla^2[(h\mathbf{u}_{\alpha_t})] + \tfrac{1}{2}\eta^2\big\{\{\nabla[\nabla \bullet (h\mathbf{u}_\alpha)]\}^2$$

$$-\nabla \bullet (h\mathbf{u}_\alpha)\nabla^2[\nabla \bullet (h\mathbf{u}_\alpha)] + 2(\nabla \bullet \mathbf{u}_\alpha)(\nabla \bullet \Gamma_\alpha)$$

$$-(\mathbf{u}_\alpha \bullet \nabla)(\nabla \bullet \Gamma_\alpha) - (\Gamma_\alpha \bullet \nabla)(\nabla \bullet \mathbf{u}_\alpha)\big\}\Big\} \qquad \text{(C.35e)}$$

$$\Lambda^8_{44} = \nabla\Big\{\tfrac{1}{24}\eta^4\nabla^2(\nabla \bullet \mathbf{u}_{\alpha_t}) + \tfrac{1}{6}\eta^3\big\{(\mathbf{u}_\alpha \bullet \nabla)\nabla^2[\nabla \bullet (h\mathbf{u}_\alpha)]$$

$$-\nabla \bullet (h\mathbf{u}_\alpha)\nabla^2(\nabla \bullet \mathbf{u}_\alpha) + 3\nabla(\nabla \bullet \mathbf{u}_\alpha) \bullet \nabla[\nabla \bullet (h\mathbf{u}_\alpha)]$$

$$-3(\nabla \bullet \mathbf{u}_\alpha)\nabla^2[\nabla \bullet (h\mathbf{u}_\alpha)]\big\}\Big\} \qquad \text{(C.35f)}$$

$$\Lambda^8_{45} = \nabla\Big\{\tfrac{1}{24}\eta^4\big\{(\mathbf{u}_\alpha \bullet \nabla)\nabla^2(\nabla \bullet \mathbf{u}_\alpha) + 3[\nabla(\nabla \bullet \mathbf{u}_\alpha)]^2 - 4(\nabla \bullet \mathbf{u}_\alpha)\nabla^2(\nabla \bullet \mathbf{u}_\alpha)\big\}\Big\}$$

$$\text{(C.35g)}$$

Equations (C.34) and (C.35) are a set of fully non-linear Boussinesq-type equations which are accurate to $O(\mu^4)$. As in Section C.3, no relation between ε and μ has been assumed in equations (C.34) and (C.35). This set of $(\mu^4,\varepsilon^5\mu^4)$ equations is identical to that of Madsen and Schäffer (1998) (see Figure C.3). If all the μ^4 terms are removed, this set of equations reduces to the equations of Wei *et al.* (1995) (see Figure C.3). In the present derivation (see Paths (1) and (2) in Figure C.3), the free surface, kinematic boundary condition has not been involved in the momentum equation (C.35).

Path (2) in Figure C.3:

Similar to Path (1), but equation (C.2) is used instead of equation (3.2) to develop a Boussinesq-type momentum equation. The resulting equation is exactly the same as that in Path (1) i.e. equation (C.35).

Path (3) in Figure C.3:

An new alternative set of $(\mu^4,\varepsilon^5\mu^4)$ equations can be developed by utilising the pressure field defined by equation (3.3), which includes the free surface kinematic and dynamic boundary conditions, instead of equation (C.3), which only includes the free surface dynamic boundary condition. Consequently, the resulting $(\mu^4,\varepsilon^5\mu^4)$ equations (FBE4O-F) are very long but they satisfy all the boundary conditions (not presented here).

C.5. Transfer functions[3] for regular waves

Following Madsen and Schäffer (1998), all the sets of Boussinesq-type equations derived in this appendix are analysed to quantify the embedded characteristics with respect to frequency dispersion and non-linearity. Although the derivation of the (ε,μ^2) equations has been based on the assumption of $\mu \ll 1$ and $O(\varepsilon) = O(\mu^2)$, and the derivation of the $(\mu^2,\varepsilon^3\mu^2)$ and $(\mu^4,\varepsilon^5\mu^4)$ equations based on $\mu \ll 1$ and arbitrary ε, the analysis will now be made under the assumption of $\varepsilon \ll 1$ (i.e. weakly non-linear solutions) and arbitrary μ. Use will be made of a Stokes-type Fourier analysis on a horizontal bottom and first- and second-order solutions of the following form will be sought.

$$\overbrace{\overbrace{\eta = \eta_1 \cos\theta}^{\text{First-order}} + \overbrace{\varepsilon\eta_2 \cos 2\theta}^{\text{Second-order correction term}}}^{\text{Second-order}} \tag{C.36a}$$

$$u_b = u_{b1} \cos\theta + \varepsilon u_{b2} \cos 2\theta \tag{C.36b}$$

$$\tilde{u} = \tilde{u}_1 \cos\theta + \varepsilon\tilde{u}_2 \cos 2\theta \tag{C.36c}$$

$$\bar{u} = \bar{u}_1 \cos\theta + \varepsilon\bar{u}_2 \cos 2\theta \tag{C.36d}$$

$$u_\alpha = u_{\alpha 1} \cos\theta + \varepsilon u_{\alpha 2} \cos 2\theta \tag{C.36e}$$

where $\theta = \omega t - kx$. η_1, η_2 are the amplitudes of η in the first-order and the second-order correction term for regular waves. A similar comment applies to u_{b1}, u_{b2}; $\tilde{u}_1, \tilde{u}_2$; $\bar{u}_1, \bar{u}_2$; and $u_{\alpha 1}$, $u_{\alpha 2}$; It is emphasised that the analysis will not involve non-linear terms with powers of ε higher than one, although such terms are retained in the complete equations of the $(\mu^2,\varepsilon^3\mu^2)$ and $(\mu^4,\varepsilon^5\mu^4)$ equations.

---

[3] The term 'transfer function' refers to that used in the work of Madsen and Schäffer (1998).

For making comparisons, the following existing sets of equations will be analysed to the first- and second-order transfer functions for regular waves[4]:

- the equations of Boussinesq (1872) [equations (2.29) and (2.30)] and
- the first and second sets of equations of Peregrine (1967) [equations (2.111)-(2.112) and (2.105)-(2.106)]
- the equations of Nwogu (1993) [equations (3.16) and (3.17)] and
- the equations of Schäffer and Madsen (1995) [equations (4.5) and (4.6)]
- The first and second sets of equations of Chen *et al.* (1998) [equations (5.17)-(5.18) and (5.22)-(5.23)],

The 1D forms of the new and existing Boussinesq-type equations corresponding to a horizontal bottom are:

- BEWCBV-B, BEWBV-D and the equations of Boussinesq (1872) reduce to

$$\eta_t + h u_{b_x} - \mu^2 \tfrac{1}{6} h^3 u_{b_{xxx}} + \varepsilon(\eta u_b)_x = O(\varepsilon\mu^2, \mu^4) \qquad \text{(C.37)}$$

$$u_{b_t} + \eta_x - \mu^2 \tfrac{1}{2} h^2 u_{b_{xxt}} + \varepsilon u_b u_{b_x} = O(\varepsilon\mu^2, \mu^4) \qquad \text{(C.38)}$$

- BEWCSV-C and the second set of equations of Peregrine (1967) reduce to

$$\eta_t + h\tilde{u}_x + \mu^2 \tfrac{1}{3} h^3 \tilde{u}_{xxx} + \varepsilon(\eta\tilde{u})_x = O(\varepsilon\mu^2, \mu^4) \qquad \text{(C.39)}$$

$$\tilde{u}_t + \eta_x + \varepsilon\tilde{u}\tilde{u}_x = O(\varepsilon\mu^2, \mu^4) \qquad \text{(C.40)}$$

[4] The sets of equations of Nwogu (1993) and Schäffer and Madsen (1995) have been analysed to the first-order transfer functions for regular waves in Section 3.3 and Section 4.3 respectively. The analysis in both sections is intended to determine the free coefficients contained in both sets of equations. Consequently, in this appendix, both sets of equations will be analysed to the second-order only.

- The first set of equations of Chen *et al.* (1998) and the first set of equations of Peregrine (1967) reduce to

$$\eta_t + h\overline{u}_x + \varepsilon(\eta\overline{u})_x = 0 \tag{C.41}$$

$$\overline{u}_t + \eta_x - \mu^2 \tfrac{1}{3}h^2\overline{u}_{xxt} + \varepsilon\overline{u}\,\overline{u}_x = O(\varepsilon\mu^2, \mu^4) \tag{C.42}$$

- BEWCAV-A, the equations of Nwogu (1993) and the second set of equations of Chen *et al.* (1998) reduce to

$$\eta_t + hu_{\alpha_x} + \mu^2\left(\alpha + \tfrac{1}{3}\right)h^3 u_{\alpha_{xxx}} + \varepsilon(\eta u_\alpha)_x = O(\varepsilon\mu^2, \mu^4) \tag{C.43}$$

$$u_{\alpha_t} + \eta_x + \mu^2\alpha h^2 u_{\alpha_{xxt}} + \varepsilon u_\alpha u_{\alpha_x} = O(\varepsilon\mu^2, \mu^4) \tag{C.44}$$

- The equations of Schäffer and Madsen (1995) reduce to

$$\eta_t + hu_{\alpha_x} + \mu^2\left[\left(\alpha - \beta + \tfrac{1}{3}\right)h^3 u_{\alpha_{xxx}} - \beta h^3 \eta_{txx}\right] + \varepsilon(\eta u_\alpha)_x = O(\varepsilon\mu^2, \mu^4) \tag{C.45}$$

$$u_{\alpha_t} + \eta_x + \mu^2[(\alpha - \gamma)h^2 u_{\alpha_{xxt}} - \gamma\, h^2\eta_{xxx}] + \varepsilon u_\alpha u_{\alpha_x} = O(\varepsilon\mu^2, \mu^4) \tag{C.46}$$

- The equations of Wei *et al.* (1995) reduce to

$$\eta_t + hu_{\alpha_x} + \mu^2\left(\alpha + \tfrac{1}{3}\right)h^3 u_{\alpha_{xxx}} + \varepsilon\left[\eta u_\alpha + \mu^2\alpha\, h^2\eta u_{\alpha_{xx}}\right]_x = O(\varepsilon^2\mu^2, \mu^4) \tag{C.47}$$

$$u_{\alpha_t} + \eta_x + \mu^2\alpha\, h^2 u_{\alpha_{xxt}} + \varepsilon u u_{\alpha_x} + \varepsilon\mu^2\left[\alpha h^2 u_\alpha u_{\alpha_{xx}} + \tfrac{1}{2}h^2(u_{\alpha_x})^2 - \eta h u_{\alpha_{xt}}\right]_x$$
$$= O(\varepsilon^2\mu^2, \mu^4) \tag{C.48}$$

- FBE2O-E reduce to

$$\eta_t + hu_{\alpha_x} + \mu^2\left(\alpha + \tfrac{1}{3}\right)h^3 u_{\alpha_{xxx}} + \varepsilon\left[\eta u_\alpha + \mu^2\alpha h^2\eta u_{\alpha_{xx}}\right]_x = O(\varepsilon^2\mu^2, \mu^4) \tag{C.47}$$

$$u_{\alpha_t} + \eta_x + \mu^2\alpha h^2 u_{\alpha_{xxt}} + \varepsilon u u_{\alpha_x} + \varepsilon\mu^2\left[\alpha h^2 u_\alpha u_{\alpha_{xx}} - \tfrac{1}{6}h^2(u_{\alpha_x})^2\right.$$
$$\left. - \eta h u_{\alpha_{xt}} - \eta_t h u_{\alpha_x}\right]_x = O(\varepsilon^2\mu^2, \mu^4) \tag{C.49}$$

- The equations of Madsen and Schäffer (1998) reduce to

$$\eta_t + hu_{\alpha_x} + \mu^2\left(\alpha + \tfrac{1}{3}\right)h^3 u_{\alpha_{xxx}} + \mu^4 \sigma_1 h^5 u_{\alpha_{xxxxx}} + \varepsilon[\eta u_\alpha + \mu^2 \alpha h^2 \eta u_{\alpha_{xx}}$$

$$+ \mu^4 \sigma_2 h^4 \eta u_{\alpha_{xxxx}}]_x = O(\varepsilon^2\mu^2, \varepsilon^2\mu^4, \mu^6) \qquad \text{(C.50)}$$

$$u_{\alpha_t} + \eta_x + \mu^2 \alpha h^2 u_{\alpha_{xxt}} + \mu^4 \sigma_2 h^4 u_{\alpha_{xxxxt}} + \varepsilon u u_{\alpha_x}$$

$$+ \varepsilon\mu^2\left[\alpha h^2 u_\alpha u_{\alpha_{xx}} + \tfrac{1}{2} h^2 (u_{\alpha_x})^2 - \eta h u_{\alpha_{xt}}\right]_x$$

$$+ \varepsilon\mu^4\left[\tfrac{1}{2}\alpha^2 h^4 (u_{\alpha_{xx}})^2 + \sigma_2 h^2 u_\alpha u_{\alpha_{xxxx}} + \left(\alpha + \tfrac{1}{3}\right)h^3 (h u_{\alpha_x} u_{\alpha_{xxx}} - \eta u_{\alpha_{xxxt}})\right]_x$$

$$= O(\varepsilon^2\mu^2, \varepsilon^2\mu^4, \mu^6) \qquad \text{(C.51)}$$

where

$$\sigma_1 = \tfrac{5}{6}\left(\alpha + \tfrac{2}{5}\right)^2, \qquad \sigma_2 = \tfrac{5}{6}\alpha\left(\alpha + \tfrac{2}{5}\right) \qquad \text{(C.52)}$$

and α is defined by equation (3.22).

In the next steps, the expression for the free surface elevation [equation (C.36a)] and the appropriate expression for the horizontal velocity [one of equations (C.36b) – (C.36e)] is substituted into the appropriate sets of governing equations. Terms of $O(\varepsilon^0)$ are collected to yield the first-order transfer functions and terms of $O(\varepsilon^1)$ are collected to yield the second-order transfer functions. In particular, substitute:

(i) equations (C.36a) and (C.36b) into (C.37) and (C.38) to give equations (C.53a) and (C.70a),

(ii) equations (C.36a) and (C.36c) into (C.39) and (C.40) to give equations (C.53b) and (C.70b),

(iii) equations (C.36a) and (C.36d) into (C.41) and (C.42) to give equations (C.53c) and (C.70c), and

(iv) equations (C.36a) and (C.36e) into (C.43) through to (C.51) to give equations (C.53d) and (C.70d), Details of the various first-order transfer functions are given in the next section.

C.5.1. First-order transfer functions for regular waves

In determining the first-order transfer functions for regular waves, those terms of $O(\varepsilon^0)$ are collected.

$$\begin{bmatrix} m_{11}^{(1)} & m_{12}^{(1)} \\ m_{21}^{(1)} & m_{22}^{(1)} \end{bmatrix} \begin{Bmatrix} \eta_1 \\ u_{b1} \end{Bmatrix} = \begin{Bmatrix} 0 \\ 0 \end{Bmatrix} \tag{C.53a}$$

$$\begin{bmatrix} m_{11}^{(1)} & m_{12}^{(1)} \\ m_{21}^{(1)} & m_{22}^{(1)} \end{bmatrix} \begin{Bmatrix} \eta_1 \\ \tilde{u}_1 \end{Bmatrix} = \begin{Bmatrix} 0 \\ 0 \end{Bmatrix} \tag{C.53b}$$

$$\begin{bmatrix} m_{11}^{(1)} & m_{12}^{(1)} \\ m_{21}^{(1)} & m_{22}^{(1)} \end{bmatrix} \begin{Bmatrix} \eta_1 \\ \bar{u}_1 \end{Bmatrix} = \begin{Bmatrix} 0 \\ 0 \end{Bmatrix} \tag{C.53c}$$

$$\begin{bmatrix} m_{11}^{(1)} & m_{12}^{(1)} \\ m_{21}^{(1)} & m_{22}^{(1)} \end{bmatrix} \begin{Bmatrix} \eta_1 \\ u_{\alpha 1} \end{Bmatrix} = \begin{Bmatrix} 0 \\ 0 \end{Bmatrix} \tag{C.53d}$$

- The coefficients $(m_{11}^{(1)}, m_{12}^{(1)}, m_{21}^{(1)}, m_{22}^{(1)})$ in equation (C.53a) for BEWCBV-B, BEWBV-D and the equations of Boussinesq (1872) including terms up to $O(\mu^2)$ are

  $$\begin{aligned} m_{11}^{(1)} &= \omega, \quad m_{12}^{(1)} = -kh\left(1+\mu^2 \tfrac{1}{6} k^2h^2\right) \\ m_{21}^{(1)} &= -k, \quad m_{22}^{(1)} = \omega\left(1+\mu^2 \tfrac{1}{2} k^2h^2\right) \end{aligned} \tag{C.54}$$

  Hence, the solution (relating the velocity and surface elevation) of the algebraic system of equations (C.53a) with the coefficients defined by equation (C.54) is

  $$u_{b1} = \frac{\omega \eta_1}{kh\left(1+\mu^2 \tfrac{1}{6} k^2h^2\right)} \tag{C.55}$$

and the dispersion relation is

$$\frac{\omega^2}{k^2h}=\frac{1+\mu^2\frac{1}{6}k^2h^2}{1+\mu^2\frac{1}{2}k^2h^2} \tag{C.56}$$

- The coefficients $(m_{11}^{(1)},m_{12}^{(1)},m_{21}^{(1)},m_{22}^{(1)})$ in equation (C.53b) for BEWCSV-C and the second set of equations of Peregrine (1967) including terms up to $O(\mu^2)$ are

$$\begin{aligned} m_{11}^{(1)} &= \omega, \quad m_{12}^{(1)} = -kh\left(1-\mu^2\tfrac{1}{3}k^2h^2\right) \\ m_{21}^{(1)} &= -k, \quad m_{22}^{(1)} = \omega \end{aligned} \tag{C.57}$$

The solution and dispersion relation for the first-order transfer function are

$$\tilde{u}_1=\frac{\omega\eta_1}{kh\left(1-\mu^2\frac{1}{3}k^2h^2\right)} \tag{C.58}$$

$$\frac{\omega^2}{k^2h}=\frac{1-\mu^2\frac{1}{3}k^2h^2}{1} \tag{C.59}$$

- The coefficients $(m_{11}^{(1)},m_{12}^{(1)},m_{21}^{(1)},m_{22}^{(1)})$ in equation (C.53c) for the first set of equations of Chen *et al.* (1998) and the first set of equations of Peregrine (1967) including terms up to $O(\mu^2)$ are

$$\begin{aligned} m_{11}^{(1)} &= \omega, \quad m_{12}^{(1)} = -kh \\ m_{21}^{(1)} &= -k, \quad m_{22}^{(1)} = \omega\left(1+\mu^2\tfrac{1}{3}k^2h^2\right) \end{aligned} \tag{C.60}$$

The solution and dispersion relation for the first-order transfer function are

$$\bar{u}_1=\frac{\omega\eta_1}{kh} \tag{C.61}$$

$$\frac{\omega^2}{k^2h}=\frac{1}{1+\mu^2\frac{1}{3}k^2h^2} \tag{C.62}$$

- The coefficients $(m_{11}^{(1)}, m_{12}^{(1)}, m_{21}^{(1)}, m_{22}^{(1)})$ in equation (C.53d) for BEWCAV-A, FBE2O-E, the second set of equations of Chen *et al.* (1998) and the equations of Wei *et al.* (1995) equations including terms up to $O(\mu^2)$ are

$$\begin{aligned} &m_{11}^{(1)} = \omega, \quad m_{12}^{(1)} = -kh\left[1-\mu^2\left(\alpha+\tfrac{1}{3}\right)k^2h^2\right] \\ &m_{21}^{(1)} = -k, \quad m_{22}^{(1)} = \omega(1-\mu^2\alpha k^2h^2) \end{aligned} \tag{C.63}$$

The solution and dispersion relation are

$$u_{\alpha 1} = \frac{\omega\eta_1}{kh\left[1-\mu^2\left(\alpha+\frac{1}{3}\right)k^2h^2\right]} \tag{C.64}$$

$$\frac{\omega^2}{k^2h} = \frac{1-\mu^2\left(\alpha+\frac{1}{3}\right)k^2h^2}{1-\mu^2\alpha k^2h^2} \tag{C.65}$$

- The coefficients $(m_{11}^{(1)}, m_{12}^{(1)}, m_{21}^{(1)}, m_{22}^{(1)})$ in equation (C.53d) for the equations of Madsen and Schäffer (1998) including terms up to $O(\mu^4)$ are

$$\begin{aligned} &m_{11}^{(1)} = \omega, \quad m_{12}^{(1)} = -kh\left[1-\mu^2\left(\alpha+\tfrac{1}{3}\right)k^2h^2+\mu^4\sigma_1k^4h^4\right] \\ &m_{21}^{(1)} = -k, \quad m_{22}^{(1)} = \omega(1-\mu^2\alpha k^2h^2+\mu^4\sigma_2k^4h^4) \end{aligned} \tag{C.66}$$

The solution is

$$u_{\alpha 1} = \frac{\omega\eta_1}{kh\left[1-\mu^2\left(\alpha+\frac{1}{3}\right)k^2h^2+\mu^4\sigma_1k^4h^4\right]} \tag{C.67}$$

and the dispersion relation is

$$\frac{\omega^2}{k^2h} = \frac{1-\mu^2\left(\alpha+\frac{1}{3}\right)k^2h^2+\mu^4\sigma_1k^4h^4}{1-\mu^2\alpha k^2h^2+\mu^4\sigma_2k^4h^4} \tag{C.68}$$

The reference solution, which is adopted herein, is the dispersion relation of Stokes or Airy, that is

$$\left(\frac{\omega^2}{k^2h}\right)_{\text{Stokes}} = \frac{\tanh(kh)}{kh} \tag{C.69}$$

The expressions (C.56) and (C.65) are Padé [2,2] expansions in kh of (C.69), expression (C.59) is a Padé [2,0] expansion in kh of (C.69), expression (C.62) is a Padé [0,2] expansion in kh of (C.69), and (C.68) is a Padé [4,4] expansion in kh of (C.69).

The phase speed or celerity ratio is C/C_{Stokes}, where $C = \omega/k$ is determined from equations (C.56), (C.59), (C.62), (C.65) and (C.68), and C_{Stokes} from equation (C.69). The various celerity ratios are depicted in Figures C.4 and C.5.

Figure C.4 shows the variation of the wave celerity ratio with the *dimensionless* depth kh of the Boussinesq-type equations including terms up to $O(\mu^2)$ based on several definitions of the horizontal velocity. It appears that the (μ^2) equations presented in terms of the horizontal velocity at an arbitrary z-elevation ($\alpha = -0.39$, see Chapter Three for α) i.e. curve no. 1 in Figure C.4 gives the minimum error in the wave celerity.

Furthermore, Figure C.5 shows the *dimensionless* dispersion relation for Boussinesq-type equations including terms up to $O(\mu^4)$ with the horizontal velocity at several arbitrary levels, where $\alpha = -0.429648$ (suggested by Madsen and Schäffer, 1998) gives excellent results.

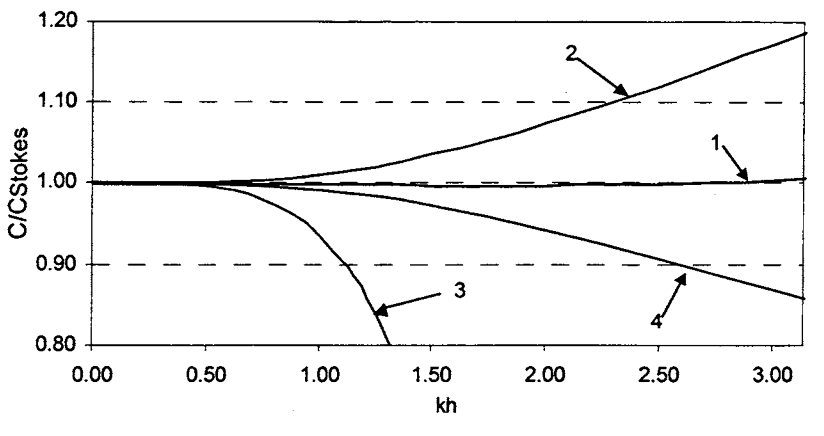

Figure C.4. Wave celerity ratio, C/C_{Stokes}, where C is determined by: (1) equation (C.65) (with $\alpha = -0.39$); (2) equation (C.56); (3) equation (C.59); and (4) equation (C.62). [Boussinesq-type equations include terms up to $O(\mu^2)$], and C_{Stokes} from (C.69).

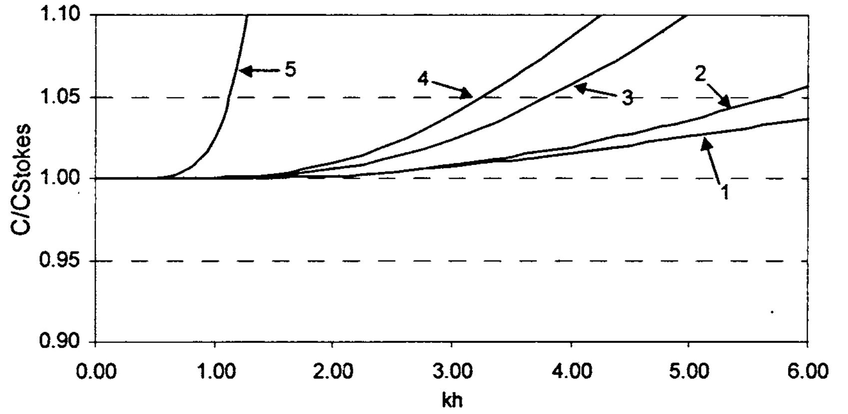

Figure C.5. Wave celerity ratio, C/C_{Stokes}, where C is determined by equation (C.68), and C_{Stokes} from equation (C.69). Boussinesq-type equations include terms up to $O(\mu^4)$. (1) $\alpha = -0.429648$, (2) $\alpha = -4/9$, (3) $\alpha = -2/5$ and (4) $\alpha = -1/2$, (2) $\alpha = 0$.

C.5.2. Second-order transfer functions for regular waves

The analysis is continued to second order for the transfer functions of regular waves by collecting those terms of $O(\varepsilon^1)$. This results in

$$\begin{bmatrix} m_{11}^{(2)} & m_{12}^{(2)} \\ m_{21}^{(2)} & m_{22}^{(2)} \end{bmatrix} \begin{Bmatrix} \eta_2 \\ u_{b2} \end{Bmatrix} = \frac{(\eta_1)^2}{h} \begin{Bmatrix} F_1 \\ F_2 \end{Bmatrix} \tag{C.70a}$$

$$\begin{bmatrix} m_{11}^{(2)} & m_{12}^{(2)} \\ m_{21}^{(2)} & m_{22}^{(2)} \end{bmatrix} \begin{Bmatrix} \eta_2 \\ \tilde{u}_2 \end{Bmatrix} = \frac{(\eta_1)^2}{h} \begin{Bmatrix} F_1 \\ F_2 \end{Bmatrix} \tag{C.70b}$$

$$\begin{bmatrix} m_{11}^{(2)} & m_{12}^{(2)} \\ m_{21}^{(2)} & m_{22}^{(2)} \end{bmatrix} \begin{Bmatrix} \eta_2 \\ \bar{u}_2 \end{Bmatrix} = \frac{(\eta_1)^2}{h} \begin{Bmatrix} F_1 \\ F_2 \end{Bmatrix} \tag{C.70c}$$

$$\begin{bmatrix} m_{11}^{(2)} & m_{12}^{(2)} \\ m_{21}^{(2)} & m_{22}^{(2)} \end{bmatrix} \begin{Bmatrix} \eta_2 \\ u_{\alpha 2} \end{Bmatrix} = \frac{(\eta_1)^2}{h} \begin{Bmatrix} F_1 \\ F_2 \end{Bmatrix} \tag{C.70d}$$

- The coefficients $(m_{11}^{(2)}, m_{12}^{(2)}, m_{21}^{(2)}, m_{22}^{(2)})$ in equation (C.70a) for BEWCBV-B, BEWBV-D and the equations of Boussinesq (1872) including terms up to $O(\mu^2,\varepsilon)$ are

$$\begin{aligned} m_{11}^{(2)} &= 2\omega, \quad m_{12}^{(2)} = -2kh\left(1+\mu^2 \tfrac{2}{3} k^2h^2\right) \\ m_{21}^{(2)} &= -2k, \quad m_{22}^{(2)} = 2\omega(1+\mu^2 2k^2h^2) \end{aligned} \tag{C.71}$$

and

$$F_1 = \frac{\omega}{1+\mu^2 \frac{1}{6} k^2h^2}, \qquad F_2 = \frac{1}{2kh\left(1+\mu^2 \frac{1}{6} k^2h^2\right)} \tag{C.72}$$

- The coefficients $(m_{11}^{(2)}, m_{12}^{(2)}, m_{21}^{(2)}, m_{22}^{(2)})$ in equation (C.70b) for BEWCSV-C and the second set of equations of Peregrine (1967) including terms up to $O(\mu^2,\varepsilon)$ are

$$\begin{aligned} m_{11}^{(2)} &= 2\omega, \quad m_{12}^{(2)} = -2kh\left(1-\mu^2 \tfrac{4}{3} k^2h^2\right) \\ m_{21}^{(2)} &= -2k, \quad m_{22}^{(2)} = 2\omega \end{aligned} \tag{C.73}$$

and

$$F_1 = \frac{\omega}{1-\mu^2 \frac{1}{3} k^2h^2}, \qquad F_2 = \frac{1}{2kh\left(1-\mu^2 \frac{1}{3} k^2h^2\right)} \tag{C.74}$$

- The coefficients $(m_{11}^{(2)}, m_{12}^{(2)}, m_{21}^{(2)}, m_{22}^{(2)})$ in equation (C.70c) for the first set of equations of Chen *et al.* (1998) and the first set of equations of Peregrine (1967) including terms up to $O(\mu^2,\varepsilon)$ are

$$\begin{aligned} m_{11}^{(2)} &= 2\omega, \quad m_{12}^{(2)} = -2kh \\ m_{21}^{(2)} &= -2k, \quad m_{22}^{(2)} = 2\omega\left(1+\mu^2 \tfrac{4}{3} k^2h^2\right) \end{aligned} \tag{C.75}$$

and

$$F_1 = \omega, \qquad F_2 = \frac{\omega^2}{2kh} \tag{C.76}$$

- The coefficients $(m_{11}^{(2)}, m_{12}^{(2)}, m_{21}^{(2)}, m_{22}^{(2)})$ in equation (C.70d) for BEWCAV-A, the equations of Nwogu (1993) and the second set of equations of Chen *et al.* (1998) including terms up to $O(\mu^2,\varepsilon)$ are

$$\begin{aligned} m_{11}^{(2)} &= 2\omega, \quad m_{12}^{(2)} = -2kh\left[1-\mu^2 4\left(\alpha+\tfrac{1}{3}\right)k^2h^2\right] \\ m_{21}^{(2)} &= -2k, \quad m_{22}^{(2)} = 2\omega(1-\mu^2 4\alpha k^2h^2) \end{aligned} \tag{C.77}$$

and

$$F_1 = \frac{\omega}{1+\mu^2\left(\alpha+\frac{1}{3}\right)k^2h^2}, \qquad F_2 = \frac{1}{2kh\left[1+\mu^2\left(\alpha+\frac{1}{3}\right)k^2h^2\right]} \tag{C.78}$$

- The coefficients $(m_{11}^{(2)}, m_{12}^{(2)}, m_{21}^{(2)}, m_{22}^{(2)})$ in equation (C.70d) for the equations of Schäffer and Madsen (1995) including terms up to $O(\mu^2,\varepsilon)$ are

$$\begin{aligned} m_{11}^{(2)} &= 2\omega(1+\mu^2 4\beta k^2h^2), \quad m_{12}^{(2)} = -2kh\left[1-\mu^2 4\left(\alpha-\beta+\tfrac{1}{3}\right)k^2h^2\right] \\ m_{21}^{(2)} &= -2k(1+\mu^2 4\gamma k^2h^2), \quad m_{22}^{(2)} = 2\omega[1-\mu^2 4(\alpha-\gamma)k^2h^2] \end{aligned} \tag{C.79}$$

and

$$F_1 = \frac{\omega(1+\mu^2\beta k^2h^2)}{1-\mu^2\left(\alpha-\beta+\frac{1}{3}\right)k^2h^2}, \qquad F_2 = \frac{\omega^2(1+\mu^2\beta k^2h^2)^2}{2kh\left[1-\mu^2\left(\alpha-\beta+\frac{1}{3}\right)k^2h^2\right]^2} \tag{C.80}$$

- The coefficients $(m_{11}^{(2)}, m_{12}^{(2)}, m_{21}^{(2)}, m_{22}^{(2)})$ in equation (C.70d) for the equations of Wei *et al.* (1995) including terms up to $O(\mu^2,\varepsilon\mu^2)$ are

$$\begin{aligned} m_{11}^{(2)} &= 2\omega, \quad m_{12}^{(2)} = -2kh\left[1-\mu^2 4\left(\alpha+\tfrac{1}{3}\right)k^2h^2\right] \\ m_{21}^{(2)} &= -2k, \quad m_{22}^{(2)} = 2\omega(1-\mu^2 4\alpha k^2h^2) \end{aligned} \tag{C.81}$$

and

$$F_1 = \omega\frac{1-\mu^2\alpha k^2h^2}{1-\mu^2\left(\alpha+\frac{1}{3}\right)k^2h^2},$$

$$F_2 = \frac{1-\mu^2\left\{1+2\alpha-2\left[1-\mu^2\left(\alpha+\frac{1}{3}\right)k^2h^2\right]\right\}k^2h^2}{2kh\left[1-\mu^2\left(\alpha+\frac{1}{3}\right)k^2h^2\right]} \tag{C.82}$$

- The coefficients $(m_{11}^{(2)}, m_{12}^{(2)}, m_{21}^{(2)}, m_{22}^{(2)})$ in equation (C.70d) for FBE2O-E including terms up to $O(\mu^2, \varepsilon\mu^2)$ are

$$\begin{aligned} m_{11}^{(2)} &= 2\omega, \quad m_{12}^{(2)} = -2kh\left[1-\mu^2 4\left(\alpha+\tfrac{1}{3}\right)k^2h^2\right] \\ m_{21}^{(2)} &= -2k, \quad m_{22}^{(2)} = 2\omega(1-\mu^2 4\,\alpha k^2h^2) \end{aligned} \tag{C.83}$$

and

$$F_1 = \omega\frac{1-\mu^2\alpha\,k^2h^2}{1-\mu^2\left(\alpha+\frac{1}{3}\right)k^2h^2},$$

$$F_2 = \frac{1-\mu^2\left\{-\frac{1}{3}+2\alpha+4\left[1-\mu^2\left(\alpha+\frac{1}{3}\right)k^2h^2\right]\right\}k^2h^2}{2kh\left[1-\mu^2\left(\alpha+\frac{1}{3}\right)k^2h^2\right]} \tag{C.84}$$

- The coefficients $(m_{11}^{(2)}, m_{12}^{(2)}, m_{21}^{(2)}, m_{22}^{(2)})$ in equation (C.70d) for the equations of Madsen and Schäffer (1998) including terms up to $O(\mu^4, \varepsilon\mu^4)$ are

$$\begin{aligned} m_{11}^{(2)} &= 2\omega, \quad m_{12}^{(2)} = -2kh\left[1-\mu^2 4\left(\alpha+\tfrac{1}{3}\right)k^2h^2+\mu^2 16\sigma_1 k^4h^4\right] \\ m_{21}^{(2)} &= -2k, \quad m_{22}^{(2)} = 2\omega(1-\mu^2 4\alpha k^2h^2+\mu^2 16\sigma_2 k^4h^4) \end{aligned} \tag{C.85}$$

and

$$F_1 = \omega\frac{1-\mu^2\alpha\,k^2h^2+\mu^4\sigma_2 k^4h^4}{1-\mu^2\left(\alpha+\frac{1}{3}\right)k^2h^2+\mu^4\sigma_1 k^4h^4},$$

$$F_2 = \frac{1-\mu^2(1+2\alpha+2\,f_{MS})k^2h^2+\mu^4\left[2\sigma_2+2\left(\alpha+\frac{1}{3}\right)(1+f_{MS})+\alpha^2\right]k^4h^4}{2kh\left[1-\mu^2\left(\alpha+\frac{1}{3}\right)k^2h^2+\mu^4\sigma_1 k^4h^4\right]} \tag{C.86}$$

where $f_{MS} = 1-\mu^2\left(\alpha+\frac{1}{3}\right)k^2h^2+\mu^4\sigma_1 k^4h^4$.

From equations (C.70), the free surface solution for the second-order transfer function is

$$\eta_2 = \frac{(\eta_1)^2}{h}\left(\frac{F_1 m_{22}^{(2)} - F_2 m_{12}^{(2)}}{m_{11}^{(2)}m_{22}^{(2)} - m_{21}^{(2)}m_{12}^{(2)}}\right) \tag{C.87}$$

The Stokes second-order solution (see, e.g. Skjelbreia and Hendrickson, 1960 and Madsen and Schäffer, 1998) for the free surface is used as a reference and is

$$\eta_{2\,\text{Stokes}} = \frac{1}{4}\frac{(\eta_1)^2}{h}\frac{kh}{\tanh(kh)}\left[\frac{3}{\tanh^2(kh)} - 1\right] \tag{C.88}$$

Figure C.6 displays the ratios of the amplitudes of the second harmonics, $\eta_2/\eta_{2\text{Stokes}}$ for the six different versions of the Boussinesq-type equations. It seems that FBE2O-E and Wei *et al.*'s (1995) Boussinesq-type equations (curve 1 in Figure C.6) are superior to the Boussinesq-type equations with the lowest order non-linearity.

Figure C.7 shows that $\alpha = -0.429648$ is still the best value for α for Boussinesq-type equations of Madsen and Schäffer (1998) in the second harmonic.

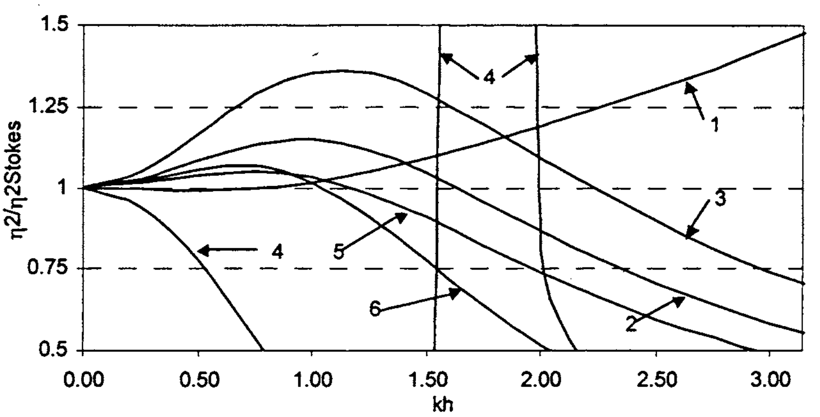

Figure C.6. Ratio of second harmonic, $\eta_2/\eta_{2\text{Stokes}}$, where η_2 is determined by equation (C.87) and $\eta_{2\text{Stokes}}$ by equation (C.88). (1) FBE2O-E and Wei *et al.*'s (1995) equations include terms up to $O(\mu^2,\varepsilon\mu^2)$; (2) BEWCAV-A, Nwogu's (1993) and Chen *et al.*'s (1998) second equations include terms up to $O(\mu^2,\varepsilon)$; (3) BEWCBV-B and BEWBV-D include terms up to $O(\mu^2,\varepsilon)$; (4) BEWCSV-C include terms up to $O(\mu^2,\varepsilon)$; (5) Chen *et al.*'s first equations include terms up to $O(\mu^2,\varepsilon)$; and (6) Schäffer and Madsen's (1995) equations include terms up to $O(\mu^2,\varepsilon)$.

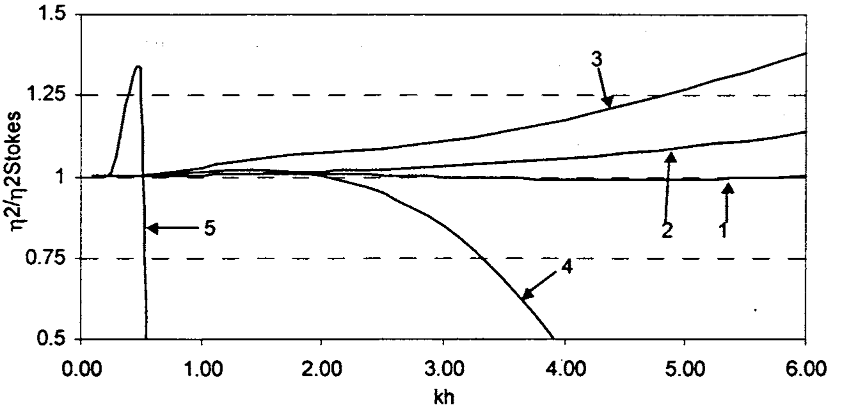

Figure C.7. Ratio of second harmonic, $\eta_2/\eta_{2Stokes}$, where η_2 is determined by equation (C.87) and $\eta_{2Stokes}$ by equation (C.88). Boussinesq-type equations include terms up to $O(\mu^4,\varepsilon\mu^4)$. (1) $\alpha = -0.429648$; (2) $\alpha = -4/9$; (3) $\alpha = -2/5$; (4) $\alpha = -1/2$; and (5) $\alpha = 0$.

C.6. Wave-current interaction and Doppler shift

Chen *et al.* (1998) and Madsen and Schäffer (1998) reported that one consequence of the non-linearity of the Boussinesq (-type) equations is the automatic inclusion of wave-averaged effects such as radiation stress, setup, undertow and wave-induced currents. This is however, not a guarantee for a correct representation of for example, the Doppler shift in association with current refraction and in fact, most Boussinesq-type equations fail to model this phenomenon accurately.

Yoon and Liu (1989) were the first to address the problem of wave-current interaction in relation to Boussinesq-type equations. Their study was followed by for example, Prüser and Zielke (1990), Chen *et al.* (1998) and Madsen and Schäffer (1998).

In the lowest order Boussinesq-type equations in which terms up to $O(\varepsilon,\mu^2)$ are retained, the inclusion of an ambient current needs special attention and scaling. This can be found in the work of Yoon and Liu (1989), Chen *et al.* (1998) and also the present study (see Section C.2). Wave-current interaction in those (ε,μ^2) equations was considered as weakly non-linear waves with slowly varying currents and topography. The magnitude of the current velocity was assumed to be larger than that of the characteristic wave orbital velocity but less than that of the wave group velocity. Chen *et al.* then allowed current speeds to exceed the intrinsic wave group velocity[5] in order to simulate wave blocking phenomenon. The spatial variation of the current was closely related to the variation of the bottom bathymetry, and these variations were assumed to be a larger scale than the characteristic wavelength. Consequently, strong currents can be treated only on weakly varying bathymetry. However, weak currents do not imply any restriction on the bathymetry variation.

Following Chen *et al.* (1998), the analysis will be restricted to 1D on a horizontal bottom.

- BEWCBV-B include terms up to $O(\varepsilon,\mu^2)$

$$\eta_t + h u_{b_x} + \varepsilon(\eta u_b)_x + \mu^2\left(-\tfrac{1}{6}h^3 - \tfrac{1}{2}h^2\eta - \tfrac{1}{2}\eta^2 h - \tfrac{1}{6}\eta^3\right)u_{b_{xxx}} = O(\varepsilon\mu^2,\mu^4) \tag{C.89}$$

$$u_{b_t} + \varepsilon u_b u_{b_x} + \eta_x + \mu^2\Big[\left(-\tfrac{1}{2}h^2 - \eta h - \tfrac{1}{2}\eta^2\right)\left(u_{b_{xxt}} + u_b u_{b_{xxx}}\right)\Big]$$

$$+\left(-\tfrac{1}{6}h^2 - \tfrac{1}{3}\eta h - \tfrac{1}{6}\eta^2\right)u_{b_x} u_{b_{xx}}\Big] = O(\varepsilon\mu^2,\mu^4) \tag{C.90}$$

- BEWCSV-C include terms up to $O(\varepsilon,\mu^2)$

$$\eta_t + h\tilde{u}_x + \varepsilon(\eta\tilde{u})_x + \mu^2\left(\tfrac{1}{3}h^3 - \tfrac{1}{2}\eta^2 h - \tfrac{1}{6}\eta^3\right)\tilde{u}_{xxx} = O(\varepsilon\mu^2,\mu^4) \tag{C.91}$$

$$\tilde{u}_t + \varepsilon\tilde{u}\tilde{u}_x + \eta_x + \mu^2\Big[\left(-\eta h - \tfrac{1}{2}\eta^2\right)\left(\tilde{u}_{xxt} + \tilde{u}\tilde{u}_{xxx}\right)$$

$$+\left(\tfrac{1}{3}h^2 - \tfrac{1}{3}\eta h - \tfrac{1}{6}\eta^2\right)\tilde{u}_x\tilde{u}_{xx}\Big] = O(\varepsilon\mu^2,\mu^4) \tag{C.92}$$

[5] Intrinsic group velocity is the group velocity relative to the current.

- The first set of equations of Chen *et al.* (1998) include terms up to $O(\varepsilon,\mu^2)$

$$\eta_t + h\bar{u}_x + \varepsilon(\eta\bar{u})_x = 0 \tag{C.93}$$

$$\bar{u}_t + \varepsilon\bar{u}\bar{u}_x + \eta_x - \mu^2\left(\tfrac{1}{3}h^2 + \tfrac{2}{3}\eta + \tfrac{1}{3}\eta^2\right)(\bar{u}_{xxt} + \bar{u}\bar{u}_{xxx}) = O(\varepsilon\mu^2,\mu^4) \tag{C.94}$$

- BEWCAV-A and the second set of equations of Chen *et al.* (1998) include terms up to $O(\varepsilon,\mu^2)$

$$\eta_t + hu_{\alpha_x} + \varepsilon(\eta u_\alpha)_x + \mu^2\left[\left(\alpha + \tfrac{1}{3}\right)h^3 + \alpha h^2\eta - \tfrac{1}{2}\eta^2 h - \tfrac{1}{6}\eta^3\right]u_{\alpha_{xxx}} = O(\varepsilon\mu^2,\mu^4) \tag{C.95}$$

$$u_{\alpha_t} + \varepsilon u_\alpha u_{\alpha_x} + \eta_x + \mu^2\left[\left(\alpha h^2 - \eta h - \tfrac{1}{2}\eta^2\right)(u_{\alpha_{xxt}} + u_\alpha u_{\alpha_{xxx}})\right.$$

$$\left. + \left(\alpha h^2 + \tfrac{1}{3}h^2 - \tfrac{1}{3}\eta h - \tfrac{1}{6}\eta^2\right)u_{\alpha_x}u_{\alpha_{xx}}\right] = O(\varepsilon\mu^2,\mu^4) \tag{C.96}$$

- The equations of Wei *et al.* (1995) include terms up to $O(\mu^2,\varepsilon^3\mu^2)$

$$\eta_t + hu_{\alpha_x} + \varepsilon(\eta u_\alpha)_x + \mu^2\left[\left(\alpha + \tfrac{1}{3}\right)h^3 u_{\alpha_{xxx}} + \varepsilon\alpha h^2(\eta u_{\alpha_{xx}})_x\right.$$

$$\left. - \varepsilon^2\tfrac{1}{2}h(\eta^2 u_{\alpha_{xx}})_x - \varepsilon^3\tfrac{1}{6}(\eta^3 u_{\alpha_{xx}})_x\right] = O(\mu^4) \tag{C.97}$$

$$u_{\alpha_t} + \varepsilon u_\alpha u_{\alpha_x} + \eta_x + \mu^2\left\{\alpha h^2 u_{\alpha_{xxt}} + \varepsilon\left[\alpha h^2(u_\alpha u_{\alpha_{xxx}} + u_{\alpha_x}u_{\alpha_{xx}})\right.\right.$$

$$\left. + h^2 u_{\alpha_x}u_{\alpha_{xx}} - h(\eta u_{\alpha_{xt}})_x\right] + \varepsilon^2\left[-\tfrac{1}{2}(\eta^2 u_{\alpha_{xt}})_x + h(\eta u_{\alpha_x}u_{\alpha_x} - \eta u_\alpha u_{\alpha_{xx}})_x\right]$$

$$\left. + \varepsilon^3\left[\tfrac{1}{2}(\eta^2 u_{\alpha_x}u_{\alpha_x} - \eta^2 u_\alpha u_{\alpha_{xx}})_x\right]\right\} = O(\mu^4) \tag{C.98}$$

- FBE2O-E include terms up to $O(\mu^2, \varepsilon^3\mu^2)$

$$\eta_t + hu_{\alpha_x} + \varepsilon(\eta u_\alpha)_x + \mu^2\Big[\big(\alpha + \tfrac{1}{3}\big)h^3 u_{\alpha_{xxx}} + \varepsilon\alpha h^2(\eta u_{\alpha_{xx}})_x$$

$$- \varepsilon^2 \tfrac{1}{2} h(\eta^2 u_{\alpha_{xx}})_x - \varepsilon^3 \tfrac{1}{6}(\eta^3 u_{\alpha_{xx}})_x\Big] = O(\mu^4) \qquad \text{(C.97)}$$

$$u_{\alpha_t} + \varepsilon u_\alpha u_{\alpha_x} + \eta_x + \mu^2\Big\{\alpha h^2 u_{\alpha_{xxt}} + \varepsilon\Big\{\alpha h^2(u_\alpha u_{\alpha_{xxx}} + u_{\alpha_x} u_{\alpha_{xx}})$$

$$- h[(\eta\, u_{\alpha_{xt}})_x + (\eta_t u_{\alpha_x})_x] - \tfrac{1}{3} h^2 u_{\alpha_x} u_{\alpha_{xx}}\Big\}$$

$$+ \varepsilon^2\Big\{\tfrac{1}{2}(\eta^2 u_{\alpha_{xt}})_x - (\eta\eta_t u_{\alpha_x})_x - h[u_\alpha(\eta u_{\alpha_x})_x]_x - \tfrac{2}{3} h\eta u_{\alpha_x} u_{\alpha_{xx}}\Big\}$$

$$+ \varepsilon^3\Big\{-\tfrac{1}{2}[u_\alpha(\eta^2 u_{\alpha_x})_x]_x - \tfrac{1}{3}\eta^2 u_{\alpha_x} u_{\alpha_{xx}}\Big\}\Big\} = O(\mu^4) \qquad \text{(C.99)}$$

- The equations of Madsen and Schäffer (1998) include terms up to $O(\mu^4, \varepsilon^5\mu^4)$

$$\eta_t + hu_{\alpha_x} + \varepsilon(\eta u_\alpha)_x + \mu^2\Big[\big(\alpha + \tfrac{1}{3}\big)h^3 u_{\alpha_{xxx}} + \varepsilon\alpha h^2(\eta u_{\alpha_{xx}})_x - \varepsilon^2 \tfrac{1}{2} h(\eta^2 u_{\alpha_{xx}})_x$$

$$-\varepsilon^3 \tfrac{1}{6}(\eta^3 u_{\alpha_{xx}})_x\Big] + \mu^4\Big[\sigma_1 h^5 u_{\alpha_{xxxxx}} + \varepsilon\sigma_2 h^4(\eta u_{\alpha_{xxxx}})_x$$

$$-\varepsilon^2 \tfrac{1}{2}\big(\alpha + \tfrac{1}{3}\big)h^3(\eta^2 u_{\alpha_{xxxx}})_x - \varepsilon^3 \tfrac{1}{6}\alpha h^2(\eta^3 u_{\alpha_{xxxx}})_x + \varepsilon^4 \tfrac{1}{24} h(\eta^4 u_{\alpha_{xxxx}})_x$$

$$+\varepsilon^5 \tfrac{1}{120}(\eta^5 u_{\alpha_{xxxx}})_x\Big] = O(\mu^6) \qquad \text{(C.100)}$$

$$u_{\alpha_t} + \varepsilon u_\alpha u_{\alpha_x} + \eta_x + \mu^2\Big\{\alpha h^2 u_{\alpha_{xxt}} + \varepsilon[\alpha h^2(u_\alpha u_{\alpha_{xxx}} + u_{\alpha_x} u_{\alpha_{xx}})$$

$$+h^2 u_{\alpha_x} u_{\alpha_{xx}} - h(\eta u_{\alpha_{xt}})_x] + \varepsilon^2[-\tfrac{1}{2}(\eta^2 u_{\alpha_{xt}})_x + h(\eta u_{\alpha_x} u_{\alpha_x} - \eta u_\alpha u_{\alpha_{xx}})_x]$$

$$+\varepsilon^3[\tfrac{1}{2}(\eta^2 u_{\alpha_x} u_{\alpha_x} - \eta^2 u_\alpha u_{\alpha_{xx}})_x]\Big\}$$

$$+\mu^4\Big\{\sigma_2 h^4 u_{\alpha_{xxxxt}} + \varepsilon[\alpha^2 h^4 u_{\alpha_{xx}} u_{\alpha_{xxx}} + \sigma_2 h^4(u_\alpha u_{\alpha_{xxxxx}} + u_{\alpha_x} u_{\alpha_{xxxx}})$$

$$+\big(\alpha + \tfrac{1}{3}\big)h^3[h(u_{\alpha_x} u_{\alpha_{xxx}})_x - (\eta u_{\alpha_{xxxt}})_x] + \varepsilon^2\Big[-\tfrac{1}{2}\alpha h^2(\eta^2 u_{\alpha_{xxxt}})_x$$

$$+\big(\alpha + \tfrac{1}{3}\big)h^3(\eta u_{\alpha_x} u_{\alpha_{xxx}} - \eta u_\alpha u_{\alpha_{xxxx}})_x + \alpha h^3(u_{\alpha_x} u_{\alpha_{xxx}} - \eta u_\alpha u_{\alpha_{xxxx}})_x\Big]$$

$$+\varepsilon^3\Big[\tfrac{1}{6} h(\eta^3 u_{\alpha_{xxxt}})_x + \tfrac{1}{2} h^2(\eta^2 u_{\alpha_{xx}} u_{\alpha_{xx}} - \eta^2 u_{\alpha_x} u_{\alpha_{xxx}})_x$$

$$+\alpha h^2\big(\eta^2 u_{\alpha_x} u_{\alpha_{xxx}} - \tfrac{1}{2}\eta^2 u_\alpha u_{\alpha_{xxxx}} - \tfrac{1}{2}\eta^2 u_{\alpha_{xx}} u_{\alpha_{xx}}\big)_x\Big]$$

$$+\varepsilon^4\{\tfrac{1}{24}(\eta^4 u_{\alpha_{xxxt}})_x + \tfrac{1}{6} h[\eta^3(u_\alpha u_{\alpha_{xxxx}} - 4u_{\alpha_x} u_{\alpha_{xxx}} + 3u_{\alpha_{xx}} u_{\alpha_{xx}})]_x\}$$

$$+\varepsilon^5\{\tfrac{1}{24}[\eta^4(u_\alpha u_{\alpha_{xxxx}} - 4\, u_{\alpha_x} u_{\alpha_{xxx}} + 3\, u_{\alpha_{xx}} u_{\alpha_{xx}})]_x\}\Big\} + O(\mu^6) \qquad \text{(C.101)}$$

The velocity field is decomposed into the wave orbital velocity and ambient current components. The ambient current speed $\hat{u}_c$ is assumed to be a known quantity, which is constant in space (horizontal and vertical) and time. This results in the following *non-dimensional* forms.

$$u_b = u_{bw} + \frac{1}{\varepsilon}\hat{u}_c \tag{C.102a}$$

$$\tilde{u} = \tilde{u}_w + \frac{1}{\varepsilon}\hat{u}_c \tag{C.102b}$$

$$\bar{u} = \bar{u}_w + \frac{1}{\varepsilon}\hat{u}_c \tag{C.102c}$$

$$u_\alpha = u_{\alpha w} + \frac{1}{\varepsilon}\hat{u}_c \tag{C.102d}$$

where subscripts w and c denote wave and current components respectively.

In the next steps, the appropriate expression for the horizontal velocity [one of equations (C.102a) – (C.102d)] is substituted in the appropriate sets of governing equations. In particular,

- Substitution of equation (C.102a) into (C.89) and (C.90) [i.e. BEWCBV-B including terms up to $O(\varepsilon,\mu^2)$] leads to

$$\eta_t + h u_{bw_x} + \hat{u}_c \eta_x - \mu^2 \tfrac{1}{6} h^3 u_{bw_{xxx}} = O(\varepsilon) \tag{C.103}$$

$$u_{bw_t} + \hat{u}_c u_{bw_x} + \eta_x - \mu^2 \tfrac{1}{2} h^2 (u_{bw_{xxt}} + \hat{u}_c u_{bw_{xxx}}) = O(\varepsilon) \tag{C.104}$$

- Substitution of equation (C.102b) into (C.91) and (C.92) [i.e. BEWCSV-C including terms up to $O(\varepsilon,\mu^2)$] leads to

$$\eta_t + h \tilde{u}_{w_x} + \hat{u}_c \eta_x + \mu^2 \tfrac{1}{3} h^3 \tilde{u}_{w_{xxx}} = O(\varepsilon) \tag{C.105}$$

$$\tilde{u}_{w_t} + \hat{u}_c \tilde{u}_{w_x} + \eta_x = O(\varepsilon) \tag{C.106}$$

- Substitution of equation (C.102c) into (C.93) and (C.94) [i.e. the first set of equations of Chen *et al.* (1998) including terms up to $O(\varepsilon,\mu^2)$] leads to

$$\eta_t + h\overline{u}_{w_x} + \hat{u}_c\eta_x = O(\varepsilon) \tag{C.107}$$

$$\overline{u}_{w_t} + \hat{u}_c\overline{u}_{w_x} + \eta_x - \mu^2\tfrac{1}{3}h^2(\overline{u}_{w_{xxt}} + \hat{u}_c\overline{u}_{w_{xxx}}) = O(\varepsilon) \tag{C.108}$$

- Substitution of equation (C.102d) into (C.95) through to (C.99) [i.e. BEWCAV-A and the second set of equations of Chen *et al.* (1998) including terms up to $O(\varepsilon,\mu^2)$, and FBE2O-E and the equations of Wei *et al.* (1995) including terms up to $O(\mu^2,\varepsilon^3\mu^2)$] leads to

$$\eta_t + hu_{\alpha w_x} + \hat{u}_c\eta_x + \mu^2\left(\alpha + \tfrac{1}{3}\right)h^3u_{\alpha w_{xxx}} = O(\varepsilon) \tag{C.109}$$

$$u_{\alpha w_t} + \hat{u}_c u_{\alpha w_x} + \eta_x + \mu^2\alpha h^2(u_{\alpha w_{xxt}} + \hat{u}_c u_{\alpha w_{xxx}}) = O(\varepsilon) \tag{C.110}$$

- Substitution of equation (C.102d) into (C.100) and also into (C.101) [i.e. the equations of Madsen and Schäffer (1998) including terms up to $O(\mu^4,\varepsilon^5\mu^4)$] leads to

$$\eta_t + hu_{\alpha w_x} + \hat{u}_c\eta_x + \mu^2\left(\alpha + \tfrac{1}{3}\right)h^3u_{\alpha w_{xxx}} + \mu^4\sigma_1 h^5u_{\alpha w_{xxxxx}} = O(\varepsilon) \tag{C.111}$$

$$u_{\alpha w_t} + \overline{u}_c u_{\alpha w_x} + \eta_x + \mu^2\alpha h^2(u_{\alpha w_{xxt}} + \hat{u}_c u_{\alpha w_{xxx}})$$
$$+ \mu^4\sigma_2 h^4(u_{\alpha w_{xxxxt}} + \hat{u}_c u_{\alpha w_{xxxxx}}) = O(\varepsilon) \tag{C.112}$$

First-order wave solutions of the following forms will be sought

$$\eta = \eta_1\cos\theta \tag{C.113a}$$

$$u_{bw} = u_{b1}\cos\theta \tag{C.113b}$$

$$\tilde{u}_w = \tilde{u}_1\cos\theta \tag{C.113c}$$

$$\overline{u}_w = \overline{u}_1\cos\theta \tag{C.113d}$$

$$u_{\alpha w} = u_{\alpha 1}\cos\theta \tag{C.113e}$$

In the next steps, the expression for the surface elevation [i.e. equation (C.113a)] and the appropriate expression for the horizontal velocity [one of equations (C.113b) – (C.113e)] is substituted in the appropriate sets of governing equations. In particular,

- Inserting equations (C.113a) and (C.113b) into (C.103) and (C.104) [i.e. BEWCBV-B including terms up to $O(\mu^2)$] leads to the algebraic system of equations (C.53a) with the coefficients $(m_{11}^{(1)}, m_{12}^{(1)}, m_{21}^{(1)}, m_{22}^{(1)})$ defined by

$$\begin{aligned} m_{11}^{(1)} &= \omega - \hat{u}_c k, & m_{12}^{(1)} &= -kh(1+\mu^2 \tfrac{1}{6} k^2h^2) \\ m_{21}^{(1)} &= -k, & m_{22}^{(1)} &= (\omega - \hat{u}_c k)(1+\mu^2 \tfrac{1}{2} k^2h^2) \end{aligned} \tag{C.114}$$

The associated dispersion relation is

$$\frac{1}{k^2h}(\omega - \hat{u}_c k)^2 = \frac{1+\mu^2 \frac{1}{6} k^2h^2}{1+\mu^2 \frac{1}{2} k^2h^2} \tag{C.115}$$

- Inserting equations (C.113a) and (C.113c) into (C.105) and (C.106) [i.e. BEWCSV-C including terms up to $O(\mu^2)$] leads to the algebraic system of equations (C.53b) with the coefficients $(m_{11}^{(1)}, m_{12}^{(1)}, m_{21}^{(1)}, m_{22}^{(1)})$ defined by

$$\begin{aligned} m_{11}^{(1)} &= \omega - \hat{u}_c k, & m_{12}^{(1)} &= -kh(1-\mu^2 \tfrac{1}{3} k^2h^2) \\ m_{21}^{(1)} &= -k, & m_{22}^{(1)} &= \omega - \hat{u}_c k \end{aligned} \tag{C.116}$$

The associated dispersion relation is

$$\frac{1}{k^2h}(\omega - \hat{u}_c k)^2 = \frac{1-\mu^2 \frac{1}{3} k^2h^2}{1} \tag{C.117}$$

- Inserting equations (C.113a) and (C.113d) into (C.107) and (C.108) [i.e. the first set of equations of Chen *et al.* (1998) including terms up to $O(\mu^2)$] leads to the algebraic systems of equation (C.53c) with the coefficients $(m_{11}^{(1)}, m_{12}^{(1)}, m_{21}^{(1)}, m_{22}^{(1)})$ defined by

$$\begin{aligned} m_{11}^{(1)} &= \omega - \hat{u}_c k, & m_{12}^{(1)} &= -kh \\ m_{21}^{(1)} &= -k, & m_{22}^{(1)} &= (\omega - \hat{u}_c k)(1+\mu^2 \tfrac{1}{3} k^2h^3) \end{aligned} \tag{C.118}$$

The associated dispersion relation is

$$\frac{1}{k^2h}(\omega-\hat{u}_c k)^2=\frac{1}{1+\mu^2\frac{1}{3}k^2h^2} \tag{C.119}$$

- Inserting equations (C.113a) and (C.113e) into (C.109) and (C.110) [i.e. BEWCAV-A, FBE2O-E, the second set of equations of Chen *et al.* (1998) and the equations of Wei *et al.*'s (1995) including terms up to $O(\mu^2)$] leads to the algebraic system of equations (C.53d) with the coefficients $(m_{11}^{(1)},m_{12}^{(1)},m_{21}^{(1)},m_{22}^{(1)})$ defined by

$$\begin{aligned} m_{11}^{(1)}&=\omega-\hat{u}_c k, & m_{12}^{(1)}&=-kh\left[1-\mu^2\left(\alpha+\tfrac{1}{3}\right)k^2h^2\right] \\ m_{21}^{(1)}&=-k, & m_{22}^{(1)}&=(\omega-\hat{u}_c k)(1-\mu^2\alpha k^2h^2) \end{aligned} \tag{C.120}$$

The associated dispersion relation is

$$\frac{1}{k^2h}(\omega-\hat{u}_c k)^2=\frac{1-\mu^2\left(\alpha+\frac{1}{3}\right)k^2h^2}{1-\mu^2\alpha k^2h^2} \tag{C.121}$$

- Inserting equations (C.113a) and (C.113e) into (C.111) and (C.112) [i.e. the equations of Madsen and Schäffer (1998) including terms up to $O(\mu^4)$] lead to the algebraic system of equations (C.53d) with the coefficients $(m_{11}^{(1)},m_{12}^{(1)},m_{21}^{(1)},m_{22}^{(1)})$ defined by

$$\begin{aligned} m_{11}^{(1)}&=\omega-\hat{u}_c k, & m_{12}^{(1)}&=-kh\left[1-\mu^2\left(\alpha+\tfrac{1}{3}\right)k^2h^2+\mu^4\sigma_1k^4h^4\right] \\ m_{21}^{(1)}&=-k, & m_{22}^{(1)}&=(\omega-\hat{u}_c k)(1-\mu^2\alpha k^2h^2+\mu^4\sigma_2k^4h^4) \end{aligned} \tag{C.122}$$

The associated dispersion relation is

$$\frac{1}{k^2h}(\omega-\hat{u}_c k)^2=\frac{1-\mu^2\left(\alpha+\frac{1}{3}\right)k^2h^2+\mu^4\sigma_1k^4h^4}{1-\mu^2\alpha k^2h^2+\mu^4\sigma_2k^4h^4} \tag{C.123}$$

Obviously, all the new Boussinesq-type equations (except BEWBV-D, this is due to BEWBV-D for waves only), the Boussinesq-type equations of Chen *et al.* (1995) (the first and second sets), of Wei *et al.* (1995) and of Madsen and Schäffer (1998) provide the correct form of the Doppler shift.

C.7. Conclusions

Three new sets of weakly non-linear Boussinesq-type (ε,μ^2) equations with an ambient current are developed by the present author. They are written in terms of the horizontal velocities at an arbitrary z-level (BEWCAV-A), the bottom (BEWCBV-B) and still water level (BEWCSV-C). The scaling assumptions for wave-current interaction follow those of the work of Chen *et al.* (1998). In the present study however, currents are allowed to be vertically sheared instead of the depth-uniform currents as in the work of Chen *et al.*. The present depth-integrated momentum equation is obtained by integrating the horizontal Euler equation of motion including the irrotationality condition instead of including the kinematic and dynamic boundary conditions as in the work of Nwogu (1993) and Chen *et al.* (1998). The free surface kinematic and dynamic boundary conditions are then inserted into the expression for the pressure field and the kinematic seabed boundary condition is inserted into the expression for the vertical velocity. Nevertheless, the present depth-integrated continuity equation remains identical to that employed by Nwogu, Chen *et al.*, Wei *et al.* (1995) and Madsen and Schäffer (1998).

Removing all dispersion terms associated with currents in BEWCBV-B leads to a new set of Boussinesq-type equations for weakly non-linear waves (BEWBV-D).

Making use of the new alternative approach for deriving the equations of Nwogu (1993) in Section 3.2, but with the free surface kinematic boundary condition excluded, the fully non-linear Boussinesq-type equations of Wei *et al.* (1995) [including terms up to $O(\mu^2,\varepsilon^3\mu^2)$] and of Madsen and Schäffer (1998) [including terms up to $O(\mu^4,\varepsilon^5\mu^4)$] are successfully re-derived.

Wei *et al.* derived their ($\mu^2,\varepsilon^3\mu^2$) equations by introducing a series expansion for ϕ at $z = -h$, and converting it to $z = z_\alpha$. This expansion was then substituted into the free surface, dynamic boundary condition to develop the Boussinesq-type momentum equation.

Madsen and Schäffer derived their $(\mu^4,\varepsilon^5\mu^4)$ equations by introducing an expansion of the velocity potential as a power series in the vertical coordinate to form the horizontal and vertical velocities and then utilising the free surface, dynamic boundary condition to develop the Boussinesq-type momentum equation.

A new alternative set of $(\mu^2,\varepsilon^3\mu^2)$ equations (FBE2O-E) is derived by use of the depth-integrated momentum equation as used in the derivation of the new (ε,μ^2) equations (BEWCAV-A, BEWCBV-B and BEWCSV-C).

Furthermore, the existing and new Boussinesq-type equations are analysed by Fourier analysis to show the dispersion relationship (first-order transfer function for regular waves) and non-linear properties (second-order transfer function for regular waves) of the corresponding governing equations.

In the first-order transfer function for regular waves, the governing equations with μ^4 terms included are superior to those with μ^2 terms. The governing equations including the lowest-order frequency dispersion (i.e. μ^2) terms presented in terms of the arbitrary horizontal velocity give an excellent dispersion relation compared to those in terms of other velocity definitions. For Boussinesq-type equations including fourth-order frequency dispersion (i.e. μ^4) terms, the horizontal velocity at $z = -0.429648\,h$ (suggested by Madsen and Schäffer, 1998) gives the best dispersion relation when compared to Stokes dispersion relation (i.e. the Stokes first-order solution). In the second-order transfer function for regular waves, the same trends apply. The reference solution is the Stokes second-order solution.

In addition, all the new Boussinesq-type equations presented in this appendix (except BEWBV-D) and the first and second sets of (ε,μ^2) equations of Chen *et al.* (1998) presented in Chapter Five provide the correct representation of the Doppler shift in association with current refraction.